Adsorption, Surface Area and Porosity

SECOND EDITION

S. J. Gregg

Formerly of the Department of Chemistry, University of Exeter, Exeter, U.K.

K. S. W. Sing

Department of Applied Chemistry, Brunel University, Uxbridge, Middlesex, U.K.

1982

ACADEMIC PRESS

A Subsidiary of Harcourt Brace Jovanovich, Publishers

LONDON · NEW YORK
PARIS · SAN DIEGO · SAN FRANCISCO
SAO PAULO · SYDNEY · TOKYO · TORONTO

ACADEMIC PRESS INC. (LONDON) LTD
24/28 Oval Road,
London NW1 7DX

United States Edition published by
ACADEMIC PRESS INC.
111 Fifth Avenue,
New York, New York 10003

British Library Cataloguing in Publication Data

Gregg, S. J.
Adsorption, surface area and porosity.—2nd ed.
1. Surface chemistry 2. Surfaces (Physical)
I. Title II. Sing, K. S. W.
541.3'453 QD506 LCCCN 66-29432

ISBN 0-12-300956-1

Filmset in 'Monophoto' Times New Roman
by Eta Services (Typesetters) Ltd., Beccles, Suffolk
Printed in Great Britain by
St Edmundsbury Press, Bury St Edmunds, Suffolk

Preface

The principal aim of the second edition of this book remains the same as that of the first edition: to give a critical exposition of the use of the adsorption methods for the assessment of the surface area and pore size distribution of finely divided and porous solids.

A vast amount of research has been undertaken on adsorption phenomena and the nature of solid surfaces over the fifteen years since the first edition was published, but for the most part this work has resulted in the refinement of existing theoretical principles and experimental procedures rather than in the formulation of entirely new concepts. In spite of the acknowledged weakness of its theoretical foundations, the Brunauer–Emmett–Teller (BET) method still remains the most widely used procedure for the determination of surface area; similarly, methods based on the Kelvin equation are still generally applied for the computation of mesopore size distribution from gas adsorption data. However, the more recent studies, especially those carried out on well defined surfaces, have led to a clearer understanding of the scope and limitations of these methods; furthermore, the growing awareness of the importance of molecular sieve carbons and zeolites has generated considerable interest in the properties of microporous solids and the mechanism of micropore filling.

The incorporation of the new material without any increase in the overall length of the book has been achieved in part by extensive re-writing, with the compression of earlier material, and in part by restricting the scope to the physical adsorption of gases (apart from a section on mercury porosimetry). The topics of chemisorption and adsorption from solution, both of which were dealt with in some detail in the first edition, have been omitted: chemisorption processes are obviously dependent on the chemical nature of the surface and therefore cannot be relied upon for the determination of the *total* surface area; and methods based on adsorption from solution have not been developed, as was once hoped, into routine procedures for surface area determination. Likewise omitted, on grounds of

space and because of the availability of commercial equipment, are the "experimental notes"; details of the various techniques can be found in the relevant publications referred to in the text. Finally, no attempt has been made to deal in detail with the zeolites. Because of their regularity of structure and the wide range of their catalytic and ion exchange properties, the zeolites constitute a self-contained field of study distinct from that of microporous solids in general.

At the outset, we were faced with the difficult decision whether to use the Ångstrom unit or the nanometre for the dimensions of molecules. After careful consideration, we have come down firmly in favour of the Ångstrom and we believe that this decision will meet with the approval of the majority of our readers. When quoting graphs and tables of data from the literature, we have retained the original units (kcal, Torr, °C, ton in^{-2}, etc.) in the belief that it is more reasonable to state the data in the form used by the original author—except where comparisons are being made between results presented in different units.

The second edition, like the first, is addressed to those workers in academic laboratories or industrial laboratories who are not necessarily specialists in the field of gas adsorption, but whose work is concerned either directly or indirectly with the characterization of finely divided or porous solids.

Finally, we have pleasure in expressing our cordial thanks for fruitful discussions, both verbal and written, to Dr. J. M. Haynes, on porosity; to Professor H. F. Stoeckli, on surface forces; to Dr. J. Rouquerol, for giving us the benefit of his extensive experience at the Marseilles school of calorimetry, in clarifying our ideas on the thermodynamics of adsorption; to Dr. A. McLeod for preparing the index; and last, but not least, to Miss Jean Ridge, who with unfailing good humour, has grappled with daunting drafts and well-nigh illegible handwriting and transformed them into polished typescript for the printer.

S. J. GREGG

December, 1981 K. S. W. SING

Preface to the First Edition

In writing the present book our aim has been to give a critical exposition of the use of adsorption data for the evaluation of the surface area and the pore size distribution of finely divided and porous solids. The major part of the book is devoted to the Brunauer–Emmett–Teller (BET) method for the determination of specific surface, and the use of the Kelvin equation for the calculation of pore size distribution; but due attention has also been given to other well known methods for the estimation of surface area from adsorption measurements, viz. those based on adsorption from solution, on heat of immersion, on chemisorption, and on the application of the Gibbs adsorption equation to gaseous adsorption.

It would be difficult to over-estimate the extent to which the BET method has contributed to the development of those branches of physical chemistry such as heterogeneous catalysis, adsorption or particle size estimation, which involve finely divided or porous solids; in all of these fields the "BET surface area" is a household phrase. But it is perhaps the very breadth of its scope which has led to a somewhat uncritical application of the method as a kind of infallible yardstick, and to a lack of appreciation of the nature of its basic assumptions or of the circumstances under which it may, or may not, be expected to yield a reliable result. This is particularly true of those solids which contain very fine pores and give rise to Langmuir-type isotherms, for the BET procedure may then give quite erroneous values for the surface area. If the pores are rather larger—tens to hundreds of Ångstroms in width—the pore size distribution may be calculated from the adsorption isotherm of a vapour with the aid of the Kelvin equation, and within recent years a number of detailed procedures for carrying out the calculation have been put forward; but all too often the limitations on the validity of the results, and the difficulty of interpretation in terms of the actual solid, tend to be insufficiently stressed or even entirely overlooked. And in the time-honoured method for the estimation of surface area from measurements of adsorption from solution, the complications introduced by

the competitive adsorption of the solvent, which are frequently ignored because they are so difficult to allow for, may completely vitiate the results.

We therefore felt it timely to attempt a critical exposition and assessment of the common methods for the evaluation of the surface area and pore size distribution of solids from adsorption measurements. Our main concern has therefore been with the *use* of adsorption data for these purposes rather than with adsorption *per se*; and it is for this reason that our treatment of theoretical matters, whilst sufficiently detailed to bring out the nature of the assumptions underlying the various methods, is not exhaustive; we have not set out to write a text-book or a treatise on adsorption, and our choice of material from the literature has been dictated solely by its seeming suitability for the explanation or illustration of the topic under discussion.

The book is addressed to those workers whether in academic institutions or in industrial laboratories, whose work is concerned, either directly or indirectly, with the surface area or the pore structure of finely divided or porous solids.

In conclusion our cordial thanks are offered to all those authors or publishers who have so readily agreed to our reproduction of diagrams and tables, whose courtesy is acknowledged at the appropriate places in the text. We are indebted to Mr. D. Geoghan for drawing our attention to some of the early history of the subject. We wish to thank the following for information supplied privately: Professor C. H. Amberg, Dr. T. A. Dorling, Dr. C. H. Giles, Professor R. J. Good, Dr. D. F. Klemperer, Dr. R. L. Moss, Dr. F. S. Stone and Dr. L. Whalley. We are grateful also to Professor A. V. Kiselev for valuable discussions. Last, but not least, we should like to pay tribute to the forbearance of our wives, who have cheerfully put up with our preoccupation during innumerable week-ends.

S. J. GREGG

March, 1967 K. S. W. SING

Contents

1

Introduction

1.1 Historical

It has long been known that a porous solid can take up relatively large volumes of condensable gas. Already in 1777 Fontana[1] had noted that freshly calcined charcoal, cooled under mercury, was able to take up several times its own volume of various gases; and in the same year Scheele[2] records that "air" expelled from charcoal on heating is taken up again on cooling. He describes the effect in the following words: "I filled a retort half full with very dry pounded charcoal and tied it to a bladder emptied of air. As soon as the retort became red-hot at the bottom, the bladder would no longer expand. I left the retort to cool, and the air returned from the bladder into the coals. I again heated the retort, and the air was again expelled; and when it was cooled, the air was again absorbed by the coals. This air filled eight times the space occupied by the coals."

It was soon realized that the volume taken up varies from one charcoal to another and from one gas to another. In suggesting that the efficiency of the solid depended on the area of exposed surface, de Saussure[3] in 1814 anticipated our present-day views on the subject. Mitscherlich[4] in 1843, on the other hand, emphasized the role of the pores in charcoal, and estimated their average diameter to be 1/2400 in; it would seem that carbon dioxide condensed into layers 0·005 mm thick in a form closely resembling liquid carbon dioxide. These two factors, surface area and porosity (or pore volume), are now recognized to play complementary parts in adsorption phenomena, not only in charcoal but in a vast range of other solids. It thus comes about that measurements of adsorption of gases or vapours can be made to yield information as to the surface area and the pore structure of a solid. The following chapters are devoted to a detailed consideration of the ways in which this can be done.

The term *adsorption* appears to have been introduced by Kayser[5] in 1881 to connote the condensation of gases on free surfaces, in contradistinction to

gaseous *absorption* where the molecules of gas penetrate into the mass of the absorbing solid. Adsorption (strictly, physical adsorption) has now been internationally defined as the enrichment (i.e. positive adsorption or simply adsorption) or depletion (i.e. negative adsorption) of one or more components in an interfacial layer.[6] Actually, in 1909, McBain[7] had proposed the term *sorption* to embrace *ad*sorption on the surface, *ab*sorption by penetration into the lattice of the solid, and capillary condensation within the pores. Perhaps for reasons of euphony the term has never enjoyed really wide usage and the designation *adsorption* is frequently employed to denote uptake whether by capillary condensation or by surface adsorption.

1.2 The adsorption isotherm

When a solid such as charcoal is exposed in a closed space to a gas or vapour at some definite pressure, the solid begins to adsorb the gas and (if the solid is suspended, for example, on a spring balance) by an increase in the weight of the solid and a decrease in the pressure of the gas. After a time the pressure becomes constant at the value p, say, and correspondingly the weight ceases to increase any further. The amount of gas thus adsorbed can be calculated from the fall in pressure by application of the gas laws if the volumes of the vessel and of the solid are known; or it can be determined directly as the increase in weight of the solid in the case where the spring balance is used.

In such an experiment the material actually adsorbed by the solid (*the adsorbent*) is termed the *adsorbate*, in contradistinction to the *adsorptive* which is the the general term for the material in the gas phase which is capable of being adsorbed. The adsorption is brought about by the forces acting between the solid and the molecules of the gas. These forces are of two main kinds—physical and chemical—and they give rise to physical (or "van der Waals") adsorption, and chemisorption respectively. The nature of the physical forces will be dealt with in the next section; meanwhile it is convenient to note that they are the same in nature as the van der Waals forces which bring about the condensation of a vapour to the liquid state.

The quantity of gas taken up by a sample of solid is proportional to the mass m of the sample, and it depends also on the temperature T, the pressure p of the vapour, and the nature of both the solid and the gas. If n is the quantity of gas adsorbed expressed in moles per gram of solid,

$$n = f(p, T, \text{gas}, \text{solid}) \tag{1.1}$$

For a given gas adsorbed on a particular solid maintained at a fixed temperature, Equation (1.1) simplies to

$$n = f(p)_{T,\text{gas},\text{solid}} \tag{1.2}$$

If the temperature is below the critical temperature of the gas, the alternative form

$$n = f(p/p^\circ)_{T,\text{gas,solid}} \tag{1.3}$$

is more useful, p° being the saturation vapour pressure of the adsorptive.

Equations (1.2) and (1.3) are expressions of the *adsorption isotherm*, i.e. the relationship, at constant temperature, between the amount of gas adsorbed and the pressure, or relative pressure, respectively.

The quantity of gas adsorbed may of course be expressed in other ways, notably as the mass of gas (usually mg) or the volume of gas reduced to stp (usually cm^3(stp)). Unless immediate convenience dictates otherwise, however, the use of moles (or in some contexts, molecules) is to be preferred. In particular the common but loose expression "volume of gas adsorbed at pressure p" is highly ambiguous.

In the literature of the subject there are recorded tens of thousands of adsorption isotherms, measured on a wide variety of solids. Nevertheless, the majority of those isotherms which result from physical adsorption may conveniently be grouped into five classes—the five types I to V of the classification originally proposed by Brunauer, Deming, Deming and Teller[8] (hereafter BDDT), sometimes referred to as the Brunauer, Emmett and Teller[9] (BET), or simply the Brunauer[10] classification. The essential features of these types are indicated in Fig. 1.1. As will be noted, the isotherms of Type IV and Type V possess a *hysteresis loop*, the lower branch of which represents measurements obtained by progressive addition of gas to the system, and the upper branch by progressive withdrawal; hysteresis effects are liable to appear in isotherms of the other types also. *The stepped isotherm*, appropriately designated Type VI, though relatively rare, is of particular theoretical interest and has therefore been included.

Besides the five classical types there are borderline cases which, as in most classifications, are difficult to assign to one group rather than another. There are indeed a not inconsiderable number of isotherms which are difficult to fit into the classification at all.

1.3 Adsorption forces

As indicated in the previous section, the adsorption of a gas by a solid is the outcome of the forces of attraction between the individual molecules of the gas and the atoms or ions composing the solid. These forces have been studied theoretically over a number of decades, and though impressive advances have been made in recent years these remain more in the nature of refinements than of fundamental changes in the ideas themselves. And since,

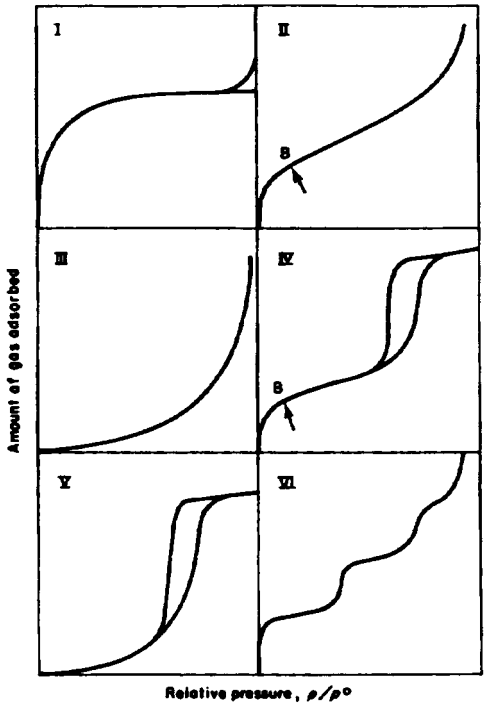

Fig. 1.1 The five types of adsorption isotherm, I to V, in the classification of Brunauer, Deming, Deming and Teller[5] (BDDT), together with Type VI, the stepped isotherm.

perforce, they are based on idealized models, their state of development has not reached the point where it would be possible to calculate the detailed course of an isotherm from known, and independently determined, parameters of the gas and the solid. Even so, they provide a valuable insight into the nature of the adsorption process by making clear the kind of factors involved. The following treatment, although elementary, should be sufficient to enable one to predict, for example, the sense in which adsorption will be affected by an increase in polarizability of the gas molecule or by a change in polarity of the solid.

The forces which bring about adsorption always include "dispersion" forces, which are attractive, together with short-range repulsive forces. In addition, there will be electrostatic (coulombic) forces if either the solid or the gas is polar in nature. *Dispersion forces* derive their name from the close connection between their origin and the cause of optical dispersion. First

characterized by London,[11] these forces arise from the rapid fluctuation in electron density within each atom, which induces an electrical moment in a near neighbour and thus leads to attraction between the two atoms. Making use of quantum-mechanical perturbation theory, London arrived at an expression for the potential energy, $\varepsilon_D(r)$, of two isolated atoms separated by a distance r. As developed by later workers it reads[12]

$$\varepsilon_D(r) = -C_1 r^{-6} - C_2 r^{-8} - C_3 r^{-10} \tag{1.4}$$

which appears to be valid so long as the atoms are not too far apart. The negative sign, of course, implies attraction. The coefficients C_1, C_2, C_3 are the dispersion constants associated with instantaneous dipole–dipole, dipole–quadrupole and quadrupole–quadrupole interactions respectively. Because of the unavoidable uncertainties and approximations inherent in the application of the expression to actual numerical calculations, the terms in r^{-8} and r^{-10}, which are relatively small, are usually omitted. Equation (1.4) thus simplifies to

$$\varepsilon_D(r) = -C_1 r^{-6} \tag{1.5}$$

An expression for the short-range repulsive force (which arises from the interpenetration of the electron clouds of the two atoms) can also be derived from quantum-mechanical considerations[13] as

$$\varepsilon_R(r) = B\exp(-ar) \tag{1.6}$$

where B and a are constants. For mathematical convenience this expression is usually simplified to the form[12]

$$\varepsilon_R(r) = Br^{-m} \tag{1.7}$$

where B is an empirical constant and the index m is usually assigned the value $m = 12$. The total potential energy between the two atoms thus becomes (writing $C_1 = C$)

$$\varepsilon(r) = -Cr^{-6} + Br^{-12} \tag{1.8}$$

which is often designated as the Lennard-Jones potential.[14] The general form of the curve of $\varepsilon(r)$ against r is indicated in Fig. 1.2.

Several relations have been devised for the calculation of the parameter C from the molecular properties of two atoms A and B. One of the best known is that of Kirkwood and Müller:[15]

$$C = \frac{6mc^2\alpha_A\alpha_B}{(\alpha_A/\chi_A) + (\alpha_B/\chi_B)} \tag{1.9}$$

where c is the speed of light, α_A and α_B are the polarizabilities, and χ_A and χ_B

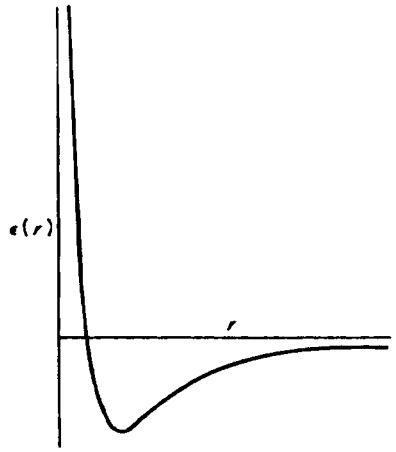

Fig. 1.2 The potential energy $\varepsilon(r)$ of two isolated atoms as a function of the distance r between their centres. The curve for the potential energy $\phi(z)$ of a molecule as a function of its distance z from the surface of a solid is similar in general shape to this curve.

are the magnetic susceptibilities of the atoms A and B. Other expressions are that of London,[11]

$$C = (3/2)\alpha_A\alpha_B h\nu_A^\circ\nu_B^\circ/(\nu_A^\circ + \nu_B^\circ) \tag{1.10}$$

where ν_A° and ν_B° are characteristic frequencies related to optical dispersion (h being the Planck quantum constant); and that of Slater and Kirkwood,[16]

$$C = (3eh/4\pi m^{1/2})\alpha_A\alpha_B/[(\alpha_A N_A)^{1/2} + (\alpha_B N_B)^{1/2}] \tag{1.11}$$

where e and m are the charge and mass of the electron and N_A and N_B are the numbers of electrons per atom of A and B which are involved in the interaction.

To apply these various equations to the adsorption of a gas on a solid, it is necessary to consider[17–20] the interaction of the surface layers of a solid composed of atoms (or ions) of a substance Y, say, with isolated molecules of gas X. The individual interactions of each atom in gas molecule X with each atom of the solid Y have to be added up to obtain the potential $\phi(z)$ of a single molecule of the gas with reference to the solid:

$$\phi(z) = \sum \varepsilon_{ij}(r_{ij}) \tag{1.12}$$

i.e.
$$\phi(z) = -C_{ij}\sum_j r_{ij}^{-6} + B_{ij}\sum_j r_{ij}^{-12} \tag{1.13}$$

Here r_{ij} is the distance between the molecule i in the gas phase (or, for a complex molecule, the centre of its atom i) and the centre of an atom j in the solid. If a particular face of a crystalline solid is being considered, the various values of r_{ij} can be expressed in terms of a single quantity z; here z is the distance between the centre of the gas molecule (or a given atom or group thereof) and the plane through the centres of the atoms in the outermost layer of the solid.

In practice, only a limited number of atoms of the solid need to be considered because of the rapid falling-off of potential with distance, implied by Equation (1.8); moreover, for larger values of r_{ij} the summation process may be replaced by volume integration. With the ready availability of computers, however, it is now possible to sum up all the individual interactions over say 100 to 200 of the nearest pairs, and to confine the integration operation to the remainder.[20]

If the solid is polar—if it consists of ions, or contains polar groups or π-electrons—it will give rise to an electric field[21] which will induce a dipole in the gas molecule X. The resulting interaction energy ϕ_P will be

$$\phi_P = -\tfrac{1}{2}\alpha^2 F \tag{1.14}$$

where F is the field strength at the centre of the molecule and α is the polarizability of the molecule. If, in addition, the molecule possesses a permanent dipole, its interaction with the field will make a further contribution $\phi_{F\mu}$ given by

$$\phi_{F\mu} = -F\mu\cos\theta \tag{1.15}$$

where μ is the dipole moment of the molecule and θ is the angle between the field and the axis of the dipole.

Finally, if the gas molecule possesses a quadrupole moment Q—examples are CO, CO_2 and N_2—this will interact strongly with the field gradient $\dot{F}$ to produce a further contribution ϕ_{FQ} to the energy.[22]

Thus the overall interaction energy $\phi(z)$ of a molecule at distance z from the surface may be represented by the general expression[23,24]

$$\phi(z) = \phi_D + \phi_P + \phi_{F\mu} + \phi_{FQ} + \phi_R \tag{1.16}$$

Here ϕ_D and ϕ_R correspond to the terms in r^{-6} and r^{-12} respectively in Equation (1.8); as already pointed out, these contributions are always present, whereas the electrostatic energies ϕ_P, $\phi_{F\mu}$ and ϕ_{FQ} may or may not be present according to the nature of the adsorbent and the adsorptive. In principle, Equation (1.16) could be used to calculate the numerical value of the interaction potential as a function of the distance z of any given molecule from the surface of a chosen solid. In practice, however, the scope has to be limited to systems composed of a simple type of gas molecule and

an idealized surface of a solid having a relatively simple lattice—such as an inert gas on potassium chloride. Even so, the inevitable uncertainties are such that the final result can be no more than a rough approximation to the actual situation: not only are the various expressions for $\varepsilon(r)$, such as the Lennard-Jones 6–12 relation, themselves approximations, but the distance z has to be defined by recourse to arbitrary assumptions as to the exact location of the surface of the solid. Nevertheless, the *general form* of the curve of $\phi(z)$ against z is not in doubt, and is similar to that for two isolated atoms given in Fig. 1.2. It is useful to note that the interaction potential becomes larger as the solid atoms become smaller relative to the size of a gas atom. This is because the number of solid atoms at a given distance from the gas atom increases when the solid becomes more closely packed.

The potential energy $\phi(z)$ depends not only on the distance z but also on the position of the gas molecule in the xy plane parallel to the surface of the solid and distant z from it. For any given position, the adsorption energy will be equal to the value of $\phi = \phi_0$ at the minimum of the potential curve (cf. Fig. 1.2), which of course represents the equilibrium position.

A number of calculations of ϕ_0, for a variety of systems, have been carried out over the years. Recently Ricca and his co-workers[25] chose a slightly unusual adsorbent, in the form of solid xenon, together with the inert gases helium, neon and argon as adsorptives. From the theoretical point of view these systems possess the merit of involving dispersion forces only, with no polar contribution, and monatomic adsorbates. Both the (100) and the (111) face of solid xenon were considered. The results for helium on these two faces are given, in the form of contour maps (with lines spaced at intervals of potential), in Fig. 1.3. Locations of particular interest are the centre of an array of nearest neighbours (S), the saddle point (P) midway between adjacent xenon atoms, and the position A immediately over a xenon atom. Corresponding values of ϕ_0 appear in Table 1.1 along with those for the other gases. Noteworthy features are: the most favourable site (maximal interaction) is at position S at the centre of an array of Xe atoms; the energy increases steadily with atomic number of the adsorptive (cf. Equation (1.11)); and for a given adsorptive the value of ϕ_0 varies considerably from point to point on the surface.

A study of Table 1.1 reveals interesting features as to the mobility of the adsorbed atoms. Thus, for an argon atom on the (100) face, the easiest path from one preferred site S to the next is over the saddle point P, so that the energy barrier which must be surmounted is $(1251 - 855)$ or 396×10^{-23} J/molecule. Since the mean thermal energy $\sim kT$ at 78 K is only 108 J/molecule, the argon molecule will have severely limited mobility at this temperature and will spend nearly all of its time in the close vicinity of site S: its adsorption will be *localized*. On the other hand, for helium on the

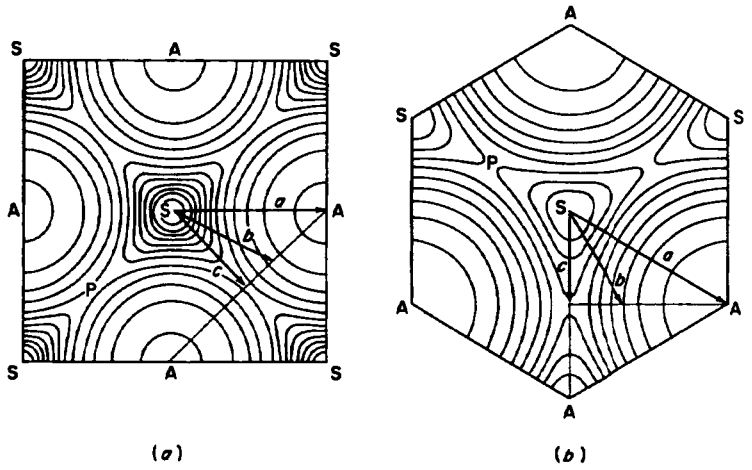

Fig. 1.3 (*a*) Isopotential curves for the adsorption of He on the (100) face of solid Xe. The interval between the isopotential lines is $1{\cdot}24 \times 10^{-22}$ J. (*b*) Isopotential curves for the adsorption of He on the (III) face of solid Xe. The interval between the isopotential lines is $1{\cdot}66 \times 10^{-22}$ J. (After Ricca[25])

TABLE 1.1

Potential energy ϕ_0 for atoms of He, Ne, and Ar adsorbed on the (100) and (111) faces of crystalline Xe.†

Adsorbed atom	Values of $-\phi_0/10^{-23}$ J/molecule (rounded to the nearest unit)					
	Position on (100) face‡			Position on (111) face‡		
	S	P	A	S	A	P
He	340	209	135	271	234	147
Ne	641	404	268	518	453	291
Ar	1251	855	608	1072	971	677

† After Ricca, Pisani and Garrone.[25]

‡ S: The centre of a square ((100) face) or triangular ((111) face) array of surface atoms of Xe.

P: Between adjacent atoms of Xe ("saddle point").

A: Directly over a surface atom of Xe.

same face the energy barrier is only 131×10^{-23} J/molecule, so that its degree of localization will be low and the adsorbed molecules will enjoy almost completely free mobility on the surface.[17]

Calculations of a similar kind, carried out by Stoeckli and Stoeckli-Evans[26] for argon on rhombic sulphur likewise reveal a marked difference in the patterns of energy distribution of sites, as between the (011) and the (111) faces of the sulphur.

An important class of adsorbents, which unlike xenon are solid at room temperature and are therefore more commonly encountered in practice, are ionic crystals. They are, however, rather more complex, not only on account of the presence of more than one type of atom (ion) but also because electrostatic forces are involved alongside the dispersion forces. To avoid the further complications arising from different possible orientations of the molecule relative to the surface, most workers have again chosen an inert gas as adsorptive. A number of studies have been made along these lines.[27-31] Recently, for example, House and Jaycock[32] have made very detailed calculations, involving lattice summations over 3000 nearest atoms of the solid, for the adsorption of He, Ne, Ar, Kr and Xe on the (100) face of NaCl and also of Ar on the (100) face of KCl; electrostatic contributions were also taken into account. From the resultant contour maps for the overall interaction energy ϕ_0, it is found that the energy barrier to translational movement along the surface is 3·81 kJ mol^{-1} for Xe on NaCl, but only 0·53 kJ mol^{-1} for Ar on KCl. Thus the adsorption of xenon on NaCl at 60 K, where RT is 0·50 kJ mol^{-1}, should be localized (this has been confirmed by low-energy electron diffraction) but that of Ar on NaCl at the same temperature should be non-localized.

From these various examples, it is clear that the adsorption energy ϕ_0 for a given kind of site can vary quite markedly from one crystal face of the adsorbent to another. For argon on solid xenon (Table 1.1), for example, the most favourable site has a ϕ_0-value of -1251×10^{-23} J on the (100) face but only -1072 on the (111) face. Such differences are in no way surprising, and they have been found also with ionic crystals.

Multilayers

The molecules in an adsorbed layer interact not only with the solid, but also with their neighbours within the layer. The effect is negligible when the fractional coverage θ of the surface is small and the adsorbed molecules are therefore far apart, but it becomes increasingly significant as the monolayer becomes more and more crowded. A densely occupied monolayer will act in some degree as an extension of the solid, and will be able to attract further molecules from the gas phase in the manner already described, though more

feebly. The result will be that at higher relative pressures an adsorbed layer several molecules thick—a multilayer—is built up.

Specific and non-specific adsorption[23,33]

The effect of polarity in enhancing the energy of interaction has been discussed by Kiselev and his associates[33-35] who distinguish between "non-specific" adsorption, where only dispersion and repulsive forces are involved (ϕ_D and ϕ_R) and "specific" adsorption, where coulombic contributions (some or all of ϕ_F, $\phi_{F\mu}$ and ϕ_{FQ}) are present in addition.

Adsorbents are divided into three classes, containing:

(I) No ions or positive groups (e.g. graphitized carbon).
(II) Concentrated positive charges (e.g. OH groups on hydroxylated oxides).
(III) Concentrated negative charges (e.g. =O, =CO).

Adsorbates are divided into four groups, having:

(a) Spherically symmetrical shells or σ-bonds (e.g. noble gases, saturated hydrocarbons).
(b) π-bonds (e.g. unsaturated, or aromatic, hydrocarbons) or lone pairs of electrons (e.g. ethers, tertiary amines).
(c) Positive charges concentrated on peripheries of molecules.
(d) Functional groups with both electron density and positive charges concentrated as above (e.g. molecules with —OH or =NH groups).

The kinds of interactions resulting from each of the possible adsorbent–adsorbate combinations are summarized in Table 1.2.

TABLE 1.2

Specific and non-specific adsorption[33]

Adsorbate group	Class of adsorbent		
	I	II	III
(a)	n	n	n
(b)	n	n + s	n + s
(c)	n	n + s	n + s
(d)	n	n + s	n + s

s = specific adsorption; n = non-specific adsorption.

The energy of the interactions was evaluated, not by *a priori* calculation, but by equating it to the difference Δq^{st} in the isosteric heats of adsorption (see Section 1.4) between a suitable pair of adsorbates, one member of the pair belonging to group (a) and therefore showing only nonspecific interaction. Thus, on dehydroxylated silica (class I adsorbent) the heats of adsorption of ethane (group (a)) and of ethylene (group (b)) were 17·6 and 15·9 kJ mol^{-1} respectively; but on hydroxylated silica (class II) the corresponding values were 18·4 and 21·8 kJ mol^{-1}, so that the energy of specific interaction of ethylene with the hydroxylated silica was (21·8 − 15·9) or ~5·9 kJ mol^{-1}. Another example was *n*-pentane (group (a) and diethyl ether (group (b)), which on graphitized carbon black gave heats of adsorption of 38·5 and 37·3 kJ mol^{-1}, respectively, whereas on hydroxylated silica (class II) the values were 30·6 and 62·8, respectively, giving an energy of specific interaction of the ether with hydroxylated silica of ~32 kJ mol^{-1}.

Argon and nitrogen constitute a particularly interesting pair of adsorbates in the present context on account of their close similarity in polarizability and molecular size, and therefore in their nonspecific adsorption behaviour. From Table 1.3 it is seen that the heat of adsorption for nitrogen is almost the same as for argon on nonpolar adsorbents such as polypropylene and dehydroxylated silica, but is significantly higher on adsorbents such as alumina or hydroxylated silica which can interact with the quadrupole of nitrogen.[23,36]

TABLE 1.3

Isosteric heat of adsorption (at half coverage) q^{st} of nitrogen and argon†

	q^{st}/(kJ mol^{-1})		Specific contribution for nitrogen q^{st}/(kJ mol^{-1})
	Argon	Nitrogen	
Graphitized carbon black	11·3, 11·7	10·9, 11·3, 11·7	~0
Bone mineral	10·9	15·5	4·6
γ-alumina	8·4	11·3	2·9
Hydroxylated silica	8·8, 10·1	11·7, 13·4	3·4
Dehydroxylated silica	8·8	9·2	~0
Polypropylene	6·7	7·1	~0

† Reduced from the table of Sing and Ramakrishna.[36]

1.4 Thermodynamics of adsorption

It has long been known that the adsorption of a gas on a solid surface is always accompanied by the evolution of heat. Various attempts have been made to arrive at a satisfactory thermodynamic analysis of heat of adsorption data, and within the past few years broad agreement has been achieved in setting up a general system of adsorption thermodynamics. Here we are not concerned with the derivation of the various thermodynamic functions but only with the more relevant definitions and the principles involved in the thermodynamic analysis of adsorption data. For more detailed treatments, appropriate texts should be consulted.[24,37-40]

In dealing with physical adsorption it is usually assumed that the adsorbent is inert, so that the loss or gain of energy is due solely to the change in state of the adsorptive brought about by the addition or removal of the adsorbate. This approach allows us to write

$$\frac{\Delta_a U}{n_a} = u_a - u_g = \Delta_a u \tag{1.17}$$

where $\Delta_a u$ is the *molar integral energy of adsorption* and u_a and u_g represent the molar internal energies of the adsorbed state and the adsorptive, respectively, and n_a is the number of moles adsorbed. The quantity $\Delta_a u$ is dependent on all the adsorbent–adsorbate and adsorbate–adsorbate interactions from zero coverage to the given surface concentration. Thus, u_a is the mean molar internal energy for all the adsorbed molecules in the particular adsorbed state under consideration.

Similarly, one may define the *molar integral enthalpy of adsorption*, $\Delta_a h$ as

$$\Delta_a h = h_a - h_g \tag{1.18}$$

To characterize the state of the adsorbed phase, it is useful to evaluate its molar entropy, s_a, defined as the mean molar value for all the molecules adsorbed over the complete range of surface coverage up to the given amount adsorbed. The *molar integral entropy of adsorption*, Δs_a, is then defined as

$$\Delta_a s = s_a - s_g \tag{1.19}$$

where s_g is the molar entropy of the gaseous adsorptive. Alternatively, the liquid adsorptive may be taken as the standard state; the expression then becomes $(S_a - S_l)$, where S_l is the molar entropy of the liquid adsorptive.

Where a differential amount, dn_a, of adsorptive is transferred to the

surface at constant gas volume, the *differential molar energy of adsorption*† is defined as

$$\Delta_a\dot{u} = \dot{u}_a - u_g \tag{1.20}$$

where the differential molar energy, $\dot{u}_a$, of the adsorbed state is given by

$$\dot{u}_a = \left(\frac{\partial u_a}{\partial n_a}\right)_{T,A} \tag{1.21}$$

Similarly, *the differential molar enthalpy of adsorption*,‡ $\Delta_a\dot{h}$ is defined as

$$\Delta_a\dot{h} = \dot{h}_a - h_g \tag{1.22}$$

where

$$\dot{h}_a = \left(\frac{\partial h_a}{\partial n_a}\right)_{T,p} \tag{1.23}$$

Also, the *differential molar entropy of adsorption*, $\Delta_a\dot{s}$, is defined as

$$\Delta_a\dot{s} = \dot{s}_a - s_g \tag{1.24}$$

where

$$\dot{s}_a = \left(\frac{\partial s_a}{\partial n_a}\right)_{T,A} \tag{1.25}$$

Determination of the energy of adsorption

The term "heat of adsorption" has been defined in a number of different ways. Unfortunately, the initial and final states of the adsorption system and the conditions under which the exchange of heat takes place have not always been adequately defined. As in all applications of thermodynamics, it is essential that the experimental data refer to a system which has reached equilibrium.

In the simplest case, adsorption occurs at constant temperature and volume and we can then write

$$\Delta_a u = -Q_{T,V} \tag{1.26}$$

where $Q_{T,V}$ is the amount of heat *evolved*.

In considering the differential energy of adsorption, it is useful to picture an experimental procedure which allows the adsorption to proceed at constant temperature and in infinitely small stages. Then

$$-\mathrm{d}U = \delta Q + \delta W \tag{1.27}$$

† Recently this quantity has been called the "derivative energy of adsorption".[40]

‡ $\Delta_a\dot{h}$ is alternatively called "derivative enthalpy of adsorption", and $\Delta_a\dot{s}$ "derivative entropy of adsorption".[40]

where δQ is the heat *evolved* and δW the work *performed.* Since the adsorption involves a change in the internal energy of both the adsorbed state and the gas, we have

$$-\left[\left(\frac{\partial u_a}{\partial n_a}\right) \mathrm{d}n_a + \left(\frac{\partial u_g}{\partial n_g}\right) \mathrm{d}n_g\right] = \delta Q + p\,\mathrm{d}V \tag{1.28}$$

where V is the volume of the gas, so that $\delta W = p\,\mathrm{d}V$. Since for a closed system, $\mathrm{d}n_a = -\mathrm{d}n_g$, Equation (1.28) may be written

$$-\Delta_a \dot{u}\,\mathrm{d}n_a = \delta Q + p\,\mathrm{d}V \tag{1.29}$$

where

$$\Delta_a \dot{u} = \left(\frac{\partial u_a}{\partial n_a}\right) - \left(\frac{\partial u_g}{\partial n_g}\right)$$

Now if the gas is perfect, $pV = n_g RT$, so that on differentiation for constant temperature,

$$-p\,\mathrm{d}V = V\,\mathrm{d}p - RT\,\mathrm{d}n_g \tag{1.30}$$

which on substituting into (1.29) gives

$$\Delta_a \dot{u}\,\mathrm{d}n = -\delta Q + V\,\mathrm{d}p + RT\,\mathrm{d}n_a \tag{1.31}$$

or

$$\Delta_a \dot{u} = -\left(\frac{\partial Q}{\partial n_a}\right)_T + V\left(\frac{\partial p}{\partial n_a}\right) + RT \tag{1.32}$$

Thus by measuring the small amount of heat δQ which is evolved when the adsorption increases by the small amount δn_a mole at constant temperature, the differential molar energy of adsorption $\Delta_a \dot{u}$ can be evaluated calorimetrically, e.g. in a Calvet calorimeter.

Now molar enthalpy is defined by the general relation

$$h = u + pV \tag{1.33}$$

but since the volume of the adsorbed phase is very small compared with that of the gas, this may be reduced to

$$h_a = u_a \qquad (\text{and} \quad \dot{h}_a = \dot{u}_a) \tag{1.34}$$

Also, if the gas is perfect,

$$h_g = u_g + RT \tag{1.35}$$

Then, on subtracting (1.35) from (1.34) and using (1.20) and (1.22), Equation (1.32) becomes

$$\Delta_a \dot{h} = \left(\frac{\partial Q}{\partial n_a}\right)_T + V\left(\frac{\partial p}{\partial n_a}\right)_T \tag{1.36}$$

since the temperature is constant.

Finally, from (1.35) and (1.36)

$$\Delta_a \dot{u} - \Delta_a \dot{h} = RT \tag{1.37}$$

The isosteric enthalpy (or isosteric heat) of adsorption

The chemical potential μ_a of the adsorbate may be defined, following standard practice, in terms of the Gibbs free energy, the Helmholtz energy, or the internal energy (U_a). Adopting the last of these, we may write

$$\mu_a = \left(\frac{\partial U_a}{\partial n_a}\right)_{s, V, n_s} \tag{1.38}$$

the conditions being those of constant entropy, volume and amount of adsorbent (n_s).

When the adsorbate is in equilibrium with the gas, we have

$$\mu_a = \mu_g \tag{1.39}$$

and

$$\mathrm{d}\mu_a = \mathrm{d}\mu_g \tag{1.40}$$

where μ_g is the chemical potential of the gas. For the gas, $\mathrm{d}\mu_g$ is given by the well known expression

$$\mathrm{d}\mu_g = -s_g \,\mathrm{d}T + V_g \,\mathrm{d}p \tag{1.41}$$

For the adsorbed state, the corresponding expression is

$$\mathrm{d}\mu_a = -\dot{s}_a \,\mathrm{d}T + \dot{V}_a \,\mathrm{d}p + \left(\frac{\partial \mu_a}{\partial n_a}\right)_{T,p} \mathrm{d}n_a \tag{1.42}$$

which may be obtained by extending the standard methods of solution thermodynamics.

At constant n_a, and in view of (1.40), Equations (1.41) and (1.42) together give

$$(s_g - \dot{s}_a)\,\mathrm{d}T = (V_g - \dot{V}_a)\,\mathrm{d}p \tag{1.43}$$

i.e.

$$(\mathrm{d}p/\mathrm{d}T)_{n_a} = (s_g - \dot{s}_a)/(V_g - \dot{V}_a) \tag{1.44}$$

or noting that $V_g \gg \dot{V}_a$, and putting $V_g = RT/p$,

$$\left(\frac{\partial \ln p}{\partial T}\right)_{a_s} = (s_g - \dot{s}_a)RT \qquad (1.45)$$
$$= -\Delta_a \dot{s}/RT$$

Since at equilibrium

$$\Delta_a \dot{h} = T\Delta_a \dot{s} \qquad (1.46)$$

we have

$$\left(\frac{\partial \ln p}{\partial T}\right)_{n_a} = -\frac{\Delta_a \dot{h}}{RT^2} \qquad (1.47)$$

Now $\Delta_a \dot{h}$. the differential molar enthalpy of adsorption, is often termed the *isosteric enthalpy of adsorption* (or alternatively the *isosteric heat of adsorption*) and is given the opposite sign. Thus

$$\left(\frac{\partial \ln p}{\partial T}\right)_{n_a} = \frac{q^{st}}{RT^2} \qquad (1.48)$$

q^{st} being positive when adsorption occurs, and heat is therefore evolved.

The equation, when integrated, allows one to calculate q^{st} from adsorption isotherms obtained experimentally at two or more temperatures, provided the range of temperature is small enough to justify the assumption that q^{st} is independent of temperature. If isotherms are available for only two temperatures, the value of q^{st} is given by the expression

$$q^{st} = \frac{RT_1T_2}{T_2 - T_1}(\ln p_2 - \ln p_1)_{n_a} \qquad (1.49)$$

where p_1 and p_2 are the equilibrium pressures at temperatures T_1 and T_2 respectively, when the amount adsorbed is n_a.

If isotherms at several temperatures are available, the appropriate form is

$$(\ln p)_{n_a} = -\frac{q^{st}}{RT} + \text{constant} \qquad (1.50)$$

This equation, which represents an *adsorption isostere*—the relation between p and T for a given amount adsorbed—can be plotted from the isotherms for a series of temperatures. The value of q^{st} is then immediately calculable from the slope of the isosteric plot.

If, as is often the case, the *net heat of adsorption* ($q^{st} - q_L$), rather than q^{st} itself, is required, it is only necessary to substitute p/p° for p in Equation (1.49) or (1.50). (q_L = molar heat of condensation; sign convention the same as for q^{st}).

It should be emphasized that the value of q^{st} resulting from use of (1.49) or (1.50) applies to a particular value of n_a. Because of the joint effects of the energetic non-uniformity of the adsorbent surface and the interaction of adsorbate molecules in the adsorbed film itself, the heat of adsorption in general varies significantly with the amount adsorbed. It is therefore essential to repeat the calculation of q^{st} for a succession of values of n_a and thereby obtain the curve of q^{st} against n_a.

1.5 Real solids

In Section 1.3 it was noted that the energy of adsorption even for a perfect crystal differs from one face to another. An actual specimen of solid will tend to be microcrystalline, and the proportion of the various faces exposed will depend not only on the lattice itself but also on the crystal habit; this may well vary amongst the crystallites, since it is highly sensitive to the conditions prevailing during the preparation of the specimen. Thus the overall behaviour of the solid as an adsorbent will be determined not only by its chemical nature but also by the way in which it was prepared.

However, not only are two or more different crystal faces exposed in the samples of solids encountered in practice, but the surfaces of the faces themselves deviate widely from the idealized models of Section 1.3. The surface of a real solid is liable to contain various kinds of imperfection, which include cleavage steps, dislocations and point defects. A *cleavage step* is illustrated diagrammatically in Fig. 1.4. The step heights such as h_1 and h_2 may vary from one to tens or even to hundreds of atomic diameters. Their existence has been directly demonstrated by the electron microscope and indirectly by the method of multiple-beam interferometry devised by Tolansky.[41] A *dislocation* is essentially a region of misfit, on an atomic scale, within the crystal; two of the most important kinds are edge dislocations and screw dislocations. The nature of the former may perhaps be better appreciated from its two-dimensional analogue in Fig. 1.5, which

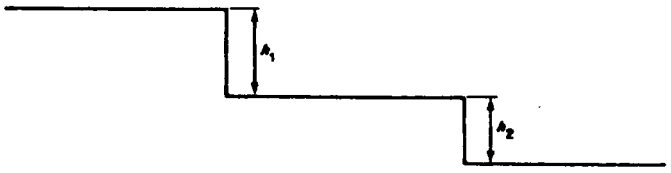

Fig. 1.4 Diagrammatic representation of a cleavage step on the surface of a solid.

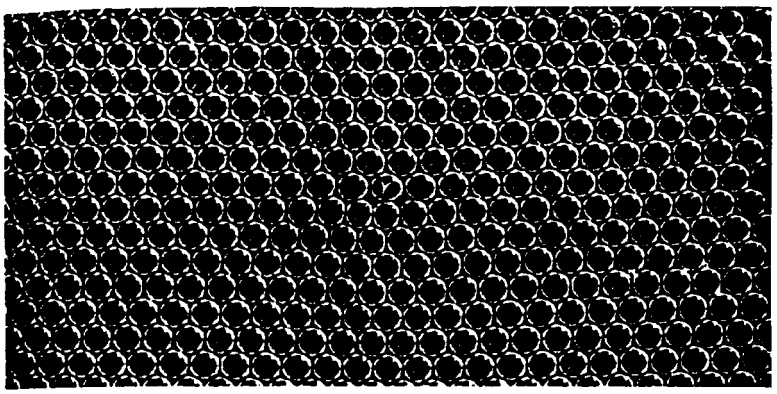

Fig. 1.5 A bubble raft illustrating the nature of a dislocation. The region of misfit near Y can be seen. (After Bragg and Nye[42])

is a photograph of a "bubble raft":[42] bubbles of uniform size represent atoms or ions, and the region of misfit near Y is clear. Finally, a *point defect* may be a vacancy where one or more ions is or are missing completely (cf. Fig. 1.6(*a*)); or an *interstitial* (cf. Fig. 1.6(*b*)), which is an ion, usually a cation, in an interstitial position rather than in a normal lattice site; or lastly, an *impurity defect*, where an ion of the substance proper is substituted by a foreign ion. *Lattice strain* may also be present, and is said to exist when a considerable proportion of the lattice ions do not occupy their equilibrium positions; strain probably consists, in essence, of a high concentration of dislocations and defects.

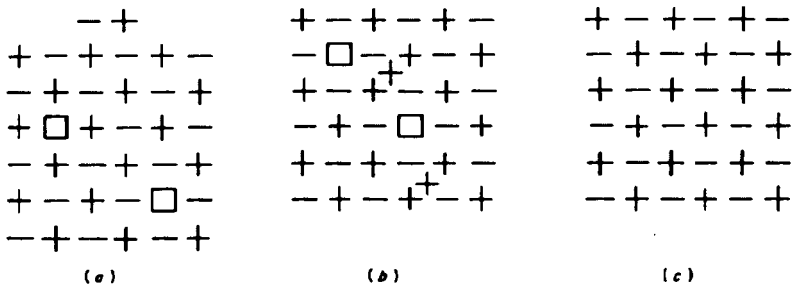

Fig. 1.6 Point defects: (*a*) vacancies (Schottky defects); (*b*) interstitials (Frenkel defects); (*c*) ideal crystal.

The presence of imperfections inevitably produces energetic heterogeneity of the surface, so that the potential curve will no longer show a simple periodicity when the molecule is moved along an imaginary straight line parallel to the surface.[43] In particular, the value of ϕ_0 varies irregularly from point to point, in a manner which in general defies detailed mathematical description; the curve in Fig. 1.7 represents an imaginary example.

The state of the surface is now best considered in terms of distribution of site energies, each of the minima of the kind indicated in Fig. 1.7 being regarded as an adsorption site. The distribution function is defined as the number of sites for which the interaction potential lies between ϕ_0 and $(\phi_0 + d\phi_0)$, and various forms of this function have been proposed from time to time. One might expect the form of $f(\phi_0)$ to be derivable from measurements of the change in the heat of adsorption with the amount adsorbed. In practice the situation is complicated by the interaction of the adsorbed molecules with each other to an extent depending on their mean distance of separation, and also by the fact that the exact proportion of the different crystal faces exposed is usually unknown. It is rarely possible, therefore, to formulate the distribution function for a given solid except very approximately.

The number and kind of defects in a given specimen, as well as the crystal habit and with it the proportion of different crystal faces exposed, will in general depend in considerable degree on the details of preparation. The production of a standard sample of a given chemical substance, having reproducible adsorptive behaviour, remains therefore as much an art as a science.

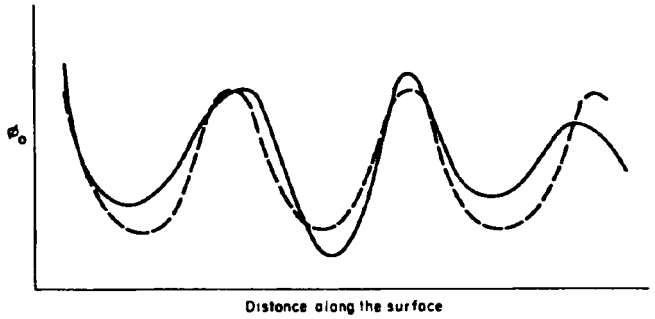

Fig. 1.7 Variation of the value of ϕ_0 as the centre of the adsorbed atom moves along a straight line parallel to the surface of a solid and distant z_0 from it. (——) For a real surface; (- - - -) for an ideal surface.

1.6 Porous and nonporous solids of high surface area

For practical reasons, the application of the adsorption method to the study of surface area and porosity has to be limited to bodies which are either very finely divided or possess an extensive pore system. It is helpful to consider the case of finely divided bodies first.

The surface area of a given mass of solid is inversely related to the size of the constituent particles. Thus, for the idealized case where these are equi-sized cubes of edge length l, the specific surface area A, being the surface area of 1 gram of solid, is given by (cf. p. 26)

$$A = \frac{6}{\rho l} \tag{1.51}$$

where ρ is the density of the solid: if, for example, $\rho = 3\,\mathrm{g\,cm^{-3}}$ and $l = 1\,\mu\mathrm{m}$ the specific surface comes to $2\,\mathrm{m^2\,g^{-1}}$. For actual powders made up of particles of different sizes and irregular shapes the relationship is of course more complicated, but Equation (1.51) still provides a rough guide to the order of magnitude of their specific surfaces.

In practice, the particles of a fine powder—the *primary particles*—will stick together more or less firmly under the action of surface forces to form *secondary particles*. If the junctions between neighbouring particles are weak, the assemblage can be readily broken down again and is termed an *aggregate*. At elevated temperatures, or by application of mechanical pressure, the primary particles become rigidly joined together, and the secondary particles are then called *agglomerates*.†

The voids between the primary particles within a secondary particle, together with those between a secondary particle and its neighbours, constitute a pore system in which the individual pores will tend to be related both in shape and size to the primary or secondary particles as the case may be.[46] Though almost any shape of primary particle is possible in principle, two particular shapes frequently turn up in practice: the sphere and the plate. The primary particles of silica gel, for example, if suitably prepared are approximately spherical and of the same size; ferric oxide and alumina gels, again if suitably prepared, are composed of plate-like particles. The walls of the pores in the aggregate or agglomerate will be made up of the surface of spheres in the first case (Fig. 1.8) and will be planar in the second (Fig. 1.9). The detailed shapes of the pores will of course depend on the size distribution of the constituent particles and on their mode of packing. With

† These definitions of *aggregate* and *agglomerate* are those recommended by the British Standards Institution,[44] which, however, are not universally followed. Rather different definitions are encountered in some fields, especially in pigment technology (cf. Sappok and Honigman.[45])

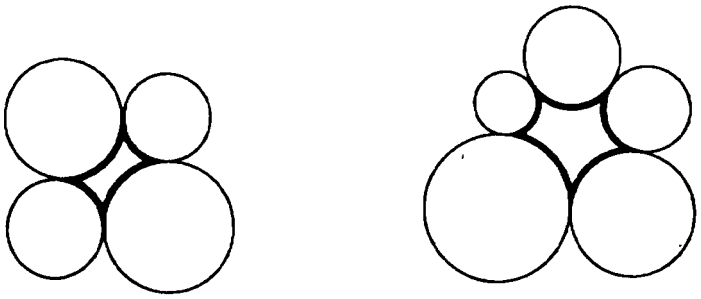

Fig. 1.8 Pores in aggregates composed of spherical particles.

Fig. 1.9 Pores in an aggregate composed of plate-like particles.

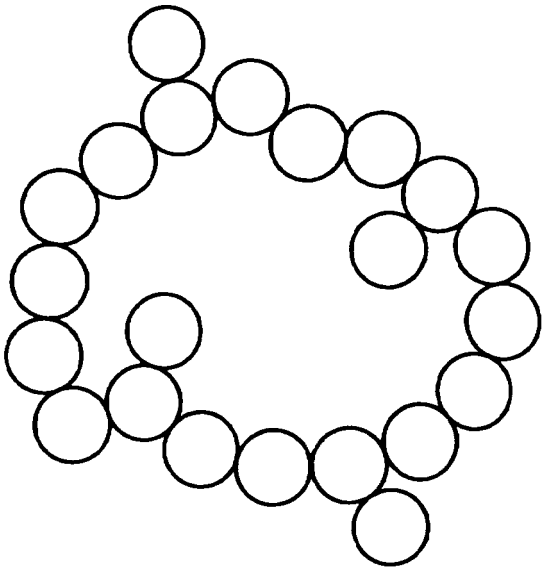

Fig. 1.10 An aggregate of spherical particles, having a very open structure.

plates, wedge-shaped pores will tend to appear, and in favourable circumstances, slits may be formed having sides which are nearly or quite parallel (Fig. 1.9). With spheres, the closeness of packing is conveniently expressed through the coordination number N, which is the average number of neighbours in immediate contact with a given particle: in the ideal case where all the spheres are equal in size, N has the value 12 for hexagonal close packing, 4 for tetrahedal packing, and may fall as low as 2 in a very open structure (Fig. 1.10).

1.7 External and internal surface

In discussions of the surface properties of solids having a large specific surface, it is convenient to distinguish between the *external* and the *internal* surface. The walls of pores such as those denoted by heavy lines in Fig. 1.8 and 1.11 clearly comprise an internal surface and equally obviously the surface indicated by lightly drawn lines is external in nature. In many cases, however, the distinction is not so clear, for the surfaces of the primary particles themselves suffer from imperfections in the forms of cracks and fissures; those that penetrate deeply into the interior will contribute to the internal surface, whereas the superficial cracks and indentations will make up part of the external surface. The line of demarcation between the two kinds of surface necessarily has to be drawn in an arbitrary way, but the external surface may perhaps be taken to include all the prominences and all of those cracks which are wider than they are deep. The internal surface will

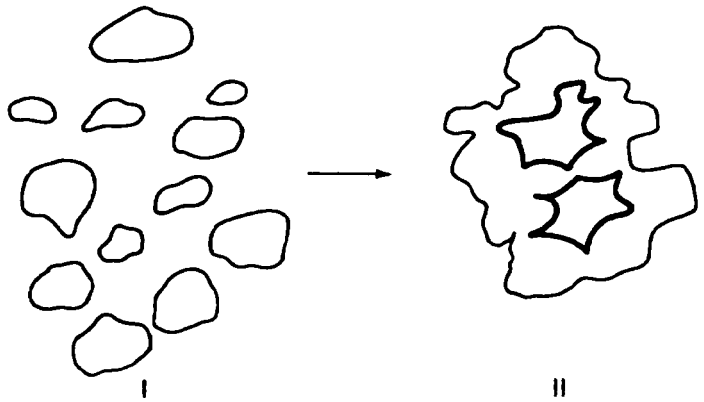

Fig. 1.11 The external surface of the individual particles in I is partially converted into an internal surface (denoted by heavy lines) when the agglomerate in II is formed.

then comprise the walls of all cracks, pores and cavities which are deeper than they are wide. Despite its arbitrariness the distinction between an external and an internal surface is useful in practice; a wide range of porous solids have an internal surface greater by several orders of magnitude than the external surface, the total surface of the solid thus being predominantly internal. Porous solids of this kind include not only those formed by the coming together of primary particles in the manner already indicated, but also solids in which the pore system, and with it a large internal surface, has been produced by the removal of part of a parent solid. The formation of an active solid by this subtraction process can come about in a number of different ways. The parent solid may, for example, have a composite structure, whence one component may be removed by preferential dissolution or evaporation, as in the preparation of Raney nickel by treatment of a nickel–aluminium alloy with caustic soda to remove the aluminium. The controlled burning of partially graphitized carbon provides an instance of production of pores by chemical means: the combustion takes place along channels which become progressively longer and wider. Another way in which a pore system can be produced is by a thermal decomposition of the type

$$\text{solid A} \rightarrow \text{solid B} + \text{gas}$$

exemplified by the production of lime by calcination of chalk or limestone, where the loss of volatile component leads to the development of a pore system with its associated surface area. It should be noted that the term internal surface is usually restricted in its application to those cavities which have an opening to the exterior of the grains, that is it does not include the walls of sealed-off pores.

An interesting example of a large specific surface which is wholly *external* in nature is provided by a dispersed aerosol composed of fine particles free of cracks and fissures. As soon as the aerosol settles out, of course, its particles come into contact with one another and form aggregates; but if the particles are spherical, more particularly if the material is hard, the particle-to-particle contacts will be very small in area; the interparticulate junctions will then be so weak that many of them will become broken apart during mechanical handling, or be prized open by the film of adsorbate during an adsorption experiment. In favourable cases the flocculated specimen may have so open a structure that it behaves, as far as its adsorptive properties are concerned, as a completely non-porous material. Solids of this kind are of importance because of their relevance to standard adsorption isotherms (cf. Section 2.12) which play a fundamental role in procedures for the evaluation of specific surface area and pore size distribution by adsorption methods.

1.8 Classification of pore sizes: micropores, mesopores and macropores

The pore systems of solids are of many different kinds. The individual pores may vary greatly both in size and in shape within a given solid, and between one solid and another. A feature of especial interest for many purposes is the *width* w of the pores, e.g. the diameter of a cylindrical pore, or the distance between the sides of a slit-shaped pore. A convenient classification of pores according to their average width originally proposed by Dubinin[47] and now officially adopted by the International Union of Pure and Applied Chemistry[6] is summarized in Table 1.4.

The basis of the classification is that each of the size ranges corresponds to characteristic adsorption effects as manifested in the isotherm. In *micropores*, the interaction potential is significantly higher than in wider pores owing to the proximity of the walls, and the amount adsorbed (at a given relative pressure) is correspondingly enhanced. In *mesopores*, capillary condensation, with its characteristic hysteresis loop, takes place. In the *macropore* range the pores are so wide that it is virtually impossible to map out the isotherm in detail because the relative pressures are so close to unity.

The borderlines between the different classes are not hard and fast, depending as they do both on the shape of the pores and on the nature (especially the polarizability) of the adsorptive molecule. Thus, the highest value of w (and therefore of p/p°) at which the enhancement of adsorption occurs, i.e. the upper limit of the micropore range, will vary from one adsorptive to another (cf. Chapter 4).

It frequently happens that the micropore effect, the enhancement of interaction potential and the resultant adsorption, ceases to appear when the value of w (and the corresponding relative pressure) is still below the beginning of the hysteresis loop. Within recent years, the micropore range

TABLE 1.4

Classification of pores according to their width w†

	Width
Micropores	Less than ~20 Å (2 nm)§
Mesopores‡	Between ~20 and ~500 Å (2 and 50 nm)
Macropores	More than ~500 Å (50 nm)

† After ref. 6.

‡ This replaces the earlier terms "intermediate pores" and "transitional pores".

§ 1 Å = 10^{-10} m = 10 nm.

has therefore been subdivided into the very narrow pores or *ultramicropores*,[48] where the enhancement effect is found, and *supermicropores*,[49] which fill the gap between the ultramicropore and the mesopore ranges. These features are discussed more fully in Chapter 4 which is devoted to micropores. Mesopores comprise the subject matter of Chapter 3.

It is perhaps worth emphasizing that, amongst solids as a whole, a wide and continuous range of pore sizes is to be found, from macropores through mesopores and micropores, to sub-atomic "pores" in the form of cleavage planes, dislocations and point defects. The analogy with the continuum of electromagnetic wave lengths in the spectrum would seem particularly apt: it serves as a reminder of the danger of unconsciously assuming that nature arranges the pore sizes in solids so as to suit the particular scientific instruments and methods that happen to have been devised so far.

1.9 Particle size distributions[50-55]

This section is devoted to the relationship between the specific surface of particulate solids and some parameter or parameters which characterize the particle size. Attention will be restricted to particles of simple shapes, but non-uniformity of particle size will be considered.

Let us take first the ideal case in which a centimetre cube of material is fragmented into equal-sized cubes of edge length l. Then the area of each will be $6l^2$ and their number will be $1/l^3$. The total area is thus $(1/l^3)6l^2$, or $6/l$; and if the density of the solid is ρ, then the specific surface A must be

$$A = \frac{6}{\rho l} \tag{1.51}$$

and is therefore inversely proportional to the particle size l.

This ideal case is rarely if ever encountered in practice; in general there will be a distribution of particle sizes rather than a single size, and in addition there will usually be a range of particle shapes, many of them highly irregular.

It will be convenient to deal first with the distribution aspect of the problem. One of the clearest ways in which to represent the distribution of sizes is by means of a *histogram*. Suppose that the diameters of 500 small spherical particles, forming a random sample of a powder, have been measured and that they range from 2·7 to 5·3 μm. Let the range be divided into thirteen class intervals 2·7 to 2·9 μm, 2·9 to 3·1 μm, etc., and the number of particles within each class noted (Table 1.5). A histogram may then be drawn in which the number of particles with diameters within any given range is plotted as if they all had the diameter of the middle of the

TABLE 1.5

Frequency distribution of particle size†

Particle size (μm)	2·8	3·0	3·2	3·4	3·6	3·8	4·0
Number of particles	4	15	20	47	63	78	88
Particle size (μm)	4·2	4·4	4·6	4·8	5·0	5·2	
Number of particles	69	59	35	10	8	4	Total = 500

† After Herdan.[51]

range. For example (Fig. 1.12), the four particles with diameters lying between 2·7 and 2·9 μm are regarded as having the diameter 2·8 μm, the fifteen particles with diameters between 2·9 and 3·1 μm are similarly regarded as having the diameter 3·0 μm and so on.

Attempts have been made to devise mathematical functions to represent the distributions that are found experimentally. The mathematical treatment is necessarily based on the assumption that the number of particles in the sample is large enough for statistical considerations to be applicable. With the 500-member sample of the previous section one could not expect any more than approximate agreement between mathematical prediction and experiment.

The only two distributions we shall consider are the Gaussian distribution ("normal law") and the log-normal distribution.

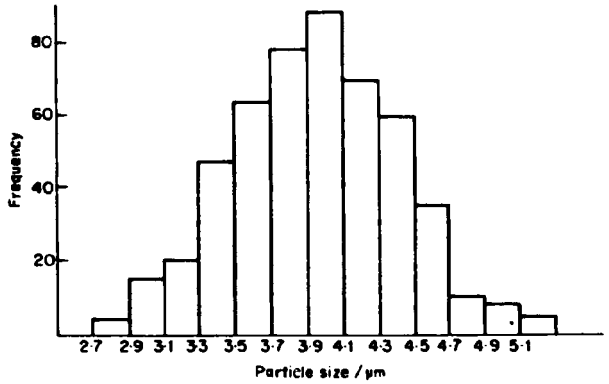

Fig. 1.12 Histogram showing the distribution of particle sizes for the sample of powder referred to in Table 1.5. (After Herdan[51])

The *Gaussian distribution* of particle size is given by

$$y = \frac{1}{\sigma_n\sqrt{2\pi}} \exp[-(l - \bar{l})^2/2\sigma_n^2] \tag{1.52}$$

where y is the probability density, l is the diameter of a given particle, $\bar{l}$ is the arithmetic mean of the diameter of all the particles in the sample; and σ_n is the number standard deviation, given by the expression

$$\sigma_n = \sqrt{\frac{\sum (l - \bar{l})^2 n_i}{N}} \tag{1.53}$$

where N is the total number of particles in the sample; $y\,dl$ then gives the fraction of the particles which have diameters lying between l and $(l + dl)$, and the fraction n_j/N of particles which have diameters between the limits l' and l'', say, is accordingly given by

$$\frac{n_j}{N} = \frac{1}{\sigma_n\sqrt{2\pi}} \int_{l'}^{l''} \exp[-(l - \bar{l})^2/2\sigma_n^2]\,dl \tag{1.54}$$

The plot of y against l gives a curve of the well known bell-shaped form (Fig. 1.13). The sharpness of the peak is determined by the value of σ_n, the peak becoming narrower as the value of σ_n decreases. Curve I of Fig. 1.13, with its sharper peak, corresponds to a more uniform size distribution than does Curve II.

The Gaussian distribution is rare amongst particulate solids, though instances have been found with aerosols and precipitates. Much more

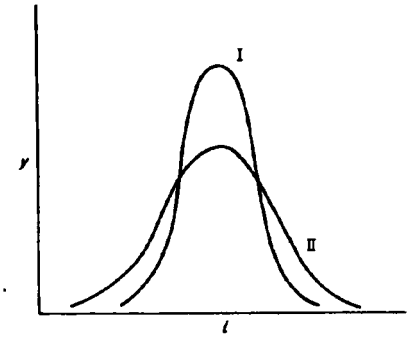

Fig. 1.13 Gaussian particle size distributions. Curve I represents a more uniform size distribution than does curve II.

common is the skewed curve (Fig. 1.14), which conforms to the "log-normal" distribution fairly well. The dispersions produced by milling, grinding or crushing provide good examples.

To obtain the expression for the log-normal distribution it is only necessary to substitute for l and σ in Equation (1.52) the logarithms of these quantities. One thus obtains

$$y = \frac{1}{\ln \sigma_g \sqrt{2\pi}} \exp\left[-\frac{(\ln l - \ln l_g)^2}{2 \ln^2 \sigma_g} \right] \tag{1.55}$$

where l_g is the geometrical mean of l, and $\ln \sigma_g$ is the standard deviation of $\ln l$.

The fraction of particles with lengths between l' and l'' is now given by

$$\frac{n_j}{N} = \frac{1}{\ln \sigma_g \sqrt{2\pi}} \int_{l'/\ln \sigma_g}^{l''/\ln \sigma_g} \exp\left[\frac{-(\ln l - \ln l_g)^2}{2 \ln^2 \sigma_g} \right] \mathrm{d} \ln l \tag{1.56}$$

The log-normal curve is obtained by plotting the frequency against $\ln l$ instead of against l itself (cf. Fig. 1.15).

The distribution curves may be regarded as histograms in which the class intervals (see p. 26) are indefinitely narrow and in which the size distribution follows the normal or log-normal law exactly. The distribution curves constructed from experimental data will deviate more or less widely from the ideal form, partly because the number of particles in the sample is necessarily severely limited, and partly because the postulated distribution

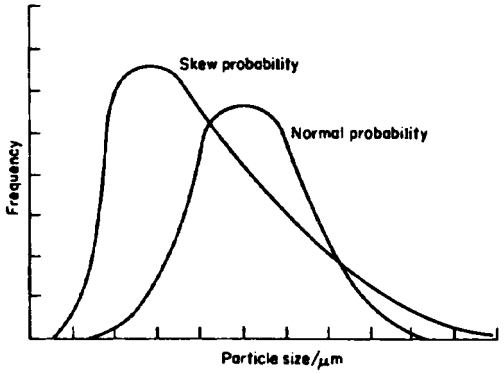

Fig. 1.14 Normal and skew probability functions. (Courtesy DallaValle[60])

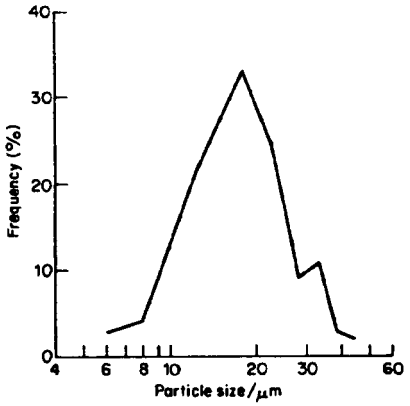

Fig. 1.15 A "log-normal" plot. Note the irregular shape, arising from the smallness of the sample. (Courtesy, DallaValle[60])

law is not obeyed perfectly. These factors account for the irregular shape of the log-normal curve illustrated in Fig. 1.15 which refers to a system in which the number of particles was only 245.

1.10 Relationship between specific surface and particle size

We will now consider the dependence of specific surface on particle size for systems composed of particles of simple shape, and exhibiting a distribution of particle sizes. The shapes chosen will, in the first instance, be cubes and spheres, rods, and plates, and will be dealt with in turn.

Cubes and spheres

Let us imagine that our centimetre cube of solid (density ρ) is broken up into cubes no longer of equal size and that there are n_1 cubes of edge length l_1, n_2 of $l_2, \ldots, n_i$ of length l_i.

The total area is then the sum

$$n_1 . 6l_1^2 + n_2 . 6l_2^2 + \ldots n_i . 6l_i^2$$

i.e.

$$\rho A = 6 \sum (n_i l_i^2) \tag{1.57}$$

and the total volume, which is 1 cm^3, is given by

$$n_1 l_1^3 + n_2 l_2^3 + \ldots n_i l_i^3$$

so that

$$\sum (n_i l_i^3) = 1 \tag{1.58}$$

Division of (1.57) by (1.58) gives the equation

$$\rho A = 6 \frac{\sum n_i l_i^2}{\sum n_i l_i^3} \tag{1.59}$$

To elucidate the role of the particle size distribution it is helpful to express the relationships implied in (1.57) and (1.58) in an alternative manner. Let $n_1, n_2, \ldots, n_i$ be stated as fractions $v_1, v_2, \ldots, v_i$, of the total number N of particles present, i.e. let

$$n_1 = v_1 N, \qquad n_2 = v_2 N, \qquad \ldots, \qquad n_i = v_i N$$

Similarly, let the lengths be expressed in terms of some characteristic length, the most suitable being the most frequently occurring length L (i.e. that corresponding to the maximum in Fig. 1.14). Thus, let

$$l_1 = \lambda_1 L, \qquad l_2 = \lambda_2 L, \qquad \ldots, \qquad l_i = \lambda_i L$$

Equation (1.57) may then be rewritten

$$A\rho = 6 \sum v_i N (\lambda_i L)^2$$

or

$$A\rho = 6NL^2 \sum (v_i \lambda_i^2) \tag{1.60}$$

Correspondingly, (1.58) becomes

$$\sum v_i N (\lambda_i L)^3 = 1$$

or

$$NL^3 \sum (v_i \lambda_i^3) = 1 \tag{1.61}$$

Division of (1.60) by (1.61) gives

$$A\rho = \frac{6}{L} \frac{\sum (v_i \lambda_i^2)}{\sum (v_i \lambda_i^3)} \tag{1.62}$$

or

$$A = \frac{6}{\rho L} \frac{\sum (v_i \lambda_i^2)}{\sum (v_i \lambda_i^3)} \tag{1.63}$$

An exactly similar expression is obtained for spherical particles, where L and λ now refer to the diameters of particles rather than their edge length.

Now the relationship between v and λ is given by the size distribution curve: the value of λ merely represents the lengths of the particles measured in terms of a particular, arbitrary, unit. Thus, if the size distribution curve remains of exactly the same shape during the grinding process, the values of

$\sum(v_i\lambda_i^2)$ and of $\sum(v_i\lambda_i^3)$ will likewise remain constant. Thus, for a given shape of size distribution curve we have that

$$A \propto 1/L\rho$$

or

$$A = f_c/L\rho \tag{1.64}$$

Here f_c is a coefficient which will approach 6 as the quotient $\sum(v_i\lambda_i^2)/\sum(v_i\lambda_i^3)$ approaches unity. The quotient actually attains the value unity when $\lambda_1 = \lambda_2 = \ldots \lambda_i$, i.e. when all the particles are of the same size; this is of course the ideal case discussed at the outset, which led to Equation (1.51).

Rods

We will consider first the case of rods of length l and of square cross-section, the square having sides of length d (Fig. 1.16(*b*)). Let the ratio l:d be denoted by γ i.e.

$$\frac{l}{d} = \gamma \quad \text{or} \quad l = \gamma d$$

We will further assume that γ has the same value for all the particles, no matter what their size, i.e. that all the particles are of the same shape.

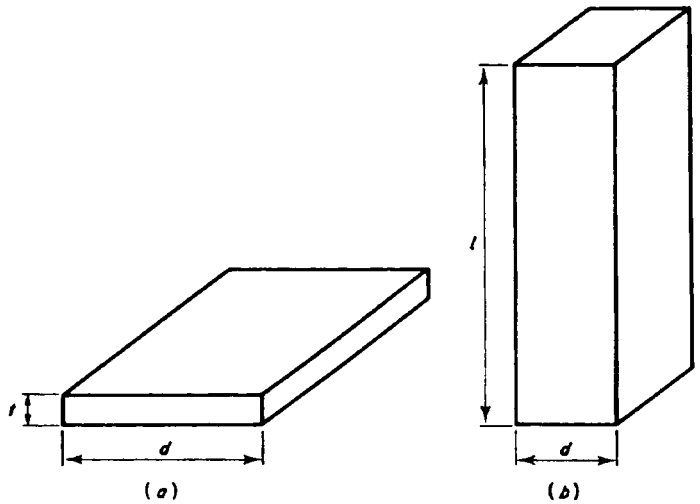

Fig. 1.16 Diagrammatic representation of particles. (*a*) Square plates, of edge length d and thickness t. (*b*) Square rods, of overall length l, with sides of square having length d.

The area of a typical particle is then

$$4d_i l_i + 2d_i^2, \quad \text{or} \quad 2d_i^2(2\gamma + 1)$$

so that the total area of all the particles is given by

$$A\rho = \sum [n_i 2d_i^2(2\gamma + 1)] \tag{1.65}$$

The volume of a typical particle is ld^2, or γd^3, and the total volume of all the particles (which is 1 cm^3) is given by

$$\sum n_i \gamma d_i^3 \tag{1.66}$$

We will now put

$$n_1 = v_1 N, \qquad n_2 = v_2 N, \qquad \ldots, \qquad n_i = v_i N$$

as before, and also

$$d_1 = \delta_1 D, \qquad d_2 = \delta_2 D, \qquad \ldots, \qquad d_i = \delta_i D$$

where D is some characteristic linear dimension, say the most frequently occurring thickness.

Equation (1.65) thus becomes

$$A\rho = 2ND^2(2\gamma + 1) \sum (v_i \delta_i^2) \tag{1.67}$$

and (1.66) becomes

$$ND^3 \gamma \sum (v_i \delta_i^3) = 1 \tag{1.68}$$

Division of (1.67) by (1.68) yields

$$A\rho = \frac{2(2\gamma + 1)}{D\gamma} \cdot \frac{\sum (v_i \delta_i^2)}{\sum (v_i \delta_i^3)} \tag{1.69}$$

or

$$A = \frac{4}{D\rho}\left(1 + \frac{1}{2\gamma}\right) \frac{\sum (v_i \delta_i^2)}{\sum (v_i \delta_i^3)}$$

If the particles are very long and narrow ($\gamma \gg 1$), Equation (1.69) reduces to

$$A = \frac{4}{D\rho} \cdot \frac{\sum (v_i \delta_i^2)}{\sum (v_i \delta_i^3)}. \tag{1.70}$$

Thus for a fixed size distribution curve we have

$$A = f_v / D\rho \tag{1.71}$$

where f_v is a parameter which will approach 4 as the quotient $\sum(v_i\delta_i^2)/\sum(v_i\delta_i^3)$ approaches unity, i.e. as the particles become more and more nearly equal in size.

If the rods are cylindrical in shape with diameter d and length l, exactly similar expressions to (1.69), (1.70) and (1.71) are obtained.

Plates

We will assume that the plates are square, the thickness being t and the length of the side of the square being d (Fig. 1.16(a). The area of a typical plate (its upper and lower faces being borne in mind) is thus

$$2d_i^2 + 4d_it_i$$

or if the ratio of $d:t$ (assumed the same for all particles) is denoted by γ so that $d = \gamma t$ this area is

$$2\gamma^2t_i^2 + 4\gamma t_i^2$$

i.e.

$$2\gamma t_i^2(\gamma + 2)$$

Thus the total area of all the particles is given by

$$A\rho = \sum t_i^2 . 2\gamma(\gamma + 2) \tag{1.72}$$

By an anolagous notation to that used earlier in this section, we can put

$$n_1 = v_1N, \quad n_2 = v_2N, \quad \ldots, \quad n_i = v_iN,$$

and also

$$t_1 = \tau_1T, \quad t_2 = \tau_2T, \quad \ldots, \quad t_i = \tau_iT$$

Equation (1.72) thus becomes

$$A\rho = 2NT^2\gamma(\gamma + 2)\sum(v_i\tau_i^2) \tag{1.73}$$

The volume of a typical particle is

$$d_i^2t_i \quad \text{or} \quad \gamma^2t_i^3$$

so that the total volume of all the particles (again equal to 1 cm^3) is given by

$$\sum v_iN.\gamma^2\tau_i^3T^3 = 1$$

or

$$NT^3\gamma^2\sum(v_i\tau_i^3) = 1 \tag{1.74}$$

Division of (1.73) by (1.74) yields

$$A\rho = \frac{2}{T}\frac{\gamma + 2}{\gamma}\frac{\sum(v_i\tau_i^2)}{\sum(v_i\tau_i^3)} \tag{1.75}$$

or

$$A = \frac{2}{T\rho}\left(1 + \frac{2}{\gamma}\right)\frac{\sum (v_i\tau_i^2)}{\sum (v_i\tau_i^3)} \tag{1.76}$$

If the plates are very thin ($t \ll d$) then γ ($= d/t$) will be large in comparison with 2, and (1.75) will become

$$A = \frac{2}{T\rho}\frac{\sum (v_i\tau_i^2)}{\sum (v_i\tau_i^3)} \tag{1.77}$$

Thus

$$A = f_p/T\rho \tag{1.78}$$

where f_p is a coefficient which approaches the value $f_p = 2$ more closely as the quotient $\sum (v_i\tau_i^2)/\sum (v_i\tau_i^3)$ approaches unity, i.e. as the size distribution becomes more and more uniform.

If the plates are circular with diameter d and thickness t, exactly similar expressions to (1.76), (1.77) and (1.78) are obtained.

From the arguments of the present section it is clear that an inverse relationship holds between the specific surface and the particle size, and if the particles are long or thin it is the *minimum* dimension, the thickness of the plates or of the rods, which mainly determines the magnitude of the specific surface.

So far in this section, the specific surface has been taken as the dependent variable and the particle size as the independent variable. In practice one is often more concerned with the converse case where the specific surface of a disperse solid has been determined directly (by methods which will be explained in the subsequent chapters) and one wishes to calculate a particle size from it.

In the rare event in which the solid is known to be composed of cubes or spheres all of the same size, the problem is simple. Equation (1.51) can be applied and we have

$$l = \frac{6}{\rho A} \tag{1.79}$$

where l is the edge length of the cubes or the diameter of the spheres.

In the even rarer event that the component particles are equal-sized rods of known length and thickness, or equal-sized platelets of known diameter and thickness, one may respectively use Equation (1.71) with $f_v = 4$, or Equation (1.78) with $f_p = 2$, if the rods or plates are very thin.

In all other cases the quantity l calculated from the specific surface is a *mean diameter*. Unless there is some definite and detailed evidence as to particle shape, the simplest such diameter to aim at is the mean diameter $\bar{d}_{vs}$ obtained by substituting the measured value of A in Equation (1.79)

$$\bar{d}_{vs} = \frac{6}{\rho A} \tag{1.80}$$

Comparison of Equations (1.80) and (1.59) shows that

$$\bar{d}_{vs} = \frac{\sum (n_i l_i^3)}{\sum (n_i l_i^2)} \tag{1.81}$$

Since the numerator of the right-hand side of (1.81) has the dimensions of volume and the denominator those of surface area, the quantity $\bar{d}_{vs}$ is termed the *volume–surface mean diameter* of the sample.

Various attempts have been made to allow for particle shapes, through the use of volumes and shape factors.[52,54] From general considerations it is clear that the volume v of the particles from ρ grams of solid will be proportional to $\sum n_i X_i^3$ and the area $A\rho$ proportional to $\sum n_i X_i^2$, i.e.

$$v = \alpha_v \sum (n_i X_i^3) = 1$$

$$A\rho = \alpha_s \sum (n_i X_i^2)$$

where α_v is the volume shape factor and α_s the surface shape factor, and X_i is a linear dimension. Consequently

$$A\rho = \frac{\alpha_s}{\alpha_v} \frac{\sum (n_i X_i^2)}{\sum (n_i X_i^3)} \tag{1.82}$$

The numerical values of α_v and α_s for a particular sample, which will depend on the kind of linear dimension chosen, cannot be calculated *a priori* except in the very simplest of cases. In practice one nearly always has to be satisfied with an approximate estimate of their values. For this purpose X is best taken as the *mean projected diameter*[52] d_p, i.e. the diameter of a circle having the same area as the projected image of the particle, when viewed in a direction normal to the plane of greatest stability; d_p is determined microscopically, and it includes no contributions from the *thickness* of the particle, i.e. from the dimension normal to the plane of greatest stability. For perfect cubes and spheres, the value of the ratio α_s/α_v ($=K$, say) is of course equal to 6. For sand, Fair and Hatch[56] found, with rounded particles 6·1, with worn particles 6·4, and with sharp particles 7·7. For crushed quartz, Cartwright[57] reports values of K ranging from 14 to 18, but since the specific surface was determined by nitrogen adsorption (p. 61) some internal surface was probably included.†

† It may be wondered why the values of α_s/α_v all turn out greater than 6, whereas the factors in Equations (1.69) and (1.65) or (1.69) and (1.77) are less than 6. The reason is that in these equations the dimensions L and T are the minimum dimensions of a particle, whereas, in applying Equation (1.81), X is the mean projected diameter. For a plate-like particle X will not include the thickness T at all, and for a rod-like particle X will be approximately proportional to the geometrical mean of the maximum and the minimum dimensions of the particle.

1.11 The application of adsorption methods

The adsorption of a gas by a solid can, in principle, be made to yield valuable information as to the surface area and pore structure of the solid. In practice the range of suitable adsorptives is quite narrow, by far the most commonly used one being nitrogen at its boiling point, 77 K.

A Type II isotherm indicates that the solid is non-porous, whilst the Type IV isotherm is characteristic of a mesoporous solid. From both types of isotherm it is possible, provided certain complications are absent, to calculate the specific surface of the solid, as is explained in Chapter 2. Indeed, the method most widely used at the present time for the determination of the surface area of finely divided solids is based on the adsorption of nitrogen at its boiling point.[58] From the Type IV isotherm the pore size distribution may also be evaluated, using procedures outlined in Chapter 3.

Type I isotherms, as will be demonstrated in Chapter 4, are characteristic of microporous adsorbents. The detailed interpretation of such isotherms is controversial, but the majority of workers would probably agree that the very concept of the surface area of a microporous solid is of doubtful validity, and that whilst it is possible to obtain an estimate of the total micropore *volume* from a Type I isotherm, only the crudest guesses can be made as to the pore size *distribution*.

Isotherms of Type III and Type V, which are the subject of Chapter 5, seem to be characteristic of systems where the adsorbent–adsorbate interaction is unusually weak, and are much less common than those of the other three types. Type III isotherms are indicative of a non-porous solid, and some halting steps have been taken towards their use for the estimation of specific surface; but Type V isotherms, which betoken the presence of porosity, offer little if any scope at present for the evaluation of either surface area or pore size distribution.

One of the most important uses of specific surface determination is for the estimation of the particles size of finely divided solids; the inverse relationship between these two properties has already been dealt with at some length. The adsorption method is particularly relevant to powders having particle sizes below about 1 μm, where methods based on the optical microscope are inapplicable. If, as is usually the case, the powder has a *range* of particle sizes, the specific surface will lead to a mean particle size directly, whereas in any microscopic method, whether optical or electron-optical, a large number of particles, constituting a representative sample, would have to be examined and the mean size then calculated.

Active solids are widely used as adsorbents of gases and vapours, and the specific surface is the most important parameter for characterizing their

adsorptive behaviour at low and medium relative pressures. The pore size distribution and the total pore volume are more important at the relative pressures of say, 0·3 or 0·4 upwards. Again, the vast majority of contact catalysts are solids of high surface area; their efficiency is determined by the area A' which is actually reached by the reactant molecules under the conditions prevailing during laboratory or industrial operation. The magnitude of A' is related to the specific surface, but the proportion of this latter surface which is actually reached by the reactant molecules will depend upon the ease of transport of the molecules from the exterior of the grains to the various parts of the internal surface, and therefore upon the pore size distribution.

1.12 Some useful definitions

Finally, a number of useful definitions of quantities directly or indirectly involved in the study of the surface area and porosity of both particulate and massive solids are given in Table 1.6.

TABLE 1.6

Some useful definitions[69]

Open pore	Cavity or channel communicating with the surface of the solid.
Closed pore	Cavity not communicating with the surface.
Void	Space or interstice between particles.
True density	Mass of the solid divided by the volume of the solid excluding open and closed pores.
Effective solid density	The density of the solid as determined by a given liquid displacement method.
Porosity	Ratio of the volume of open pores to the total volume of the solid.
Agglomerate†	Assemblage of particles rigidly held together.
Aggregate†	Assemblage of particles which is loosely coherent.

† But see footnote on p. 21.

References

1. F. Fontana, *Memorie Mat. Fis. Soc. Ital Sci.* I, 679 (1777).
2. C. W. Scheele, "Chemical Observations on Air and Fire", 182 (1780).
3. N. T. de Saussure, *Gilbert's Ann.* **47**, 113 (1814).
4. E. Mitscherlich, *Pogg. Ann.* **59**, 94 (1843).
5. H. Kayser, *Wied. Ann.* **14**, 451 (1881).
6. IUPAC Manual of Symbols and Terminology, Appendix 2, Pt. 1, Colloid and Surface Chemistry. *Pure Appl. Chem.* **31**, 578 (1972).
7. J. W. McBain, *Z. Phys. Chem.* **38**, 471 (1909); *Phil. Mag.* **18** (6), 916 (1909).
8. S. Brunauer, L. S. Deming, W. S. Deming and E. Teller, *J. Amer. Chem. Soc.* **62**, 1723 (1940).
9. S. Brunauer, P. H. Emmett and E. Teller, *J. Amer. Chem. Soc.* **60**, 309 (1938).
10. S. Brunauer, "The Adsorption of Gases and Vapours", Oxford University Press (1945).
11. F. London, *Z. Physik* **63**, 245 (1930); *Z. Physik. Chem.* 11, 222 (1930).
12. D. M. Young and A. D. Crowell, "Physical Adsorption of Gases", pp. 9, 18, Butterworths, London (1962).
13. A. A. Abrahamson, *Phys. Rev.* **130**, 693 (1963).
14. J. E. Lennard-Jones, *Physica (Eindhoven)* **4**, 941 (1937).
15. J. G. Kirkwood, *Phys. Zeits.* **33**, 57 (1932); A. Muller, *Proc. Roy. Soc*, **154A**, 624 (1936).
16. J. C. Slater and J. G. Kirkwood, *Phys. Rev.* **37**, 682 (1931).
17. W. A. Steele, "The Interaction of Gases with Solid Surfaces", p. 13, Pergamon Press, Oxford (1974).
18. R. M. Barrer, *Proc. Roy. Soc.* **A161**, 476 (1937).
19. A. D. Crowell and D. M. Young, *Trans. Faraday Soc.* **49**, 1080 (1953).
20. N. N. Avgul and A. V. Kiselev, *Chem. Phys. Carbon* p. 1 (1970).
21. J. H. de Boer, *Advances in Catalysis* **8**, 33, Academic Press, New York and London (1956).
22. L. E. Drain and J. L. Morrison, *Trans. Faraday Soc.* **49**, 654 (1953).
23. R. M. Barrer, *J. Colloid Interface Sci.* **21**, 415 (1966).
24. R. M. Barrer, "Zeolites and Clay Minerals as Sorbents and Molecular Sieves", p. 174, Academic Press, London and New York (1978).
25. F. Ricca, *Suppl. Nuovo Cimento* **1**, **5**, 339; F. Ricca, C. Pisani and E. Garrone, "Adsorption-Desorption Phenomena, Proc. 2nd. Intern. Conf. 1971, p. 111, Academic Press, London and New York (1972); C. Pisani, F. Ricca and C. Roetti, *J. Phys. Chem.* **77**, 657 (1973).
26. H. Stoeckli-Evans and F. Stoeckli, *Helvetica Chim. Acta* **58**, 194 (1975).
27. W. J. C. Orr, *Trans. Faraday Soc.* **35**, 1247 (1939).
28. J. M. Honig, *Ann. N.Y. Acad. Sci.* **58**, 749 (1954).
29. P. J. Anderson and F. R. Horlock, *Trans. Faraday Soc.* **65**, 251 (1969).
30. P. R. Anderson, *Surface Sci.* **27**, 60 (1971).
31. M. Leard and A. Mellier, *Compt. Rend.* **B272**, 1477 (1971).
32. W. A. House and M. J. Jaycock, *J. Chem. Soc. Faraday Trans. I*, **70**, 1348 (1974).
33. A. V. Kiselev, *Discuss. Faraday Soc.* **40**, 205 (1965).
34. A. V. Kiselev, N. V. Kovaleva and Yu. S. Nikitin, *J. Chromatography* **58**, 19 (1971).

35. G. Curthoys, V. Ya. Davydov, A. V. Kiselev, S. A. Kiselev and B. V. Kuznetsov, *J. Colloid Interface Sci.* **48**, 58 (1974).
36. K. S. W. Sing and V. R. Ramakrishna, Colloques Internationaux de Centre National de la Recherche Scientifique, No. 201, 435 (1971).
37. T. L. Hill, *J. Chem. Phys.* **15**, 767 (1947).
38. D. H. Everett, *Trans. Faraday Soc.* **46**, 453, 942, 957 (1950).
39. C. Létoquart, F. Rouquerol and J. Rouquerol, *J. Chim. Phys.* **70**, 559 (1973).
40. F. Rouquerol, J. Rouquerol and D. H. Everett, *Thermochimica Acta* **41**, 311 (1980).
41. S. Tolansky, "Multiple Beam Interferometry of Surfaces and Films", Oxford University Press, London (1948).
42. W. L. Bragg and J. F. Nye, *Proc. Roy. Soc.* **190A**, 474 (1947).
43. S. Ross and J. P. Olivier, "Physical Adsorption", Interscience, New York (1964).
44. British Standard 2955 (1958): British Standard 4359: Part 2 (1971).
45. R. Sappok and B. Honigmann, *in* "Characterization of Powder Surfaces" (eds. G. D. Parfitt and K. S. W. Sing), p. 239, Academic Press, London and New York (1976).
46. A. P. Karnaukhov, *Kinetika i Kataliz* **8**, 172 (1967) (transl.).
47. M. M. Dubinin, *Zhur. Phys. Chem.* **34**, 959 (1960); *Chem. Rev.* **60**, 235 (1960).
48. S. Brunauer, *in* "Surface Area Determination", Proc. Int. Symp 1969 (eds. D. H. Everett and R. H. Ottewill), p. 90, Butterworths, London (1970).
49. M. M. Dubinin, *in* "Characterisation of Porous Solids", Proc. Int. Symp. 1978 (eds. S. J. Gregg, K. S. W. Sing and H. F. Stoeckli), p. 1, Soc. Chem. Ind., London (1979).
50. C. Orr and J. M. DallaValle, "Fine Particle Measurement", Macmillan, London (1959).
51. G. Herdan, "Small Particle Statistics", Butterworths, London (1960).
52. H. Heywood, Proc. Intern. Symp. on Surface Area Determination. (eds. D. H. Everett and R. H. Ottewill), p. 375, Butterworths, London (1970).
53. H. Heywood, *in* "Particle Size Analysis, 1970" (eds. M. Groves and J. L. Wyatt-Sargent), p. 1, Soc. Analytical Chem., London (1972).
54. "Particle Size Analysis", Proc. Conf. Analytical Div. Chem. Soc. 1977 (ed. M. J. Groves), Heyden, London (1978).
55. T. Allen, "Particle Size Measurement", 2nd ed., Chapman and Hall, London (1975).
56. G. M. Fair and L. P. Hatch, *J. Amer. Waterworks Assoc.* **25**, 1551 (1933).
57. J. Cartwright, *Ann. Occup. Hygiene* **5**, 163 (1962).
58. British Standard 4359, Pt. 1 (1969); draft revision (1981).
59. K. S. W. Sing, *in* "Characterization of Powder Surfaces", (eds. G. D. Parfitt and K. S. W. Sing), p. 3, Academic Press, London and New York (1976).
60. J. M. DallaValle, "Micromeritics", Pitman, New York (1948).

2

The Physical Adsorption of Gases by Nonporous Solids: The Type II Isotherm

2.1 Introduction

The physical adsorption of gases by non-porous solids, in the vast majority of cases, gives rise to a Type II isotherm. From the Type II isotherm of a given gas on a particular solid it is possible in principle to derive a value of the *monolayer capacity* of the solid, which in turn can be used to calculate the specific surface of the solid. The monolayer capacity is defined as the amount of adsorbate which can be accommodated in a completely filled, single molecular layer—a *monolayer*—on the surface of unit mass (1 g) of the solid. It is related to the specific surface area A, the surface area of 1 g of the solid, by the simple equation

$$A = n_m a_m L \tag{2.1}$$

where a_m is the average area occupied by a molecule of adsorbate in the completed monolayer and L is the Avogadro constant, n_m being expressed in moles of adsorbate per gram of adsorbent. If the amount adsorbed is expressed in other units, an appropriate conversion factor is invoked. Thus, with adsorption stated in grams and a_m in Å^2 per molecule the relation becomes

$$A = \frac{x_m}{M} a_m L \times 10^{-20} \tag{2.2}$$

where M is the molecular weight of the adsorbate, x_m is the monolayer capacity in grams of adsorbate per gram of solid and A is the specific surface in square metres per gram.

Alternatively, if the monolayer capacity expressed as the volume of gas

(reduced to stp). is v_m, the specific surface (again in m^2g^{-1}) is given by

$$A = \frac{v_m}{22414} a_m L \times 10^{-20} \tag{2.3}$$

To obtain the monolayer capacity from the isotherm, it is necessary to interpret the (Type II) isotherm in quantitative terms. A number of theories have been advanced for this purpose from time to time, none with complete success. The best known of them, and perhaps the most useful in relation to surface area determination, is that of Brunauer, Emmett and Teller. Though based on a model which is admittedly over-simplified and open to criticism on a number of grounds, the theory leads to an expression—the "BET equation"—which, when applied with discrimination, has proved remarkably successful in evaluating the specific surface from a Type II isotherm.

2.2 The BET model[1]

The BET treatment is based on a kinetic model of the adsorption process put forward more than sixty years ago by Langmuir,[2] in which the surface of the solid was regarded as an array of adsorption sites. A state of dynamic equilibrium was postulated in which the rate at which molecules arriving from the gas phrase and condensing on to bare sites is equal to the rate at which molecules evaporate from occupied sites.

If the fraction of sites occupied is θ_1 and the fraction of bare sites is θ_0 (so that $\theta_0 + \theta_1 = 1$) then the rate of condensation on unit area of surface is $a_1\kappa\theta_0$ where p is the pressure and κ is a constant given by the kinetic theory of gases ($\kappa = \frac{1}{2}L/(MRT)^{1/2}$); a_1 is the condensation coefficient, i.e. the fraction of incident molecules which actually condense on a surface. The evaporation of an adsorbed molecule from the surface is essentially an activated process in which the energy of activation may be equated to the isosteric heat of adsorption q_1. The rate of evaporation from unit area of surface is therefore equal to

$$z_m\theta_1 v_1 \, e^{-q_1/RT}$$

where z_m is the number of sites per unit area (so that $z_m\theta_1$ is the corresponding number of adsorbed molecules) and v_1 is the frequency of oscillation of the molecule in a direction normal to the surface. Thus at equilibrium:

$$a_1\kappa p\theta_0 = z_m\theta_1 v_1 \, e^{-q_1/RT} \tag{2.4}$$

so that, since $\theta_0 = 1 - \theta_1$

$$\theta_1 = \frac{a_1 \kappa p}{a_1 \kappa p + z_m \nu_1 \, e^{-q_1/RT}} \tag{2.5}$$

If n (in moles) is the amount adsorbed on 1 g of adsorbent, then $\theta_1 = n/n_m$, where n_m is the monolayer capacity. Insertion into (2.5) leads to

$$\frac{n}{n_m} = \frac{Bp}{1 + Bp} \tag{2.6}$$

where

$$B = \frac{a_1 \kappa}{z_m \nu_1} e^{q_1/RT} \tag{2.7}$$

Equation (2.6) is the familiar Langmuir equation[2] for the case when adsorption is confined to a monolayer. In practice B is an empirical constant and cannot be evaluated from the relationship in Equation (2.7). The question as to how well the Langmuir equation reproduces experimental isotherms will be dealt with in Chapter 4.

Langmuir[3] referred to the possibility that the evaporation–condensation mechanism could also apply to second and higher molecular layers, but the equation he derived for the isotherm was complex and has been little used. By adopting the Langmuir mechanism but introducing a number of simplifying assumptions; Brunauer, Emmett and Teller[1] in 1938 were able to arrive at their well known equation for multilayer adsorption, which has enjoyed widespread use ever since.

When extended to the second layer, the Langmuir mechanism requires that the rate of condensation of molecules from the gas phase on to molecules already adsorbed in the first layer, shall be equal to the rate of evaporation from the second layer, i.e.

$$a_2 \kappa p \theta_1 = z_m \theta_2 \nu_2 \, e^{-q_2/RT} \tag{2.8}$$

and for the ith layer

$$a_i \kappa p \theta_{i-1} = z_m \theta_i \nu_i \, e^{-q_i/RT} \tag{2.9}$$

The model implies that at any pressure below the saturation vapour pressure, the fractions of the surface covered with 1, 2, ..., i molecules will be $\theta_1, \theta_2, \ldots, \theta_i$ respectively, so that the thickness of the adsorbed layer will not be constant throughout. On the specific surface area A, therefore, the total number Z of molecules adsorbed will be

$$Z = A z_m (\theta_1 + 2\theta_2 + \ldots + i\theta_i) \tag{2.10}$$

so that n, the amount adsorbed in moles, will be given by

$$n = \frac{A z_m}{L} \sum_1^i (i\theta_i) \tag{2.11}$$

Now in principle each layer will have its own values of a, q, and v, and consequently the summation of Equation (2.11) cannot be carried out unless simplifying assumptions are made. Brunauer, Emmett and Teller[1] made three such assumptions: (a) that in all layers except the first the heat of adsorption is equal to the molar heat of condensation q_L; (b) that in all layers except the first the evaporation–condensation conditions are identical, i.e. that

$$v_2 = v_3 = \ldots = v_i \quad \text{and} \quad a_2 = a_3 = \ldots = a_i$$

(c) that when $p = p^\circ$, the adsorptive condenses to a bulk liquid on the surface of the solid, i.e. that the number of layers becomes infinite (p° = saturation vapour pressure). The summation,[4] though straightforward, is somewhat tedious, and little purpose would be served by reproducing the steps here; it leads to the relatively simple equation

$$\frac{n}{n_m} = \frac{c(p/p^\circ)}{(1 - p/p^\circ)(1 + \overline{c-1}\,p/p^\circ)} \tag{2.12}$$

often termed the BET equation. For convenience of plotting it is rewritten as

$$\frac{p/p^\circ}{n(1 - p/p^\circ)} = \frac{1}{n_m c} + \frac{c-1}{n_m c}\frac{p}{p^\circ} \tag{2.13}$$

or, if preferred, as

$$\frac{p}{n(p^\circ - p)} = \frac{1}{n_m c} + \frac{c-1}{n_m c}\frac{p}{p^\circ} \tag{2.14}$$

Strictly, the parameter c is given by

$$c = \frac{a_1 v_2}{a_2 v_1} e^{(q_1 - q_L)/RT} \tag{2.15}$$

but in practice is nearly always taken as

$$c = e^{(q_1 - q_L)/RT} \tag{2.16}$$

where $(q_1 - q_L)$ is the net heat of adsorption (p. 17). The alternative form of (2.16) in which $(q_1 - q_L)$ is the dependent variable is, of course

$$q_1 - q_L = RT \ln c \tag{2.17}$$

The approximate nature of the relationship in Equations (2.16) and (2.17) needs to be emphasized. Not only does the heat of adsorption q_1 in the first layer vary, in general, with the coverage θ_1, but theoretical considerations as well as analysis of experimental data suggest that the factor $a_1 v_2 / a_2 v_1$ ($= m$,

say) may differ significantly from the figure $m = 1$, assumed in simplifying Equation (2.15) to (2.16). A range of m-values from 0·02 to 20 (or even, according to Kemball and Schreiner,[5] from 10^{-5} to 10) is not impossible.

If the number of molecular layers, even at saturation pressure, is restricted to the finite number N (by the walls of a narrow pore, for example), the BET treatment leads to the modified equation

$$\frac{n}{n_m} = \frac{c(p/p^\circ)}{1 - p/p^\circ} \frac{1 - (N+1)(p/p^\circ)^N + N(p/p^\circ)^{N+1}}{1 + (c-1)(p/p^\circ) - c(p/p^\circ)^{N+1}} \tag{2.18}$$

obtained by summing Equation (2.11) to N rather than to an infinite number of terms. Equation (2.18) reduces to the Langmuir equation by putting $N = 1$.

Statistical-mechanical derivations[6,7]

An alternative way of deriving the BET equation is to express the problem in statistical-mechanical rather than kinetic terms. Adsorption is explicitly assumed to be localized: the surface is regarded as an array of identical adsorption sites, and each of these sites is assumed to form the base of a stack of sites extending out from the surface; each stack is treated as a separate system, i.e. the occupancy of any site is independent of the occupancy of sites in neighbouring stacks—a condition which corresponds to the neglect of lateral interactions in the BET model. The further postulate that in any stack the site in the ith layer can be occupied only if all the underlying sites are already occupied, corresponds to the BET picture in which condensation of molecules to form the ith layer can only take place on to molecules which are present in the $(i-1)$th layer.

Finally, the molecules in all layers above the first are postulated to have the same partition function q_i as in the bulk liquid, so that $q_i = q_{\text{liquid}}$ for $i > 1$. This is of course equivalent to the BET assumption of liquid-like properties for these higher layers.

By following the standard procedures of statistical mechanics, one arrives at an equation which can be converted into the BET equation (2.12) by the simple substitution $q_1/q_{\text{liquid}} = c$. Thus parameter c acquires a significance different from that in the BET theory: in essence it now involves entropic terms as well as energetic terms.

2.3 The mathematical nature of the BET equation

If plotted as n/n_m against p/p°, Equation (2.12) gives a curve having the shape of a Type II isotherm so long as c exceeds 2. From Fig. 2.1 it is seen

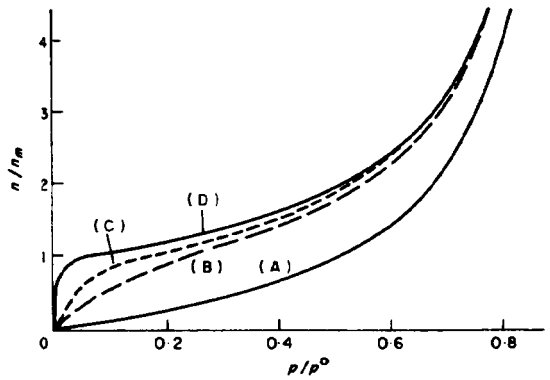

Fig. 2.1 Curves of n/n_m against p/p°, calculated from the BET equation (2.12) for different values of c: (A) $c = 1$; (B) $c = 11$; (C) $c = 100$; (D) $c = 10000$.

that the shape of the knee depends on the value of c, becoming sharper as the value of c becomes greater.

It is interesting to note that the BET equation is equivalent to the difference between the upper branches of two rectangular hyperbolae,[8,9] as may be seen by breaking up the right-hand side of Equation (2.12) into partial fractions:

$$\frac{n}{n_m} = \frac{1}{1 - p/p^\circ} - \frac{1}{1 + c - 1\,p/p^\circ} \tag{2.19}$$

The graph of n/n_m against p/p° will thus be obtained as the difference between the two hyperbolae represented by the equations

$$\frac{n}{n_m} = \frac{1}{1 - p/p^\circ} \tag{2.20}$$

and

$$\frac{n}{n_m} = \frac{1}{1 + c - 1\,p/p^\circ} \tag{2.21}$$

Equation (2.20) has asymptotes at $n/n_m = 0$ and $p/p^\circ = 1$ and it cuts the n/n_m axis at $n/n_m = 1$. Equation (2.21) has asymptotes at $n/n_m = 0$ and $p/p^\circ = -1(c - 1)$. and likewise cuts the n/n_m axis at $n/n_m = 1$. The plots are shown in Fig. 2.2 together with their differences, given as a dotted line.

When c is less than 2 but still positive, the BET equation results in a curve having the general shape of a Type III isotherm (cf. Fig. 2.1, Curve A and Fig. 2.3).

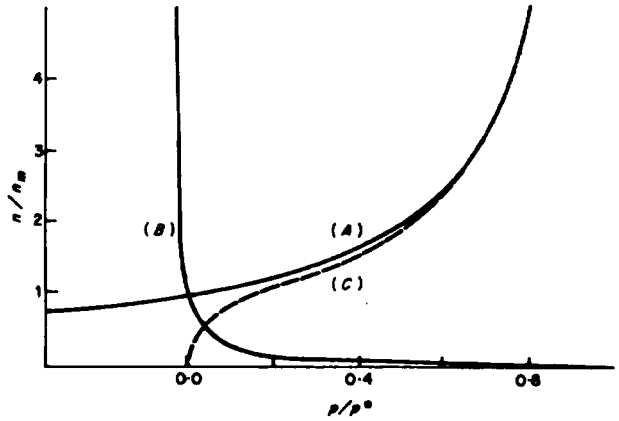

Fig. 2.2 The BET equation: (A) graph of equation $n/n_m = 1/(1 - p/p^\circ)$; (B) graph of equation $n/n_m = 1/(1 + c - 1\ p/p^\circ)$ for $c = 30$; (C) graph of Equation (2.19) for $c = 30$.

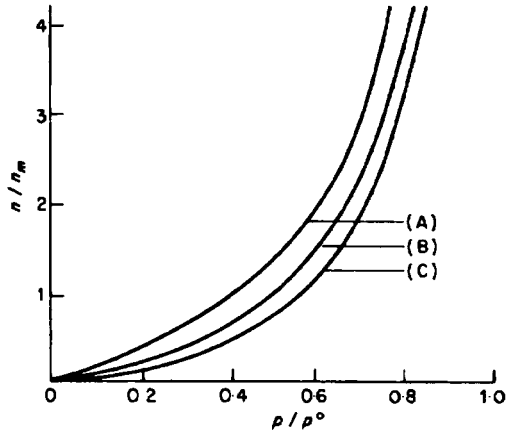

Fig. 2.3 Isotherms calculated according to the BET equation (2.12) for the following values of c: (A) $c = 2$; (B) $c = 1$; (C) $c = 0{\cdot}5$.

The point of inflection

As is seen from Fig. 2.1, the BET equation yields an isotherm which (so long as c exceeds 2) has a point of inflection; this point is close to, but not necessarily coincident with, the point where the amount adsorbed is equal to the BET monolayer capacity.

The relation between the two points is of some interest, and may be elucidated by simple mathematics.

Referring to Equation (2.12), put $n/n_m = X$ and $p/p^\circ = Y$ for the sake of convenience, and differentiate twice to obtain d^2X/dY^2. Equating the resulting expression to zero and solving for Y gives Y_F, the value of p/p° at the point of inflection:[10]

$$Y_F = (p/p^\circ)_F = \frac{(c-1)^{2/3} - 1}{(c-1) + (c-1)^{2/3}}$$

Insertion of this value into Equation (2.12) gives the value, X_F, of X at the point of inflection:

$$X_F = (n/n_m)_F = \frac{1}{c}[(c-1)^{1/3} + 1][(c-1)^{2/3} - 1] \qquad (2.22)$$

In Fig. 2.4, the location of the point of inflection thus calculated is plotted for different values of c. Clearly, the value of n/n_m at the point of inflection may deviate considerably from unity. At the one value of $c = 9$ the value of n/n_m is actually equal to unity and the point of inflection then coincides with the point corresponding to the monolayer capacity; but for values of c

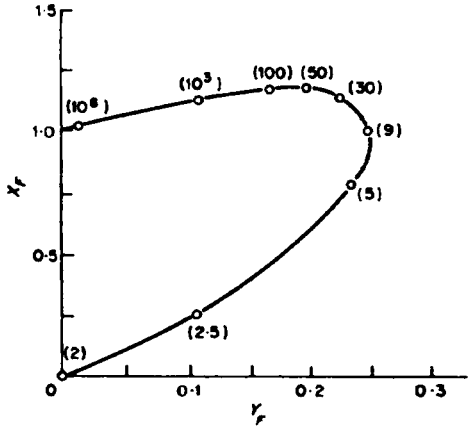

Fig. 2.4 The BET equation. Plot[10] of X_F, calculated for different values of c, against Y_F. X_F is the value of n/n_m at the point of inflection in the isotherm; Y_F is the relative pressure at the point of inflection. Each point on the curve is marked with the corresponding value of c in brackets.

between 9 and infinity the adsorption at the point of inflection may exceed the BET monolayer capacity by as much as 15 per cent and for values of c below 9 the two quantities deviate more and more widely till at $c = 2$ the point of inflection had disappeared. When c is less than 2 the isotherm is of Type III and discussion of the point of inflection is meaningless.

Criticisms of the BET model[6,7,11-14]

From the earliest days, the BET model has been subject to a number of criticisms. The model assumes all the adsorption sites on the surface to be energetically identical, but as was indicated in Section 1.5 (p. 18) homogeneous surfaces of this kind are the exception and energetically heterogeneous surfaces are the rule. Experimental evidence—e.g. in curves of the heat of adsorption as a function of the amount adsorbed (cf. Fig. 2.14)—demonstrates that the degree of heterogeneity can be very considerable. Indeed, Brunauer, Emmett and Teller[1] adduced this non-uniformity as the reason for the failure of their equation to reproduce experimental data in the low-pressure region.

A second criticism is that the model restricts attention to the forces between the adsorbent and the adsorbate molecules—the "vertical" interactions—and neglects the forces between an adsorbate molecule and its neighbours in the same layer—the "horizontal" interactions. From the nature of intermolecular forces (p. 5) it is certain that these adsorbate–adsorbate interactions must be far from negligible when a layer is approaching completion and the average separation of the molecules is therefore small in relation to their size.

It is also questionable how far the molecules in all layers after the first should be treated as completely equivalent.[12,13] From Section 1.2 it follows that the interaction must diminish significantly as distance from the surface increases: this falling-off is, indeed, the basis of Halsey's treatment[11] for the multilayer region of the isotherm, which is dealt with in Section 2.11.

It will be noted that these various limitations cannot be removed merely by adopting a statistical-mechanical approach rather than the original BET treatment.

2.4 Application of the BET equation to experimental data

The most convenient form of the BET equation for application to experimental data is that already given in Equation (2.13), viz

$$\frac{p/p^\circ}{n(1 - p/p^\circ)} = \frac{1}{n_m c} + \frac{c - 1}{n_m c}(p/p^\circ) \qquad (2.13)$$

The plot of $(p/p^\circ)/n(1 - p/p^\circ)$ (or if more convenient, of $p/n(p^\circ - p)$) against p/p° should therefore be a straight line with slope $s = (c - 1)/n_m c$ and intercept $i = 1/n_m c$. Solution of these two simultaneous equations gives n_m and c:

$$n_m = \frac{1}{s + i} \tag{2.23}$$

$$c = \frac{s}{i} + 1 \tag{2.24}$$

Some typical examples of BET plots are given in Figs 2.5–2.7. Those in Fig. 2.5 for nitrogen adsorption at 90 K on various catalysts, taken from the

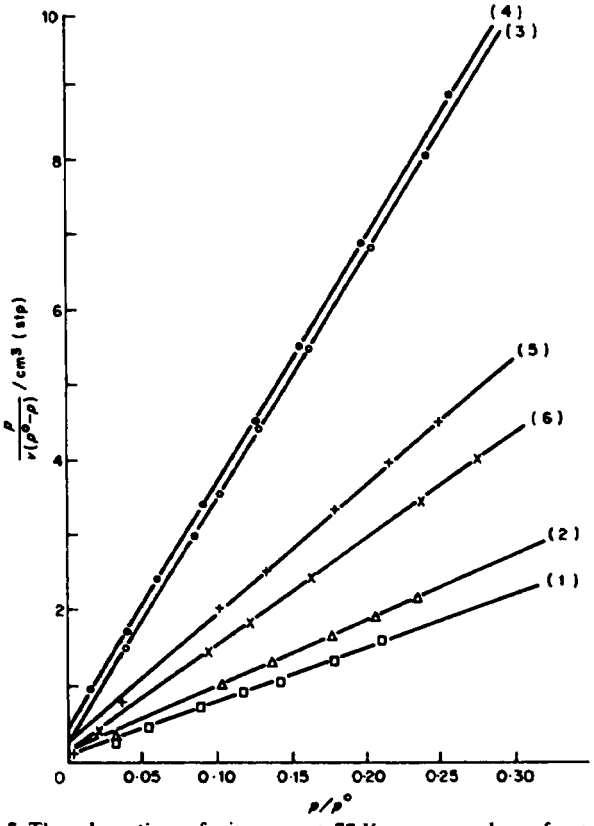

Fig. 2.5 The adsorption of nitrogen at 77 K on a number of catalysts.[1] Plot of $p/v(p^\circ - p)$ against p/p° (v is expressed in cm^3 (stp)). (1) Unpromoted Fe catalyst; (2) Al_2O_3-promoted Fe catalyst; (3) Al_2O_3–K_2O-promoted Fe catalyst; (4) fused copper catalyst; (5) chromium oxide gel; (6) silica gel. (Courtesy Brunauer, Emmett and Teller.)

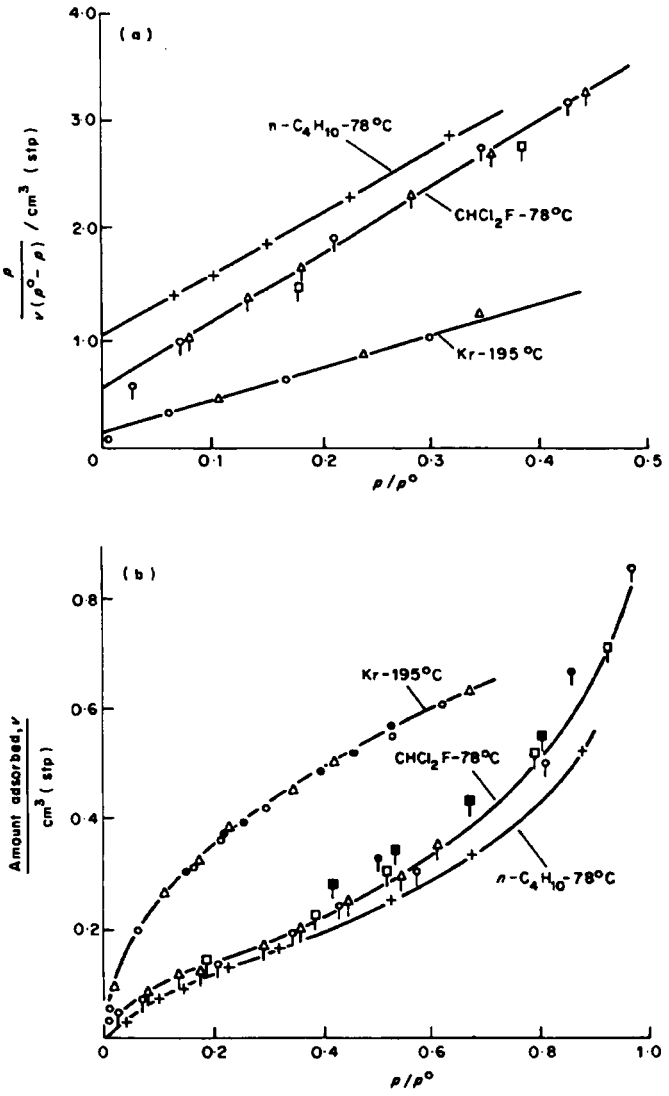

Fig. 2.6 Adsorption of gases on silver foil.[15] (*a*) BET plots; (*b*) adsorption isotherms. (Solid symbols are desorption points.) (Courtesy Davis, De Witt and Emmett.)

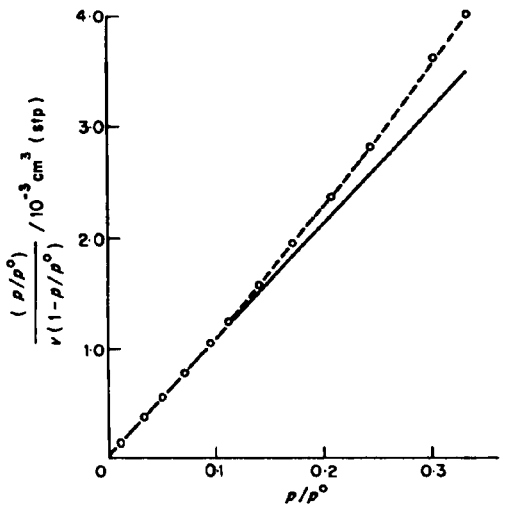

Fig. 2.7 The BET plot for nitrogen adsorbed at 78 K on sodium chloride.[16] $(p/p^\circ)/v(1 - p/p^\circ)$ is plotted against p/p°; v = amount adsorbed in cm^3 (stp). (Courtesy MacIver and Emmett.)

original paper of Brunauer, Emmett and Teller are linear between relative pressures of about 0·05 and 0·35. On extrapolation they pass close to the origin (a feature which is typical of nitrogen adsorption on oxides and hydrated oxides) and this indicates a relatively large value of c, which is associated with the presence of a distinct knee in the adsorption isotherm (p. 46). The isotherms and BET plots in Fig. 2.6 illustrate cases where c is small (e.g. for n-C_4H_{10}, $c = 11{\cdot}6$ at 195 K); the knee of the isotherm is much less pronounced and the intercept on the $p/n(p^\circ - p)$ axis is greater. The range of linearity of the BET plot is roughly the same as before, however.

Contrary to what had at one time been supposed, the range of validity of the BET equation does not always extend over the range of relative pressures ~0·05 to ~0·30. In Fig. 2.7, which refers to the adsorption of nitrogen on pure sodium chloride, the straight line portion of the BET plot covers the relative pressure range 0·01 to 0·1; the point where the adsorption has the value n_m (calculated from the plot) lies at a relative pressure of ~0·05. On ungraphitized carbon black, Dubinin[17] obtained a linear BET plot for nitrogen over the relative pressure range 0·005 to 0·15, which changed to 0·01 to 0·20 when the surface of the black was 80 per cent covered with a layer of pre-adsorbed methanol. There are numerous other examples (not only with nitrogen) where departure from linearity commences at relative pressures below ~0·2 (cf. Table 2.1). Cases are also

TABLE 2.1

Adsorption on rutile[18]

Vapour	Temperature (K)	v_B† cm³ (stp)	$p/p°$ point B	v_m‡ cm³ (stp)	Range of linearity of BET plot ($p/p°$)
Nitrogen	75	760 ± 20	0·043	780	0·024–0·10
				846	0·10–0·29
Nitrogen	85	715 ± 10	0·035	720	0·015–0·06
				801	0·07–0·28
Oxygen	85	745 ± 5	0·070	745	0·02–0·08
				786	0·05–0·30
Argon	85	720 ± 10	0·068	740	0·03–0·08
				768	0·08–0·3

† v_B = adsorption at point B.
‡ v_m = monolayer capacity calculated from the BET equation (2.13).

known where the BET plot is not linear at all, e.g. from cyclohexane on alumina[19] at 0°C.

The degree to which the BET equation fails to reproduce experimental data in the multilayer region of the isotherm is brought out in Fig. 2.8. The results for the adsorption of nitrogen are plotted in the reduced form of n/n_m for a number of nonporous samples of silica and alumina. Despite the differences in surface area and crystal structure of the samples,[20] the experimental points are grouped around a common curve (A), which when $p/p°$ exceeds 0·3 deviates widely from curve (B), the theoretical BET isotherm calculated from Equation (2.12) with $c = 100$ or $c = 200$. (The theoretical isotherms are almost indistinguishable for values of c between 100 and 200; when c is below 100 or above 200 the divergencies between curves (A) and (B) become even greater.)

A number of attempts have been made[21-23] to modify the BET equation so as to obtain better agreement with the experimental isotherm data in the multilayer region. One of the most recent is that of Brunauer and his co-workers:[23]

$$\frac{k(p/p°)}{n(1 - k(p/p°))} = \frac{1}{n_m c} + \frac{c - 1}{n_m c} k(p/p°) \tag{2.25}$$

which is based on the assumption that the number of molecular layers at saturation pressure $p°$, even on an open surface, is finite (~5 or 6) and that n/n_m tends to infinity only at a hypothetical pressure in excess of $p°$. This

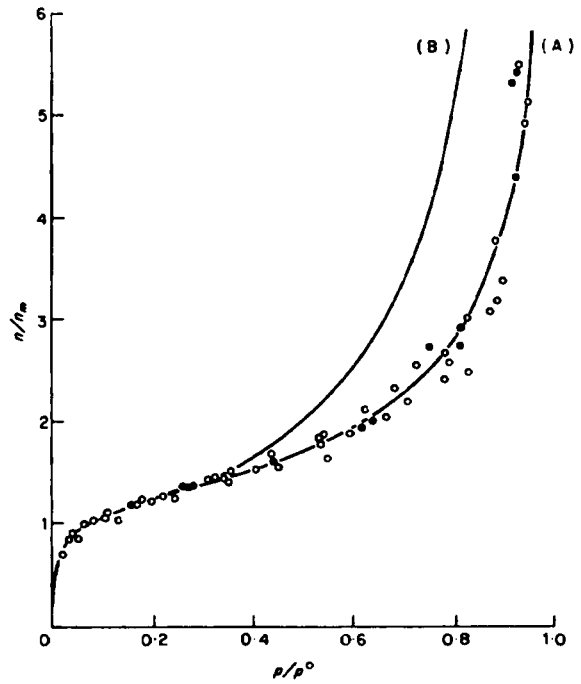

Fig. 2.8 The adsorption of nitrogen at 77 K on nonporous samples of silica and alumina,[20] ranging from 2·6 to 11·5 $m^2 g^{-1}$ for silica and from 58 to 153 $m^2 g^{-1}$ for alumina. n/n_m is plotted against p/p°. (A) ○, silica; ●, alumina. (B) BET isotherm (Equation 2.12) with c values of 100–200.

assumption is allowed for by introducing the coefficient k which has a value less than unity. With $k = 0{\cdot}79$ Brunauer found that the equation is able to reproduce the experimental composite isotherm of Shull[24] (p. 91) reasonably well in the multilayer range up to a relative pressure ~0·8. Actually, the equation is identical in form with one proposed by Anderson[22] many years earlier, but is based on a different model.

2.5 Point B

The Type II isotherms obtained experimentally often display a rather long straight portion (BC in Fig. 2.9), a feature not strictly compatible with the properties of the BET equation which, as we have seen, yields a point of

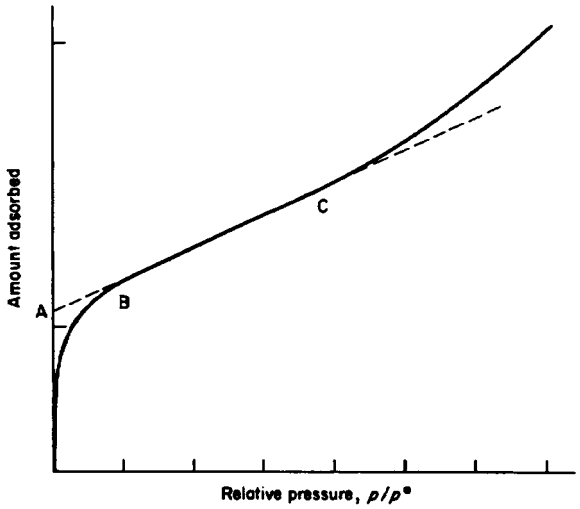

Fig. 2.9 A typical Type II isotherm, showing "Point A" and "Point B".

inflection. The point at which this linear portion begins was termed by Emmett and Brunauer[25] "Point B" and was taken by them to indicate the completion of the monolayer, so that the adsorption at Point B, say n_B, should be equal to the monolayer capacity. In an early paper, Brunauer and Emmett[26] suggested that Point A—the point where the extrapolated linear branch cuts the adsorption axis—might represent the monolayer capacity, but after a detailed study[25] of various characteristic points on the Type II isotherm, Point A was discarded in favour of Point B. This choice was supported by the finding[1] that the value of n_B for a variety of systems, agreed well with n_m as calculated from the BET equation. Subsequent experience, however, has shown that the two quantities frequently show appreciable divergence.

Thus, Young and Crowell,[27] summarizing the results from the literature for nitrogen at 77 K on sixty-eight different solids, reported values of the ratio $n_m:n_B$ ranging from 0·75 to 1·53, though the grand average was close to unity, at 1·03. Brennan and his collaborators,[28] investigating the adsorption of krypton and xenon on a number of evaporated films, found that n_m and n_B could differ by as much as 20 per cent. In common with a number of other workers, they noted that satisfactory agreement between the two quantities may not be achieved unless the BET equation is applied over a range of the isotherm which contains Point B. Sing,[18] for example, found that n_m and n_B obtained from the nitrogen isotherms for a number of

samples of silica and alumina, agreed within about 5 per cent in those cases where Point B lay within the pressure range corresponding to a linear BET plot, but differed by 16 per cent in the one case where Point B lay outside this range.

Consideration of the results of Drain and Morrison[29] for the low-temperature adsorption of nitrogen, oxygen and argon on rutile, serves to confirm the importance of reference to Point B when calculating the monolayer capacity from BET plots. The isotherms were all of well defined Type II, but each gave *two* almost linear BET plots:[18] a short one at low relative pressure and a longer one over the higher and more usual range of relative pressures. The former, which included point B, gave a value of n_m which agreed well with n_B, but the value of n_m from the latter was significantly higher than n_B (cf. Table 2.1).

The ease of locating Point B depends on the shape of the knee of the isotherm.[27] If the knee is sharp, corresponding to a high value of c, Point B can be located with accuracy even if the linear branch of the isotherm is short (see Fig. 2.10, curve (i)). When the knee is rounded, when c is small, Point B becomes difficult to locate, and the estimated value of n_B may then differ widely from the BET monolayer capacity n_m. As will be seen shortly it is doubtful, indeed, how far isotherms in which Point B cannot be identified easily should be used for the estimation of monolayer capacity from either Point B or the BET plot. In practice, this reservation would include all isotherms having a value of c below ~ 20.

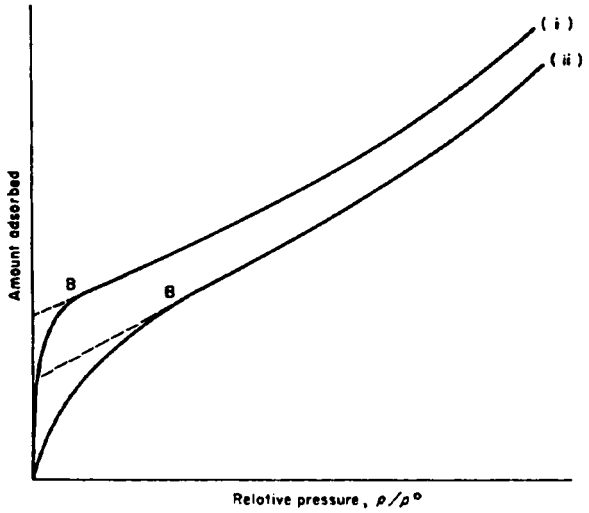

Fig. 2.10 Typical Type II isotherms: (i) with sharp "knee"; (ii) with rounded "knee".

2.6 Test of the validity of the BET monolayer capacity

Supporting evidence for the validity of the monolayer capacity calculated by the BET equation is afforded by curves for the heat of adsorption against the amount adsorbed. Some of the most detailed work has been carried out on carbon black which had been heated at elevated temperature to induce graphitization. Figure 2.11 gives plots of the calorimetric heat of adsorption of nitrogen on carbon black, against n/n_m (n_m having been calculated by the BET equation). Graphs (*a*) to (*d*) refer to progressive increases in the degree of graphitization, and therefore in surface uniformity, resulting from heat treatment at successively higher temperatures. Despite their differences in the sub-monolayer region ($n/n_m < 1$), all of the curves show a very distinct fall in the heat of adsorption in the region where $n/n_m = 1$, to a value little in excess of the molar heat of condensation—just as would be expected for completion of the monolayer and inception of the multilayer. The slight rise in the curves in the sub-monolayer region in curves (*a*) and (*b*), and the peaks in curves (*c*) and (*d*), are plausibly explained in terms of the lateral

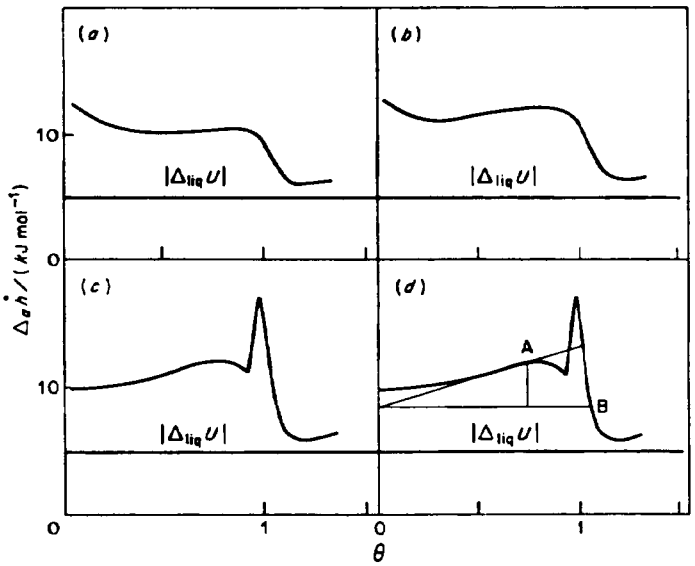

Fig. 2.11 Curves of the differential enthalpy of adsorption[30] $\Delta_a\dot{h}$ of nitrogen against surface coverage θ ($= n/n_m$) for samples of Sterling carbon black heated at the following temperatures: (*a*) 1500°C; (*b*) 1700°C; (*c*) 2200°C; (*d*) 2700°C. The curve for 2000°C was similar to (*c*), but with a lower peak. The calorimetric temperature was 77·5, 77·7, 77·4, 77·4 K in (*a*), (*b*), (*c*) and (*d*) respectively.

interaction of the adsorbed molecules as they become more tightly packed in the monolayer.[30]

Similar results with graphitized carbon blacks have been obtained for the heat of adsorption of argon,[17,30,31] krypton,[32] and a number of hydrocarbons[33,34] (Fig. 2.12). In all these cases the heat of adsorption falls to a level only slightly above the molar heat of condensation, in the vicinity of the point where $n = n_m$.

Surface heterogeneity tends to mask the effect of monolayer completion,

Fig. 2.12 Plot of the calorimetric differential enthalpy of adsorption ($\Delta_a h$) against amount adsorbed (n), for (*a*) *n*-pentane, (*b*) *n*-hexane, (*c*) *n*-heptane, (*d*) *n*-octane, all adsorbed on graphitized carbon black.[33] The point corresponding to $n = n_m$ is marked on each curve. (Courtesy Kiselev.)

as can be seen from Fig. 2.13, in which the adsorbent was a typical carbon black which was similar to that in Fig. 2.11, but which had not been graphitized.

Surface heterogeneity is difficult to remove from crystalline inorganic substances, such as metal oxides, without causing large loss of surface areas by sintering. Thus in Fig. 2.14 in which the adsorbent was rutile (TiO_2) all three adsorbates show a continuous diminution in the heat of adsorption as the surface coverage increases, but with an accelerated rate of fall as monolayer completion is approached.

It should be noted that with low-energy surfaces the sudden fall in the heat of adsorption is absent. This is illustrated in Fig. 2.15, where the contrast between the behaviour of nitrogen on the carbons (high-energy surfaces) and on the molecular solids (low-energy surfaces) is very clear.

Some further evidence as to the validity of the BET monolayer capacity is provided by data for the variation in the entropy of adsorption over the course of the isotherm.[29,31,38] Figure 2.16, which refers to a sample of graphitized carbon provides an example. The molar entropy of nitrogen at 84 K exhibits a well defined minimum when $n = n_m$, which has been explained in terms of the BET model by taking into account the changes in configurational entropy (arising from the different ways of arranging molecules on the available sites) and neglecting changes in non-configurational entropy arising from mobility of the molecules.

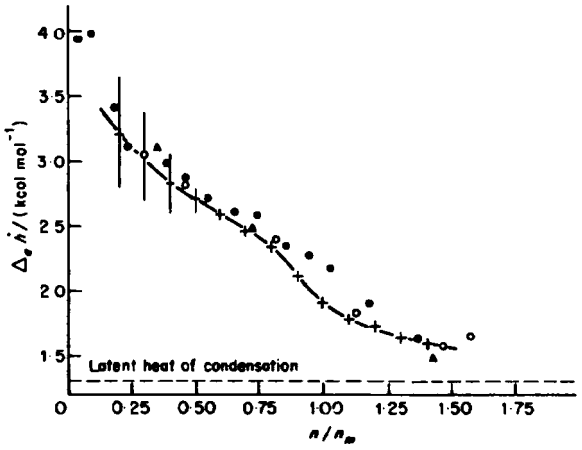

Fig. 2.13 Adsorption of nitrogen on a carbon black before graphitization.[35] The differential heat of adsorption $\Delta_a h$, plotted against n/n_m, was determined calorimetrically at 78 K (○, ●, △) and was also calculated from the isotherms at 78·6 and 90·1 K (+). (Courtesy Joyner and Emmett.)

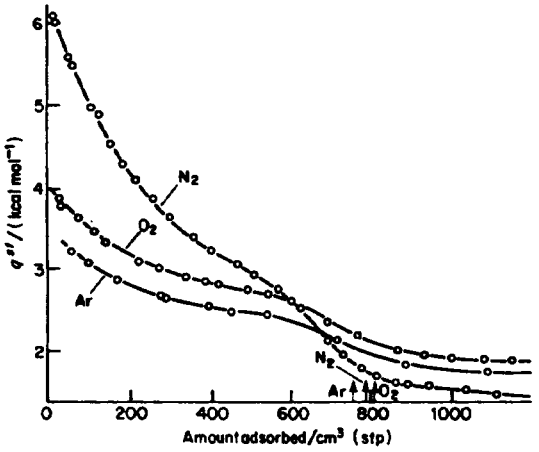

Fig. 2.14 The isosteric heat of adsorption (q^{st}) of argon, nitrogen and oxygen of rutile[36] at 95 K, plotted as a function of the amount adsorbed (expressed in cm^3 (stp). The uptake of each gas corresponding to the completion of a monolayer is marked. Note the more rapid decrease in q^{st} as the amount adsorbed approaches monolayer completion. (After Drain.)

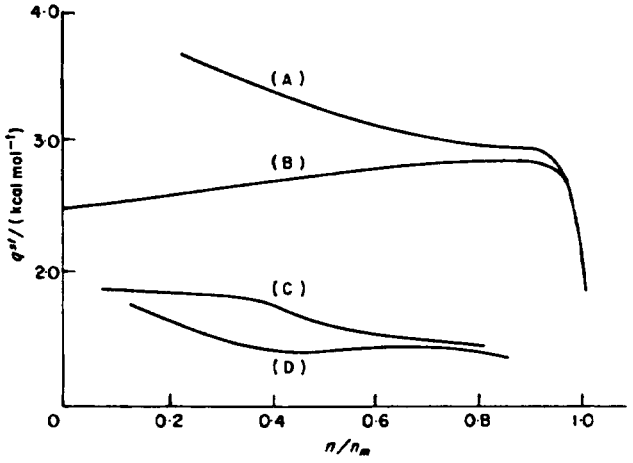

Fig. 2.15 Isosteric heat of adsorption of nitrogen on molecular (low-evergy) solids and on carbons (high-energy solids), plotted as a function of n/n_m. (A) Diamond; (B) graphitized carbon black, P.33; (D) Benzene; (E) Teflon. The curve for amorphous carbon was very close to Curve (A). (Redrawn from a Figure of Adamson[37].)

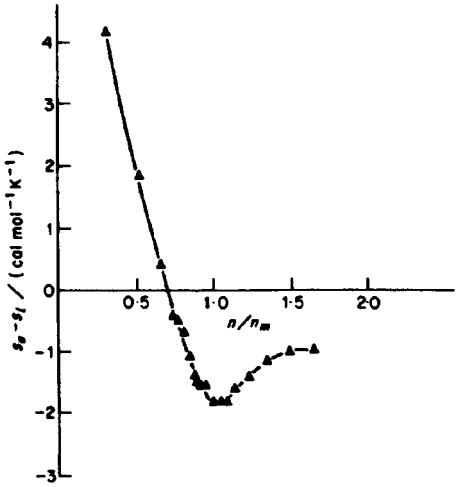

Fig. 2.16 The molar entropy for nitrogen adsorbed on graphitized carbon[142] (Graphon) at −189·3°C, as a function of the amount adsorbed: s_a = molar entropy of adsorbed nitrogen; s_l = molar entropy of liquid nitrogen. (Courtesy Hill, Emmett and Joyner.)

The kind of results adduced in the present section justify the conclusion that the quantity n_m calculated by means of the BET equation from the Type II isotherm corresponds reasonably well to the actual monolayer capacity of the solid. The agreement lies within, say, ±20 per cent, or often better, provided the isotherm has a well defined Point B.

2.7 Comparison of BET areas from nitrogen isotherms with independent values

In practice, the monolayer capacity is of interest, not so much in itself, but as a means of calculating the specific surface with the relation quoted at the beginning of the Chapter, viz

$$A = Ln_m a_m \tag{2.1}$$

where a_m is the molecular area of the adsorbate, i.e. the area occupied by an adsorbate molecule in the completed monolayer. An obvious way of testing the validity of the monolayer capacity obtained by the BET equation or from Point B, is to compare the specific surface of a variety of adsorbents calculated from their monolayer capacities by means of Equation (2.1), with

their areas evaluated by an independent method. The majority of tests of this kind have been carried out with nitrogen at its boiling point, 77 K, as adsorbate, with the value of a_m, following an early suggestion of Emmett and Brunauer,[25] calculated from the density ρ_L of the liquid nitrogen. The tacit assumption is made that the arrangement of the adsorbed molecules on the surface is just the same as it would be on a plane surface placed within the bulk liquid without disturbing the pre-existing arrangement. This leads to the formula

$$a_m = f\left(\frac{M}{\rho_L L}\right)^{2/3} \tag{2.26}$$

where f is a packing factor, which for 12 nearest neighbours in the bulk liquid and six on the plane surface, is equal to 1·091. Equation (2.26) thus becomes

$$a_m = 1{\cdot}091\left(\frac{M}{\rho_L L}\right)^{2/3} \tag{2.27}$$

Insertion of $\rho_L = 0{\cdot}81\ \mathrm{g\,cm^{-3}}$ gives the value of a_m for nitrogen at 77 K as $a_m(N_2) = 16{\cdot}2 \times 10^{-20}\ \mathrm{m^2}$ or $16{\cdot}2\ \text{Å}^2$. Consideration of the a_m values of other adsorbates is deferred to Section 2.8.

The most direct test is to compare the BET area with the *geometrical* area of the solid. Unfortunately, comparisons of this kind are relatively rare on account of experimental difficulties. The choices are to work with, say, single crystals having a well defined surface, when techniques of quite extraordinary sensitivity will be needed for measurement of the adsorption; or, to obtain a larger surface area by use of thin sheets, narrow rods or small spheres, and run the risk that the surface will not be truly smooth so that the actual area will exceed the geometrical area.

Rhodin[39] chose the first alternative. With the aid of a very sensitive microbalance he measured the adsorption isotherms of nitrogen on single crystals of copper and zinc in the form of electropolished thin plates (at 78·1, 83·5 and 89·2 K). He found the ratio r of the BET area to the geometrical area to be 1·20 for copper and $1{\cdot}16 \pm 0{\cdot}01$ for zinc, taking a_m for nitrogen to be $16{\cdot}1\ \text{Å}^2$. Since the roughness factor r, even for single crystals, would almost certainly exceed unity the agreement between the BET and the actual area of the solids is considerably better than the 16 to 20 per cent implied by these figures. This inference is supported in further experiments where a sample of polycrystalline copper was progressively oxidized and its surface area measured by nitrogen adsorption at intervals: the value of r fell continuously from 2·45 to 1·00 as the average thickness t of the oxide film increased from zero up to 75 Å, but then remained constant as

t increased further to 100 Å. Thus the values of r in excess of unity must have represented roughness which was eliminated by the oxidation.

More recently Deitz and Turner[40] have employed a special technique to produce glass fibre fine enough and sufficiently uniform in diameter ($\sim 8\,\mu m$) to give a reasonably large geometrical surface area, around $0{\cdot}2\,m^2\,g^{-1}$, which could be calculated within 0·5 per cent; the surface (as checked by electron microscopy) was believed to be free of roughness. The BET plot for nitrogen was linear for p/p° values between 0·01 and 0·04, and exact correspondence between the geometrical area and the BET area could be obtained by putting $a_m(N_2)$ equal to $16{\cdot}4\,Å^2$ at 77 K and $16{\cdot}6\,Å^2$ at 90·2 K; thus the conventional value of $16{\cdot}2\,Å^2$ gave agreement within 2 per cent with the geometrical area.

Most tests of the validity of the BET area have been carried out with finely divided solids, where independent evaluation of the surface area can be made from optical microscopic or, more often, electron microscopic observations of particle size, provided the size distribution is fairly narrow. As already explained (Section 1.10) the specific surface A_d obtained in this way is related to the mean projected diameter d_p through the equation

$$A_d = \frac{K \sum n_p d_p^2}{\rho \sum n_p d_p^3} \tag{2.28}$$

where K is the shape factor α_s/α_v of Equation (1.82) (for spheres and cubes, $K = 6{\cdot}0$), ρ is the true density of the material, and n_p is the number of particles having diameter d_p.

Equation (2.28), being statistical in nature, requires a large number of particles to be measured, especially if the spread of particle size is wide. The possibility of error from this source is stressed by Arnell and Henneberry[41] who found that in a particular sample of finely ground quartz, two particles in a total of 335 had a diameter about twenty times the most probable diameter, and that if these were overlooked the calculated value of A_d would be nearly doubled.

The shape factor K is another indeterminate source of error, the most reliable results being obtained with particles that are spherical or nearly so. From this point of view, carbon blacks, when non-porous, are particularly satisfactory and they possess the additional advantage of being obtainable with a high degree of uniformity in particle size. The porosity that is usually present in ungraphitized blacks can be largely eliminated by graphitization through heating at temperatures around 3000°C, a procedure which unfortunately induces some deviation from the spherical shape. Pioneer work by Anderson and Emmett[42] (taking $a_m(N_2) = 16{\cdot}2\,Å^2$) led to values of the apparent roughness factor r for four blacks ranging from 0·96 to 1·43;

whilst Arnell and Henneberry,[41] who examined eleven blacks, obtained ten values between 0·87 and 1·71, with one value of 5·4. Values in excess of unity are plausibly explained by the presence of an internal surface which is registered by gas adsorption, but not by electron microscopy. In the experiments of Hofmann and his collaborators,[43] the specific surface A_N measured by nitrogen adsorption invariably diminished considerably on graphitization, whereas the value of A_d calculated from the electron micrographs was much less affected. Thus the value of r decreased (Table 2.2), as would be expected if graphitization reduced or eliminated the porosity. The values of r for five out of the eight graphitized samples ranged between 0·95 and 1·10; the two high values of 1·40 and 1·24 could be due to incomplete graphitization, since the r-values for the corresponding ungraphitized samples were unusually high. However, the low value of 0·77 is somewhat puzzling.

TABLE 2.2

Specific surface area of carbon blacks[43] before and after graphitization, determined by electron microscopy (A_d) end by nitrogen adsorption (A_N)†

Sample	$\frac{A_d}{m^2 g^{-1}}$	$\frac{A_N‡}{m^2 g^{-1}}$	$r = A_N/A_d$
Thermax	6·50	7·63	1·17
Thermax graph.	6·45	6·37	0·99
CK	97·1	92·3	0·95
CK graph.§	69·8	72·8	1·04
Philblack A	46	44	0·96
Philblack A graph.	48·4	37·0	0·77
Philblack O	73	87·2	1·19
Philblack O graph.	65	69·9	1·07
Spheron C	96	252	2·62
Spheron C graph.	101	126	1·24
Spheron I	132	170	1·29
Spheron I graph.	96	103·5	1·08
Spheron 6	106	124	1·17
Spheron 6 graph.	79	87	1·10
Luv 36	10·2	17·8	1·74
Luv 36 graph.	11·0	15·4	1·40

† Reduced from the Table of Hofmann *et al.*[43]

‡ A_N is based on $a_m(N_2) = 16{\cdot}2$ Å^2.

§ Graph = graphitized by heating at 3000°C.

TABLE 2.3

Comparison of specific surface of anatase and zinc oxide[45] determined by electron microscopy (A_d) and by nitrogen adsorption (A_N)

Sample	$\frac{A_d}{m^2 g^{-1}}$	$\frac{A_N}{m^2 g^{-1}}$	$r = A_N/A_d$
Anatase-1	9·5	10·3–11·0	1·08–1·16
Anatase-2	8·3–9·7	7·0	0·84–0·72
Anatase-3	6·7	5·6	0·84
Zinc oxide-1	4·3	4·2	0·98
Zinc oxide-2	8·9	7·9	0·89

Various other substances have also been used in tests. Robens,[44] for example, with glass spheres 20 to 60 μm in diameter, obtained a BET area (taking $a_m(N_2) = 16{\cdot}2\,Å^2$) which was only 5 per cent higher than the geometrical area obtained from microscopic particle size analysis. In view of the uncertainties inherent in the latter procedure (p. 63) this result may be taken to confirm the BET value within 5 per cent or less. Ewing and Lui[45] worked with pigmentary anatase and zinc oxide and found concordance within ±20 per cent between the two measures of specific surface (Table 2.3). The experiments of Alexander and Iler[46] involved the techniques of light scattering, nitrogen adsorption and electron microscopy, the adsorbents being a series of fractions of colloidal silica. As is seen from Table 2.4, there is good agreement, except for the coarsest fraction, between the

TABLE 2.4

Comparison of particle diameter of colloidal silica[46] by electron microscopy (d_d), by nitrogen adsorption (d_N) and by light scattering (d_l)

Fraction number	Particle diameter		
	$\frac{d_d}{Å}$	$\frac{d_N}{Å}$	$\frac{d_l}{Å}$
1	165	147	175
9	188	189	230
18	211	218	300
27	284	281	430
35	352	325	530
50	592	400	660

particle size as measured by the electron microscopy and by nitrogen adsorption.

Recently a different approach, based on calorimetry, has been used by Rouquerol and his co-workers,[47] in their revival of the Harkins–Jura "absolute" method for surface area determination.[48] Harkins' and Jura's idea was to cover the adsorbent with a film of adsorbate thick enough to present an external surface identical in nature with the bulk liquid. When the adsorbent thus treated was immersed in the liquid adsorptive, the enthalpy change per unit area would be equal to the surface enthalpy h_L of the bulk liquid adsorptive, which is calculable from the surface tension of the liquid and its temperature coefficient ($h_L = \gamma - T\mathrm{d}\gamma/\mathrm{d}T$); the surface area would therefore be given by the relation $q^i = Ah_L$ where q^i is the heat of immersion per unit mass of the sample. Harkins and Jura believed that a thickness of 5 to 7 molecular layers was necessary, and the corresponding relative pressure was then so near saturation as to run the risk of appreciable capillary condensation in the interstices between the particles of solid. However, Rouquerol and his co-workers,[47] as a result of a careful microcalorimetric study, concluded that (with water) two molecular layers was adequate. Eleven samples, comprising nine different substances, ranging in BET area from 0·6 to 129 $m^2\,g^{-1}$, were studied. If the sample of lowest area is omitted, along with one result for kaolin which was believed to be anomalous, the ratio of the calorimetric area to the BET-nitrogen area, ranged from 0·98 to 1·23 with an average value of 1·07. The results described in this section show that the specific surface A calculated from the BET monolayer capacity of nitrogen with $a_m(N_2) = 16{\cdot}2$ Å^2, agrees to within ± 20 per cent and often better, with geometrical or other independent estimates of A. Much of the discrepancy can be reasonably attributed to uncertainties inherent in the independent estimates of A and to the difficulty of ensuring that the solid was completely non-porous. The overall consistency of results is such that the figure $a_m(N_2) = 16{\cdot}2$ Å^2 has gained widespread acceptancy as a working value for the determination of specific surface from Type II nitrogen isotherms by the BET method. Even so, there is little doubt that the molecular area of nitrogen can vary somewhat with the nature of the solid, and this possibility must always be borne in mind when absolute rather than relative values of specific surface are being sought. The reasons for such variation are indicated in the following section.

2.8 Factors determining the molecular area a_m

Numerous vapours besides nitrogen have been used from time to time for the determination of surface area by the BET method. These include argon,

krypton and xenon, oxygen, benzene, toluene, the shorter chain hydrocarbons, Freon-1 ($CHCl_2F$), carbon dioxide and nitrous oxide, as well as water vapour. In the earlier stages of the subject the molecular area a_m was calculated from the liquid density by Equation (2.27) and inserted into Equation (2.1) to obtain the specific surface of the solid. It soon became evident that this procedure was leading to anomalous results, for significantly different values were obtained for the area of a given solid according to the particular adsorbate used. Although the anomalies could often be diminished by use of suitably but arbitrarily modified values of a_m, they could not be eliminated.

Table 2.5, based on the pioneer work of Davies, DeWitt and Emmett,[15]

TABLE 2.5

Comparison of the specific surface estimated by the adsorption of different vapours on some powders and metal foils[15]

(i) Adsorbent	(ii) Gas	(iii) A† / $m^2 g^{-1}$	(iv) A / A(N)	(v) A'‡ / $m^2 g^{-1}$	(vi) A' / A(N)	(vii) c(BET)
Glass spheres (7 μm)	N_2 (78 K)	0·434	1·00	0·434	1·00	150
	Kr (78 K)	0·322	0·74	0·441	1·02	32
	C_4H_{10} (195 K)	0·333	0·77	0·489	1·12	7
	$CHCl_2F$ (195 K)	0·315	0·73	0·479	1·10	106
Tungsten Powder	N_2 (78 K)	2·69	1·00	2·69	1·00	81
	Kr (78 K)	1·96	0·73	2·68	1·00	290
	C_4H_{10} (273 K)	1·67	0·62	2·43	0·90	26
	$CHCl_2F$ (273 K)	1·73	0·64	2·62	0·97	21
Zinc oxide	N_2 (78 K)	9·40	1·00	9·40	1·00	155
	Kr (98 K)	6·82	0·72	9·34	0·99	150
	C_4H_{10} (273 K)	6·93	0·74	10·1	1·07	52
	$CHCl_2F$ (273 K)	6·63	0·71	10·1	1·07	215
Silver Foil§	Kr (78 K)	1·56	—	2·14	—	19
	C_4H_{10} (195 K)	1·22	—	1·78	—	6
	$CHCl_2F$ (195 K)	1·13	—	1·72	—	11
Monel ribbon‖	Kr (78 K)	0·456	—	0·622	—	13
	C_4H_{10} (195 K)	0·652	—	0·952	—	4
	$CHCl_2F$ (195 K)	0·577	—	0·878	—	7

† Based on a_m values of column 3 of Table 2.6.

‡ Based on a_m values of column 4 of Table 2.6.

§ Geometrical area = 1·56 $m^2 g^{-1}$.

‖ Geometrical area = 0·579 $m^2 g^{-1}$.

TABLE 2.6

Values of molecular area a_m es used by Davis, DeWitt and Emmett[15]

Adsorbate	T/K	a_m/Å^2 (Equation 2.27)	a_m/Å^2 (Revised)
Nitrogen	78	16·2	16·2
Krypton	78	15·2	20·8
	195	29·7	43·4
Butane	273	32·1	46·9
	195	24·7	37·5
Freon-21	273	26·4	40·1

with nitrogen, krypton, *n*-butane and Freon-1 as adsorbates, illustrates the point. Five adsorbents were used, two of them having known geometrical areas. Column (iii) gives the values of the BET surface area A obtained by using the molecular areas calculated from the liquid density (Equation (2.27)), (cf. Table 2.6). As is seen—especially by reference to column (iv)—the values of A for a given adsorbent differ, sometimes widely, amongst themselves. A revised set of values of molecular area (Table 2.6, column (iv)) was then tried in an attempt to bring the various values of A into concordance with the "nitrogen" values and with each other. Columns (v) and (vi) of Table 2.5 show that the divergences were diminished though not always eliminated, in the case of the first three adsorbents, and that with the silver foil and the monel ribbon there were still quite wide divergences both from the geometrical area and amongst the different adsorbates.

Similar discrepancies were found for other vapours by Harris and Emmett,[49] who quoted their results as the ratio Ω of the BET area calculated from the isotherm of the particular adsorbate to the BET "nitrogen" area (Table 2.7). The value of Ω varied, again sometimes widely, for any one gas on different adsorbents, so that the divergences could not be removed by use of a single revised value of a_m for a given vapour.

Examination of these and other results indicates that the value of a_m for a given adsorptive which needs to be used in order to arrive at a value of specific surface consistent with that from nitrogen adsorption, varies according to the nature of the adsorbent. The existence of these variations shows that the conventional picture, in which the value of a_m corresponds to a monolayer which is completely filled with adsorbate molecules in a liquid-like packing, is over-simplified. Two factors can upset the simple picture: (a) there may be a tendency for adsorbed molecules to become localized on lattice sites, or on more active parts of the solid surface; and (b) the process

TABLE 2.7

Value of $\Omega = S_{vap}/S_N$ for a number of solids and various vapours[49] (S_N and S_{vap} are the specific surfaces determined by use of nitrogen and of another vapour† respectively)

Solid		Value of Ω						
		C_2H_5OH	C_6H_6	$C_6H_5CH_3$	C_5H_{12}	CS_2	H_2S	H_2O
Glass spheres		0·97	0·8	0·72	0·52	0·38	0·72	
Porous Glass‡	No. 1	0·4	0·53	0·53				
	No. 2	–	0·54	0·54				
	No. 1a	–	–	–	0·6	0·31	–	0·59
	No. 2a						0·65	
Iron 973		0·69 (75°C)	0·65	0·57				
		0·86 (20°C)						
Iron 652		–	0·67	0·53				
Ground Pyrex					0·48	0·27		
Pptd. Silver	No. 1				0·71			
	No. 2				0·62	0·76		

† Using liquid density in Equation (2.27); $a_m(N_2) = 16{\cdot}2$ Å^2.

‡ Type IV isotherm; but the argument as to surface area is still valid (cf. Chapter 3).

of monolayer formation may not be clearly separated from the building-up of the multilayer.

The way in which localization can have a disturbing effect is fairly clear: if adsorption is completely localized, the adsorbed molecules will reside on the adsorption sites, whose positions are determined by the crystal structure of the adsorbent; the value of a_m will thus be determined, not by the molecular size of the *adsorbate*, but (unless this is large enough to block more than one site) by the lattice parameters of the *adsorbent*. At the other extreme when the adsorbate is freely mobile, a_m will be determined by the size and shape of the molecules and the way they can pack together; if the ordering is the same as in the bulk liquid, a_m will be given by Equation (2.27). The degree of mobility will be determined by the height of the energy barrier $\Delta\phi$ between a given site and its immediate neighbours, relative to the thermal energy kT (cf. p. 8). If $\Delta\phi/kT < 1$ there will be virtually complete mobility, and if $\Delta\phi/kT > 10$, say, there will be almost complete localization. In the intermediate—and much more common—cases where $\Delta\phi/kT$ lies between 1 and 10, the adsorption will be partly localized and partly mobile, and the time which a molecule spends in the vicinity of the adsorption sites will increase as the value of $\Delta\phi/kT$ increases: a_m will be expected to lie between the two extremes just referred to.

In general one would expect a high value of $\Delta\phi$ to be associated with a high value of ϕ itself (cf. Table 1.1 and p. 10) which will be reflected in a high value of c. Thus a highly localized film is likely to yield an isotherm having a high value of c, whereas a largely mobile film should lead to a lower value of c. Both of the factors (a) and (b) should therefore cause the value of a_m to vary with the value of c. Such a variation is demonstrated, for example, by the set of isotherms of *n*-pentane in Fig. 2.17(*a*), which vary markedly in shape according to the nature of the adsorbent.[50] The corresponding values of a_m (calculated from these and additional isotherms of pentane) show a marked correspondence with the value of c (Fig. 2.17(*b*): at low c-values (rounded knee) a_m varies rapidly with c, whereas at higher c-values a_m becomes almost constant. Moreover all the values of a_m are in excess of the figure, 36·2 Å^2, calculated from the liquid density at 293 K, which corresponds to nonlocalized adsorption.

The dependence of a_m on the nature of the surface can also be studied by modifying a well defined nonporous surface in a systematic way. Thus, Dubinin and his co-workers[17] have measured the isotherms of nitrogen on a graphitized carbon black which had undergone surface modification by pre-adsorption of different amount of methanol, thereby producing surfaces of lower energy. Both c and the BET surface area calculated with $a_m(N_2) = 16{\cdot}2$ Å^2 progressively decreased in value as the coverage of methanol increased (Table 2.8). Whilst the true area of the sample would indeed decrease somewhat owing to the increase in particle size produced by the film of methanol, the change would be quite small (around 2 per cent) and it is more likely that the value of $a_m(N_2)$ itself has increased. Day, Parfitt and Peacock[51] likewise found an apparent reduction, from 10·2 to 7·5 m^2 g^{-1}, in the nitrogen area of a rutile sample after pre-adsorption of methanol, with a

TABLE 2.8

Effect of pre-adsorption of methanol on BET parameters for adsorption of nitrogen at 77·6 K on graphitized carbon black CT ($a_m(N_2) = 16{\cdot}2$ Å^2)

Fractional coverage with MeOH	A(BET)/(m^2 g^{-1})	c
0	39·1	150
0·50	31·4	90
0·80	30·0	40
1·3	29·9	32

† After Dubinin.[17]

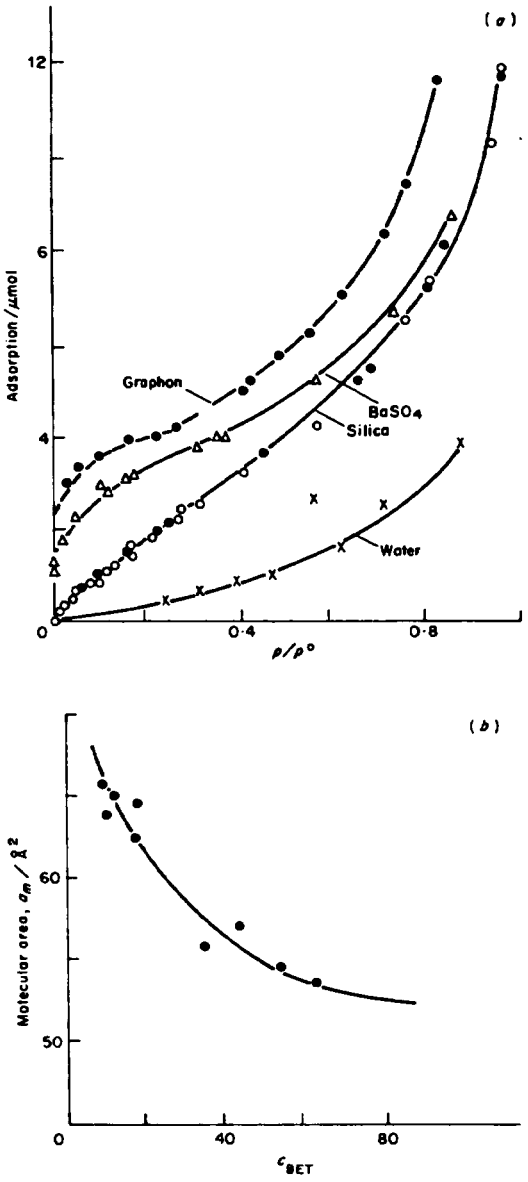

Fig. 2.17 The adsorption of pentane on different adsorbents. (*a*) Effect of the nature of the adsorbent on the shape of the isotherm (each isotherm is labelled with the name of the adsorbent). (*b*) Dependence of a_m(pentane) on the value of parameter *C*. (Courtesy Kiselev and Eltekov.[50])

corresponding diminution in the value of c from 400 to 39. This result also is best explained in terms of an increase in $a_m(N_2)$ from 16·2 to 22 Å^2.

From all these considerations it is seen that the attainment of a constant value of a_m characteristic of a given adsorbate involves two opposing requirements: it is necessary that c shall be high enough to ensure adequate separation between monolayer and multilayer formation; but on the other hand c must be low enough to avoid appreciable localization of the adsorbate. It seems that with nitrogen, these two opposing requirements can be met reasonably well on a wide range of adsorbents; the kind of evidence discussed earlier indicates that, as a general rule, use of the working value $a_m(N_2) = 16{\cdot}2$ Å^2 will result in a value of specific surface lying within, say, 20 per cent of the true figure. The selection of nitrogen for surface area determination so long ago by Brunauer and Emmett[25] must be reckoned a most happy inspiration. Even so, there are bound to be adsorbents for which the standard figure of 16·2 Å^2 needs to be modified. For example, Pierce and Ewing,[52] as well as Zettlemoyer,[53] give reasons for supposing that the nitrogen monolayer on the uniform surface of graphitized carbon is localized in the form of an open array, with $a_m(N_2) \sim 20$ Å^2; interestingly, this figure is close to that calculated for nitrogen molecules rotating freely in a plane parallel to the surface.[54] Sing and his co-workers suggest[55] that on α-alumina the value of $a_m(N_2)$ is about 18 Å^2, whereas Rouquerol[56] has argued, from calorimetric data, that on graphitized carbon and hydroxylated silica the nitrogen molecules are steeply oriented so as to give a value significantly less than 16·2 Å^2. The adsorption measurements of Chung and Dash[57] also provide evidence for a monolayer structure of nitrogen more dense than the liquid type of packing implied by $a_m(N_2) = 16{\cdot}2$ Å^2.

A complicating factor quite different in nature from factors (a) and (b) above may occasionally appear. It is well known that variation in the conditions of outgassing, in particular the temperature, can lead to considerable differences in the isotherm and the calculated value of specific surface. This is especially true of the hydrated metal oxides; outgassing at progressively higher temperatures causes the loss of H_2O ligands and OH groups, producing gaps in the surface layer and consequent departure from atomic planarity.[58]

Finally, it needs to be noted that the pressures involved in the BET range for nitrogen, from ~ 10 to ~ 200 Torr with the actual figures depending on the system, whilst making for experimental convenience, limit the scope of routine nitrogen determination to specific surfaces in excess of ~ 1 m^2 g^{-1}; this is because of the magnitude of the correction for the gas remaining unadsorbed in the "dead space" in the volumetric method, and of the buoyancy correction in the gravimetric technique.

2.9 Adsorptives other than nitrogen

Of the large number of readily available gases, the proportion that turn out to be suitable for surface area determination is quite small, because a number of conditions have to be met. In the first place it is necessary that the isotherm of the adsorptive on a wide range of adsorbents shall have the characteristics described in the previous Section, 2.8: the isotherm must have a sharp knee and a well defined Point B. A number of requirements of a practical kind must also be satisfied: the adsorptive must be chemically inert towards the solid; the saturation vapour pressure, p°, at the working temperature must be large enough to allow the accurate measurement of the relative pressure over a reasonably wide range ($\sim 0{\cdot}001 < p/p^\circ < \sim 0{\cdot}5$); but, for reasons of experimental convenience, p° should not exceed 1 to 2 atmospheres. In addition, the working temperatures tend to be limited to those which can be obtained with the common refrigerants, notably nitrogen (b.p. 77 K), oxygen (b.p. 90 K), carbon dioxide slush (195 K), melting ice (273 K), along with the range, 253 to 323 K, which can be conveniently attained by an adjustable thermostat bath. Finally, it is desirable that the shape of the adsorbate molecule shall not be far removed from spherical symmetry, so as to minimize the uncertainty in a_m arising from the different possible orientations on the surface.

These rather exacting requirements explain why the number of adsorptives suitable for surface area determinations is severely limited. In a very comprehensive survey of the literature published in 1967 and covering 188 references, McClellan and Harnsberger[59] found 128 substances each of which had been used in at least two, and often several, surface area determinations. Yet from this large number they felt able to arrive at "recommended" values of a_m for only five adsorptives, viz nitrogen, argon, krypton, *n*-butane and benzene. The remainder of the present section is devoted to a consideration of the a_m-values for the last four of these adsorptives, together with certain others (xenon, oxygen, carbon dioxide and the lower alkanes) which are, or have been, widely used for surface area determination.

Water is another adsorptive which has often been used, but its complexity of behaviour renders it generally unsuitable for the evaluation of total surface area. Consideration of this important topic is deferred to Chapter 5.

Argon

Argon is frequently used for the determination of surface area, usually at 77 K. Like the other noble gases, argon is of course chemically inert and is composed of spherically symmetrical monatomic molecules. Argon stands in

the middle of the range of noble gases, and its physical properties, such as boiling point, heat of vaporization and polarizability, are not far removed from those of nitrogen. From the experimental standpoint, therefore, the adsorption of argon is relatively easy to measure at the temperature of liquid nitrogen ($\sim$77 K), provided the specific surface exceeds $\sim 1\ m^2\ g^{-1}$. However, since this temperature is below the triple point of argon (88·8 K) there is doubt as to the appropriate reference state. At first sight it would seem reasonable to take p° as the saturation vapour pressure of the solid; but when this is done, the argon isotherm on a non-porous solid is found to approach the saturation pressure axis at an angle rather than asymptotically (Fig. 2.18). For this reason, it has been usual to take the effective saturation vapour pressure as that of the supercooled liquid state ($p_L^\circ = 220$ Torr at 77·2 K), though in recent years this choice has been questioned (cf. p. 76).

In their pioneer work, Brunauer and Emmett[61] adopted the value $a_m(\mathrm{Ar}) = 13{\cdot}8\ \text{Å}^2$ for the molecular area of argon, by insertion of the *liquid* density ρ_L in the standard equation (2.27). The same figure was recommended by McClellan and Harnsberger[59] as a result of their comprehensive survey of the literature, already referred to. These workers noted that the recorded values of a_m (based on $a_m(\mathrm{N_2}) = 16{\cdot}2\ \text{Å}^2$) extended over the wide range 10–19 Å^2, and concluded that the area occupied per molecule of argon in the completed monolayer varied from one adsorbent to another.

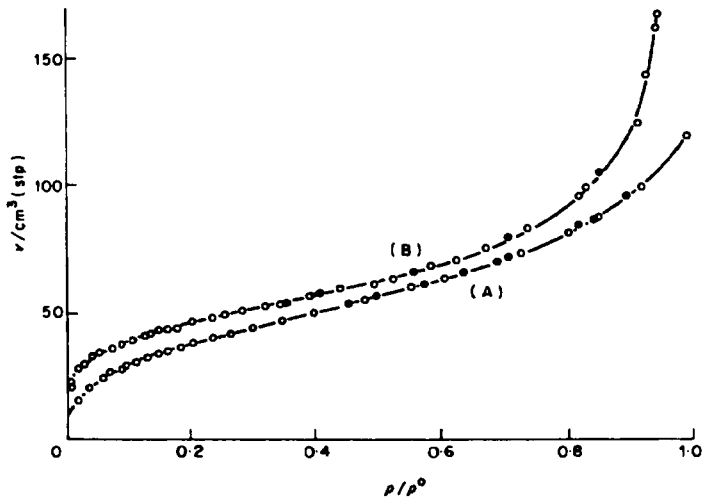

Fig. 2.18 Isotherms of argon (A) and of nitrogen (B) at 78 K on a non-porous silica[60] (TK800-III). Open circles, adsorption; solid circles, desorption.

In the light of Section 2.8 such a variation could be connected with the fact that argon isotherms often have low values of c (~ 50), so that the monolayer is not very well defined. On this argument, it would seem helpful to compare the BET monolayer capacities for argon and nitrogen in selected cases where the argon Point B happens to be clearly distinguishable. One of the most suitable adsorbents for this purpose is graphitized carbon black. The results of such a comparison are given in Table 2.9 as a_m values for argon, based on $a_m(N_2) = 16{\cdot}2\,Å^2$. As is seen, the divergence between the values for different samples is not very great, and could be largely accounted for by the fact that the range of linearity of the BET plot for argon is short. The average, $13{\cdot}8\,Å^2$, coincides with the value calculated from the liquid density with Equation (2.27), already referred to. It is possible that this identity is only fortuitous, however, since according to several authorities the adsorption of nitrogen on graphitized carbon is localized, with $a_m \sim 19\,Å^2$. If Pierce's figure[52] of $a_m(N_2) = 19{\cdot}3\,Å^2$ is adopted, the average for argon in Table 2.9 would be raised to $a_m(Ar) = 16{\cdot}5\,Å^2$.

The results obtained when the adsorbents are non-porous oxides are somewhat different. The values of $a_m(Ar)$ referred to $a_m(N_2) = 16{\cdot}2\,Å^2$ are

TABLE 2.9

Molecular area, $a_m(Ar)$ of argon at 77 K on graphitized carbon blacks (Argon BET plots constructed with p^* (liquid); surface areas determined by BET-nitrogen, with $a_m(N_2) = 16{\cdot}2\,Å^2$)

$a_m(Ar)/Å^2$	Reference
13·8	62
14.3†	63
13·7	64
15·1	65
13·7	17
14·3	66
12·9‡	56
13·0§	67
Average $13{\cdot}85 \pm 0{\cdot}7$	

† At 87·5 K.

‡ From Point B.

§ From flattest part of first tread (at 64·5 K).

N.b. If $a_m(N_2) = 19{\cdot}3\,Å^2$, $a_m(Ar) = 16{\cdot}5\,Å^2$.

TABLE 2.10

Molecular area, a_m(Ar), of argon at 77 K on nonporous oxides (Argon BET plots constructed with p^*(liquid); BET surface areas calculated from nitrogen isotherms, with $a_m(N_2) = 16{\cdot}2\,Å^2$)

Oxide	a_m(Ar)/Å^2	Reference
Silica (Aerosil)	16·3	137
Silica (Aerosil)	17·7	69
Silicas (Crystalline)	16·1, 16·7	70
Silica (HiSil)	16·6	71
Aluminas (Precipitates)	15·3, 16·6	70
Alumina (γ-Al_2O_3)	17·6	72
Titanium dioxide (Anatase)	16·6	73
Titanium dioxide (Anatase)	16·7	74
Titanium dioxide (Rutile)	16·4	73
Titanium dioxide (Rutile)	17·2	79
Titanium dioxide (Rutile)	16·5	58
Thorium oxide	16·6	75
Magnesium oxide (smoke)	16·9	76
	Average 16·65 ± 0·6 Å^2	

higher, and now average 16·6 (cf. Table 2.10) which, incidentally, is close to the figure proposed by Harkins[68] many years ago.

As already mentioned, the choice of the supercooled liquid as reference state has been questioned by some workers[55,70] who use the saturation vapour pressure of the solid, which is measured at the working temperature in the course of the isotherm determination. The effect of this alternative choice of p° on the value of a_m for argon adsorbed on a number of oxide samples, covering a wide range of surface areas, is clear from Table 2.11: the average value of a_m(Ar) is seen to be somewhat higher, i.e. 18·0 Å^2.

Thus, on oxide surfaces, the molecular area of argon based on $a_m(N_2) = 16{\cdot}2\,Å^2$, shows little variation from one solid to another, the average value being $a_m(Ar) = 16{\cdot}6\,Å^2$ with the supercooled liquid, or $a_m(Ar) = 18{\cdot}0\,Å^2$ with the solid, as the reference state. With graphitized carbon, the situation is less clear, because there are now two options: either to keep the molecular area of nitrogen the same as on oxides, at 16·2 Å^2, when a_m(Ar) becomes 13·8 Å^2; or to maintain a_m for argon constant throughout, at 16·6 Å^2, when the value for nitrogen on graphite has to be raised to $a_m(N_2) = 19{\cdot}3\,Å^2$, a figure which agrees with Pierce's proposal of a few years ago.[52]

The idea of a constant value for the molecular area of argon on different solids would seem reasonable in view of the non-specific nature of argon

TABLE 2.11

Molecular area, a_m(Ar) of argon at 77 K on nonporous oxides (Argon BET plots constructed with p^*(solid))

Oxide	$A_{BET}(N_2)$ ($a_m(N_2) = 16{\cdot}2$ Å^2) / $m^2\,g^{-1}$	a_m(Ar) / Å^2	References
Quartz	6·2	18·2	55
Silica (TK70)	36·3	18·5	55
Silica (Fransil)	38·7	17·9	60
Silica (TK800)	163	18·2	60
δ-Al_2O_3	111	18·1	55
Amorphous Al_2O_3	85	17·9	55
Anatase	20·5	17·4	77
Anatase	145	17·8	77
		Average 18·0 ± 0·3 Å^2	

adsorption;[64,71,78] the disadvantage of argon in relation to surface area determination, however, is the poor definition of Point B, associated with the relatively low value of c, which results in uncertainty as to the precise value of the monolayer capacity.

At sufficiently low temperatures the isotherm of argon on high-energy surfaces tends to assume a step-like character (cf. p. 86).

Krypton

Following the pioneer work of Beebe[79] in 1945, the adsorption of krypton at 77 K has come into widespread use for the determination of relatively small surface areas because its saturation vapour pressure is rather low (p° ~ 2 Torr). Consequently the "dead space" correction for unadsorbed gas is small enough to permit the measurement of quite small adsorption with reasonable precision. Estimates of specific surface as low as 10 cm^2 g^{-1} have been reported. Unfortunately, however, there are some complications in the interpretation of the adsorption isotherm.

The working temperature, 77 K, is well below the triple point of krypton, 116 K, but if the solid is taken as the reference state the isotherm shows an unusually sharp upward turn at the high-pressure end. The usual practice, following Beebe, is therefore to take p° as the saturation vapour pressure of the supercooled liquid (p° = 2·49 Torr at 77·35 K and 27·5 Torr at 90·2 K).

A further complication is that the BET plot is frequently not linear; with

forty out of fifty catalysts studied by Malden and Marsh,[80] for example, the plot was somewhat convex to the relative pressure axis when p° referred to the supercooled liquid state and became more so when p° was that of the solid state. The calculated monolayer capacity therefore varied according to where the tangent was drawn.

The molecular area, calculated from the density of the supercooled liquid at 77 K is $a_m(\mathrm{Kr}) = 15{\cdot}2\ \text{Å}^2$, but Beebe found it necessary to adopt the higher value $19{\cdot}5\ \text{Å}^2$ to bring the krypton-based area into line with the area of Harkins' reference sample of anatase.[48]

McClellan's and Harnsberger's survey,[59] which embraced a considerable variety of solids including carbons, metal oxides and organic polymers such as polythene, arrived at a mean value of $20{\cdot}2\ \text{Å}^2$, with a standard deviation of $\pm 1{\cdot}6\ \text{Å}^2$. Other more recent results, likewise based on $a_m(\mathrm{N_2}) = 16{\cdot}2\ \text{Å}^2$, are 19·9 to $21{\cdot}4\ \text{Å}^2$ with an average of $20{\cdot}4\ \text{Å}^2$ (glass fibre of known area[40]); $20{\cdot}2\ \text{Å}^2$ (stainless steel[81]); 19·2 to $20{\cdot}8\ \text{Å}^2$, with a mean of $20{\cdot}1\ \text{Å}^2$ (boron phosphate[82]). All values are well in excess of the $15{\cdot}2\ \text{Å}^2$ calculated from liquid density, and indicate an appreciable degree of localization. The wide spread in c-values (Table 2.12) suggests a considerable variation in the degree of localization, which might have been expected to result in a larger range of a_m-values than actually found. However, the solids showing very high c-values were metals having small surface areas, where the isotherms tend to be restricted to low relative pressures so as to minimize the "dead space" correction; consequently these values of c are rather uncertain.

The Beebe value of $a_m = 19{\cdot}5\ \text{Å}^2$ still remains a useful working figure, but in view of the various complications just enumerated, it is always advisable

TABLE 2.12

Values of BET parameter c for adsorption of krypton[83] at 77 K

Adsorbent	c
Organic materials	10–70
Glass	20–80
Silica	25–50
Ferric oxide	30–75
Nickel oxide	70–120
Silica gel	80
Ferrites	60–200
Micas	100–130
Tungsten powders	215, 290
Carbon black	230
Nickel films	
contaminated	400, 1000
clean	1200, 2300

to calibrate against nitrogen adsorption. This is often difficult in practice because the reason for choosing krypton in any particular case is that the specific surface is too low for accurate measurement by nitrogen adsorption. In the absence of nitrogen calibration an uncertainty of at least ± 20 per cent in the value of the specific surface has to be accepted.

The step-like nature of krypton isotherms on highly uniform surfaces is referred to in Section 2.10.

Xenon

Xenon is another adsorptive which has a low vapour pressure, $\sim 1{\cdot}7 \times 10^{-3}$ Torr, at its usual working temperature of 77 K, which should in principle render it suitable for the measurement of low surface areas; in practice its use seems to have been largely restricted to well defined surfaces. The position as to its molecular area still remains somewhat unclear. On account of its high polarizability ($\alpha(\text{Xe}) = 4{\cdot}09 \times 10^{-24}\,\text{cm}^3$; $\alpha(\text{Kr}) = 2{\cdot}46$, $\alpha(\text{Ar}) = 1{\cdot}63$ and $\alpha(\text{N}_2) = 1{\cdot}74 \times 10^{-24}\,\text{cm}^3$), its dispersion interaction with solids will be large and a high degree of localization might be expected. The finding of Brennan,[84] working with nine metals as evaporated films, that the monolayer capacities of xenon and krypton on the same metal were equal, supports this idea; and the wide range of values quoted in McClellan and Harnsberger's paper[59] for $a_m(\text{Xe})$ on various apparently nonporous materials, viz 18·2 to 25 Å^2 (at 77 or 90 K) points in the same direction. Using the LEED technique, Lander and Morrison[85] found that $a_m(\text{Xe})$ on graphite at 90 K was only 15·7 Å^2, which is actually less than the area per atom in the close-packed plane of bulk solid xenon, viz 16·8 Å^2; they concluded that the Xe atoms were in register with the carbon hexagons, having suffered the necessary lateral compression.

On the other hand, Pritchard,[86] more recently, has found that on the (111) plane of both silver and copper, the value of $a_m(\text{Xe})$ is close to 17·0 Å^2 (17·7 for Ag, 16·9 Å^2 for Cu) and this corresponds to the spacings in solid xenon rather than in the metal adsorbents.[87]

The picture therefore remains obscure. The degree of localization may well depend on variable factors such as the purity of the surface (ultra high vacuum is now known to be essential), the temperature, and the magnitude of the lattice parameters relative to the (rather large) size of the xenon atom.

Alkanes

Several of the lower alkanes, from C_2 to C_7, have been used from time to time for surface area determination. They possess the virtue of chemical inertness towards the majority of adsorbents, and their saturation pressures

are such that (apart from ethane) they can be worked with conveniently at temperatures around ambient. As with most adsorbates, however, the values for molecular area in the literature vary considerably. Except for the lowest members of the series, the area occupied will depend markedly on the orientation of the molecule relative to the surface. On *a priori* grounds a flat orientation would be expected, and on Graphon, at least, the experimental evidence bears this out. Thus Kiselev,[88] for the alkanes C_5 to C_8, and more recently, Clint[89] for C_5 to C_{12}, found that the value of a_m calculated from the isotherm varies almost linearly with the chain length. The actual values of a_m obtained (in Å^2) were:

C_5	C_6	C_7	C_8	C_9	C_{10}	C_{11}	C_{12}
45	51·5	57·3	61·0	–	–	–	–
46·6	51·8	56·8	64·5	66·7	74·9	81·8	82·8

Extrapolation from these two sets of values to C_4 gives $a_m(C_4H_{10})$ = 40·5 Å^2 for *n*-butane, which may be compared with the figure of 44·4 Å^2 (with a standard deviation of ±4 Å^2) given in McClellan and Harnsberger's final list of recommended values[59] and the value of 40 Å^2 found by Davis[76] for *n*-butane on graphitized carbon at 195 K. A contributory factor to the variation in a_m-values is that the value of *c* tends to be low,[90] e.g. on $CaCO_3$ (p. 251) *c* for butane is around 25.

Finally, ethane merits special mention on account of its early appearance in the field of surface area evaluation from adsorption isotherms usually at 78 and 90 K. Its saturation vapour pressure at these temperatures is so low (0·0017 and 0·0083 Torr respectively) that the "dead space" correction for unadsorbed gas is nearly or quite negligible. In 1947, Brown and Uhlig,[91] in their estimates of the surface roughness of chrome-plated nickels from ethane adsorption at 90 K, used the value a_m (C_2H_6) = 20·5 Å^2, calculated from the lattice spacing of *solid* ethane (m.p. of ethane = 90·4 K); this figure has been adopted by a number of workers.[59] Later, Kiselev and his collaborators,[92] working with graphitic carbon of known area, obtained 22·7 Å^2 from the BET monolayer capacity (at 173 K), as compared with 20·4 Å^2 from a molecular model and 22·2 Å^2 from the liquid density (taking the van der Waals thickness of an ethane monolayer as 4 Å). The use of ethane for surface area determination seems to have fallen off in recent years, however.

Benzene

Benzene has enjoyed some popularity as an adsorbate for surface area determination over a number of years. It can be used conveniently at temperatures around ambient, but assignment of a value to its molecular

area encounters difficulties. The area occupied by a molecule of benzene on the surface of a solid is very different according as the molecule is lying flat or standing end-on. For the flat position Isirikyan and Kiselev[93] estimate a_m from the simple relation $a_m = V_L/Lt$ (where V_L is the molar volume of the bulk liquid adsorptive and t is the van der Waals thickness, taken as 3·7 Å^2) and obtain a_m(flat) = 40 Å^2. For the end-on orientation a_m has been estimated as a_m(upright) = 25 Å^2; the value calculated from the liquid density by Equation (2.27)—which corresponds to random orientation—is 30·7 Å^2. Values of a_m in the literature are always higher than these last two values, so that a flat orientation is strongly indicated, and receives further support from recent work on the neutron diffraction of benzene adsorbed on graphitized carbon.[94]

In their review McClellan and Harnsberger[59] arrived at a "recommended" value of $a_m(C_6H_6)$ = 43 Å^2 with a standard deviation of ±3 Å^2 (based on $a_m(N_2)$ = 16·2 Å^2) as a result of examining fifteen papers covering eleven adsorbents. More recently Wade[19] has obtained the value 42·3 Å^2 for benzene on α-alumina.

One of the factors responsible for the rather wide variation in a_m values for benzene is the presence of π-electrons in the molecule, which can cause its adsorption to acquire a specific character if the adsorbent is polar (Chapter 1, p. 11). On hydroxylated silica, for example, the heat of adsorption is much higher than on the dehydroxylated material;[95,96] on the latter solid indeed the interaction is so weak that a Type III isotherm results (Fig. 2.19). Unfortunately c-values are rarely quoted in the literature, but

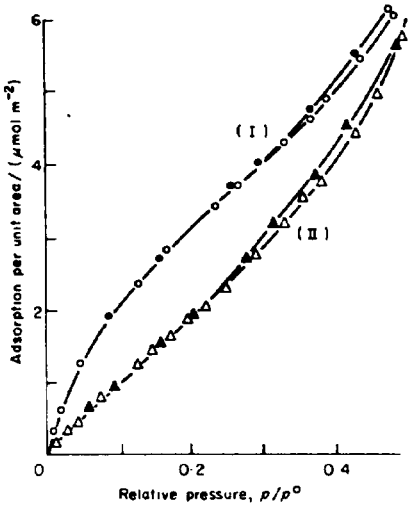

Fig. 2.19 Adsorption isotherm of benzene on (I) hydrated, and (II) dehydrated silica gel. (After Kiselev[50].)

such as do appear are relatively low, e.g. $c = 10$ for benzene on hydroxylated silica;[96] the rounding of the knee of the isotherms, with ill-defined Point B, introduces an element of uncertainty into the calculated values of monolayer capacity.

Oxygen

In the early days of the BET method, oxygen at its boiling point was frequently used for surface area determination, but its use has fallen off now that liquid nitrogen is readily available. Apart perhaps from the greater hazards attendant on the use of liquid oxygen as refrigerant, the possibility of chemisorption or chemical reactivity even at the low temperature of its boiling point (90 K) cannot be entirely ruled out. The molecular area of oxygen, calculated from the liquid density at 90 K, is $a_m(O_2) = 14{\cdot}1$ Å^2. The majority of values in McClellan and Harnsberger's list[59] at (or near) 90 K or 77 K, and on a variety of non-porous adsorbents, including titanias, silicas and carbon blacks, fall within the range 13·5 to 15·2 Å^2. More recently, Brunauer and his co-workers[97] gave $a_m(O_2) = 14{\cdot}3$ Å^2 at 77·3 K and $a_m(O_2) = 15{\cdot}4$ Å^2 at 90 K on four adsorbents, taking $a_m(N_2)$ as 16·2 Å^2. Isirikyan and Kazmenko[98] obtained $a_m(O_2) = 16{\cdot}2$ Å^2 with rutile outgassed at various temperatures, in good agreement with the value 15·8 Å^2 reported by Smith and Ford.[65]

Carbon dioxide

Carbon dioxide is another adsorptive which finds relatively little use in surface area determination, despite its general experimental convenience and simple molecular structure: not only is the possibility of chemisorption a complicating factor, but the high quadrupole moment of CO_2(3·1–3·4 $\times 10^{-26}$ e.s.u.) means that its adsorption isotherm is very sensitive to the presence of polar groups or ions in the surface of the solid. The quadrupole effect is clearly brought out in Fig. 2.20, due to Lemcoff and Sing,[99] where the adsorbent was a well investigated nonporous silica (TK800, cf. Table 2.16). In curves (i) and (ii) the outgassing temperatures were 25°C and 1000°C, respectively, so that surface OH groups were present in (i) but absent in (ii). Removal of the OH groups led to a marked change in the isotherm from clear Type II ($c = 21$) to a near Type III ($c = 4$). Somewhat unexpectedly the a_m value, based on nitrogen, remained unchanged 22·2 Å^2, but this may well have been fortuitous in view of the uncertainty attaching to the BET monolayer capacity when c is small.

The low c-values and the sensitivity to surface polarity are no doubt major causes of the rather wide variation in a_m-values for CO_2 in the

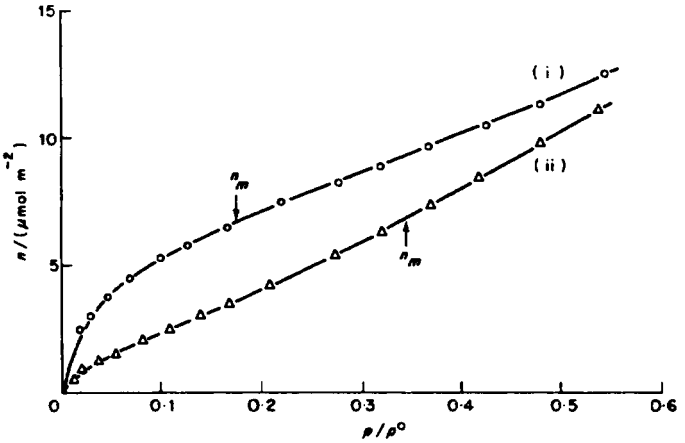

Fig. 2.20 Adsorption isotherms of carbon dioxide[99] at −78·5°C in TK 800 outgassed at 25°C and 1000°C (triangles). The BET monolayer is indicated as n_m on each isotherm.

literature. The values listed by McClellan and Harnsberger[59] range from 14·1 to 22·0 Å^2 at 195 K ($a_m(CO_2)$ from liquid density = 16·3 Å^2); other values are 20·6 Å^2 (on carbon black and titania,[69] based on a_m(Ar) = 13·8 Å^2), and 19·1 Å^2 (on porous aluminas[100]).

Carbon dioxide cannot be recommended for routine determinations of specific surface: on the other hand, it should be particularly suitable for the study of the polarity of surfaces in systems where chemisorption can be excluded from consideration.

Conclusion

The survey in the present section shows quite clearly that it is not possible to assign a fixed value of a_m to a given adsorptive, which will remain valid for its adsorption on all adsorbents. As demonstrated in Section 2.7, nitrogen and argon would seem to provide the best approximation to a constant effective molecular area, with $a_m(N_2) = 16{\cdot}2$ Å^2 and a_m(Ar) = 16·6 Å^2. When another adsorptive is used, it needs to be calibrated against nitrogen or argon; consequently, if the specific surface of a single sample only is being sought, there is no point in resorting to an alternative adsorptive, since the nitrogen or argon isotherm had to be determined in any case. (If the solid has a very low surface area however, recourse to krypton is unavoidable, since nitrogen or argon calibration would be too inaccurate.)

When it is desired to evaluate the specific surfaces of a set of closely related samples of solid, however, only one of the samples needs to be calibrated against nitrogen (or argon), provided that all the isotherms of the alternative adsorptive can be shown to have indentical shape. A simple device for testing this identity, by use of the α_s-plot, is described in Section 2.13; by means of the α_s-plot it is also possible to proceed directly to calculation of the specific surface without having to assign a value to a_m, or to evaluate the BET monolayer capacity, of the alternative adsorptive.

2.10 Step-like isotherms

The existence of step-like (Type VI) isotherms, has already been mentioned (Chapter 1). As long ago as 1948, it was argued by Halsey[101] that if the surface of the (non-porous) adsorbent is completely uniform, or nearly so, the isotherm should assume a step-like form rather than the sigmoid shape of the Type II isotherm. Halsey's analysis took account of the "horizontal" interactions (cf. Nicholson and Silvester[102]), which were neglected in the BET model, and also allowed for the rapid falling-off in the interaction energy ϕ with distance from the surface, which is implied by the 6–12 and similar relations of Chapter 1 (Section 1.3). On the other hand, the analysis neglected the entropic contribution. The arguments of the present section apply in the first instance to molecules such as argon and krypton which are spherically symmetrical and nonpolar in nature.

Because of the large difference in ϕ between successive molecular layers, each layer becomes complete at a relative pressure $(p/p^\circ)_\theta$ which is determined by the value of ϕ/kT for that layer, viz ϕ_θ/kT (here θ is of course restricted to integral values). Each layer will therefore give rise to a step, such that the "riser" corresponds to the cooperative build-up of the layer and the "tread" to the transition between the layer and the next higher one.

An example of a stepped isotherm, for krypton at 90 K, is shown in Fig. 2.21(*a*), where the adsorbent is graphitized carbon black, which is known to possess a very uniform surface. Figure 2.21(*b*) shows the steps obtained, also with krypton, on cadmium bromide.

Since the sharpness of the steps depends on ϕ_θ/kT, the steps will become less pronounced as ϕ_θ becomes smaller or T becomes higher. The temperature effect is well illustrated by the isotherms of argon on graphitized carbon at a series of temperatures, given in Fig. 2.22: with increasing temperature the steps become more and more rounded until at the highest temperature mere vestiges remain and the isotherm has become a wavy line.[105]

The effect of a diminution in ϕ is brought out in the comparison of the

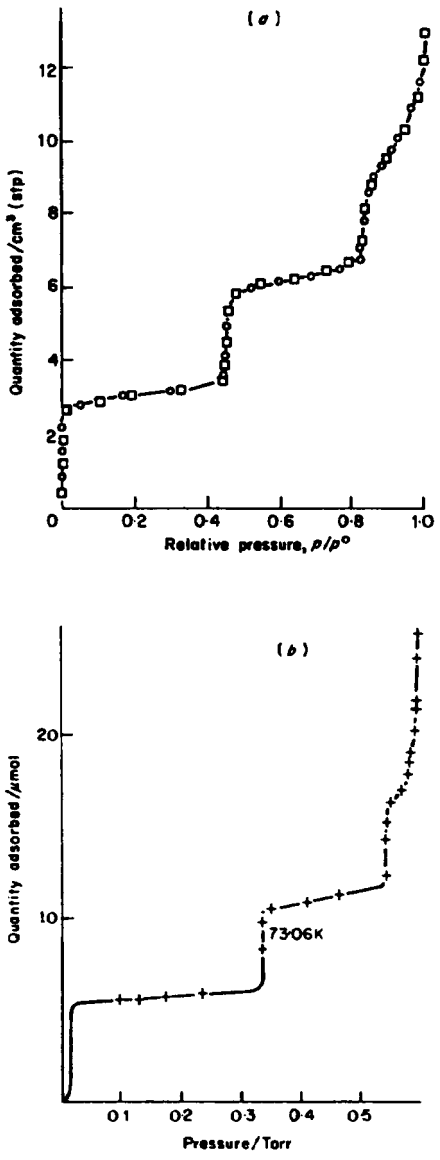

Fig. 2.21 Stepped isotherms of (*a*) krypton at 90 K on a carbon black graphitized at 2700°C. (*a*) (○) Run 1; (□) Run 2; (*b*) krypton at 73·1 K on crystals of cadmium bromide. (Courtesy (*a*) Amberg, Spencer and Beebe;[103] (*b*) Larher[104].)

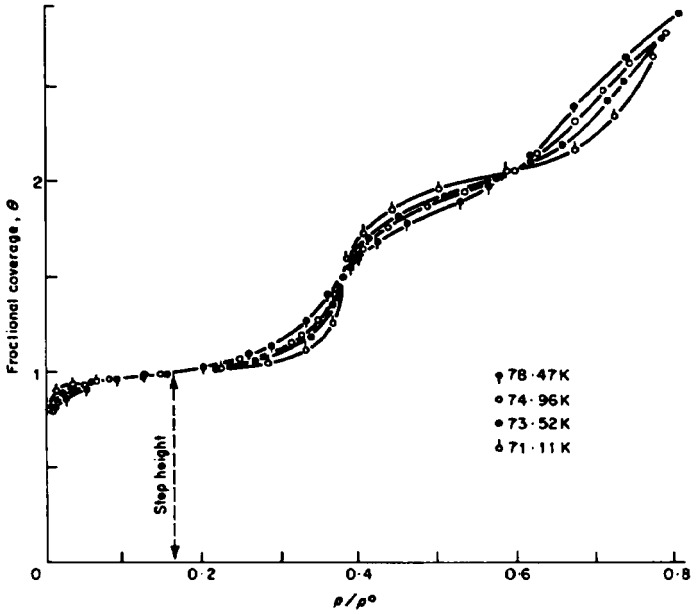

Fig. 2.22 Adsorption isotherms of argon on graphitized carbon black at a number of temperatures,[105] plotted as fractional coverage θ against relative pressure p/p°. (Courtesy Prenzlow and Halsey.)

isotherms of argon and krypton, at the same temperature 77 K, on graphitized carbon black (Fig. 2.23). With krypton the steps are well defined, whereas with argon they have almost disappeared; correspondingly the value of ϕ (at a given value of θ) is higher for krypton than for argon by virtue of its higher polarizability (cf. Equations 1.9–1.11; $\alpha(\text{Kr}) = 2{\cdot}48 \times 10^{-24}\,\text{cm}^3$; $\alpha(\text{Ar}) = 1{\cdot}63 \times 10^{-24}\,\text{cm}^3$).

Another spherical, nonpolar molecule is methane; its isotherms on both graphite and molybdenite at 77 K have a step-like character.[107] Ethane, whilst slightly less symmetrical, is still nonpolar and it gives two distinct steps on cadmium at 97·4 K, the second step being nonhorizontal.[108]

With nitrogen, the departure from spherical symmetry combined with the relatively strong quadrupole moment, leads to a blurring of the step-like character of the isotherm in the multilayer region[109] (cf. Fig. 2.29(b)).

If the surface of the adsorbent is energetically heterogeneous rather than homogeneous each step of the isotherm will be replaced by an assortment of steps, corresponding to the completion of a monolayer on the different homogeneous patches of the surface. If the steps are sufficiently numerous

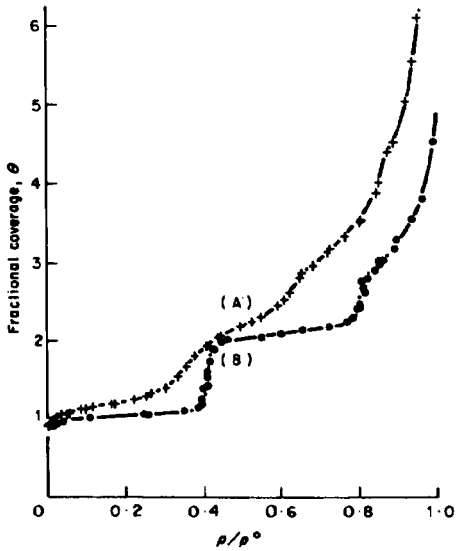

Fig. 2.23 Adsorption isotherms on graphitized carbon black at 77 K.[106] (A) argon; (B) krypton. (Courtesy Dash.)

the result will be a smooth isotherm of the familiar Type II shape. On this argument, therefore, the Type II isotherm obtained with a noble gas at sufficiently low temperature is characteristic not of a homogeneous surface (as tacitly assumed in the BET treatment) but of a highly heterogeneous one. Striking confirmation is provided by the isotherms of argon on carbon black heat-treated at progressively higher temperatures, reproduced in Fig. 2.24. The untreated black gives an ordinary Type II isotherm, but as the temperature of heat treatment, and with it the degree of graphitization, is raised, the isotherm becomes more and more steplike. That the change in isotherm shape is indeed associated with an increase in energetic uniformity brought about by the heat treatment is clear from a comparison of the curves for heat of adsorption against surface coverage n/n_m, for a carbon black before and after graphitization (Fig. 2.25). With the ungraphitized black, the heat of adsorption falls continuously with a barely perceptible acceleration in the region of monolayer completion, indicating a high degree of nonuniformity of the surface; but after graphitization the heat varies only slightly in the monolayer region (showing, indeed a small rise due to lateral interaction) and then falls sharply when the monolayer is complete—behaviour which shows the surface to be much more uniform.

Evaluation of the monolayer capacity from a stepped isotherm raises

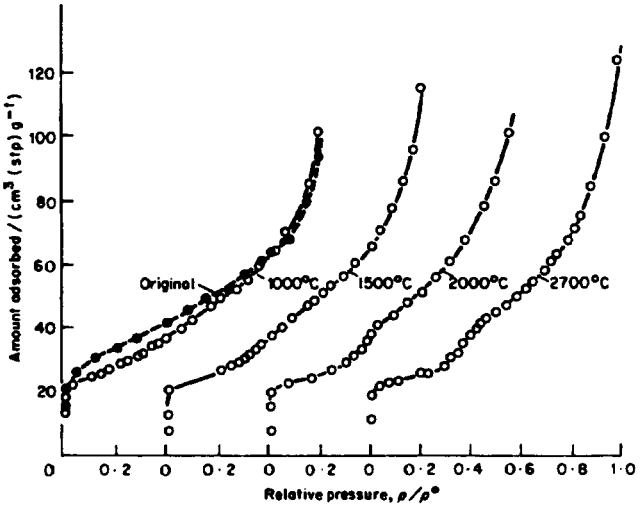

Fig. 2.24 Adsorption isotherms of argon at 78 K on Spheron-6 carbon black, heated to various temperatures indicated in °C on each isotherm. (After Polley, Schaeffer and Smith.[110])

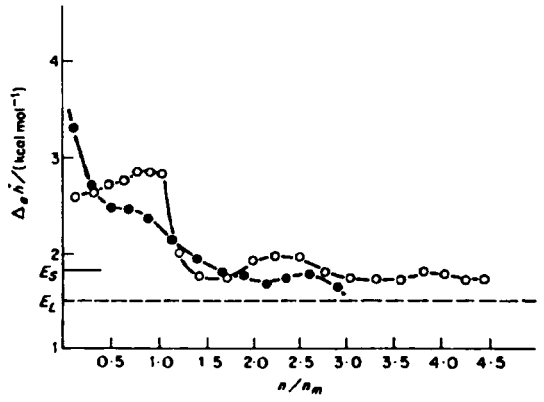

Fig. 2.25 The differential heat of adsorption of argon on carbon blacks[111] at 78 K, before and after graphitization. ●, Spheron; ○, Graphon. E_s and E_l denote molar heat of sublimation and of evaporation respectively.

some points of interest. From general considerations, it seems clear that the point corresponding to monolayer completion will be located somewhere on the tread of the first step. Halsey and his co-workers[105] favour the idea that the *step height* corresponds to the monolayer capacity, this height being measured at the point of inflection of the tread. It has the distinct advantage over Point B, of being almost independent of temperature (cf. Fig. 2.22); and application of the BET method encounters the difficulty that the range of linearity of the BET plot is short.[105]

A further complication which not infrequently appears is the occurrence of a phase transition within the adsorbed film. Detailed investigation of a number of step-like isotherms by Rouquerol,[56,112] Thomy and Duval,[113] and by others[114] has led to the discovery of a kink, or sub-step within the first riser, which has been interpreted in terms of a two-dimensional phase change in the first molecular layer.

2.11 The multilayer region. The Frenkel–Halsey–Hill (FHH) equation

When the film thickens beyond two or three molecular layers, the effect of surface structure is largely smoothed out. It should therefore be possible, as Hill[115] and Halsey[101] have argued, to analyse the isotherm in the multilayer region by reference to surface forces (Chapter 1), the partial molar entropy of the adsorbed film being taken as equal to that of the liquid adsorptive.[116] By application of the 6–12 relation of Chapter 1 (with omission of the r^{-12} term as being negligible except at short distances) Hill was able to arrive at the isotherm equation

$$\ln (p^\circ/p) = b/\theta^3 \tag{2.29}$$

Here b is a parameter, calculable in principle from the properties of the adsorbent and adsorptive, but in practice empirical; the index 3 arises from the integration of the r^{-6} term in Equation (1.8).

Halsey[101] obtained the more general equation

$$\ln (p^\circ/p) = b/\theta^s \tag{2.30}$$

where the index s is no longer necessarily integral, and may be expected to be somewhere between 2 and 3; the constant b is a function of the energy of adsorption in the first layer, but for most purposes must again be regarded as empirical.

The validity of Equation (2.30) may be tested by plotting log log (p°/p) against log (n/n_m) (or, if more convenient, against log n) when a straight line of slope $-s$ should be obtained for the multilayer region of the isotherm. In

practice such a straight line is often obtained,[117] but the slope is rarely equal to $s = 3$ as would be required by Equation (2.29). For nitrogen at 77 K, for example, Zettlemoyer[53] reported values around 2·75 for hydroxylated silicas and lower values (e.g. 2·20 and 2·48) for dehydroxylated silicas; and for low-energy surfaces such as polyethylene or Nylon, s was only 2·1. The value of s may, according to Halsey,[101] be taken as a rough guide to the strength of interaction between the adsorbate and the solid: a large value indicates the presence of specific forces (Section 1.3) and a small value the operation of dispersion forces only.

Recent work,[143] however, has shown that provided the solid is truly non-porous, the value of s for nitrogen does not differ greatly from 2·7, even when the surface of the solid is nonpolar (cf. lines (ii) and (v) of Table 2.13).

TABLE 2.13

Values of the index s in the FHH equation $\ln(p^\circ/p) = b\theta^{-s}$, for adsorption of nitrogen at 77 K on nonporous solids

Solid	s	Reference
Hydroxylated silicas	2·69–2·76	118
Dehydroxylated silica	2·63	118
Aluminas	2·65–2·68	119
Rutile	2·61–2·69	120
Copper phthalocyanines	2·48, 2·51	121

The rather low value obtained with the copper phthalocyanine,[121] a low-energy solid (line (v)), is probably explicable by some reversible capillary condensation in the crevices of the aggregate, the effect of which would be to increase the uptake at a given relative pressure; the plausibility of this explanation is supported by the fact that very low values of s, 1·47–1·77, were obtained with certain other phthalocyanines known to be mesoporous[121] (cf. Chapter 3).

2.12 The concept of a standard isotherm

From a consideration of the nature of the forces bringing about physical adsorption (cf. Chapter 1), it is evident that the detailed course of the isotherm of a given gas on a particular solid at a given temperature must depend on the nature of both the gas and the solid: each adsorbent–adsorbate system will have a unique isotherm. Nevertheless for a given gas,

such as nitrogen, adsorbed on a series of substances differing in total area but not too dissimilar otherwise (such as metal oxides) one might expect the variation in shape from solid to solid to be relatively slight. To a first approximation the different isotherms should thus be superposable by mere adjustment of the scale of units of adsorption. Therefore it should be possible to bring the isotherms into coincidence by expressing the adsorption in normalized units—the amount n/A adsorbed per unit area (Kiselev[122]); or the number n/n_m of statistical monolayers (Harris and Sing,[123] Pierce[124]); or the statistical thickness t of the adsorbed film (Shull,[125] Lippens, Linsen and de Boer[126]) $t = (n/n_m)\sigma$ where σ is the thickness of a single molecular layer.

A pioneer in the search for a standard isotherm was Shull[125] who showed that the isotherms of nitrogen at 77 K on a number of typical solids could be represented by a single curve, though with some scatter. Cranston and Inkley[127] made a similar finding a few years later, for the adsorption of nitrogen on fifteen nonporous solids including glass spherules, precipitated silver and tungsten powder. In 1959 Pierce[124] referred to a "composite isotherm" for nitrogen, again based on the isotherms on numerous solids such as carbon, metal oxides and ionic crystals; this isotherm could be represented over the multilayer range by the FHH equation with index $s = 2{\cdot}75$ and constant $b = 2{\cdot}99$ (Equation (2.30)). Somewhat later de Boer, Linsen and Osinga[109] put forward a "universal t-curve," and tested its validity against the experimental isotherms of nitrogen on a number of metal oxides and other substances. They found that most of them fitted the t-curve well, though there was some deviation at high pressures with silica (Aerosil) and at low pressures ($<0{\cdot}3\,p^\circ$) with graphitized carbon black. A few years later Pierce[128] compared the values of n/n_m for the various isotherms over the range of relative pressures 0·2 to 0·9 and found reasonably good agreement (± 5 per cent) amongst the isotherms of Shull,[125] Cranston and Inkley,[127] Pierce,[124] and Harris and Sing;[123] the isotherm of de Boer and his co-workers[109] deviated more widely (cf. Fig. 2.26).

With the passage of time, it has become increasingly evident that, when reasonably high precision is required, a single standard isotherm (for each adsorptive) is inadequate. In 1969, de Boer[129] suggested that different common isotherms might be needed for different groups of substances: perhaps one curve for metal oxides and graphite, another, slightly different, for metal halides, and a third for metals themselves. Some workers incline to the view that even these classes are too broad. Sing and his co-workers,[130] for example, have put forward a standard isotherm for silica, based on individual isotherms of nitrogen on a wide variety of silicas having surface areas ranging from ~ 1 to $\sim 200\,m^2\,g^{-1}$, and including ground quartz as

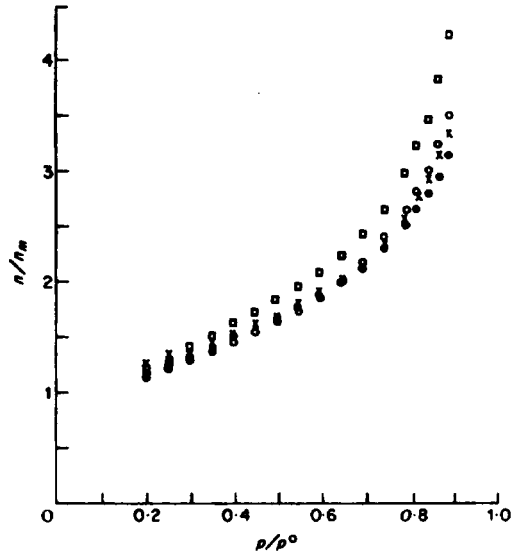

Fig. 2.26 Comparison of a number of standard isotherms of nitrogen at 77 K, plotted as n/n_m against $p/p°$. ○, Shull;[125] ×, Pierce;[124] □, de Boer *et al.*;[109] ●, Cranston and Inkley.[127]

well as various samples of nonporous but amorphous silica. They found that the points fitted on to a common curve very closely, which may be plotted from Table 2.14. A corresponding curve, though based on fewer samples, was put forward[131] for γ-alumina. The two curves are close to one another, but the divergence between them is greater than that between different samples of the same substance. Standard isotherm data for *argon* (at 77 K) on silica have been obtained by various workers.[60,72,137]

The problem of standard isotherms has engaged the attention of Brunauer and his associates,[132] who have put forward five standard isotherms for nitrogen, oxygen and water, characterized by different ranges of the BET c-constant: $200 > c > 50$; $c = 23$; $14{\cdot}5 > c > 10$; $c = 5{\cdot}2$; and (for relative pressures above 0·5), $200 > c > 10$.

The subject has also been taken up recently by Lecloux and Pirard;[133] they have measured the adsorption isotherms of nitrogen on a variety of materials including metal oxides, metal chlorides and some organic polymers, together with the isotherms of argon and oxygen (occasionally of carbon monoxide and carbon dioxide) on a smaller range of solids. From the results they also derived five standard isotherms, again characterized by

TABLE 2.14

Standard data for the adsorption of nitrogen at 77 K on nonporous hydroxylated silica[130]

Relative p/p°	Adsorption per unit area / mol m^{-2}	α_s $(=n/n_{0.4})$
0·001	4·0	0·26
0·005	5·4	0·35
0·01	6·2	0·40
0·02	7·7	0·50
0·03	8·5	0·55
0·04	9·0	0·58
0·05	9·3	0·60
0·06	9·4	0·61
0·07	9·7	0·63
0·08	10·0	0·65
0·09	10·2	0·66
0·10	10·5	0·68
0·12	10·8	0·70
0·14	11·3	0·73
0·16	11·6	0·75
0·18	11·9	0·77
0·20	12·4	0·80
0·22	12·7	0·82
0·24	13·0	0·84
0·26	13·3	0·86
0·28	13·6	0·88
0·30	13·9	0·90
0·32	14·2	0·92
0·34	14·5	0·94
0·36	14·8	0·96
0·38	15·1	0·98
0·40	15·5	1·00
0·42	15·6	1·01
0·44	16·1	1·04
0·46	16·4	1·06
0·50	17·0	1·10
0·55	17·8	1·14
0·60	18·9	1·22
0·65	19·9	1·29
0·70	21·3	1·38
0·75	22·7	1·47
0·80	25·0	1·62
0·85	28·0	1·81
0·90	37·0	2·40

their c-values, but with somewhat different ranges, viz $c > 300$; $300 > c > 100$; $100 > c > 40$; $40 > c > 30$; and $30 > c > 20$). They claim that the standard isotherm for any adsorbent-adsorbate pair can be selected on the basis of the c-value alone.

As will be demonstrated in Chapter 4, however, the presence of micropores distorts the Type II isotherm in a sense which is reflected in a much increased value of the constant c. In such cases the value of c is no guide at all to the course of the isotherm on the external surface. Consequently the appropriate criterion for choosing the correct t-curve for a particular system is the similarity in chemical properties and *not* in c-values between the solid under test and the reference solid.

It is therefore of the utmost importance to ensure that the standard isotherm is based on a solid known to be free of pores, and especially of micropores. Unfortunately, it is not easy to establish the complete absence of porosity in the solids used in adsorption isotherm measurement; the unsuspected presence of such pores may well account for some, at least, of the discrepancies between different published versions of the "standard isotherm" for a given adsorptive.

Deviation from the standard isotherm in the high-pressure region offers a means of detecting the occurrence of capillary condensation in the crevices between the particles of a solid and in any mesopores present within the particles themselves. A convenient device for detecting deviations from the standard is the "t-plot".[134] In the next section the nature and uses of t-plots will be discussed, together with α_s-plots, a later development from them. As will be shown, both of these plots may be used not only for the detection of capillary condensation in mesopores, but also for showing up the presence of micropores and evaluating their volume.

2.13 Analysis of isotherms: t-plots α_s-plots, comparison and f-plots

t-Plots

The task of detecting deviation from the standard isotherm is essentially one of comparing the shape of the isotherm under test with that of the standard, by finding whether the two can be brought into coincidence by mere adjustment of the scale of ordinates. A convenient means of testing for such superposability is provided by the t-plot of Lippens and de Boer.[134] It is based on the *t-curve*, which is a plot of the standard isotherm with t, the statistical thickness of the film, rather than n/n_m, as the dependent variable. The conversion is accomplished by taking n/n_m to be equal to the number of

statistical molecular layers in the film and multiplying by the thickness of a single molecular layer, so that $t = (n/n_m)\sigma$ (t of course represents the *average* thickness; actual thickness must vary from place to place). For nitrogen at 77 K, Lippens, Linsen and de Boer[135] put $\sigma = 3{\cdot}54$ Å, on the assumption that the arrangement of molecules in the film is hexagonal close packing.

The isotherm under test is then re-drawn as a t-plot, i.e. a curve of the amount adsorbed plotted against t rather than against p/p°; the change of independent variable from p/p° to t is effected by reference to the standard t-curve. If the isotherm under test is identical in shape with the standard, the t-plot must be a straight line passing through the origin; its slope ($=b_t$, say) must be equal to n_m/σ, since the number of molecular layers is equal to both t/σ and n/n_m:

$$\frac{n}{n_m} = \frac{t}{\sigma} \tag{2.31}$$

Thus

$$n = \frac{t}{\sigma} n_m \tag{2.32}$$

or

$$n = b_t t \tag{2.33}$$

where

$$b_t = \frac{n_m}{\sigma} \tag{2.34}$$

Consequently, since (cf. Equation (2.1))

$$A = n_m a_m L$$

the specific surface A is related to the slope b_t by the expression

$$A = a_m \sigma L b_t \tag{2.35}$$

For nitrogen at 77 K with $a_m = 16{\cdot}2 \times 10^{-20}$ m^2/molecule, $\sigma = 3{\cdot}54$ Å and t also expressed in Å, we obtain

$$A = 3{\cdot}45 \times 10^5 b_t \tag{2.36}$$

where n is, as usual, expressed in mol g^{-1}. If adsorption is expressed in other units, the coefficient of b_t must be modified proportionately. Thus the specific surface is immediately calculable from the t-plot. The t-plot does not, of course, furnish an independent value of the specific surface, but merely provides a different, and sometimes more convenient, way of arriving at the same value as that obtained from the BET plot (Equation (2.13)).

If the adsorbent contains *mesopores*, capillary condensation will occur in each pore when the relative pressure reaches a value which is related to the radius of the pore by the Kelvin equation, and a Type IV isotherm will

result (cf. Fig. 1.1). A detailed treatment of capillary condensation is deferred to Chapter 3; meanwhile it will be noted that when capillary condensation takes place the uptake at a given relative pressure will be enhanced by the amount of adsorbate condensing in the pores. The *t*-plot will therefore show an upward deviation commencing at the relative pressure at which the finest pores are just being filled (Fig. 2.27).

If *micropores* are introduced into a solid which originally gave a standard Type II isotherm, the uptake is enhanced in the low-pressure region and the isotherm is correspondingly distorted. The effect on the *t*-plot is indicated in

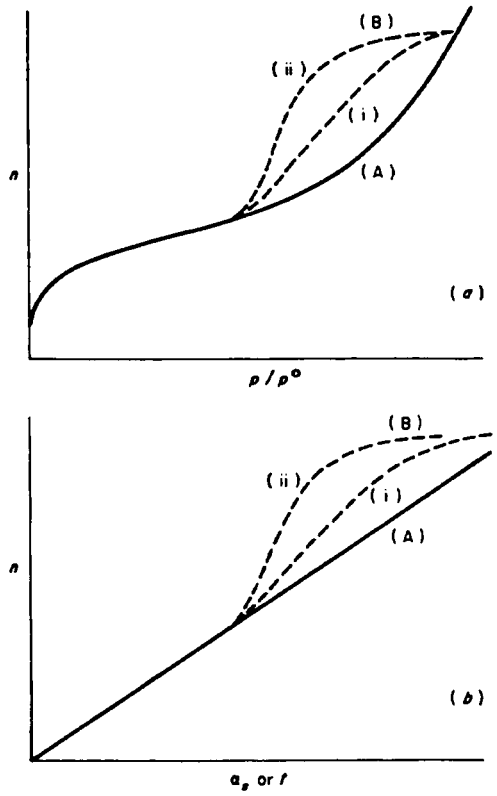

Fig. 2.27 Effect of mesoporosity on the adsorption isotherm and the *t*- (or α_s-) plot. (*a*) (A) is the isotherm on a nonporous sample of the adsorbent; (B) is the isotherm on the same solid when mesopores have been introduced into it, (i) being the adsorption, and (ii) the desorption branch. (*b*) *t*- (or α_s-) plots corresponding to the isotherms in (*a*) (Schematic only.)

Fig. 2.28. The high-pressure branch is still linear (provided mesopores are absent), but when extrapolated to the adsorption axis it gives a positive intercept which is equivalent to the micropore volume. The slope of the linear branch is now proportional to the *external* surface area of the solid. Microporosity is dealt with in detail in Chapter 4.

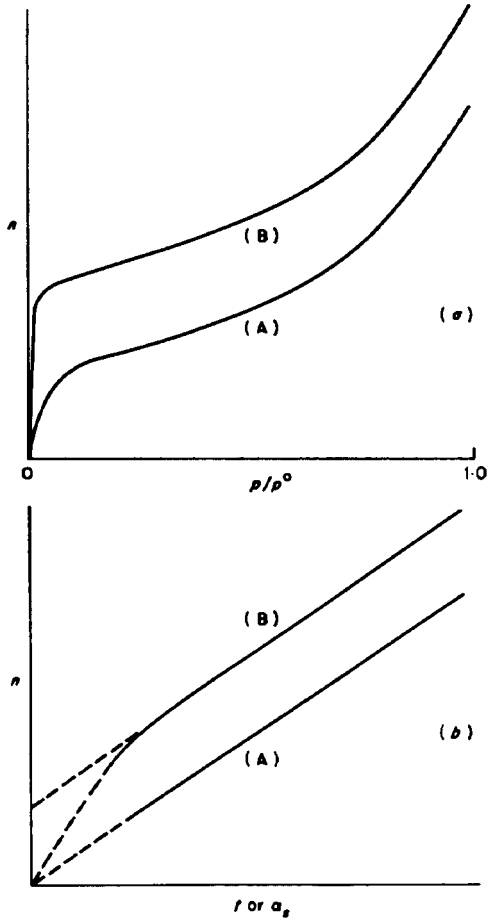

Fig. 2.28 Effect of microporosity of the isotherm and t- (or α_s-) plot. (*a*) (A) is the isotherm on a nonporous sample of the adsorbent; (B) is the isotherm of the same solid when micropores have been introduced into it. (*b*) t- (or α_s-) plots corresponding to the isotherms of (*a*). (Schematic only.)

α_s-Plots

The *t*-curve and its associated *t*-plot were originally devised as a means of allowing for the thickness of the adsorbed layer on the walls of the pores when calculating pore size distribution from the (Type IV) isotherm (Chapter 3). For the purpose of testing for conformity to the standard isotherm, however, a knowledge of the numerical thickness is irrelevant; since the object is merely to compare the shape of the isotherm under test with that of the standard isotherm, it is not necessary to involve the number of molecular layers n/n_m or even the monolayer capacity itself.

It is sufficient, as Sing has pointed out,[136] merely to replace n_m as normalizing factor by n_s, the amount adsorbed at some fixed relative pressure $(p/p^\circ)_s$, in practice taken as $(p/p^\circ)_s = 0{\cdot}4$. The normalized adsorption $n/n_{0{\cdot}4}$ $(=\alpha_s)$, obtained from the isotherm on a reference sample of the solid, is then plotted against p/p°, to obtain a standard α_s-curve rather than a *t*-curve. The α_s-curve can then be used to construct an α_s-plot from the isotherm of a test sample of the solid, just as the *t*-curve can be used to produce a *t*-plot. If a straight line through the origin results, one may infer that the isotherm under test is identical in shape with the standard; the slope b_α of the linear branch of the α_s-plot will be equal to $n_{0{\cdot}4}$, just as the slope b_t of the *t*-plot was equal to n_m/σ (cf. Equation (2.34)).

A particular advantage of the α_s-method is that its applicability is not restricted to nitrogen.[136] It offers a simple but effective means of testing for the identity in shape of the isotherms of any suitable adsorptive on a given set of samples of the same substance (obtained, for example, by grinding for different periods of time). Any one of the samples may be taken as reference material for the construction of the α_s-curve. If the samples differ only in surface area and not in porosity, their α_s-plots will be straight lines passing through the origin, with slope $= b_\alpha$, say; if mesoporosity or macroporosity has developed in the samples, there will be deviation from linearity of the kind indicated in Figs 2.27 and 2.28.

To estimate the specific surface A(test) of a test sample from the slope of its α_s-plot, one notes that

$$\frac{b_\alpha(\text{test})}{b_\alpha(\text{reference})} = \frac{n_{0{\cdot}4}(\text{test})}{n_{0{\cdot}4}(\text{reference})} = \frac{A(\text{test})}{A(\text{reference})} \tag{2.37}$$

i.e.
$$A(\text{test}) = \frac{b_\alpha(\text{test})}{b_\alpha(\text{reference})} \times A(\text{reference}) \tag{2.38}$$

Thus, if the specific surface of the reference material is known (e.g. from the nitrogen isotherm) the specific surface of the test sample can be calculated from the ratio of the slopes of the α_s-plots. The specific surfaces of all the

samples of a series can therefore be calculated without any reference to their monolayer capacities or to the value of a_m for the adsorbate in question. The way is thereby opened up to the user of a wide range of adsorptives in surface area determination, no matter whether c turns out to be small, Point B to be ill-defined, or the value of a_m to be questionable. The α_s-method is still applicable even when the isotherm, as with carbon tetrachloride on nonporous silica, is of Type III (cf. Chapter 5).

In view of the widespread use of nitrogen and argon in surface area and porosity studies, data for the construction of the standard α_s-curves for these adsorbates on hydroxylated silica, are given in Table 2.14 (p. 93) for nitrogen and in Table 2.15 for argon. From the arguments of Section 2.12, these should be adequate for other oxides such as alumina, if high accuracy is not called for.

TABLE 2.15

Standard data for the adsorption of argon at 77 K on nonporous hydroxylated silica[80]

Relative pressure p/p°	α_s $(=n/n_{0.4})$	Relative pressure p/p°	α_s $(=n/n_{0.4})$
0·01	0·243	0·30	0·876
0·02	0·324	0·32	0·900
0·03	0·373	0·34	0·923
0·04	0·413	0·36	0·948
0·05	0·450	0·38	0·973
0·06	0·483	0·40	1·000
0·07	0·514	0·42	1·022
0·08	0·541	0·44	1·048
0·09	0·563	0·46	1·064
0·10	0·583	0·48	1·098
0·11	0·602	0·50	1·123
0·12	0·620	0·52	1·148
0·13	0·638	0·54	1·172
0·14	0·657	0·56	1·198
0·15	0·674	0·58	1·225
0·16	0·689	0·60	1·250
0·17	0·705	0·62	1·275
0·18	0·719	0·64	1·300
0·19	0·733	0·66	1·327
0·20	0·748	0·68	1·354
0·22	0·773	0·70	1·387
0·24	0·801	0·72	1·418
0·25	0·813	0·74	1·451
0·26	0·826	0·76	1·486
0·28	0·851	0·78	1·527

As may be seen from Table 2.14, the uptake of nitrogen at $p/p^\circ = 0{\cdot}4$ was $15{\cdot}5\ \mu\text{mol}\,\text{m}^{-2}$, so that b_s(reference) when A(reference) $= 1\ \text{m}^2$ was $15{\cdot}5\ \mu\text{mol}\,\text{m}^{-2}$. Insertion of these values in Equation (2.38) gives

$$A(\text{test}) = 6{\cdot}5 \times 10^4 b_s(\text{test})$$

if the uptake on the test samples is expressed in $\text{mol}\,\text{g}^{-1}$. Thus the specific surface of any member of the series of test samples can be calculated at once from the slope of its α_s-plot. If the uptake is expressed in other units, a modified value of the coefficient of b_s is required.

Comparison plots

A simple device for comparing the shapes of two isotherms of a given gas on two different adsorbents is merely to plot the amount adsorbed on one adsorbent with that adsorbed on the other at the same pressure or relative pressure.[66] If the isotherms are identical in shape throughout their course, the comparison plot will be a straight line passing through the origin, its slope being equal to the ratio of the surface areas of the two adsorbents.[141] Figure 2.29(*a*) shows a comparison plot for nitrogen adsorption on a carbon black before and after graphitization, the corresponding isotherms being given in Fig. 2.29(*b*). The high-pressure branch BC of the comparison plot (which corresponds to the third and higher layers) is linear and when back-extrapolated passes through the origin. This clearly shows that the effect of the localized structure of the monolayer on graphitized carbon which is obvious in the lower-pressure region has virtually disappeared once the thickness of the film exceeds two molecule layers (cf. p. 91).

The comparison plot offers a particularly simple and direct means of comparing the shapes of a pair of isotherms; but for more general applications which involve a number of samples of a solid covering a wide range of specific surface, the α_s-method is preferable. The α_s-curve represents a convenient way of recording and using the reference isotherm.

f-Plots

Another simple way of comparing the shape of the isotherm on a given solid with that on a reference sample is to read off the ordinates of the two isotherms at regular intervals of relative pressure, calculate the value f of their ratio, and plot f against p/p°. Changes in the shape of the isotherm on the given solid from that on the reference sample will show up as deviations of the f-plot from the horizontal.[138,139]

The method may be illustrated by reference to a study of the effect of compaction of a non-porous powder. The nitrogen isotherm on a silica

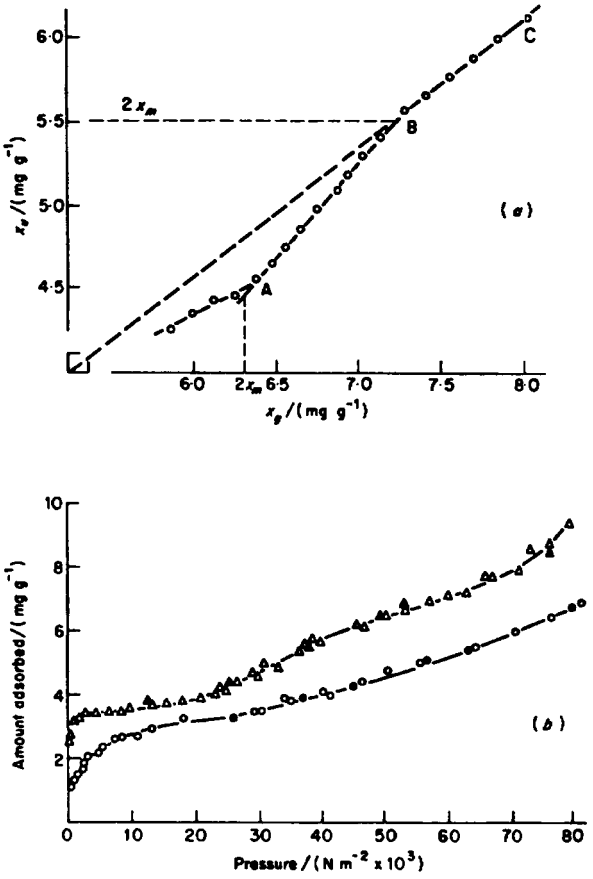

Fig. 2.29 Comparison of nitrogen adsorption at 78 K on a carbon black (Sterling FT) before and after graphitization[66] (*a*) The amount x_u adsorbed on the ungraphitized sample plotted against the amount x_g adsorbed on the graphitized sample, at the same pressure. (*b*) The corresponding isotherms: ○, adsorption, ●, desorption on the ungraphitized sample (4 runs); △, adsorption; ▲ desorption, on the graphitized sample (4 runs).

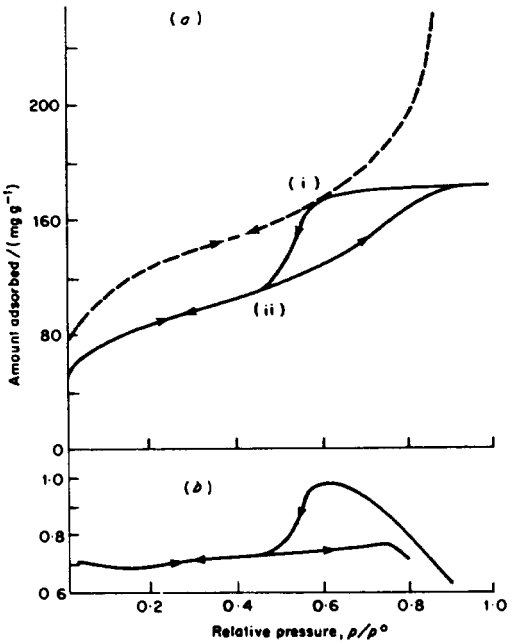

Fig. 2.30 Adsorption of nitrogen at 77 K on a silica powder:[138] (*a*) adsorption isotherms (*b*) *f*-plot. Broken line, uncompacted powder; continuous line, power compacted at $2{\cdot}00 \times 10^9$ N m^2 (130 ton in^2). (→) adsorption; (←) desorption. *f* is the ratio of the amount adsorbed on the powder to the amount adsorbed on the compact at the same relative pressure.

powder before compaction is shown in curve (i) of Fig. 2.30(*a*), and after compaction in curve (ii). The corresponding *f*-plot (with the uncompacted powder taken as reference sample) is given in Fig. 2.30(*b*); it shows that the *adsorption* branch is not greatly affected in shape by compaction even though its level (and with it, the surface area) has diminished considerably.

2.14 General conclusions: determination of specific surface from adsorption isotherms

The BET method for calculation of specific surface A involves two steps: evaluation of the monolayer capacity n_m from the isotherm, and conversion of n_m into A by means of the molecular area a_m.

To obtain a reliable value of n_m from the isotherm it is necessary that the monolayer shall be virtually complete before the build-up of higher layers commences; this requirement is met if the BET parameter c is not too low, and will be reflected in a sharp knee of the isotherm and a well defined Point B. For conversion of n_m into A, the ideal adsorptive would be one which is composed of spherically symmetrical molecules and always forms a non-localized film, and therefore gives the same value of a_m on all adsorbents. Non-localization demands a low value of c; as c increases the adsorbate molecules move more and more closely into registry with the lattice of the adsorbent, so that a_m becomes increasingly dependent on the lattice dimensions of the adsorbent, and decreasingly dependent on the molecular size of the adsorbate.

The net result of these two opposing requirements for the successful application of the BET method is that c shall be neither too high nor too low—in practice, that it shall lie between, say, ~ 50 and ~ 150. It is because nitrogen comes closest to meeting these conditions when adsorbed on an extensive range of solids that it has become the most generally used adsorptive for surface area determination, except when the specific surface is below $\sim 1\,m^2\,g^{-1}$. The widely accepted value of $a_m(N_2) = 16{\cdot}2\,Å^2$, whilst satisfactory in the majority of cases, may need modification with a minority of adsorbents such as graphitized carbon black. Within recent years, the claims of argon as a rival to nitrogen have been increasingly heard, with $a_m = 16{\cdot}6\,Å^2$ or $18{\cdot}0\,Å^2$ according as the supercooled liquid or the solid is taken as the reference state.

When other adsorptives, such as those detailed in Section 2.9, are employed for surface area determination, calibration against nitrogen or argon is strongly recommended, so long as the specific surface exceeds $\sim 1\,m^2\,g^{-1}$. For areas below this figure the calibration becomes too inaccurate, and an alternative adsorptive, usually krypton, has to be used.

As explained in Section 2.13, the use of α_s-plots makes it possible to avoid the involvement of either n_m or a_m when an alternative adsorptive is being used for evaluating the surface areas of a set of related solids. It is then no longer necessary to exclude the use of isotherms having a low value of c, consequently the method is applicable even if the isotherm of the alternative adsorptive is of Type III (cf. Chapter 5). Calibration of one sample by nitrogen or argon adsorption is still required.

As will be demonstrated in Chapter 4, an isotherm which is reversible and of Type II is quite compatible with the presence of micropores. If such pores are present, the isotherm will be distorted in the low-pressure region, the value of c will be greatly enhanced, and the specific surface derived by the BET procedure will be erroneously high. In particular, a BET specific surface in excess of $\sim 500\,m^2\,g^{-1}$ should be taken as a warning that

considerable microporosity may be present. Also, a value of c of the order of several hundreds is a strong indication of either the presence of microporosity, or adsorption on active sites, or even of chemisorption—which must be taken into account in calculation of the surface area.

Accuracy

The high degree of accuracy attainable in some branches of chemistry and physics is out of the question where evaluation of specific surface from adsorption data is concerned. Even in the favourable case of nitrogen or argon, a divergence of at least ± 10 per cent from the actual area of the solid must be reckoned with, owing to theoretical factors as yet not susceptible of accurate quantitative assessment. In addition, there are far from negligible uncertainties of an experimental origin, the importance of which is strikingly illustrated by results of a project in the United Kingdom,[140] designed to establish a bank of substances to serve as surface area standards. The project embraced thirteen laboratories, all well experienced in the field, and the participants determined detailed isotherms of nitrogen (often 30–40 points), calculating both the specific surface, based on $a_m(N_2) = 16{\cdot}2\,\text{Å}^2$, and the value of BET parameter c.

Surprising differences emerged between the results from different laboratories, even though Point B was reasonably well defined. Only four of the original eight substances were deemed suitable to become standards, and even amongst these the range of values reported was quite wide: 267 to $289\,m^2\,g^{-1}$ for the best, and 144 to $174\,m^2\,g^{-1}$ for the worst. Critical assessment of all the results caused elimination of many of them and led to the final list of Table 2.16.

The differences between the various laboratories were traced to a number of factors including: imperfect control of the conditions of outgassing (time, temperature, final pressure); variation in temperature of the sample during the experiment; inadequate monitoring of the saturation vapour pressure; purity of nitrogen (e.g. unsuspected presence of oxygen); and incidence of leaks in the apparatus. In addition, since the BET plot is never linear over the whole range of relative pressure, there is some latitude in locating the best straight line.

The degree of uncertainty of ± 10 per cent or more, inseparable from estimates of specific surface from adsorption isotherms, even those of nitrogen, may seem disappointing. In fact, however, attainment of this level of accuracy is a notable achievement in a field where, prior to the development of the BET method, even the order of magnitude of the specific surface of highly disperse solids was in doubt. The adsorption method still provides the only means of determining the specific surface of a mass of non-

TABLE 2.16

Surface area standard, based on $a_m(N_2) = 16{\cdot}2\,Å^2$

Solid	Specific surface/($m^2\,g^{-1}$) with standard deviation	No. of laboratories (see text)
Graphitized carbon (Vulcan 36-2700)	$71{\cdot}3 \pm 2{\cdot}7$	6
Graphitized carbon (Sterling FT-2700)	$11{\cdot}0 \pm 0{\cdot}8$	5
Plasma produced silica (TK 800)	$165{\cdot}8 \pm 2{\cdot}1$	4
Mesoporous silica gel (Gasil (1))	$286{\cdot}2 \pm 3{\cdot}5$	3

† U.K. Project[140] organized by Society of Chemical Industry, International Union of Pure and Applied Chemistry Commission on Surface and Colloid Chemistry, and National Physical Laboratory.

porous powder or of a porous solid large enough to constitute a representative sample. Microscopic examination is necessarily confined to a minute sample of the material, so that large numbers of such samples have to be examined if meaningful results for the external specific surface area are to be obtained; and any estimates of the internal area—formed by the walls of pores or the sides of crevices—are necessarily very crude.

Furthermore, it must be remembered that highly disperse materials are, from their very nature, difficult to prepare with exactly reproducible surface properties, in respect of either the extent of the surface or the nature of the surface itself. Consequently, highly precise values of the absolute area of individual samples, even if attainable by some method as yet undeveloped, would be of little more value in practice than the BET specific surface, calculated from carefully measured isotherms.

References

1. S. Brunauer, P. H. Emmett and E. Teller, *J. Amer. Chem. Soc.* **60**, 309 (1938).
2. I. Langmuir, *J. Amer. Chem. Soc.* **38**, 2221 (1916).
3. I. Langmuir, *J. Amer. Chem. Soc.* **40**, 1361 (1918).
4. J. H. de Boer, "The Dynamical Character of Adsorption", p. 61, Oxford University Press, London (1953).
5. C. Kemball and G. D. L. Schreiner, *J. Amer. Chem. Soc.* 72, 5605 (1950).
6. T. L. Hill, *J. Chem. Phys.* **14**, 263 (1946).

7. W. A. Steele, "The Interaction of Gases with Solid Surfaces", p. 222, Pergamon Press, Oxford (1974); K. S. W. Sing *in* "Colloid Science" (ed. D. H. Everett), Vol. 1, p. 1, Specialist Periodical Reports, Chemical Society, London (1973).
8. S. J. Gregg and J. Jacobs, *Trans. Faraday Soc.* **44**, 574 (1948).
9. D. C. Jones, *J. Chem. Soc.* 126 (1951); B. Génot, *J. Colloid Interface Sci.* **50**, 413 (1975).
10. Locke White, *J. Phys. Chem.* **51**, 644 (1947).
11. G. D. Halsey, *J. Chem. Phys.* **16**, 931 (1948).
12. M. A. Cook, *J. Amer. Chem. Soc.* **70**, 2925 (1948).
13. R. M. Barrer, N. MacKenzie and D. McLeod, *J. Chem. Soc.* 1736 (1952).
14. D. M. Young and A. D. Crowell, "Physical Adsorption of Gases", p. 156, Butterworths, London (1962).
15. R. T. Davis, T. W. De Witt and P. H. Emmett, *J. Phys. Chem.* **51**, 1232 (1947).
16. D. S. MacIver and P. H. Emmett, *J. Amer. Chem. Soc.* **60**, 824 (1956).
17. Yu. F. Berezkina, M. M. Dubinin and A. I. Sarakhov, *Akac. Nauk S.S.S.R. Ser. Khim.* 2653 (1969 (*Bull. Akad. Sci. USSR, Chem. Sci.* 2495 (1969)).
18. K. S. W. Sing, *Chem. and Ind.* p. 321 (1964).
19. H-H. Hsing and W. H. Wade, *J. Colloid Interface Sci.* **47**, 490 (1974).
20. M. R. Harris and K. S. W. Sing, *Chem. and Ind.* p. 487 (1959).
21. G. Pickett, *J. Amer. Chem. Soc.* **67**, 1958 (1945).
22. R. B. Anderson, *J. Amer. Chem. Soc.* **68**, 686 (1946).
23. S. Brunauer, J. Skalny and E. E. Bodor, *J. Colloid Interface Sci.* **30**, 546 (1969).
24. C. G. Shull, *J. Amer. Chem. Soc.* **70**, 1410 (1948).
25. P. H. Emmett and S. Brunauer, *J. Amer. Chem. Soc.* **59**, 1553 (1937).
26. S. Brunauer and P. H. Emmett, *J. Amer. Chem. Soc.* **57**, 1754 (1935).
27. D. M. Young and A. D. Crowell, "Physical Adsorption of Gases", p. 198, Butterworths, London (1962).
28. D. Brennan, M. J. Graham and F. H. Hayes, *Nature* **199**, 1152 (1963).
29. L. E. Drain and J. L. Morrison, *Trans. Faraday Soc.* **48**, 840 (1952); **49**, 654 (1953).
30. Y. Grillet, F. Rouquerol and J. Rouquerol, *J. Colloid Interface Sci.* **70**, 239 (1979).
31. T. L. Hill, P. H. Emmett and L. G. Joyner, *J. Amer. Chem. Soc.* **73**, 5102 (1952); E. L. Pace and A. R. Siebert, *J. Phys. Chem.* **64**, 961 (1960); J. R. Sams, G. Constabaris and G. D. Halsey, *J. Phys. Chem.* **66**, 2154 (1962); J. de D. Lopez-Gonzalez, F. G. Carpenter and V. R. Deitz, *J. Phys. Chem.* **65**, 1112 (1961).
32. C. H. Amberg, W. B. Spencer and R. A. Beebe, *Canad. J. Chem.* **33**, 305 (1955); F. A. Putnam and T. Fort, *J. Phys. Chem.* **79**, 459 (1975).
33. A. V. Kiselev, *in* "Proceedings of the Second International Congress on Surface Activity", **II**, p. 168, Butterworths, London (1957).
34. A. A. Isirkyan and A. V. Kiselev, *J. Phys. Chem.* **65**, 601 (1961); **66**, 205, 210 (1962); N. N. Avgul, A. V. Kiselev, I. A. Lygina and E. A. Mikhailova, *Izv. Akad. Nauk, Ot. Khim. Nauk.* 769 (1962); G. I. Berezin and A. V. Kiselev, *J. Colloid Interface Sci.* **22**, 161 (1966); J. H. Clint, *J. Chem. Soc., Faraday Trans. I*, **68**, 2239 (1972).
35. L. G. Joyner and P. H. Emmett, *J. Amer. Chem. Soc.* **70**, 2353 (1948).
36. L. E. Drain, *Sci. Progr.* **42**, 608 (1954).
37. L. M. Dormant and A. W. Adamson, *J. Colloid Interface Sci.* **28**, 459 (1968).

38. R. A. Beebe and D. M. Young, *J. Phys. Chem.* **58**, 95 (1954); S. Ross and W. W. Pultz, *J. Colloid Sci.* **13**, 397 (1958); B. G. Aristov and A. V. Kiselev, *Russ. J. Phys. Chem. (transl.)* **38**, 1077 (1964).
39. T. N. Rhodin, *J. Amer. Chem. Soc.* **72**, 569 (1950); T. N. Rhodin, *J. Phys. Chem.* **57**, 1437 (1953).
40. V. R. Deitz and N. H. Turner, *in* "Surface Area Determination", Proc. Int. Symp. 1969 (eds. D. H. Everett and R. H. Ottewill) p. 43, Butterworths, London (1970).
41. J. C. Arnell and G. O. Henneberry, *Canad. J. Research* **26A**, 29 (1948).
42. R. B. Anderson and P. H. Emmett, *J. Appl. Phys.* **19**, 367 (1948).
43. A. Claus, H. P. Boehm and U. Hofmann, *Z. Anorg. Chem.* **290**, 35 (1957).
44. E. Robens, *in* "Surface Area Determination", Proc. Int. Symp. 1969 (eds. D. H. Everett and R. H. Ottewill), p. 51, Butterworths, London (1970).
45. W. W. Ewing and F. W. J. Liu, *J. Colloid Sci.* **8**, 205 (1953).
46. G. B. Alexander and R. K. Iler, *J. Phys. Chem.* **57**, 933 (1953).
47. S. Partyka, F. Rouquerol and J. Rouquerol, *J. Colloid Interface Sci.* **68**, 21 (1979).
48. W. D. Harkins and G. Jura, *J. Amer. Chem. Soc.* **66**, 1362 (1944).
49. B. L. Harris and P. H. Emmett, *J. Phys. Chem.* **53**, 811 (1949).
50. A. V. Kiselev and Y. A. Eltekov, *in* "Proceedings of the Second International Congress on Surface Activity", II, pp. 213, 228, Butterworths, London (1957).
51. R. E. Day, G. D. Parfitt and J. Peacock, *Disc. Faraday Soc.* **52**, 215 (1971).
52. C. Pierce and B. Ewing, *J. Phys. Chem.* **68**, 2562 (1964); C. Pierce, *J. Phys. Chem.*, **73**, 813 (1969); B. W. Davis and R. G. Varsanik, *J. Colloid Interface Sci.* **37**, 870 (1971).
53. A. C. Zettlemoyer, *J. Colloid Interface Sci.* **28**, 343 (1968).
54. G. J. C. Frohnsdorff and G. L. Kington, *Trans. Faraday Soc.* **557**, 1173 (1959).
55. J. D. Carruthers, D. A. Payne, K. S. W. Sing and L. J. Stryker, *J. Colloid Interface Sci.* **36**, 205 (1971).
56. J. Rouquerol, S. Partyka and F. Rouquerol, *J. Chem. Soc., Faraday Trans. I*, **73**, 306 (1977); J. Rouquerol, F. Rouquerol, C. Pérès, Y. Grillet and M. Boudellal, *in* "Characterisation of Porous Solids", Proc. Int. Symp. 1978 (eds. S. J. Gregg, K. S. W. Sing and H. F. Stoeckli), p. 107, Soc. Chem. Ind., London (1979).
57. T. T. Chung and J. G. Dash, *Surface Science* **66**, 559 (1977).
58. D. N. Furlong, F. Rouquerol, J. Rouquerol and K. S. W. Sing, *J. Chem. Soc. Faraday Trans.* **1**, **76**, 774 (1980).
59. A. L. McClellan and H. F. Harnsberger, *J. Colloid Interface Sci.* **23**, 577 (1967).
60. D. A. Payne, K. S. W. Sing and D. H. Turk, *J. Colloid Interface Sci.* **43**, 287 (1973).
61. S. Brunauer and P. H. Emmett, *J. Amer. Chem. Soc.* **59**, 2682 (1937).
62. P. L. Walker, R. J. Foresti and C. C. Wright, *Ind. Eng. Chem.* **45**, 1703 (1953).
63. E. L. Pace and A. R. Siebert, *J. Phys. Chem.* **64**, 961 (1960).
64. B. G. Aristov and A. V. Kiselev, *Russ. J. Phys. Chem. (transl.)*, **37**, 1359 (1963).
65. W. R. Smith and D. G. Ford, *J. Phys. Chem.* **69**, 3587 (1965).
66. C. E. Brown and P. G. Hall, *Trans. Faraday Soc.* **67**, 3558 (1971).
67. C. F. Prenzlow, H. R. Beard and R. S. Brundage, *J. Phys. Chem.* **73**, 969 (1969).
68. W. D. Harkins, "The Physical Chemistry of Surface Films", p. 227, Reinhold, New York (1952).

69. K. Kodera and Y. Onishi, *Bull. Chem. Soc. Japan* **33**, 338 (1960).
70. M. R. Harris and K. S. W. Sing, *Chem. and Ind.* 757 (1967).
71. D. R. Bassett, E. A. Boucher and A. C. Zettlemoyer, *J. Colloid Interface Sci.* **27**, 649 (1968).
72. G. A. Nicolaon and S. J. Teichner, *J. Colloid Interface Sci.* **38**, 172 (1972).
73. M. L. Corrin, *J. Amer. Chem. Soc.* **73**, 4061 (1951).
74. H. L. Pickering and H. C. Eckstrom, *J. Amer. Chem. Soc.* **64**, 4775 (1952).
75. R. B. Gammage, E. L. Fuller and H. F. Holmes, *J. Colloid Interface Sci.* **34**, 428 (1970).
76. B. W. Davis, *J. Colloid Interface Sci.* **31**, 353 (1969).
77. D. H. Turk, Ph.D. Thesis, Brunel University (1972).
78. B. G. Aristov and A. V. Kiselev, *Koll. Zhur.* **27**, 299 (1965); N. K. Nair and A. W. Adamson, *J. Phys. Chem.* **74**, 2229 (1970); R. Sh. Mikhail and S. Brunauer, *J. Colloid Interface Sci.* **52**, 572 (1975).
79. R. A. Beebe, J. B. Beckwith and J. M. Honig, *J. Amer. Chem. Soc.* **67**, 1554 (1945).
80. P. J. Malden and J. D. F. Marsh, *J. Phys. Chem.* **63**, 1309 (1959).
81. M. Troy and J. P. Wightman, *J. Vac. Sci. Technol.* **8**, 743 (1971).
82. A. Knowles and J. B. Moffatt, *J. Colloid Interface Sci.* **37**, 860 (1971).
83. K. S. W. Sing and D. Swallow, *Proc. Brit. Ceram. Soc.* No. 5, 39 (1965).
84. D. Brennan, M. J. Graham and F. H. Hayes, *Nature* **199**, 1152 (1963).
85. J. J. Lander and J. Morrison, *Surface Sci.* **6**, 1 (1967).
86. R. H. Roberts and J. Pritchard, *Surface Sci.* **54**, 687 (1976).
87. D. Nicholson and K. S. W. Sing, *in* "Colloid Science" (ed. D. H. Everett), Vol. 3, p. 1, Specialist Periodical Reports, Chemical Society, London (1979).
88. A. V. Kiselev, *in* "Proceedings of the Second International Congress on Surface Activity", II, p. 168, Butterworths, London (1957).
89. J. H. Clint, *J. Chem. Soc., Faraday Trans. I* **68**, 2239 (1972).
90. R. B. Gammage, Ph.D. Thesis, Exeter University (1964).
91. C. Brown and H. H. Uhlig, *J. Amer. Chem. Soc.* **69**, 462 (1947).
92. A. G. Bezus, V. P. Dreving and A. V. Kiselev, *Russ. J. Phys. Chem.* (transl.), **38**, 30 (1964).
93. A. A. Isirikyan and A. V. Kiselev, *J. Phys. Chem.* **65**, 601 (1961).
94. P. Meehan, T. Rayment, R. K. Thomas, G. Bomchil and J. W. White, *J. Chem. Soc., Faraday Trans. I*, **76**, 2011 (1980).
95. G. Curthoys, V. Ya Davydov, A. V. Kiselev, S. A. Kiselev and B. V. Kuznetsov, *J. Colloid Interface Sci.* **48**, 58 (1974).
96. A. V. Kiselev, *in* "The Structure and Properties of Porous Materials" (eds. D. H. Everett and F. S. Stone), p. 195. Butterworths, London (1958).
97. K. M. Hanna, I. Odler, S. Brunauer, J. Hagymassy and E. E. Bodor, *J. Colloid Interface Sci.* **45**, 27 (1973).
98. A. A. Isirikyan and I. A. Kazmenko, *Koll. Zhur.* **30**, 220 (1968).
99. N. O. Lemcoff and K. S. W. Sing, *J. Colloid Interface Sci.* **61**, 227 (1977).
100. P. S. Clough and M. R. Harris, *Chem. and Ind.* 343 (1969).
101. G. D. Halsey, *J. Chem. Phys.* **16**, 931 (1948); *Adv. Catalysis* 263 (1952).
102. D. Nicholson and R. G. Silvester, *J. Colloid Interface Sci.* **62**, 447 (1977).
103. C. H. Amberg, W. B. Spencer and R. A. Beebe, *Canad. J. Chem.* **33**, 305 (1955).
104. Y. Larher, *J. Colloid Interface Sci.* **37**, 836 (1971).
105. C. F. Prenzlow and G. D. Halsey, *J. Phys. Chem.* **61**, 1158 (1957).

106. J. D. Dash, "Films on Solid Surfaces", p. 217, Academic Press, New York and London (1975); J. H. Singleton and G. D. Halsey, *J. Phys. Chem.* **58**, 330, 1011 (1954); *Canad. J. Chem*, 33, 184 (1955); A. Thomy and X. Duval, *J. Chim. Phys.* **66**, 1966 (1969).
107. L. Bonnetain, X. Duval and M. Letort, *Comp. Rend.* **234**, 1363 (1952); L. Bonnetain, X. Duval, M. Letort and P. Souny, *Comp. Rend.* **244**, 75 (1957); A. Thomy and X. Duval, *J. Chim. Phys.* **67**, 286 (1970).
108. B. Gènot, *J. Chim. Phys.* **70**, 1565 (1973).
109. J. H. de Boer, B. G. Linsen and Th. J. Osinga, *J. Catalysis* **4**, 643 (1965).
110. M. H. Polley, W. D. Schaeffer and W. R. Smith, *J. Phys. Chem.* **57**, 469 (1953).
111. R. A. Beebe, B. Millard and J. Cynarski, *J. Amer. Chem. Soc.* **75**, 839 (1953).
112. Y. Grillet, F. Rouquerol and J. Rouquerol, *J. Colloid Interface Sci.* **70**, 239 (1979).
113. A. Thomy and X. Duval, *J. Chim. Phys.* **67**, 1101 (1970).
114. D. Nicholson and K. S. W. Sing, *in* "Colloid Science" (ed. D. H. Everett), Vol. 3, p. 6, Specialist Periodical Report, Chemical Society, London (1979); C. G. Shaw and S. C. Fain, *Surface Sci.* **83**, 1 (1979).
115. T. L. Hill, *Adv. Catalysis* **IV**, 236 (1952).
116. W. A. Steele, *J. Colloid Interface Sci.* **75**, 13 (1980).
117. C. Pierce, *J. Phys. Chem.* **64**, 1184 (1960); C. Pierce and B. Ewing, *J. Amer. Chem. Soc.* **84**, 4070 (1962); K. S. W. Sing, *in* "Colloid Science" (ed. D. H. Everett), Vol. 1, p. 48, Specialist Periodical Reports, Chemical Society, London (1973).
118. F. S. Baker and K. S. W. Sing, *J. Colloid Interface Sci.* **55**, 605 (1976).
119. D. A. Payne, Ph.D. Thesis, Brunel University (1970).
120. A. McLeod, Ph.D. Thesis, Brunel University (1979).
121. C. R. S. Dean, R. R. Mather, D. L. Segal and K. S. W. Sing, *in* "Characterisation of Porous Solids" (eds. S. J. Gregg, K. S. W. Sing and H. F. Stoeckli), p. 359, Soc. Chem. Ind., London (1979).
122. A. V. Kiselev, *in* "Structure and Properties of Porous Materials" (eds. D. H. Everett and F. S. Stone), p. 200, Butterworths, London (1958).
123. M. R. Harris and K. S. W. Sing, *in* "Proceedings of the Third International Congress Surface Activity (Cologne)", **II**, p. 42 (1960); *Chem. Ind.* 487 (1959).
124. C. Pierce, *J. Phys. Chem.* **63**, 1076 (1959).
125. C. G. Shull, *J. Amer. Chem. Soc.* **70**, 1405 (1948).
126. B. C. Lippens, B. G. Linsen and J. H. de Boer, *J. Catalysis* **3**, 32 (1964).
127. R. W. Cranston and F. A. Inkley, *Adv. Catalysis* **9**, 143 (1957).
128. C. Pierce, *J. Phys. Chem.* **72**, 3673 (1968).
129. J. H. de Boer, *in* "Surface Area Determination", Proc. Int. Symp., 1968 (eds. D. H. Everett and R. H. Ottewill, p. 24, Butterworths, London (1970).
130. J. D. Carruthers, P. A. Cutting, R. E. Day, M. R. Harris, S. A. Mitchell and K. S. W. Sing, *Chem. and Ind.* 1772 (1968); M. R. Bhambhani, P. A. Cutting, K. S. W. Sing and D. H. Turk, *J. Colloid Interface Sci.* **38**, 109 (1972).
131. D. A. Payne and K. S. W. Sing, *Chem. and Ind.* 918 (1969).
132. S. Brunauer, R. Sh. Mikhail and E. E. Bodor, *J. Colloid Interface Sci.* **24**, 451 (1967); K. M. Hanna, I. Odler, S. Brunauer, J. Hagymassy and E. E. Bodor, *J. Colloid Interface Sci.* **45**, 27 (1973).
133. A. Lecloux and J. P. Pirard, *J. Colloid Interface Sci.* **70**, 265 (1979).
134. B. C. Lippens and J. H. de Boer, *J. Catalysis* **4**, 319 (1965).
135. B. C. Lippens, B. G. Linsen and J. H. de Boer, *J. Catalysis* **3**, 32 (1964).

136. K. S. W. Sing, *in* "Surface Area Determination", Proc. Int. Symp., 1969 (eds. D. H. Everett and R. H. Ottewill), p. 25, Butterworths, London (1970).
137. B. G. Aristov and A. V. Kiselev, *Koll. Zhur.* **27**, 299 (1965).
138. S. J. Gregg, *J. Chem. Soc. Chem. Comm.* 699 (1975).
139. S. J. Gregg and J. F. Langford, *J. Chem. Soc. Faraday Trans. I.* **73**, 747 (1977).
140. D. H. Everett, G. D. Parfitt, K. S. W. Sing and R. Wilson, *J. Appl. Chem. Biotechnol.* **24**, 199 (1974).
141. C. E. Brown and P. G. Hall, *Surface Sci.* **30**, 379 (1972).
142. T. L. Hill, P. H. Emmett and L. G. Joyner, *J. Amer. Chem. Soc.* **73**, 5102 (1952).
143. P. J. M. Carrot, A. I. McLeod and K. S. W. Sing, Colloque International du C.N.R.S. sur l'Adsorption aux Interfaces gaz/solide et liquide/solide, Aix-en-Provence (1981).

3

The Physical Adsorption of Gases by Mesoporous Solids: The Type IV Isotherm

3.1 Introduction

The study of the pore structure of mesoporous solids is closely connected with the interpretation of the Type IV isotherm; indeed, the mesopore range of pore size is usually taken to be that range which gives rise to a Type IV isotherm. In the low-pressure region, a Type IV isotherm follows the same path (e.g. ABC in Fig. 3.1) as the corresponding Type II isotherm (ABC), but at a certain point it begins to deviate upwards (CDE) until at higher pressures its slope decreases (EFG). As the saturation vapour pressure is approached, the amount adsorbed may show little variation (along FGH), or alternatively it may show a final upward turn (GH').

A characteristic feature of a Type IV isotherm is its hysteresis loop. The exact shape of the loop varies from one adsorption system to another, but, as indicated in Fig. 3.1, the amount adsorbed is always greater at any given relative pressure along the "desorption" branch FJD than along the "adsorption" branch DEF. The loop is reproducible provided that the desorption run is started from a point beyond F which marks the upper limit of the loop.

Type IV isotherms are often found with inorganic oxide xerogels and other porous solids. With certain qualifications, which will be discussed in this chapter, it is possible to analyse Type IV isotherms (notably those of nitrogen at 77 K) so as to obtain a reasonable estimate of the specific surface and an approximate assessment of the pore size distribution.

Isotherms of the type now characterized as Type IV have played an essential part in the development of adsorption theory and practice, as being the first kind of isotherm to be studied in detail. Already in 1888, half a century before the BDDT classification had appeared, van Bemmelen[1] had

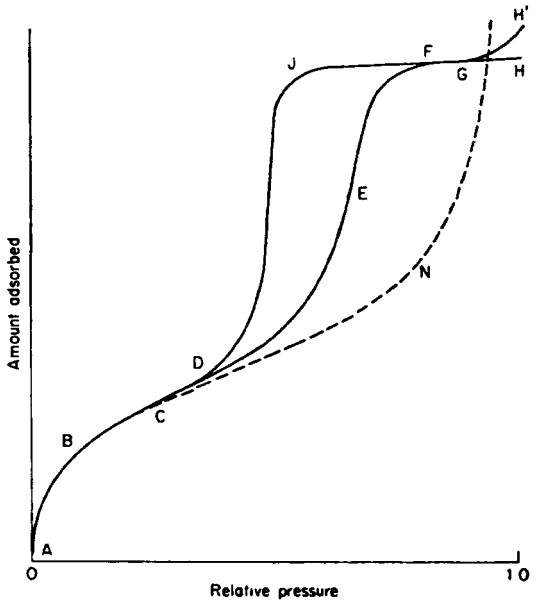

Fig. 3.1 A Type IV isotherm. The corresponding Type II isotherm follows the course ABCN (cf. dashed line).

commenced his classical studies, extending over twenty years, of the adsorption of vapours on a number of xerogels including silica. The majority of the resulting isotherms were found to possess the hysteresis loop characteristic of Type IV. It was in order to provide an interpretation of these isotherms that Zsigmondy,[2] put forward his capillary condensation theory which in one form or another has served as a basis for virtually all subsequent theoretical treatments of Type IV isotherms. Zsigmondy made use of the principle, which had been established some time earlier by Thomson[3] (later, Lord Kelvin) on thermodynamic grounds, that the equilibrium vapour pressure, p, over a concave meniscus of liquid, must be less than the saturation vapour pressure, p°, at the same temperature; this implied that a vapour will be able to condense to a liquid in the pores of a solid, even when its relative pressure is less than unity.

Thomson's original equation is not suitable for direct application to adsorption data; the form used by later workers, the "Kelvin equation", is

$$\ln \frac{p}{p^\circ} = \frac{-2\gamma V_L}{RT} \frac{1}{r_m} \tag{3.1}$$

Here p/p° is the relative pressure of vapour in equilibrium with a meniscus having a radius of curvature r_m, and γ and V_L are the surface tension and molar volume respectively, of the liquid adsorptive. R and T have their usual meanings.

The model proposed by Zsigmondy—which in broad terms is still accepted to-day—assumed that along the initial part of the isotherm (ABC of Fig. 3.1), adsorption is restricted to a thin layer on the walls, until at D (the inception of the hysteresis loop) capillary condensation commences in the finest pores. As the pressure is progressively increased, wider and wider pores are filled until at the saturation pressure the entire system is full of condensate.

Following Zsigmondy, early workers in the field assumed the pores to be cylindrical and the angle of contact to be zero, so that the meniscus was hemispherical. The mean radius of curvature r_m thus became equal to the radius of the pore less the thickness of the adsorbed film on the walls. By application of the Kelvin equation it was therefore possible to calculate the minimum radius of pores in which capillary condensation can take place, from the relative pressure at D, the lower limit of the hysteresis loop. General experience from the time of Anderson[4] (working in Zsigmondy's laboratory) onwards, shows that this minimum radius varies from system to system, but is rarely below $r_m \sim 10$ Å. The upper limit of the applicability of the Kelvin equation, $r_m \sim 250$ Å, is a practical one, set by the experimental difficulty of measuring very small lowerings of vapour pressure (cf. Table 3.8). The justification for defining mesopores by reference to the limits ~ 10 to ~ 250 Å therefore rests on the fact that the classical capillary equations, especially the Kelvin equation, are applicable in this range.

If the region FGH of the isotherm represents the filling of all the pores with liquid adsorbate, then the amount adsorbed along to plateau FGH, when expressed as a volume of liquid (by use of the normal liquid density) should be the same for all adsorptives on a given porous solid. This prediction is embodied in a generalization put forward many years ago by Gurvitsch[5] and usually known as the Gurvitsch rule.

The subsequent literature shows the rule to be generally valid, within a few per cent, amongst systems which give Type IV isotherms; in the typical example of Table 3.1, the data refer to adsorptives differing widely in their physical and chemical properties, yet the deviation of the saturation volume v_s from the mean is within 6 per cent.

This widespread conformity to the Gurvitsch rule constitutes powerful support for the capillary condensation hypothesis in relation to Type IV isotherms. It is perhaps hardly necessary to stress that in order to test data for conformity to the rule it is essential that the stage which corresponds to the complete filling of the pores shall be clearly identifiable—as in the

TABLE 3.1

Uptake at saturation by a ferric oxide gel[6] at 25°C, calculated as a volume of liquid (v_s)

Adsorbate	$v_s/(cm^3\,g^{-1})$
Benzene†	0·281
Carbon tetrachloride	0·270
Chloroform†	0·282
Cyclohexane	0·295
Deuterium oxide	0·302
Ethanol	0·300
Ethyl iodide	0·295
n-Hexane	0·308
Morpholine	0·282
n-Octane	0·278
$(isoPr)_2O$	0·290
Triethylamine	0·300
Water	0·302
Toluene	0·272

† Adsorption at 20°.

isotherms of Fig. 3.2, but not in the isotherm of Fig. 3.3. The deviations from exact obedience to the rule no doubt originate in part from this difficulty in identification.

A number of attempts have been made to demonstrate the connection between mesoporosity and the Type IV isotherm by comparing the isotherm of a vapour on a nonporous powder before and after it has been formed into a compact. The process of compaction produces pores in the form of interstices between the particles of the original powder; such pores will tend to have dimensions of the same order as those of the constituent particles, and it can be arranged that these shall fall within the mesopore range of size.

Examples are provided by the work of Carman and Raal[9] with CF_2Cl_2 on silica powder, of Zwietering[10] with nitrogen on silica spherules and of Kiselev[11] with hexane on carbon black; and more recently of Gregg and Langford[8] with nitrogen on alumina spherules compacted at a series of pressures. In all cases, a well defined Type II isotherm obtained with the loose powder became an equally well defined Type IV isotherm with the compact; moreover both branches of the hysteresis loop were situated *above* the isotherm for the uncompacted powder, but the pre-hysteresis region was scarcely affected (cf. Fig. 3.4). The results of all these and similar

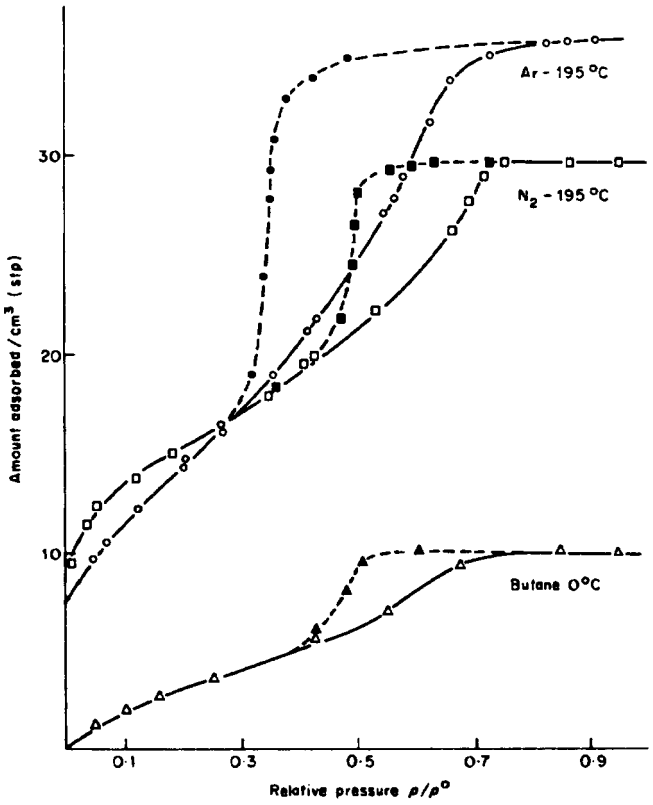

Fig. 3.2 Adsorption isotherms[7] for argon and nitrogen at 78 K and for n-butane at 273 K on porous glass No. 3. Open symbols, adsorption; solid symbols, desorption (courtesy Emmett and Cines). The uptake at saturation (calculated as volume of liquid) was as follows: argon at 78 K, 0·0452; nitrogen at 78 K, 0·0455; butane at 273 K, 0·0434 $cm^3 g^{-1}$.

experiments clearly demonstrate that the presence of mesopores brings about an increase in adsorption. The capillary condensation hypothesis offers the most reasonable explanation for this enhancement.

Closer examination reveals that the swing upwards in the Type IV isotherm not infrequently commences before the loop inception, showing that enhanced adsorption, not accompanied by hysteresis, can occur. The implications of this important fact are explored in Section 3.7.

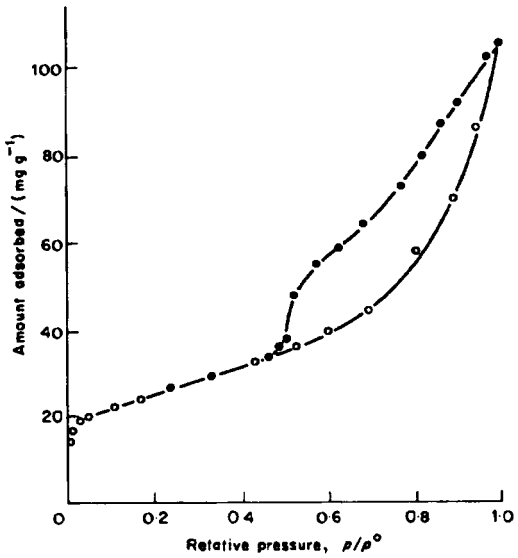

Fig. 3.3 Adsorption isotherm of nitrogen at 77 K on halloysite. Open circles, adsorption; solid circles, desorption.[8]

3.2 Types of hysteresis loop†

The hysteresis loops to be found in the literature are of various shapes. The classification originally put forward by de Boer[12] in 1958 has proved useful, but subsequent experience has shown that his Types C and D hardly ever occur in practice. Moreover in Type B the closure of the loop is never characterized by the vertical branch at saturation pressure, shown in the de Boer diagrams. In the revised classification presented in Fig. 3.5, therefore, Types C and D have been omitted and Type B redrawn at the high-pressure end. The designation E is so well established in the literature that it is retained here, despite the interruption in the sequence of lettering.

3.3 Capillary condensation and the Kelvin equation

As already indicated in Section 3.1, the study of mesoporous solids is closely bound up with the concept of capillary condensation and its quantitative expression in the Kelvin equation. This equation is, indeed, the basis of virtually all the various procedures for the calculation of pore size

† See Appendix for a new classification of hysteresis loops.

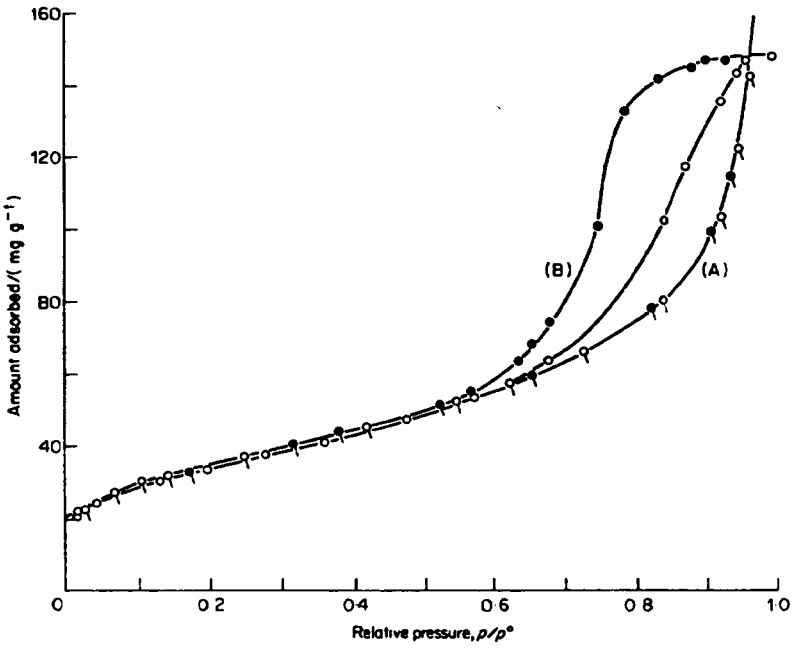

Fig. 3.4 Compaction of alumina powder.[8] Isotherms of nitrogen at 77 K, on (A) the uncompacted powder, and (B) on the powder compacted at a pressure of 1480 GN m^{-2} (96 ton in^{-2}). Open symbols, adsorption; solid symbols, desorption.

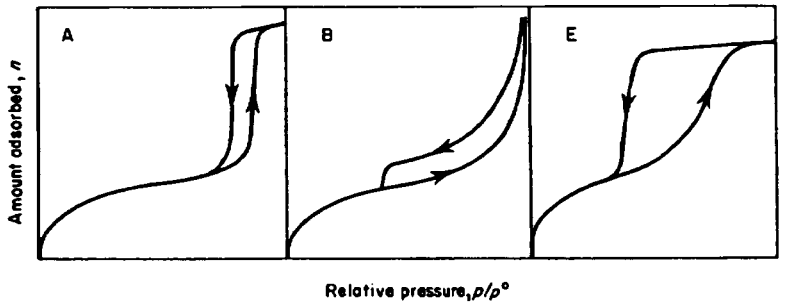

Fig. 3.5 Types of hysteresis loop.

distribution from the Type IV isotherm which have appeared over the last seventy years. Rightly used the equation can provide information on the pore system of a mesoporous solid which can be obtained in no other way; but it is imperative to recognize the limitations imposed by the thermodynamic basis of the equation, and to be fully aware of the various assumptions, often tacit, which have to be made when it is applied to actual calculations of pore size. These are best appreciated through a derivation of the equation, with accompanying discussion of relevant parameters.

As with all thermodynamic relations, the Kelvin equation may be arrived at along several paths. Since the occurrence of capillary condensation is intimately bound up with the curvature of a liquid meniscus, it is helpful to start out from the Young–Laplace equation, the relationship between the pressures on opposite sides of a liquid-vapour interface.

The Young–Laplace equation[13,14]

Picture a small element of a curved interface between a liquid α and a vapour β, having two radii of curvature r_1 and r_2 (Fig. 3.6). These radii are defined by taking two planes at right angles to one another, each of them

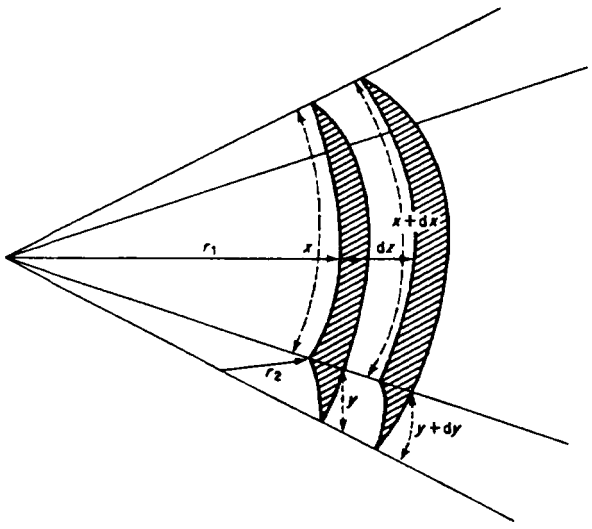

Fig. 3.6 A small section of an interface between a liquid α and a vapour β, having two radii of curvature r_1 and r_2.

passing through a normal erected from a point on the surface. Both radii are taken as constant over the area under discussion. Let the surface be displaced by a small distance dz. The change dA in surface area is

$$dA = (x + dx)(y + dy) - xy$$

i.e.
$$dA = x\,dy + y\,dx \tag{3.2}$$

if dx dy be neglected. Since the system is assumed to be in equilibrium, the total work done in making the small displacement must be zero; thus the work which has to be performed in expanding the surface must be equal to the work provided by the vapour β in expanding under the excess pressure $p^\beta - p^\alpha$. The former quantity is $\gamma\,dA$ or $\gamma(x\,dy + y\,dx)$, and the latter is $(p^\beta - p^\alpha)xy\,dz$, since the increment in volume is $xy\,dz$.

Thus

$$\gamma(x\,dy + y\,dx) = (p^\beta - p^\alpha)xy\,dz \tag{3.3}$$

Comparison of similar triangles in Fig. 3.6 gives

$$\frac{x + dx}{r_1 + dz} = \frac{x}{r_1} \tag{3.4}$$

so that

$$dx = \frac{x}{r_1}dz$$

Similarly

$$dy = \frac{y}{r_2}dz.$$

Substitution for dx and dy in Equation (3.3) gives the Young–Laplace equation:

$$p^\beta - p^\alpha = \gamma\left(\frac{1}{r_1} + \frac{1}{r_2}\right) \tag{3.5}$$

An alternative form is

$$p^\beta - p^\alpha = \frac{2\gamma}{r_m} \tag{3.6}$$

where r_m is the mean radius of curvature given by

$$\frac{1}{r_1} + \frac{1}{r_2} = \frac{2}{r_m} \tag{3.7}$$

Since the curvature of the surface is given by

$$C^{\alpha\beta} = \frac{2}{r_m} = \frac{1}{r_1} + \frac{1}{r_2} \tag{3.8}$$

relation (3.6) may be formulated alternatively as

$$p^{\beta} - p^{\alpha} = \gamma C^{\alpha\beta} \tag{3.9}$$

The Kelvin equation[15]

Let us now consider the process of capillary condensation. For the pure liquid (α) in equilibrium with its vapour (β), the condition for mechanical equilibrium is given by Equation (3.6) and that for physicochemical equilibrium by

$$\mu^{\alpha} = \mu^{\beta}$$

where μ is chemical potential.

If we now pass from one equilibrium state to another (an "equilibrium displacement") at constant temperature, then (cf. Equation (3.6)

$$\mathrm{d}p^{\beta} - \mathrm{d}p^{\alpha} = \mathrm{d}(2\gamma/r_m) \tag{3.10}$$

also

$$\mathrm{d}\mu^{\beta} = \mathrm{d}\mu^{\alpha} \tag{3.11}$$

Each of the coexisting phases will be governed by a Gibbs–Duhem equation so that

$$s^{\alpha}\,\mathrm{d}T + V^{\alpha}\,\mathrm{d}p^{\alpha} + \mathrm{d}\mu^{\alpha} = 0 \tag{3.12}$$

$$s^{\beta}\,\mathrm{d}T + V^{\beta}\,\mathrm{d}p^{\beta} + \mathrm{d}\mu^{\beta} = 0 \tag{3.13}$$

where s^{α}, s^{β} and V^{α} and V^{β} are the molar entropies and molar volumes, respectively, of the two phases.

At constant temperature, Equation (3.11) together with (3.12) and (3.13) lead to the simple relationship

$$V^{\alpha}\,\mathrm{d}p^{\alpha} = V^{\beta}\,\mathrm{d}p^{\beta} \tag{3.14}$$

whence

$$\mathrm{d}p^{\alpha} = \frac{V^{\beta}}{V^{\alpha}}\,\mathrm{d}p^{\beta} \tag{3.15}$$

Thus Equation (3.10) may be rewritten as

$$\mathrm{d}\left(\frac{2\gamma}{r_m}\right) = \frac{V^{\alpha} - V^{\beta}}{V^{\alpha}}\,\mathrm{d}p^{\beta} \tag{3.16}$$

Since the molar volume of the liquid, V^{α}, is very small compared with that of the vapour, and if the vapour β behaves as a perfect gas, then Equation (3.16) becomes

$$\mathrm{d}\left(\frac{2\gamma}{r_m}\right) = -\frac{RT}{V^{\alpha}}\frac{\mathrm{d}p^{\beta}}{p^{\beta}} \tag{3.17}$$

or

$$\mathrm{d}\left(\frac{2\gamma}{r_m}\right) = -\frac{RT}{V^{\alpha}}\mathrm{d}\ln p^{\beta} \tag{3.18}$$

On integration between the limits (r_m, p) and (∞, p°), this becomes

$$\frac{2\gamma}{r_m} = \frac{RT}{V_L}\ln\left(\frac{p^{\circ}}{p}\right) \tag{3.19}$$

or

$$\ln\frac{p}{p^{\circ}} = -\frac{2\gamma V_L}{RT}\frac{1}{r_m} \tag{3.20}$$

where $V_L(=V^{\alpha})$ is the molar volume of the liquid adsorptive and p° its saturation vapour pressure, which of course corresponds to $r_m = \infty$.

Equation (3.20) is conventionally termed *the* Kelvin equation. The tacit assumption is made at the integration stage that V^{α} is independent of pressure, i.e. that the liquid is incompressible.

From the Kelvin equation it follows that the vapour pressure p over a concave meniscus must be less than the saturation vapour pressure p°. Consequently "capillary condensation" of a vapour to a liquid should occur within a pore at some pressure p determined by the value of r_m for the pore, and less than the saturation vapour pressure—always provided that the meniscus is concave (i.e. angle of contact $< 90°$).

3.4 Relation of r_m to pore size

It must always be borne in mind that when capillary condensation takes place during the course of isotherm determination, the pore walls are already covered with an adsorbed film, having a thickness t determined by the value of the relative pressure (cf. Chapter 2). Thus capillary condensation occurs not directly in the pore itself but rather in the inner *core*[16] (Fig. 3.7). Consequently the Kelvin equation leads in the first instance to values of the core size rather than the pore size. The conversion of an r_m value to a pore size involves recourse to a model of pore shape, and also a knowledge of the angle of contact θ between the capillary condensate and the adsorbed film on the walls. The involvement of θ may be appreciated by consideration

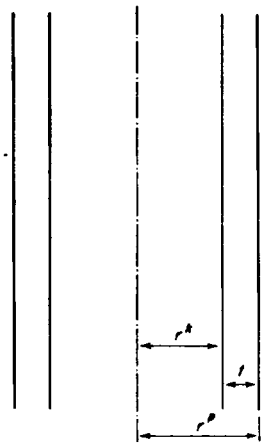

Fig. 3.7 Cross-section, parallel to the axis of a cylindrical pore of radius r^p, showing the "inner core" of radius r^k and the adsorbed film of thickness t.

of the simple model, the cylinder, which was first assumed, no doubt on grounds of simplicity, in the pioneer work of Zsigmondy[2] and Anderson[4] already referred to.

In a cylindrical pore the meniscus will be spherical in form, so that the two radii of curvature are equal to one another and therefore to r_m (Equation (3.8)). From simple geometry (Fig. 3.8) the radius r^k of the core is related to r_m by the equation

$$r^k = r_m \cos\theta \tag{3.21}$$

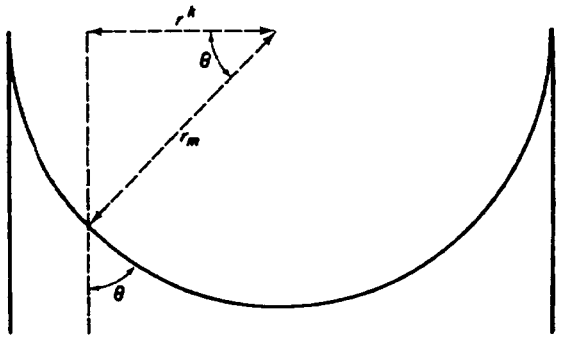

Fig. 3.8 Relation between r_m of the Kelvin equation (Equation (3.20)) and the core radius r^k for a cylindrical pore with a hemispherical meniscus; θ is the angle of contact.

Now, in principle, the angle of contact between a liquid and a solid surface can have a value anywhere between 0° and 180°, the actual value depending on the particular system. In practice θ is very difficult to determine with accuracy even for a macroscopic system such as a liquid droplet resting on a plate, and for a liquid present in a pore having dimensions in the mesopore range is virtually impossible of direct measurement. In applications of the Kelvin equation, therefore, it is almost invariably assumed, mainly on grounds of simplicity, that $\theta = 0$ ($\cos\theta = 1$). In view of the arbitrary nature of this assumption it is not surprising that the subject has attracted attention from theoreticians.

In general there are two factors capable of bringing about the reduction in chemical potential of the adsorbate, which is responsible for capillary condensation: the proximity of the solid surface on the one hand (adsorption effect) and the curvature of the liquid meniscus on the other (Kelvin effect). From considerations advanced in Chapter 1 the adsorption effect should be limited to a distance of a few molecular diameters from the surface of the solid. Only at distances in excess of this would the film acquire the completely liquid-like properties which would enable its angle of contact with the bulk liquid to become zero: thinner films would differ in structure from the bulk liquid and should therefore display a finite angle of contact with it.

Now by the Young–Dupré equation[17,18] we have

$$\gamma^{sg} = \gamma^{lg}\cos\theta + \gamma^{sl}$$

where γ^{sg} and γ^{sl} are the interfacial free energies of the solid when covered with the film and with the bulk liquid respectively, and γ^{lg} is the surface tension of the liquid. Since γ^{sg} is a function of the amount adsorbed it follows that θ should be a function of the thickness of the adsorbed film, decreasing towards zero as the film approaches the critical thickness where the "adsorption effect" vanishes.

At the junction of the adsorbed film and the liquid meniscus the chemical potential of the adsorbate must be the resultant of the joint action of the wall and the curvature of the meniscus. As Derjaguin pointed out,[19] the conventional treatment involves the tacit assumption that the curvature falls jumpwise from $2/r_m$ to zero at the junction, whereas the change must actually be a continuous one. Derjaguin put forward a "corrected" Kelvin equation to take this state of affairs into account; but it contains a term which is difficult to evaluate numerically, and has aroused little practical interest.

The question has been taken up again recently by L. R. White[20] who distinguishes between the *macroscopic* and the *microscopic* contact angles (Fig. 3.9). The macroscopic contact angle θ_c is governed by the slope of a

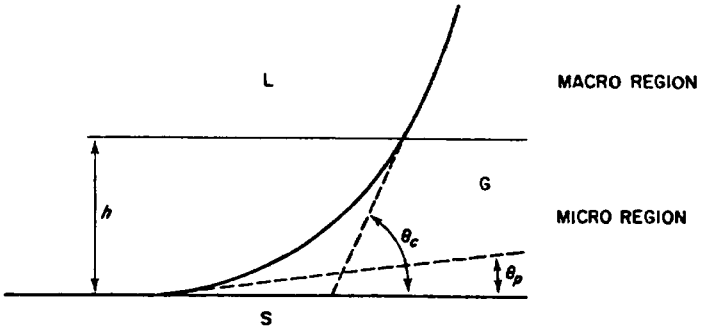

Fig. 3.9 Macroscopic contact angle θ_c and microscopic contact angle θ_p. S = solid; L = liquid; G = gas. (White[20].)

tangent to the liquid–vapour interface at a distance in excess of h, say, sufficiently remote from the solid surface for the effect of the surface on the chemical potential of the liquid to be negligible; the microscopic angle θ_p is given by the slope at the boundary line of the liquid and the adsorbed film. White concludes that when dispersion forces only are involved, the value of h will be less than 10 Å; and furthermore that if, as is probably the case in practice, the microscopic angle θ_p is equal to zero, the macroscopic angle θ_c will obey the Young–Dupré equation.

The problem has been discussed in terms of chemical potential by Everett and Haynes,[21] who emphasize that the condition of diffusional equilibrium throughout the adsorbed phase requires that the chemical potential shall be the same at all points within the phase; and since, as already noted, the interaction energy varies wtih distance from the wall, the internal pressure must vary in sympathy, so as to enable the chemical potential to remain constant.

Figure 3.10 is a plot of potential against distance from the wall for a liquid in a capillary of sufficient width for its middle A to be outside the range of forces from the wall. Since the capillary condensate is in equilibrium with the vapour, its chemical potential μ^a ($=\mu^g$), represented by the horizontal line GF, will be lower than that of the free liquid $\mu^{o,l}$; the difference in chemical potential of the condensate at A, represented by the vertical distance AF, is brought about entirely by the pressure drop, $\Delta p = 2\gamma/r_m$, across the meniscus (cf. Equation (3.6)) but at some point B, say, nearer the wall, the chemical potential receives a contribution represented by the line BC, from the adsorption potential. Consequently, the reduction Δp in pressure across the meniscus must be less at B than at A, so that again

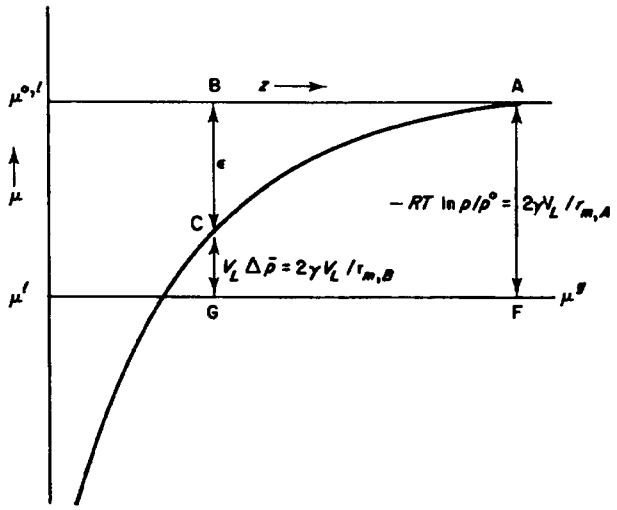

Fig. 3.10 Contributions to the lowering of chemical potential of the condensed liquid in a capillary, arising from adsorption forces (ε) and meniscus curvature ($V_L \Delta\bar{p}$). The chemical potential of the free liquid is $\mu^{\circ,l}$, and that of the capillary condensed liquid is μ^{l} ($=\mu^{g}$); z is the distance from the capillary wall. (After Everett[21].)

by Equation (3.6), the radius of curvature of the meniscus must be larger at B than at A.

At the middle of the capillary where the effect of the walls on chemical potential is negligible, the radius of curvature will be equal to r_m as calculated by the Kelvin equation (3.20); but it will become progressively larger as the wall is approached.

Broekhoff and de Boer[22] have addressed themselves to the same problem, putting forward an analysis based on an expression for the chemical potential of the adsorbed film as a function of its thickness t. The status of the de Boer treatment has been discussed in some detail by Everett and Haynes.[21]

All in all, it is clear that the value of the macroscopic contact angle, the angle θ of Equation (3.21), is subject to a great deal of uncertainty. It probably varies according to the thickness t of the adsorbed layer lining the walls of the pores, decreasing as t increases and finally becoming zero when t reaches perhaps 3 or 4 molecular diameters. At present there appear to be no means for its direct evaluation, and in practice the simplifying assumption that $\theta = 0$ is almost invariably made in the context of capillary condensation.

3.5 Hysteresis associated with capillary condensation

In calculations of pore size from the Type IV isotherm by use of the Kelvin equation, the region of the isotherm involved is the hysteresis loop, since it is here that capillary condensation is occurring. Consequently there are *two* values of relative pressure for a given uptake, and the question presents itself as to what is the significance of each of the two values of r_m which would result from insertion of the two different values of relative pressure into Equation (3.20). Any answer to this question calls for a discussion of the origin of hysteresis, and this must be based on actual models of pore shape, since a purely thermodynamic approach cannot account for two positions of apparent equilibrium.

The formation of a liquid phase from the vapour at any pressure below saturation cannot occur in the absence of a solid surface which serves to nucleate the process. Within a pore, the adsorbed film acts as a nucleus upon which condensation can take place when the relative pressure reaches the figure given by the Kelvin equation. In the converse process of evaporation, the problem of nucleation does not arise: the liquid phase is already present and evaporation can occur spontaneously from the meniscus as soon as the pressure is low enough. It is because the processes of condensation and evaporation do not necessarily take place as exact reverses of each other that hysteresis can arise.

The working out of these ideas will be illustrated by reference to a number of simple pore models: the cylinder, the parallel-sided slit, the wedge-shape and the cavity between spheres in contact.

These models, though necessarily idealized, are sufficiently close to the actual systems found in practice to enable useful conclusions to be drawn from a given Type IV isotherm as to the pore structure of a solid adsorbent. To facilitate the discussion, it is convenient to simplify the Kelvin equation by putting $\gamma V_L/RT = K$, and on occasion to use the exponential form:

$$p/p^\circ = \exp(-2K/r_m) \tag{3.22}$$

We consider first a cylinder closed at one end, B (Fig. 3.11(*a*)). Capillary condensation commences at that end to form a hemispherical meniscus; r_1 and r_2 are equal to one another and therefore to r_m, which in turn is equal to r^k, the radius of the core (cf. Equation (3.7) and Fig. 3.7). Thus capillary condensation, to fill the whole pore, takes place at the relative pressure

$$(p/p^\circ)_1 = \exp(-2K/r^k)$$

The process of evaporation can commence at the hemispherical meniscus at A, and continues at the same relative pressure $(p/p^\circ)_1$, so that there is no hysteresis.

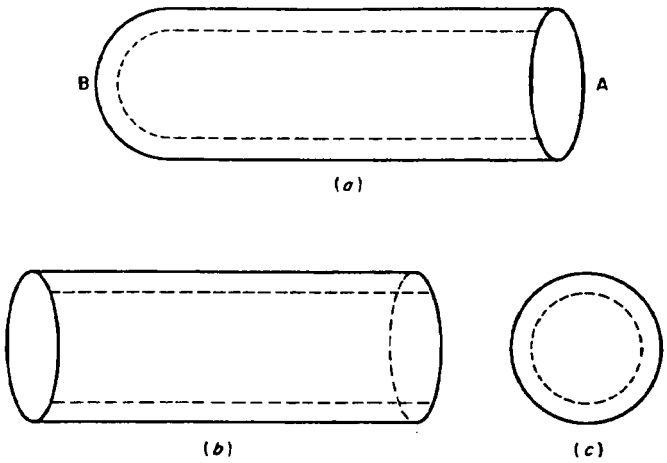

Fig. 3.11 Capillary condensation in cylindrical pores. (*a*) Cylinder closed at one end, B. The meniscus is hemispherical during both capillary condensation and capillary evaporation. (*b*) and (*c*) Cylinder open at both ends. The meniscus is cylindrical during capillary condensation and hemispherical during capillary evaporation. Dotted lines denote the adsorbed film.

If the cylinder is open at both ends, the course of events is different, because condensation has to be nucleated by the film on the walls of the cylinder.[23,24] The meniscus is now cylindrical in form (cf. Fig. 3.11(*b*) and (*c*)); thus $r_1 = r^k$ and $r_2 = \infty$, so that by Equation (3.7), $r_m = 2r^k$. Condensation therefore occurs at the relative pressure $(p/p^\circ)_{ads} = \exp(-2K/r_m) = \exp(-K/r^k)$ and completely fills the pore. (The process is spontaneous since as condensation progresses, the core radius is correspondingly reduced and the equilibrium pressure falls more and more below the actual pressure). *Evaporation* from the full pore can take place from the hemispherical meniscus at each end, and the core empties itself at a relative pressure of

$$(p/p^\circ)_{des} = \exp(-2K/r_m) = \exp(-2K/r^k)$$

Thus, as pointed out by Cohan[23] who first suggested this model, condensation and evaporation occur at different relative pressures and there is hysteresis. The value of r_m calculated by the standard Kelvin equation (3.20) for a given uptake, will be equal to the core radius r_K if the desorption branch of the hysteresis loop is used, but equal to twice the core radius if the adsorption branch is used. The two values of r_K should, of course, be the same; in practice this is rarely found to be so.

The variant of the cylindrical model which has played a prominent part in the development of the subject is the "ink-bottle",[26] composed of a cylindrical pore closed one end and with a narrow neck at the other (Fig. 3.12(*a*)). The course of events is different according as the core radius r_w of the body is greater or less than twice the core radius r_n of the neck. Nucleation to give a hemispherical meniscus, can occur at the base B at the relative pressure $(p/p^\circ)_I = \exp(-2K/r_w)$; but a meniscus originating in the neck is necessarily cylindrical so that its formation would need the pressure $(p/p^\circ)_{II} = \exp(-K/r_n)$. If now $r_w/r_n < 2$, $(p/p^\circ)_I$ is lower than $(p/p^\circ)_{II}$, so that condensation will commence at the base B and will fill the whole pore, neck as well as body, at the relative pressure $\exp(-2K/r_w)$. Evaporation from the full pore will commence from the hemispherical meniscus in the neck at the relative pressure $(p/p^\circ)_{III} = \exp(-2K/r_n)$ and will continue till the core of the body is also empty, since the pressure is already lower than the equilibrium value $(p/p^\circ)_I$) for evaporation from the body. Thus the adsorption branch of the loop leads to values of the core radius of the body, and the desorption branch to values of the core radius of the neck.

In the converse case where $r_w/r_n > 2$, $(p/p^\circ)_I = \exp(-K/r_n)$ will be lower than $(p/p^\circ)_{II} = \exp(-2K/r_w)$ so that condensation takes place in the neck, but will not be able to extend into the body until the pressure rises to $(p/p^\circ)_I$. Evaporation will occur just as before, and the core will empty completely at the pressure $(p/p^\circ)_{III} = \exp(-2K/r_n)$, so that hysteresis will be found.

If the body of the bottle is tapered (Fig. 3.12(*b*) and (*c*)) the exact way in which the pores are filled or emptied will depend on the values of the ratios $r_n : r_w$ and $r_n : r_W$, where r_w is the core radius of the narrowest end of the body

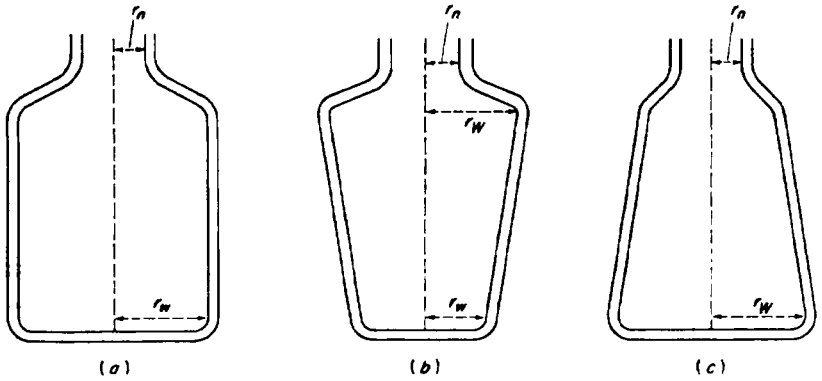

Fig. 3.12 Ink bottle pores; with (*a*) cylindrical body and (*b*), (*c*), tapering body; the neck is cylindrical in each case.

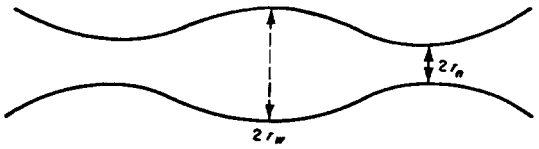

Fig. 3.13 A pore of circular cross-section and gradually varying radius.

and r_W that of the widest. Typical cases are readily analysed by application of the general principles already described.

As Everett points out, however,[27] the analogy of a pore as a narrow-necked bottle is over-specialized, and in practice a series of interconnected pore spaces rather than discrete bottles is more likely. The progress of capillary condensation and evaporation in pores of this kind (cf. Fig. 3.13) has been discussed by de Boer,[12] and more recently by Everett.[27]

Both the cone-shaped and the wedge-like pore give rise to simple, hysteresis-free behaviour. The meniscus is nucleated at the apex of the cone (Fig. 3.14(*a*)) or at the intersection of the two planes of the wedge (Fig. 3.14(*b*)), giving a spherical meniscus in the first case and a cylindrical one in the second. In both systems the process of evaporation is the exact reverse of that of condensation, and hysteresis is therefore absent.

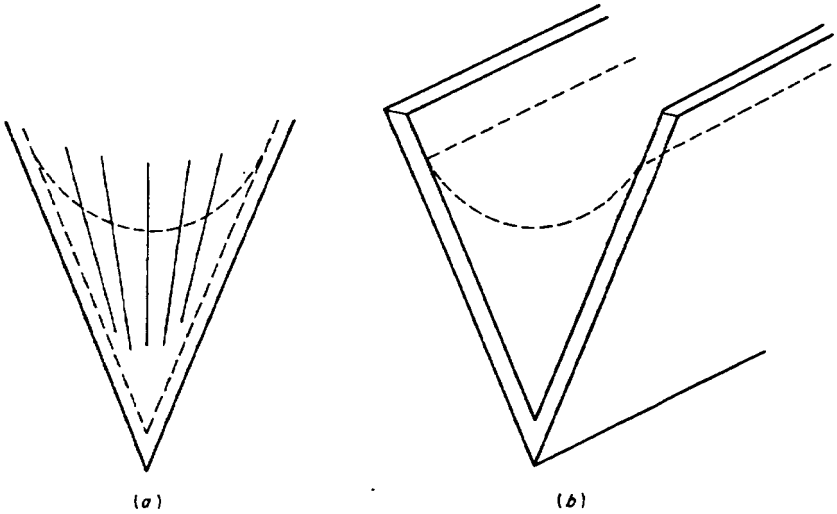

Fig. 3.14 (*a*) A cone-shaped pore with hemispherical meniscus. (*b*) A wedge-shaped pore with cylindrical meniscus.

Numerous porous solids are made up of spherical particles, each in contact with two or more of its neighbours (cf. Section 1.6). For discussion of capillary condensation and evaporation in solids of this kind, a simplified model consisting of equal-sized spheres in some form of close-packing must be resorted to. In the pore illustrated in Fig. 3.15(*a*) condensation will be nucleated by the adsorbed film in the crevices between contiguous spheres to give a torus of liquid which, as pressure increases, will extend inwards until adjacent tori coalesce; the spherical cavity, of radius r_c, say, will then suddenly fill up, the relative pressure being $\exp(-2K/r_c)$. During desorption from a filled cavity, the state of affairs is somewhat similar to that in the ink-bottle model: evaporation commences at a hemispherical meniscus in the foramen (window) of the cavity, and the cavity then empties jumpwise at the relative pressure $\exp(-2K/r_f)$ where r_f is the radius of a circle inscribed in the foramen. Since $r_f < r_c$, hysteresis is present and the isotherm should have the general form illustrated in Fig. 3.15(*b*).

The slit-shaped model has come into prominence in recent years, as electron microscopy has revealed the prevalence of solids composed of plate-like particles; the technique, indeed, has now developed to the point where it is possible to identify the presence of slit-shaped pores, and even to measure their width. In the ideal case where the sides of the slit are truly planar and parallel, the hysteresis takes an extreme form: since the mean radius of curva-

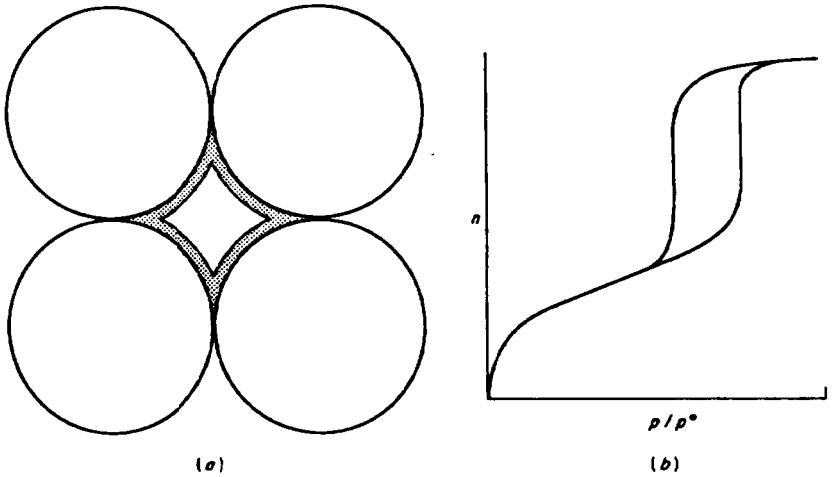

Fig. 3.15 (*a*) A pore in the form of an interstice between close-packed and equal-sized spherical particles. The adsorbed film which precedes capillary condensation is indicated. (*b*) Adsorption isotherm (idealized).

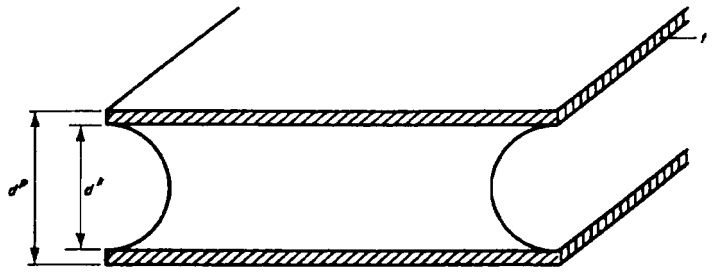

Fig. 3.16 A slit-shaped pore of width d^p, showing adsorbed film of thickness t and core of width d^k.

ture of a plane is infinite, capillary condensation cannot occur at any pressure below saturation. The adsorbed films on opposite walls will increase in thickness up to $d^k/2$ (d^k = width of slit core), when the films meet each other and the pore becomes full of adsorbate. Provided the width of the pore exceeds a few molecular diameters (cf. p. 123) the state of the adsorbate will be indistinguishable from that of the liquid. Evaporation can commence at the cylindrical menisci (Fig. 3.16) at the relative pressure $\exp(-2K/d^k)$ and will continue at that same pressure until the core is completely empty. Thus the mechanisms of filling and emptying are completely different: multilayer formation on the one hand and capillary evaporation on the other. In actual solids, of course, not only will there be a distribution of slit widths, but the sides will rarely be exactly parallel or truly planar; and some plates will touch their neighbours so as to produce wedge-shaped pores. Furthermore, the adsorbent is frequently nonrigid, so that the slit-width increases during adsorption, and decreases, though not reversibly, during desorption.[25] The loops encountered in practice, therefore, have the general form of Type B, exemplified in Fig. 3.17.

Finally, the simplifying assumption that $\theta = 0$ (p. 125) should always be borne in mind. In principle, the angle of contact during capillary condensation can differ from zero. This is particularly likely when the adsorbed film has a considerable degree of localization (p. 8), for its molecular order will then differ significantly from that of a bulk liquid; moreover the molecular order of the film could well be different during adsorption than during desorption, since in the latter situation the film has been part of the liquid condensate. However, in view of the intractable nature of the theoretical problem in its quantitative aspects,[29] the possible divergence of θ from zero is ignored in calculations of pore size from capillary condensation data.

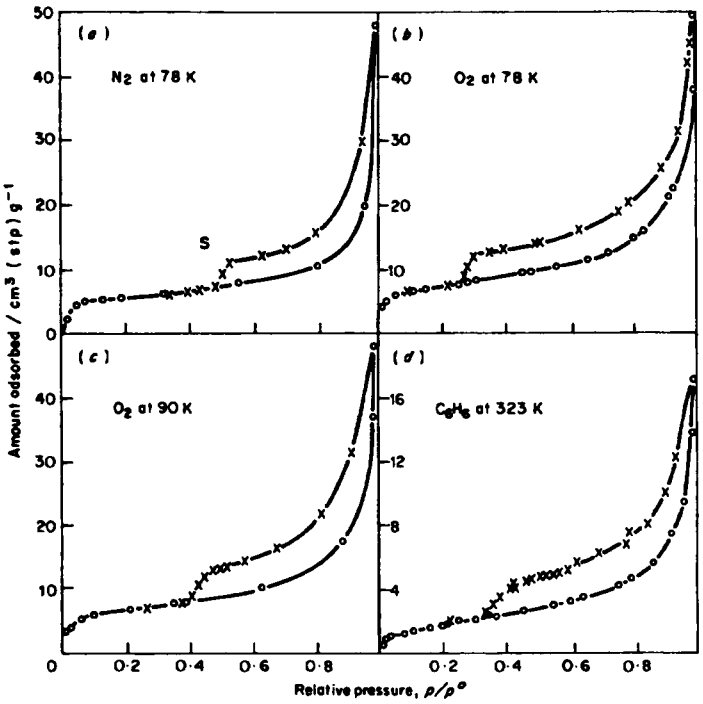

Fig. 3.17 Isotherms on a natural sodium-rich montmorillonite.[28] Circles denote adsorption, crosses desorption. (Courtesy Barrer.)

3.6 Use of the Kelvin equation for calculation of pore size distribution

The possibility of calculating the pore size distribution of a porous solid from the capillary condensation region of its Type IV isotherm has long been recognized.[4] In the pioneer work of Foster[30] the amount adsorbed on the walls of the pores was neglected; then, for any point $(n_i, p_i/p^\circ)$ on the isotherm, the volume v^p of all the pores having r_m-values up to and including $r_{m,i}$ was given by $n_i V_L$. Since a cylindrical model was assumed, r_m was taken as equal to the pore radius r^p itself. From the curve of v^p against r^p the size distribution curve, i.e. dv^p/dr^p against r^p was immediately obtainable. In present-day terms the result was a *core* size distribution rather than the pore size distribution itself.

Foster's neglect of the role of the adsorbed film was unavoidable in the then absence of any reliable information as to the thickness of the film. It is now known that in fact the effect of the film on the calculated result is far from negligible, as will be demonstrated shortly. Since, however, all the methods of calculating pore size distributions involve a decision as to the upper limit of the range to be studied, this question needs to be discussed first. In effect one has to choose a point corresponding to point G in Fig. 3.1, where the mesopores are deemed to be full up. If the isotherm takes the course GH there are no further cores to be considered in any case; but if it swings upwards as at GH', the isotherm is usually so steep that the Kelvin-type approach becomes too inaccurate (cf. p. 114) to be useful.

The precise value chosen for the upper limit is inevitably somewhat arbitrary; and a relative pressure of 0·95, corresponding to $r^p = 200$ Å (cylindrical pores), is common, but the lower figure $p/p^\circ = 0{\cdot}90$ ($r^p = 100$ Å) has been adopted on occasion. The difference between the two limits is perhaps less significant than might appear, since in many pore systems the volume of pores having radii in excess of 100 Å is relatively small; in any case the Kelvin method is beginning to lose accuracy in this range, so that mercury porosimetry is becoming more attractive (p. 173).

The importance of the role played by the adsorbed film can be appreciated by picturing the progressive emptying of a pore system initially full up at relative pressure p_s/p°, as the relative pressure is lowered in steps to p_1/p°, p_2/p° etc. Let the pores be divided into groups 1, 2, etc. having r_m-values corresponding to p_1/p°, p_2/p° etc. (the r_m-values being assumed constant within a group). When the relative pressure is reduced to p_1/p°, the first group of pores loses its capillary condensate, but still retains a film of thickness t on its walls. Since the amount of capillary-evaporated liquid is $(n_s - n_1)$, the volume δv_1^k of the first group of *cores* is $(n_s - n_1)V_L$, where n_s and n_1 are the amounts adsorbed at the beginning and end of the step respectively, and V_L as usual is the molar volume of the liquid adsorptive. The corresponding volume δv_1^p of the *pores* is $Q_1 \delta v_1^k$, where Q_1, the factor converting core volume into pore volume is a function of both pore shape and film thickness (cf. p. 142).

When the relative pressure falls to p_2/p°, the second group of pores loses its capillary condensate, but in addition the film on the walls of the first group of pores yields up some adsorbate, owing to the decrease in its thickness from t_1 to t_2. Similarly, when the relative pressure is further reduced to p_3/p°, the decrement $(n_2 - n_3)$ in the uptake will include contributions from the walls of both groups 1 and 2 (as the film thins down from t_2 to t_3), in addition to the amount of capillary condensate lost from the cores of group 3. It is this composite nature of the amount given up at each step which complicates the calculation of the pore size distribution.

In the pioneer work of Foster the correction due to film thinning had to be neglected, but with the coming of the BET and related methods for the evaluation of specific surface, it became possible to estimate the thickness of the adsorbed film on the walls. A number of procedures have been devised for the calculation of pore size distribution, in which the adsorption contribution is allowed for. All of them are necessarily somewhat tedious and require close attention to detail, and at some stage or another involve the assumption of a pore model. The "model-less" method of Brunauer and his colleagues[31] represents an attempt to postpone the introduction of a model to a late stage in the calculations.

The procedures are based on an imaginary emptying of the pores by the step-wise lowering of relative pressure, from the point already referred to where the mesopore system is taken as being full up; a relative pressure of $0{\cdot}95p_0$ is frequently adopted as starting point with isotherms having a hysteresis loop of Type A or Type E. (With Type B, as will appear later, the validity of pore size calculations is doubtful.)

The steps may be so chosen as to correspond to consecutive points on the experimental isotherm. In practice it is more convenient to divide the desorption process into a number of standard steps, either of relative pressure, or of pore radius, which is of course a function of relative pressure. The amount given up during each step i must be converted into a liquid volume δv_i (by use of the normal liquid density); in some procedures the conversion is deferred to a late stage in the calculation, but conceptually it is preferable to undertake the conversion at the outset. As indicated earlier, the task then becomes: (i) to calculate the contribution δv^f due to thinning of the adsorbed film, and thus obtain the core volume δv^k associated with the mean core radius $\bar{r}^k$ by the subtraction $\delta v_i - \delta v^f = \delta v^k$; and (ii) to convert the core volume into the corresponding pore volume δv^p, and the core radius into the corresponding mean pore radius $\bar{r}p$.

Both (i) and (ii) necessitate recourse to a model of pore shape. By far the commonest, chosen on grounds of simplicity, is the cylinder; but the slit model is being increasingly used where the primary particles are plate-like, and the model where the pore is the cavity between touching spheres is beginning to receive attention.

Various methods have been devised for incorporating the δv^f correction into calculations of pore size distribution. Some of them involve the length of the pores and the area of their walls; others the area of the walls only; and yet others avoid the direct involvement of either the length or the area. Up to the present, virtually all the procedures have been restricted to nitrogen as the adsorptive.

A selection of methods drawn from the fairly extensive literature will be described, not necessarily in chronological order of appearance.

Since they all necessitate a knowledge of the value of t, and of both r^k and r^p either directly or indirectly, all as a function of p/p°, these data are given in tabular form for reference (Table 3.2). If required, intermediate values of t may be obtained to sufficient accuracy by graphical interpolation, and the corresponding values of r^k can be calculated with the Kelvin formula. The values of r^k refer to the most commonly used model, the cylindrical pore, so that $r^p = r^k + t$. The values of t are derived from the standard nitrogen isotherm for hydroxylated silica;[32] and though the values do differ somewhat from one substance to another (p. 90), the resultant effect on the calculated pore size distribution is relatively small. In the absence of strong evidence to the contrary, the set of values in the table may be regarded as adequate for most practical purposes, particularly in view of the other uncertainties inseparable from pore size calculations in general.

Before proceeding to detail, however, it is necessary to consider the question as to which branch of the hysteresis loop—the adsorption or the desorption branch—should be used. Though the mode of calculation is

TABLE 3.2

Values of r^p, and t at different values of p/p° for nitrogen at 77·4 K[32]

A			B		
p/p°	r^p/Å	t/Å	p/p°	r^p/Å	t/Å
0·40	15·60	5·35	0·439	17	5·5
0·45	17·40	5·60	0·490	19	5·8
0·50	19·45	5·85	0·555	21	6·1
0·55	21·85	6·15	0·574	23	6·3
0·60	24·9	6·5	0·605	25	6·5
0·65	28·7	6·85	0·667	30	7·05
0·70	33·7	7·35	0·711	35	7·4
0·75	40·5	7·85	0·746	40	7·7
0·80	50·7	8·6	0·800	50	8·6
0·85	67·5	9·65	0·832	60	9·2
0·90	101·9	12·75	0·856	70	9·8
0·95	|199|	|16|	0·875	80	10·5
			0·889	90	11·7
			0·899	100	12·75

t calculated from Table 2.14 with $\sigma = 3{\cdot}54$ Å (t/Å = 0·345 × number of μmol m^{-2}). $r^p = r^k + t$.

r^k calculated from Kelvin equation with $\gamma = 8{\cdot}72$ mN m^{-1}, $V_l = 34{\cdot}68$ cm^3 mol^{-1}, $T = 77{\cdot}4$ K. i.e. r^k/Å = 4·078/log(p°/p).

All values rounded to nearest 0·05 Å. Cylindrical pores are assumed.

based on a visualization of desorption from the completely filled pore system, this is purely for conceptual convenience, and, considered mathematically, the procedure is equally valid for either branch of the loop; but since, as demonstrated in the foregoing section, spontaneous processes are frequently involved, neither branch represents thermodynamic equilibrium. Even so, as pointed out by Everett[21,48] and by Karnaukhov,[33] the pressures at which instability sets in are directly determined by the curvature of the meniscus at the onset of instability, irrespective of the lack of reversibility of the ensuing process. Consequently, spontaneous processes should not in themselves render the Kelvin equation (3.20) inapplicable. However, the significance of the resulting values of r_m will of course be different for the two branches of the loop, and the interpretation of the pore size distribution curves may be particularly difficult when, as is often the case, the pore system forms a network (cf. p. 150).

Methods based on the area of the pore walls

A procedure involving only the wall area and based on the cylindrical pore model was put forward by Pierce[34] in 1953. Though simple in principle, it entails numerous arithmetical steps the nature of which will be gathered from Table 3.3; this table is an extract from a fuller work sheet based on the Pierce method as slightly recast by Orr and DallaValle,[35] and applied to the desorption branch of the isotherm of a particular porous silica.

The uptake, in column 10, has been converted into a liquid volume at the outset rather than at a later stage as in the original papers. Columns 1–8 are based on Table 3.2. In the original papers the values of p/p° corresponded to actual points on the experimental isotherm, but the work sheet is much simplified by the choice of standard intervals of p/p° (or of r^p; cf. p. 135).

An essential feature is the involvement of δA, the additional area of multilayer exposed during the particular step as the group of pores loses its capillary condensate. δA is calculated from the volume and radius of the group, using the geometry of the cylinder (column 15). The total area of multilayer which is thinned down during any step is obtained by summing the δA contributions in all the lines above the line of the step itself (column 16).

The significance of the various columns is explained in the notes below the table, which enable the calculations of $\delta v^p/\delta r^p$ to be followed through. Only the first few lines are reproduced, by way of illustration; the pore size distribution curve resulting from the complete table is given in Fig. 3.18 (Curve A), as a plot of $\delta v^p/\delta r^p$ against $\bar{r}^p$.

TABLE 3.3

Calculation of pore size distribution
(Method of Pierce,[34] also of Orr and DallaValle[35])

(1) p / p°	(2) r^k / Å	(3) $\bar{r}^k$ / Å	(4) r^p / Å	(5) δr^p / Å	(6) $\bar{r}^p$ / Å	(7) t / Å	(8) δt / Å	(9) Q	(10) V / mm^3	(11) δV / mm^3	(12) δv^f / mm^3	(13) δv^k / mm^3	(14) δv^p / mm^3	(15) δA^p / m^2	(16) $\sum(\delta A^p)$ / m^2	(17) $\delta v^p / \delta r^p$
0·90	89·1		101·9			12·8										
0·85	57·8	73·4	67·5		84·7	9·9	2·1	1·28	709							
0·80	42·1	50·0	50·7	16·8	58·7	8·6	1·1	1·37	707	2	0	2	3	1	1	0·2
0·75	32·7	37·4	40·5	10·2	45·6	7·8	0·8	1·45	705	2	0·1	1·9	2·8	1·2	2·2	0·3
0·70	26·4	29·5	33·7	6·5	37·1	7·3	0·5	1·55	694	11	0·1	10·9	16·2	9·1	11·3	2·6
0·65	21·8	24·1	28·7	5·0	31·2	6·9	0·4	1·65	635	59	0·6	58·4	96·4	61·8	73·1	19·3
. .	. .	. .	. .	. .	. .	. .	. .	. .	. .	. .	. .	. .	. .	. .	. .	. .

Columns [1] to [8] based on Table 3.2.

Column [10], adsorption values from isotherm for silica gel GS50 (desorption branch).

Column [9] $Q = \left(\frac{\bar{r}_1^p}{\bar{r}_1^p - t_1}\right)^2$

[12] $\delta v^f = 0{\cdot}1 \times \delta t \sum(\delta A^p)$[$\sum(\delta A^p)$ from line above].

[13] $\delta v^k = \delta V - \delta v^f$ = [11] − [12].

[14] $\delta v^p = \delta v^k \times Q$ = [13] × [9].

[15] $\delta A^p = 20 \times \delta v^p / \bar{r}^p = 20 \times$ [14]/[6] (geometry of cylinder).

Volumes in mm^3(liquid); radii and film thicknesses in Å; area in $m^2\,g^{-1}$. The remainder of the standard columns ([1] to [9]) may be built up from Table 3.2A; an alternative table, based on regular intervals of r^p, may be built up from Table 3.2B.

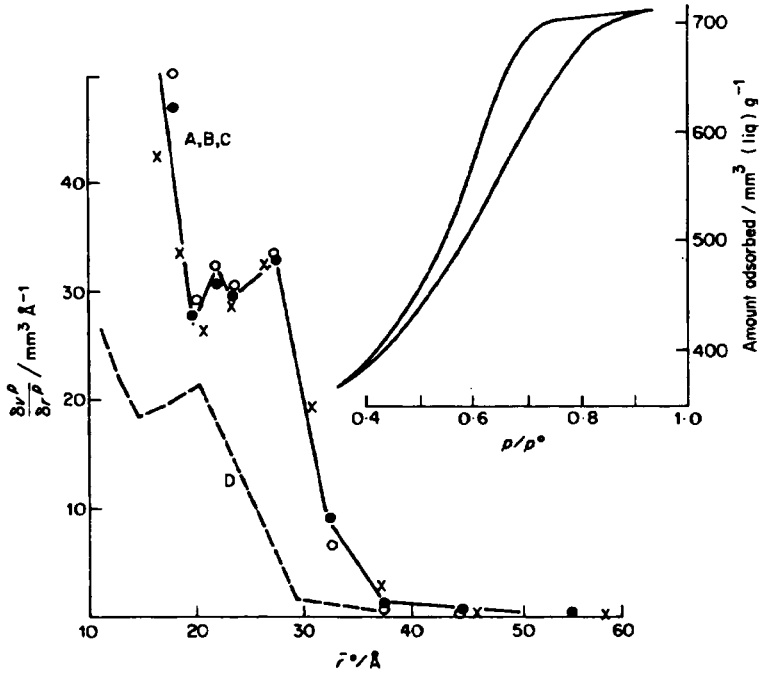

Fig. 3.18 Pore size distributions of a silica gel[36] GS50, calculated from the desorption branch of the isotherm at 77 K by different methods. (A) ×, Orr-DallaValle[35]; (B) O, Dollimore-Heal[41]; (C) ●, Roberts[42]; (D) ----, is the core-size distribution (Foster[30]), i.e. plot of $\delta v^k/\delta r^k$. Curves (A) and (D) were based on regular intervals of $p/p°$; (B) and (C) on regular intervals of r^p. The relevant part of the isotherm is shown in the inset.

Methods involving the length and area of pore walls

A procedure based primarily on the length of the pores was proposed by Wheeler[37] in 1945, and developed by a number of workers, including Shull,[38] Barrett, Joyner and Halenda[39] and Cranston and Inkley.[40] Wheeler introduced a pore size distribution function $L(r)\mathrm{d}r$, defined as the length of pores (per unit mass of adsorbent) which have radii in the range r to $(r - \mathrm{d}r)$. The calculations are somewhat involved and a simplified procedure has been put forward by Dollimore and Heal;[41] the pore radius rather than relative pressure is taken as the independent variable, and the pore system is divided into groups of pores ranging in average radius from 95 Å down to 7·5 Å. Since only the pore *radius* and not the *core* radius

appears directly in the analysis, the superscript p will be omitted for simplicity during the major part of the analysis.

Consider stage i in the desorption process where the thickness of the adsorbed film is t_i and the pores of radius r_i have just lost their capillary condensate. The volume of multilayer lining the pores of any radius r, where $r > r_i$, will then be (since the pores are cylindrical):

$$\pi[r^2 - (r - t_i)^2]L(r)\,\mathrm{d}r$$

or

$$\pi[2rt_i - t_i^2]L(r)\,\mathrm{d}r \tag{3.23}$$

The volume $v^f(>r_i)$ of the multilayer film on the walls of all pores which have already given up their capillary condensate is

$$\begin{aligned} v^f(>r_i) &= \int_{r_i}^{\infty} \pi[2rt_i - t_i^2]L(r)\,\mathrm{d}r \\ &= t_i \int_{r_i}^{\infty} 2\pi r L(r)\,\mathrm{d}r - \pi t_i^2 \int_{r_i}^{\infty} L(r)\,\mathrm{d}r \\ &= t_i A(>r_i) - \pi t_i^2 L(>r_i) \end{aligned} \tag{3.24}$$

Here $A(>r_i)$ is the total wall area, and $L(>r_i)$ the total length, of all pores having radius greater than r_i.

Thus the diminution $\mathrm{d}v^f(>r_i)$ in the volume of the film corresponding to an infinitesimal reduction in relative pressure is

$$\mathrm{d}v^f(>r_i) = A(>r_i)\,\mathrm{d}t_i - 2\pi L(>r_i)t_i\,\mathrm{d}t_i,$$

and for the small but finite step i, the reduction $\delta v^f(>r_i)$ in film volume is

$$\delta v^f(>r_i) = A(>r_i)\,\delta t_i - 2\pi(L > r_i)t_i\,\delta t_i \tag{3.25}$$

If now δV_i is the total amount of adsorbate (read off from the isotherm and expressed as a volume of liquid) which is released during the stage i, then the volume δv_i^k of *cores* emptied during the stage must be

$$\delta v_i^k = \delta V_i - \delta v_i^f \tag{3.26}$$

The corresponding pore volume will be

$$\delta v_i^p = Q_i(\delta V_i - \delta v_i^f) \tag{3.27}$$

where the conversion factor Q_i is given by

$$Q_i = \left(\frac{\bar{r}_i^p}{\bar{r}_i^p - t_i}\right)^2 \tag{3.28}$$

since the pores are cylindrical; $\bar{r}_i^p$ is the mean radius of the group i of pores, the actual radii of which cover a small but finite range; (the superscript to r

has now been restored, to provide conformity with the rest of the section.) Q_i is identified with Q_{ii} of the Roberts method (p. 142).

The calculation implicit in Equation (3.27) is carried out for each stage commencing with stage $i = 0$, where all the pores are full, so that the terms in A and L in Equation (3.25) are zero and δv_i is therefore also zero. Thus, the volume δv_1^p of the first group of pores characterized by the mean radius $\bar{r}_1^p$ is

$$\delta v_1^p = Q_1 \, \delta V_1 \tag{3.29}$$

Next the value of δv_2^f for stage 2 is calculated with Equation (3.25); $A(>r_2)$ is now the wall area of the group 1 of pores and may be written A_1, and similarly $L(>r_2)$ in the length of the group and may be written L_1. From the geometry of the cylinder we have

$$A_1 = 2\frac{\delta v_1^p}{\bar{r}_1^p} \qquad \text{and} \qquad L = \frac{A_1}{2\pi r_1^p} \tag{3.30}$$

The core volume δv_2^k of group 2 is then given by

$$\delta v_2^k = \delta V_2 - \delta v_2^f \tag{3.31}$$

and its pore volume by

$$\delta v_2^p = Q_2 \, \delta v_2^k \tag{3.32}$$

Stages 2, 3, 4 ... can be dealt with in an analogous manner. In stage 3, for example, we have by comparison with Equation (3.25),

$$\delta v_3^f = \delta t_3(A_1 + A_2) - 2\pi t_3 \, \delta t_3(L_1 + L_2) \tag{3.33}$$

$$= (t_2 - t_3)(A_1 + A_2) - 2\pi t_3(t_2 - t_3)(L_1 + L_2) \tag{3.34}$$

Also

$$A_2 = 2\frac{\delta v^p}{r_2^p} \qquad \text{and} \qquad L_2 = \frac{A_2}{2\pi r_2^p} \tag{3.35}$$

and

$$\delta v_3^p = Q_3(\delta V_3 - \delta v_3^f) \tag{3.36}$$

$$= \left(\frac{\bar{r}_3^p}{\bar{r}_3^p - t_3}\right)^2 (\delta V_3 - \delta v_3^f) \tag{3.37}$$

The pore size distribution is the plot of $\delta v^p/\delta r^p$ against $\bar{r}^p$.

To facilitate application of the method, Dollimore and Heal[41] gave a standard table of the relevant parameters, based on regular intervals of r^p extending from 100 Å down to 7 Å; t-values were calculated with Halsey's equation (p. 89). Table 3.2B retains the essential features of their original table, but r^p no longer extends below 17 Å (cf. p. 160) and the t-values are now based on an experimentally determined standard isotherm.[32] (p. 93).

The numerical steps are illustrated by the extract given in Table 3.4 from

TABLE 3.4

Calculation of pore size distribution
(Method of Dollimore and Heal[41])

(1)	(2)	(3)	(4)	(5)	(6)	(7)	(8)	(9)	(10)	(11)	(12)	(13)	(14)	(15)	(16)	(17)	(18)	(19)	(20)
p / p°	r^p / Å	$\bar{r}^p$ / Å	δr^p / Å	t / Å	$\bar{t}$ / Å	δt / Å	Q	V / mm³	δV / mm³	B / mm³	C / mm³	D / mm³	δv^p / mm³	$\sum(\delta v^p)$ / mm³	δA / m²	$\sum(\delta A)$ / m²	$\frac{\delta A}{\bar{r}^p}$ / m²/Å	$\sum\left(\frac{\delta A}{\bar{r}^p}\right)$ / m²/Å	$\frac{\delta v^p}{\delta r^p}$ / mm³/Å
0·832	60	65	10	9·2	9·5	0·6	1·36	712	0	0	0	0	0	0	0	0	0	0	0
0·800	50	55	10	8·6	8·9	0·6	1·41	712	3	0	0	3	4	4	1·4	1·4	0·02	0·02	0·4
0·746	40	45	10	7·7	8·15	0·9	1·45	705	4	0·1	0·01	3·9	5·7	9·7	2·5	3·9	0·06	0·08	0·6
0·711	35	37·5	5	7·4	7·55	0·3	1·56	700	5	0·1	0·02	4·9	7·6	17·3	4·1	8·0	0·11	0·19	1·5
0·667	30	32·5	5	7·0	7·2	0·4	1·63	671	29	0·3	0·05	28·7	46·8	64·1	28·8	36·8	0·89	1·08	9·3
0·605	25	27·5	5	6·5	6·75	0·5	1·71	572	99	1·84	0·36	97·5	167	231	121	150	4·44	5·52	33·4
. .	. .	. .	. .	. .	. .	. .	. .	. .	. .	. .	. .	. .	. .	. .	. .	. .	. .	. .	. .

Columns [1] to [8] based on Table 3.2B.

Column [9], adsorption values from isotherm for silica gel GS50 (desorption branch).

Column [11]: $B = 0{\cdot}1 \times \delta t \times \sum(\delta A) = 0{\cdot}1 \times$ [7] $\times$ [17] ($\sum(\delta A)$ from line above).

[12]: $C = 0{\cdot}1 \times \delta t \times \bar{t} \times \sum(\delta A/\bar{r}^p) = 0{\cdot}1 \times$ [7] $\times$ [6] $\times$ [19].

[13]: $D = \delta V - B + C =$ [10] $-$ [11] $+$ [12] (=core volume).

[14]: $\delta v^p = Q \times$ D $=$ [8] $\times$ [13].

[16]: $\delta A = 20 \times (\delta v^p/\bar{r}^p) = 20 \times$ [14]/[3].

[18]: $\delta A/\bar{r}^p =$ [16]/[3] $= 2\pi L^p$ (L^p = length of pore wall).

Volumes in mm³(liquid); radii and film thicknesses in Å; areas in $m^2\,g^{-1}$. The complete table commences at $r^p = 100$ Å ($p/p^\circ = 0{\cdot}899$), and continues down to $r^p = 17$ Å ($p/p^\circ = 0{\cdot}439$); it may be based on Table 3.2B. An alternative table, based on regular intervals of p/p°, may be built up from Table 3.2A.

a work sheet for the same sample of silica as that in Table 3.3 (again for the desorption branch of the isotherm). The pore size distribution curve derived from the complete work sheet is shown as Curve B in Fig. 3.18.

A method based on neither length nor area of pore walls

The method devised by Roberts[42] represents a further simplification of procedure whilst still fully allowing for the thinning of the multilayer. The idea of subdividing the pore system into a number of fixed groups of pores, each characterized by a narrow range of pore sizes, is retained, but the number of groups is rather small: in the original paper the range from 100 Å to 10 Å was divided into ten groups, which were numbered 1 to 10. By the particular manner in which the group numbers were incorporated into the symbols, Roberts was able to devise a considerably simplified work sheet and procedure.

The actual set of size intervals chosen by Roberts has the virtue of simplicity, but it suffers from the disadvantage that the values of relative pressure are crowded together at the upper end of the isotherm and spread out widely at the lower. In the modified Table given here (Table 3.5), the range from 100 Å to 40 Å is divided into intervals of 10 Å, that from 40 Å to 25 Å into intervals of 5 Å, and that from 25 Å to 17 Å into intervals of 2 Å, giving 13 groups in all. This arrangement achieves a reasonably even spacing of relative pressure whilst avoiding an inconveniently large number of groups. For reasons which will be explained later (p. 154) the procedure is not extended below 17 Å.

For each group of pores, the pore volume δv_i^p is related to the core volume by means of a model, either the cylinder or the parallel-sided slit as the case may be. Allowance is made for the succession of film thicknesses corresponding to the progressive thinning of the multilayer in each pore, as desorption proceeds. Thus for group i, with radius $\bar{r}_i^p$ when the film thickness is t_j ($j \geqslant i$) and the core volume is δv_{ij}^k, the pore volume δv_i^p will be given by

$$\frac{\delta v_i^p}{\delta v_{ij}^k} = \left(\frac{\bar{r}_i^p}{\bar{r}_i^p - t_j}\right)^2 \tag{3.38}$$

if the pores are cylindrical.

Thus
$$\delta v_i^p = Q_{ij} v_{ij}^k \tag{3.39}$$
where
$$Q_{ij} = \left(\frac{\bar{r}_i^p}{\bar{r}_i^p - t_j}\right)^2 \tag{3.40}$$

TABLE 3.5

Calculation of pore size distribution (Roberts method[42]). Work sheet

Pore group	13	12	11	10	9	8	7	6	5	4	3	2	1	0
r^p/Å	17	19	21	23	25	30	35	40	50	60	70	80	90	100
$\bar{r}^p$/Å	18	20	22	24	27·5	23·5	37·5	45	55	65	75	85	95	
t/Å	5·5	5·85	6·1	6·3	6·5	7·05	7·4	7·7	8·6	9·2	9·8	10·5	11·7	
p/p^o	0·439	0·490	0·535	0·574	0·605	0·667	0·711	0·746	0·800	0·832	0·856	0·875	0·889	0·899
V/mm³														
w/mm³														
12	528													
11	556	539												
10	588	572	556											
9	634	620	606	594										
8	685	673	660	650	640									
7	724	712	701	692	683	659								
6	767	757	747	740	732	711	698							
5	807	799	790	784	778	760	749	739						
4	835	828	821	816	810	795	785	777	753					
3	856	850	844	839	834	821	812	805	784	770				
2	873	867	862	857	852	841	832	827	808	795	783			
1	886	881	876	872	868	857	850	827	816	804	791	769		
Q_{ii}	2·11	2·00	1·92	1·84	1·715	1·63	1·56	1·455	1·41	1·32	1·33	1·30	1·31	
δr^p	2	2	2	2	5	5	5	10	10	10	10	10	10	Å
B														mm³
$C = w - B$														mm³
$\delta v^p = Q_{ii}C$														mm³
$\delta v^p/\delta r^p$														mm³/Å

Values of $10^3/Q_{ij}$

B = sum of products $\left(\delta v^p \times \frac{1}{Q_{ij}}\right)$ in the rows above (cf. Equation (3.47) and Table 3.6).

It will be noted that the first suffix of Q_{ij} refers to the pore radius of the group, and the second to the film thickness.

For parallel-sided slits the conversion factor (cf. Fig. 3.16) is

$$Q_{ij}(\text{slits}) = \frac{d_i^p}{d_i^p - 2t_{ij}} \tag{3.41}$$

where d_i^p is the width of the slits.

Consider the process of progressive emptying of the pore system, from the point, on the isotherm corresponding to $r^p = 100$ Å, where all the pores are presumed full (cf. p. 133). When the relative pressure falls to the value p_1/p° which corresponds to $r^p = 90$ Å, the first group of pores will have lost their capillary condensate and a film of thickness t_1 will remain on their walls. The core volume δv_{ii}^k of the group will be equal to the amount w_1 of adsorbate given up during the step, expressed as a liquid volume; the pore volume δv_i^p of the first group is therefore

$$\delta v_1^p = Q_{11}\,\delta v_{11}^k = Q_{11} w_1 \tag{3.42}$$

When the relative pressure falls to p_2/p°, corresponding to $r^p = 80$ Å, the second group of pores will have given up a volume of adsorbate equal to δv_{22}^k. But since the film thickness has now diminished to t_2, there will have been an additional loss from the walls of group 1: the *total* loss from group 1 is therefore δv_{12}^k so that the *total* loss w_2 from both groups is

$$w_2 = \delta v_{22}^k + \delta v_{12}^k \tag{3.43}$$

w_2 is of course obtained from the experimental isotherm as the difference between the uptakes at the *starting point* and at p_2/p° respectively, expressed as a liquid volume.

By Equation (3.39) the *pore* volume of group 2 is

$$\delta v_2^p = Q_{22}\,\delta v_{22}^k \tag{3.44}$$

or, from (3.43)

$$\delta v_2^p = Q_{22}(w_2 - \delta v_{12}^k) \tag{3.45}$$

$$= Q_{22}\left(w_2 - \frac{\delta v_{12}^p}{Q_{12}}\right) \tag{3.46}$$

The procedure may be extended to groups 3 and 4:

$$\delta v_3^p = Q_{33}\left\{w_3 - \left(\frac{\delta v_2^p}{Q_{23}} + \frac{\delta v_1^p}{Q_{13}}\right)\right\} \tag{3.47}$$

$$\delta v_4^p = Q_{44}\left\{w_4 - \left(\frac{\delta v_3^p}{Q_{34}} + \frac{\delta v_2^p}{Q_{24}} + \frac{\delta v_1^p}{Q_{14}}\right)\right\} \tag{3.48}$$

and so on up to group 13.

It is convenient to draw up a Table of values of Q_{ij} calculated by Equation (3.40) for cylindrical pores (Table 3.5), or Equation (3.41) for slit-shaped pores, for all values of i and j from 1 to 13. The value of $\bar{r}_i^p$ will correspond to the *mid-point* of the range covered by the group, e.g. for group 1, $\bar{r}_1^p = 95$ Å; and t_j is the value of t corresponding to the pressure at the *end* of the step, when the core is empty (e.g. for group 1, t_1 is the value of t at relative pressure p_1/p° corresponding to $r^p = 90$ Å).

In using the table for pore size calculations, it is necessary to read off the values of the uptake from the experimental isotherm for the values of p/p° corresponding to the different r^p values given in the table. Unfortunately, these values of relative pressure do not correspond to division marks on the scale of abscissae, so that care is needed if inaccuracy is to be avoided. This difficulty can be circumvented by basing the standard table on even intervals of relative pressure rather than of r^p; but this then leads to uneven spacings of r^p. Table 3.6 illustrates the application of the standard table to a specific example—the desorption branch of the silica isotherm already referred to. The resultant distribution curve appears as Curve C in Fig. 3.18.

From Fig. 3.18 it will be seen that the curves calculated by the three methods agree well. Actually, the Pierce procedure tacitly assumes the film area of a group—the area of the core "walls"—to be identical with the area of the pore walls, whereas the other two methods allow for the increase in the core area of each group as desorption progresses. Otherwise all three methods amount to slightly different ways of applying the same model to the same experimental data, consequently the good agreement between the three curves is not surprising.

The curve for core size distribution—Foster's[30] plot of $\delta v^k/\delta r^k$ against $\bar{r}^k$—is also shown, as Curve D, in Fig. 3.18. It differs markedly from the pore size distribution curves, clearly showing that the corrections for the film thinning effect which have become possible since Foster's day, are of first-order importance.

The "modelless" method of Brunauer, Mikhail and Bodor[31]

The procedures described so far have all required a pore model to be assumed at the outset, usually the cylinder, adopted on the grounds of simplicity rather than correspondence with actuality. Brunauer, Mikhail and Bodor[31] have attempted to eliminate the over-dependence on a model by basing their analysis on the hydraulic radius r_H rather than the Kelvin radius r_m. The hydraulic radius r_H is defined as the ratio of the cross-sectional area of a tube to its perimeter, so that for a capillary of uniform cross-section r_H is equal to the ratio of the volume of an element of core to

TABLE 3.6

Calculation of pore size distribution (Roberts Method[42]). Worked example from desorption branch of nitrogen isotherm on silica gel GS50[36]

(Entries from the experimental data are in bold type)

Pore group		13	12	11	10	9	8	7	6	5	4	3	2	1	0
r^p/Å		17	19	21	23	25	30	35	40	50	60	70	80	90	100
$\bar{r}^p$/Å		18	20	22	24	27·5	23·5	37·5	45	55	65	75	85	95	
t/Å		5·5	5·85	6·1	6·3	6·5	7·05	7·4	7·7	8·6	9·2	9·8	10·5	11·7	
p/p°		0·439	0·490	0·535	0·574	0·605	0·667	0·711	0·746	0·800	0·832	0·856	0·875	0·889	0·899
V/mm³		**418**	**465**	**500**	**537**	**572**	**671**	**700**	**705**	**709**	**712**	**712**	**712**	**712**	
δt^{r^p}*	w_i/mm³	**294**	**247**	**212**	**175**	**140**	**41**	**12**	**7**	**3**	**0**	**0**	**0**	**0**	
56	12	528 (**29**)													
62	11	556 (**35**)	539 (**34**)												
61	10	588 (**36**)	572 (**35**)	556 (**34**)											
167	9	634 (**106**)	620 (**104**)	606 (**101**)	594 (**99**)										

← Values of $10^3/Q_{ij}$

47	8	685 (32)	673 (32)	660 (31)	650 (31)	640 (30)									
8	7	724 (6)	712 (6)	701 (6)	692 (5)	683 (5)	659 (5)								
6	6	767 (5)	757 (5)	747 (5)	740 (4)	732 (4)	711 (4)	698 (4)							
4	5	807 (3)	799 (3)	790 (3)	784 (3)	778 (3)	760 (3)	9 (3)	739 (3)						
	..	..	..	..	..	..	..	..	..						
	Q_{ii}	2·11	2·00	1·92	1·84	1·715	1·63	1·56	1·455	1·41	1·32	1·33	1·30	1·31	
	δr^p	2	2	2	2	5	5	5	10	10	10	10	10	10	Å
	B	**249**	**219**	**180**	**142**	**42**	**12**	**7**	**3**	**0**	**0**	**0**	**0**	**0**	mm^3
	$C = w - B$	**45**	**28**	**32**	**33**	**98**	**5**	**4**	**4**	**3**	**0**	**0**	**0**	**0**	mm^3
	$\delta v^p = Q_{ii}C$‡	**95**	**56**	**62**	**61**	**167**	**47**	**8**	**6**	**4**					mm^3
	$\delta v^p/\delta r^p$	**47**	**28**	**31**	**30**	**33**	**9**	**1·6**	**0·6**	**0·4**					$mm^3/Å$

B = sum of products $\left(\delta v^p \times \frac{1}{Q_{ij}}\right)$ in the rows above (cf. Equation (3.47) and Table 3.5).

* Value of δv^p, re-entered from penultimate line marked ‡.
Entries in bold type in each line were obtained by multiplying the stated value of $1/Q_{ij}$ by the value of δv_i^p for the line.

the surface area of its walls, or

$$r_H = \mathrm{d}v^k/\mathrm{d}A^k \tag{3.49}$$

As in the other methods, the "modelless" procedure visualizes the progressive emptying of the pore system, initially full up, by the stepwise reduction in relative pressure. At each step the value of additional core wall area which becomes exposed is calculated by means of the equation (see p. 170):

$$\gamma\,\mathrm{d}A^k = -(\mu^a - \mu^\circ)\,\mathrm{d}n \tag{3.50}$$

Here $\mathrm{d}A^k$ is the additional wall area exposed when the uptake diminishes by $\mathrm{d}n$ moles through evaporation from the capillary; μ^a is the chemical potential of the capillary condensate and μ° that of the bulk liquid adsorptive. The negative sign is necessary because the area A exposed increases as the uptake diminishes. If the adsorptive vapour behaves as a perfect gas,

$$\mu^a - \mu^\circ = RT\ln(p/p^\circ)$$

so that Equation (3.50) becomes[43]

$$\gamma\,\mathrm{d}A^k = -RT\ln(p/p^\circ)\,\mathrm{d}n \tag{3.51}$$

Integration of Equation (3.51) over the finite step i gives

$$\gamma(A_i^k - A_{i-1}^k) = -\int_{n_{i-1}}^{n_i} RT\ln(p/p^\circ)\,\mathrm{d}n \tag{3.52}$$

where n_i is the amount adsorbed, and A_i^k the total area of core walls exposed at the end of the step; n_{i-i} and A_{i-i}^k are the corresponding quantities at the beginning of the step. Thus $(A_i^k - A_{i-i}^k)$ is the area δA_i^k of the core walls of group i of pores.

Equation (3.52) is applied in succession to all steps from step 1 onwards, commencing from the uptake n_0 where all pores are deemed full (often at $p/p^\circ = 0{\cdot}95$; cf. p. 132), to obtain the values of δA_1, δA_2 etc. If no correction is made for the thinning of the multilayer as the emptying process continues, the core volumes will be given by $\delta v_i^k = (n_i - n_{i-i})V_L$, and the uncorrected modelless core distribution curve—a plot of $\delta v^k/\delta r_H$ against $\bar{r}_H$—can be constructed.

In order to allow for the thinning of the multilayer, it is necessary to assume a pore model so as to be able to apply a correction to n_1, n_2, etc., in turn for re-insertion into Equation (3.52). Unfortunately, with the cylindrical model the correction becomes increasingly complicated as desorption proceeds, since the wall area of each group of cores changes progressively as the multilayer thins down. With the slit model, on the other hand, δA^k for a

given group remains constant. According to Brunauer, it turns out that the difference between the two corrections is so small that the simpler parallel-plate correction is adequate for most practical purposes. To convert the corrected core size distribution into a pore size distribution a model must again be used.

Closer examination reveals however that the Brunauer method is not fundamentally distinct from methods based on the Kelvin equation. As pointed out by de Vleesschauwer,[44] equations such as (3.52) are not really employed in the integral form, inasmuch as the aim is to evaluate the surface areas of successive groups of cores. In effect Equation (3.52) is used after adaptation to small rather than infinitesimal increments and becomes

$$\delta A^k = -\frac{RT}{\gamma}\ln(p/p^\circ)\,\delta n \tag{3.53}$$

where p/p° is the relative pressure at the mid-point of the step. Rearrangement of this equation with substitution of $\delta n = \delta v^k/V_L$ (where δv^k = core volume of the group) gives

$$\frac{\delta v^k}{\delta A} = -\frac{\gamma V_L}{RT\ln(p/p^\circ)} \tag{3.54}$$

Now the left-hand side of Equation (3.54) is equal to the hydraulic radius r_H of the group of cores (cf. Equation (3.49)) and the right-hand side by the Kelvin equation (cf. Equation (3.20)) is equal to $r_m/2$. Consequently,

$$r_H = \frac{r_m}{2} \tag{3.55}$$

and Equation (3.54) is thus equivalent to the Kelvin equation itself. The "modelless" method must therefore embody the same limitations as those involved in methods based directly on the Kelvin equation. In view of the rather more cumbersome calculations required, the "modelless" method would seem to offer no advantage over the more conventional procedures such as those already described.

In conclusion, it should further be noted that, as will be explained in Section 3.8, the quantity dA^k of the basic equation (3.51) is equal to the area of the core walls only if the capillary is of constant cross-section. If it tapers either outwards or inwards, a correction to dA^k is required.

Packed sphere model[45]

A model which is attracting increasing attention, because of its relevance to actual solids composed of globular particles (Section 1.6), is the packed sphere model. By applying the same general principles as those outlined

above, it is possible to carry out size calculations for pores made up of the interstices between packed spheres. Simplifying assumptions are necessary, viz that all the spheres are of the same size and that the same coordination N holds throughout the assembly. (N = number of neighbours contacted by each globule). The procedure is necessarily complicated, and must take care of the separate processes of multilayer formation, condensation to form pendulate rings around points of contact of spheres, and condensation in the cavities between spheres. Calculations of this kind have been carried out by Dollimore and Heal[46] on the nitrogen isotherms of two silica gels, one with medium-sized pores (peak ~85 Å) and one with narrow pores (peak ~17 Å), the adsorption branch being used. Several points of interest emerged from the results: the distribution curve was very nearly the same whether the correction for the pendulate rings (torus correction) was included or not; variation in the coordination number N between 4 and 8 had very little effect; and in particular, the distribution curve hardly differed from that obtained by use of the simple cylindrical model. These findings were substantially confirmed by Havard and Wilson[47] in their detailed study on Gasil 1, one of the standard materials used in the surface area project referred to in Chapter 2 (p. 105). They concluded, from calculations on the adsorption branch of the hysteresis loop (Type A loop) that there is little advantage in using models for this kind of system which are any more complicated than the open-ended cylindrical capillary.

Network effects[48,49]

Conventional methods for calculations of pore size distribution are based on the tacit assumption that, in assemblies of pores of simple geometrical form, the processes taking place in a given pore occur independently of those taking place in other pores. From a comprehensive study of scanning behaviour, Everett[27,48] has been led to the conclusion that in numerous cases desorption from a pore is, in fact, influenced by the state in the neighbouring pores, and in particular that the course of events will depend on whether there is a clear channel linking the pore to the outer surface of the material. The probability that such a channel will be present will depend on the amount of condensate remaining in the structure, which can give rise to "pore-blocking" effects.[48,49] It is suggested that the adsorption branch of the loop will be free of such effects; this is because, if any empty pore is surrounded by a filled pore space, the bubble of vapour it contains will condense as soon as the relative pressure has reached the value given by the Kelvin equation for the pore dimension; the pore can then fill up by flow of liquid from neighbouring pores. During desorption, however, pore blocking will occur because bubbles of vapour cannot nucleate at the pressure which

would produce capillary evaporation if the pores were freely exposed (the blocking of an ink-bottle pore by condensate in the neck is a simple example; cf. p. 128).

Everett concludes[48] that in systems where pore blocking can occur, pore size distribution curves derived from the desorption branch of the isotherm are likely to give a misleading picture of the pore structure; in particular the size distribution will appear to be much narrower than it actually is. Thus the *adsorption* branch is to be preferred unless network effects are known to be absent.

The importance of these considerations may be judged from Fig. 3.19,

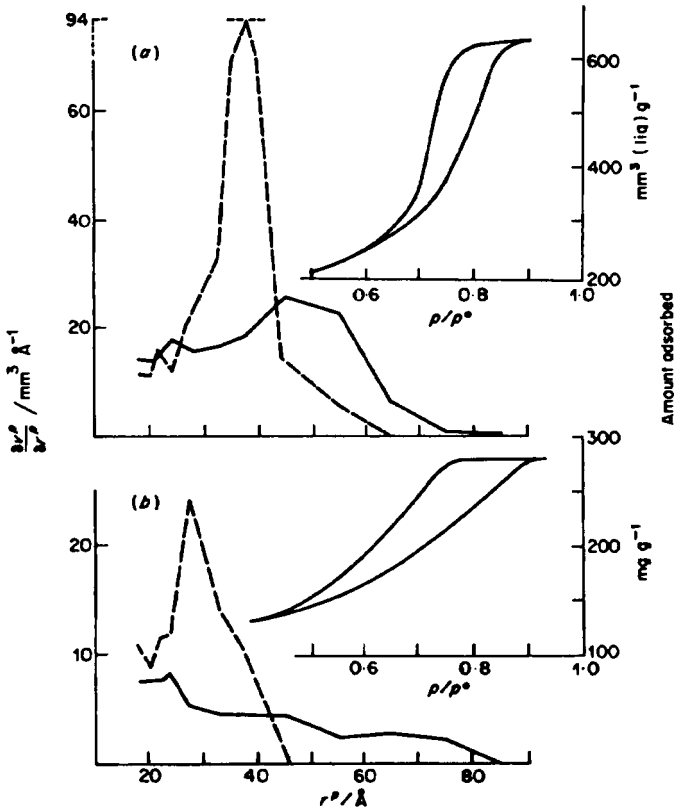

Fig. 3.19 Contrast between the pore size distribution curves based on the adsorption and the desorption branch of the hysteresis loop respectively. ——, adsorption, – – – –, desorption. (*a*) For silica gel GS80;[36] (*b*) for a compact[8] prepared from a silica powder at 64 ton in^{-2}. The relevant parts of the isotherms are shown in the insets.

where the pore size distributions, calculated from both branches of the loop, are given for two typical cases. In each case, the two distributions differ markedly from each other and give quite different pictures of the pore structure: the distribution calculated from the adsorption branch is, for each solid, much broader than that from the desorption branch, and according to Everett's argument gives a better guide to the actual pore structure.

Despite difficulties of interpretation, curves of pore size distribution can give useful indications of significant differences between pore systems, particularly in related sets of solids. Figure 3.20, which refers to graphs from compacts of silica powder prepared at successively higher pressures, provides an illustration. The curves derived from the desorption (Fig. 3.20(*a*)) and the adsorption (Fig. 3.20(*b*)) branches of the loop are again very different in shape, but both kinds show a progressive shift as the compacting pressure is increased.

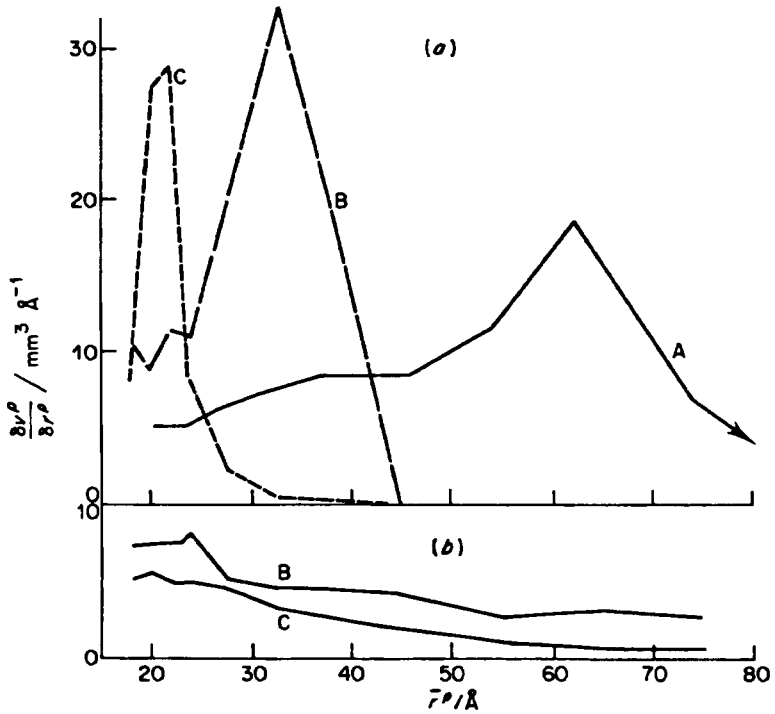

Fig. 3.20 Pore size distributions (calculated by the Roberts method) for silica powder[8] compacted at: (A) 16 ton in^{-2}; (B) 64 ton in^{-2}; (C) 130 ton in^{-2}. The distributions in (*a*) were calculated from the desorption branch of the isotherms of nitrogen, and in (*b*) from the adsorption branch.

3.7 The range of validity of the Kelvin equation

The curvature effect

It has long been realized that in very fine pores, having widths of the order of a few molecular diameters, the Kelvin equation could no longer remain strictly valid. Not only would the values of the surface tension γ and molar volume V_L deviate from those of the liquid adsorptive in bulk, but the very concept of a meniscus would eventually become meaningless. The question as to the value of the curvature at which the deviations become large enough to produce appreciable effects on the calculated pore size is a long-standing one and not easy to answer with precision. Since direct experimental measurements of γ and V_L are ruled out by the smallness of the dimensions involved, indirect approaches are inevitable. On statistical-mechanical grounds, Guggenheim[50] concluded that the surface tension must begin to depend on the radius of curvature of a liquid surface when this falls below $r \sim 500$ Å. Melrose,[51] extending the treatment of Willard Gibbs,[52] was able to derive an expression for γ/γ_∞ as a function of the radius of curvature that indirectly involved the thickness of the interfacial region. A curve from Melrose's paper, reproduced in Fig. 3.21, is based on the assumption, regarded as reasonable, that the interfacial region is 4 to 6 molecular diameters thick. As is seen, the surface tension begins to deviate appreciably from its "bulk" value γ_∞ when r falls below ~ 500 Å; at $r = 100$ Å, γ already exceeds γ_∞ by 10 per cent and at $r = 20$ Å, the excess has become 30 per cent. Inserted in the Kelvin equation, these values of γ will elevate r_m in the same proportions, so that the corrected values of r_m would be 110 Å and 27 Å respectively.

Chang and his co-workers,[53] adopting a statistical-mechanical rather than thermodynamic approach, made calculations for five different

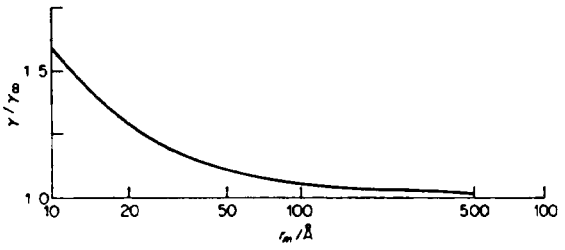

Fig. 3.21 The effect of meniscus curvature on surface tension. Plot of γ/γ_∞ against r_m. γ is the surface tension of the meniscus having the mean radius of curvature r_m and γ_∞ that of a plane surface of liquid, according to Melrose.[51] The value of γ/γ_∞ was calculated by the equation $\gamma = \gamma_\infty(1 - \Delta\lambda/r_m)$ with $\Delta\lambda = 3$ Å.

adsorptives—nitrogen, argon, benzene, cyclohexane and water—and found that with nitrogen, for example, the value of γ/γ_∞ was 1·05 for $r = 148$ Å and rose to the high figure of 1·49 at $r = 20$ Å.

These various calculations indicate that, for most of the range covered in pore size calculations, the actual value of γ will differ appreciably from the normal value. The effect of using the corrected values would be to raise the calculated value of r_m in the proportion $\gamma:\gamma_\infty$.

The time is perhaps not yet ripe, however, for introducing this kind of correction into calculations of pore size distribution: the analyses, whether based on classical thermodynamics or statistical mechanics are being applied to systems containing relatively small numbers of molecules where, as stressed by Everett and Haynes,[21] the properties of matter must exhibit wide fluctuations. A fuller quantitative assessment of the situation in very fine capillaries must await the development of a thermodynamics of small systems. Meanwhile, enough is known to justify the conclusion that, at the lower end of the mesopore range, the calculated value of r_m is almost certain to be too low by many per cent.

The tensile strength effect

In 1965 Harris[54] drew attention to the fact that the lower closure point of the hysteresis loop of nitrogen at 77 K is frequently situated at a relative pressure close to 0·42 but never below: of more than one hundred nitrogen isotherms in the literature examined by Harris, one-half showed a sharp fall in adsorption, with loop closure, in the relative pressure range 0·42 to 0·50. Interpreted naively by a Kelvin type analysis, these observations would imply that a large proportion of adsorbents possess an extensive pore system in the very narrow range $17\text{ Å} < r^p < 20\text{ Å}$, with a sudden cut-off around 17 Å, which corresponds to $p/p^\circ = 0{\cdot}42$ (cf. p. 135). The improbability of this state of affairs led Harris to suggest that a change in the mechanism of adsorption occurred at this point, though he did not speculate as to its nature.

The evidence obtained in compaction experiments is of particular interest in the present context. Figure 3.22 shows the results obtained by Avery and Ramsay[55] for the isotherms of nitrogen on compacts of silica powder. The hysteresis loop moved progressively to the left as the compacting pressure increased, but the lower closure point did not fall below a relative pressure of ~0·40. Similar results were obtained in the compaction of zirconia powder both by Avery and Ramsay[55] (cf. Fig. 4.5), and by Gregg and Langford,[8] where the lower closure point moved down to $0{\cdot}42$–$0{\cdot}45p^\circ$ but not below. With a mesoporous magnesia[56] (prepared by thermal decomposition of the hydrated carbonate) the position of the closure point

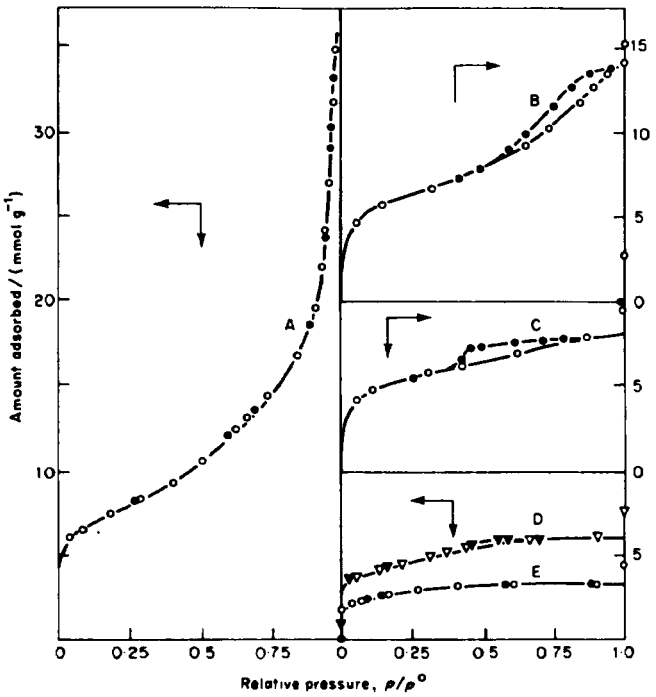

Fig. 3.22 Adsorption isotherms of nitrogen at 77 K on silica powder and its compacts.[55] (A) uncompressed; (B) 10 ton in^{-2}; (C) 40 ton in^{-2}; (D) 50 ton in^{-2}; (E) 100 ton in^{-2}. Open symbols represent adsorption, solid symbols desorption. (Courtesy Ramsay.)

was almost the same, at $\sim 0{\cdot}42p^{\circ}$, both before and after the solid had been compacted at 920 MN m^{-2} (60 ton in^{-2}). Similarly, compacts of MgO prepared by thermal dehydration of $Mg(OH)_2$ gave closure points sometimes above but never below $\sim 0{\cdot}42$.

For other adsorptives the experimental evidence, though less plentiful than with nitrogen, supports the view that at a given temperature the lower closure point is never situated below a critical relative pressure which is characteristic of the adsorptive. Thus, for benzene at 298 K Dubinin[57] noted a value of 0·17 on active carbons, and on active charcoals Everett and Whitton[58] found $\sim 0{\cdot}19$; other values, at 298 K, are 0·20 on alumina xerogel,[59] 0·20–0·22 on titania xerogel[60,61] and 0·17–0·20 on ammonium silicomolybdate.[62] Carbon tetrachloride at 298 K gives indication of a minimum closure point at 0·20–0·25 on a number of solids including

dehydrated gibbsite,[59] titania,[60,61] dehydrated gypsum,[63] ferric oxide,[64] calcined vermiculite,[65] and compacted ammonium phosphotungstate.[56,66]

The results of Hickman[67,68] for the adsorption of butane at 273 K on samples of ball-milled artificial graphite, are of particular interest in the present context. The graphite was milled for 1040 hours and the isotherms of butane were measured on samples withdrawn at intervals. The monolayer capacity increased almost sixty-fold during this period, from 2·5 to 145 mg g^{-1}, yet all six of the isotherms showed a steep fall at the same relative pressure of 0·5. (The low pressure hysteresis, cf. Fig. 3.23, was almost certainly an extraneous effect, caused by swelling.) The pore structure must have varied widely throughout the series, so that the constancy of this "closure" point is all the more striking: it is difficult to find any reason why all the pore systems should show a peak in size distribution at $r_m = 19{\cdot}2$ Å, the Kelvin value corresponding to $p/p^\circ = 0{\cdot}5$.

A possible explanation for the existence of a minimum value of relative pressure for loop closure was hinted at by Schofield[69] in 1948, who suggested

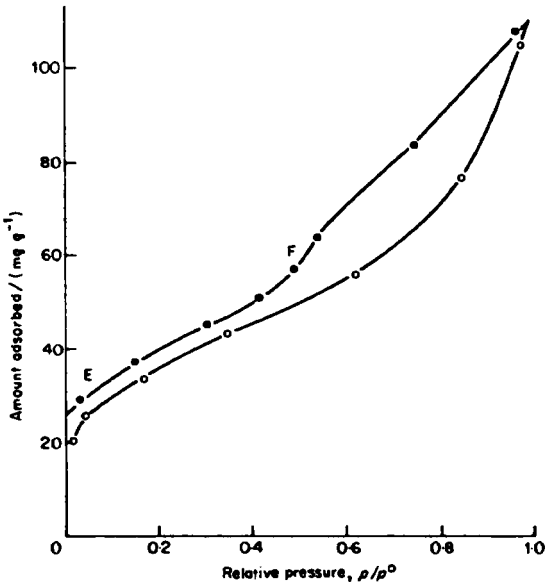

Fig. 3.23 Adsorption isotherm of n-butane[67] at 273 K on a sample of artificial graphite ball-milled for 192 b. The shoulder F appeared at a relative pressure which was the same for all six samples in the first milling run, all six in the second milling run, and also for two of the milled samples which had been compacted. The milling time varied between 0 and 1024 h, and the BET-nitrogen areas of the surfaces between 9 and 610 $m^2 g^{-1}$.

that the absence of hysteresis in the isotherms of fine-pored xerogels might be attributed to the tensile strength of the liquid adsorbate. This idea has been elaborated by Dubinin,[70] Flood,[71] Everett and Burgess,[72] and Melrose.[51]

According to the Young–Laplace equation, the pressure difference across a meniscus separating capillary-condensed liquid from its vapour is given by (cf. Equation (3.6)):

$$p^g - p^l = 2\gamma/r_m \tag{3.56}$$

where g and l refer to the vapour and liquid phase respectively. Since in the range under consideration p^g is much smaller than p^l, the liquid experiences a tension τ given by

$$\tau = -p^l \tag{3.57}$$

and therefore in turn by

$$\tau = 2\gamma/r_m \tag{3.58}$$

But by the Kelvin equation

$$\frac{2\gamma}{r_m} = -\frac{RT}{V_L}\ln(p/p^\circ) \tag{3.59}$$

and therefore

$$\tau = -\frac{RT}{V_L}\ln(p/p^\circ) \tag{3.60}$$

so that the tension increases as the value of p/p°, and with it the value of r_m, diminishes. Now the maximum tension that a liquid can withstand is equal to its tensile strength τ_0: consequently there will be a minimum value $(p/p^\circ)_h$, say, compatible with the continued existence of capillary-condensed liquid, and given by

$$\ln(p/p^\circ)_h = -\left(\frac{V_L}{RT}\right)\tau_0 \tag{3.61}$$

This minimum value should be constant for a given adsorptive at a given temperature, irrespective of the nature of the adsorbent. Any liquid present in pores finer than those given by $r_{m,h}$ of the appropriate Kelvin expression

$$r_{m,h} = -\frac{2\gamma V_L}{RT}\ln(p/p^\circ)_h \tag{3.62}$$

should therefore evaporate as soon as the relative pressure falls to the critical value $(p/p^\circ)_h$.

Thus the hysteresis loop should close at a relative pressure determined by the tensile strength of the liquid adsorptive, no matter whether the pore system extends to finer pores than those characterized by $r_{m,h}$ or not.

The most direct test of the tensile strength hypothesis would be to compare the value of τ_0 calculated from the closure point of the isotherm by Equation (3.61) with the tensile strength of the bulk liquid determined directly. Unfortunately, experimental measurement of the tensile strength is extremely difficult because of the part played by adventitious factors such as the presence of solid particles and dissolved gases, so that the values in the literature vary widely (between 9 and 270 bar for water at 298 K, for example).

It is, however, possible to calculate the tensile strength of a liquid by extrapolation of an equation of state for the fluid into the metastable region of negative pressure. Burgess and Everett[72] in their comprehensive test of the tensile strength hypothesis, plot the theoretical curves of T/T_c against τ_0/p_c, calculated from the equations of state of van der Waals, Guggenheim, and Berthelot (Fig. 3.24) (T_c and p_c are the critical temperature and critical

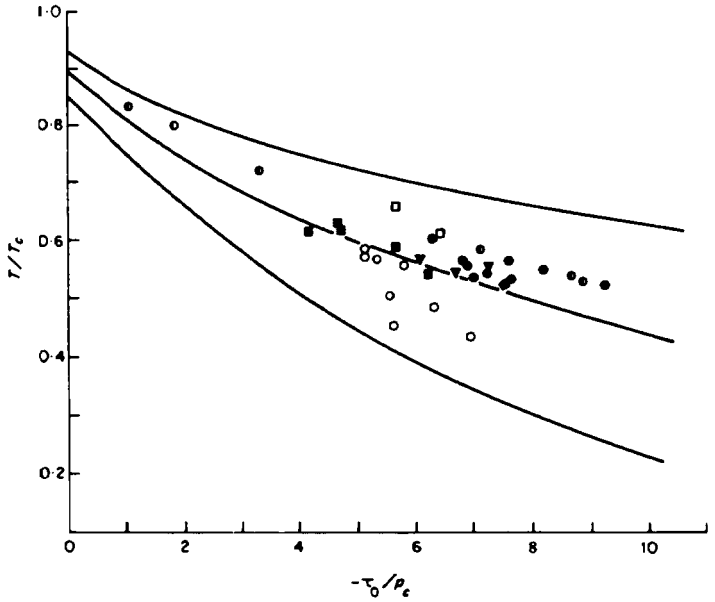

Fig. 3.24 Test of the "tensile strength" hysteresis of hysteresis (Everett and Burgess[72]). T/T_c is plotted against $-\tau_0/p_c$, where T_c is the critical temperature and p_c the critical pressure, of the bulk adsorptive; τ_0 is the tensile strength calculated from the lower closure point of the hysteresis loop. ◐, benzene; ○, xenon; □, 2-2 dimethyl benzene; ■, nitrogen; ▼, 2,2,4-trimethylpentane; ●, carbon dioxide; ◆ n-hexane. The lowest line was calculated from the van der Waals equation, the middle line from the van der Waals equation as modified by Guggenheim, and the upper line from the Berthelot equation. (Courtesy Everett.)

pressure). On the same diagram they plot the values of τ_0/p_c from the values of τ_0 calculated by Equation (3.61) from the lower closure point of the isotherms of eight different adsorptives including nitrogen, usually at several temperatures and on a number of adsorbents. Though the points show considerable scatter, they all fall within the limits set by the van der Waals and Berthelot equations, tending to cluster around the line from the Guggenheim equation. As stressed by the authors, Equation (3.61) is valid only if τ_0 is a *hydrostatic* tension and therefore equal in all directions; it breaks down if τ is a tensor, as it could well be in a very narrow slit-like pore.

A different approach is followed by Kadlec and Dubinin[70] who calculate the theoretical tensile strength from a 6–12 relation for molecular forces (cf. Section 1.3) as

$$\tau_0 = (2{\cdot}06/d_0)\gamma \tag{3.63}$$

Here d_0 is the mean separation of nearest neighbours in the bulk liquid, and is calculable from the liquid density. Substitution of $\tau_0 = 2\gamma/r_{m,h}$ (cf. Equation (3.58)) gives the further relation

$$d_0/r_{m,h} = 1{\cdot}03 \tag{3.64}$$

which should hold for all adsorption systems. Results for five different adsorptives on silica gel, porous glass and a number of active carbons are given in Table 3.7; as is seen, the values of $d_0/r_{m,h}$ (apart from that for water) are reasonably close together, though they do deviate considerably from the theoretical figure of 1·03. In view of the inevitable crudity of the model of the liquid state, however, Dubinin and Kadlec consider the agreement between expectation and experiment to be satisfactory.[70]

The evidence in favour of the tensile strength hypothesis accumulated so far is encouraging, but further work is needed before it can be regarded as fully substantiated. In particular, the existence of a minimum value of relative

TABLE 3.7

Test of "tensile strength" hypothesis

	d_0/Å	$r_{m,h}$/Å (Eq. 3.62)	$d_0/r_{m,h}$
Argon	3·87	10·9–11·9	0·32–0·36
Benzene	5·60	13·0–15·4	0·36–0·43
n-Hexane	0·40	16·8	0·38
Dimethyl formamide	5·37	15·1	0·36
Water	3·30	11·0–15·5	0·21–0·30

After Kadlec and Dubinin.[70]

pressure for loop closure, characteristic of each adsorptive at a given temperature, needs to be clearly demonstated for a reasonably wide and representative range of adsorptives other than nitrogen. Meanwhile, as a valuable working hypothesis, it leads to an important implication for pore size calculations: the Kelvin equation can give no information as to the presence or absence of pores having a value of r_m below 10 to 15 Å (the exact value depending on the particular adsorbate and the temperature). In the case of nitrogen, if the closure point is taken as $p/p^\circ = 0{\cdot}45$, the value of r_m would be $\sim 11{\cdot}3$ Å and the pore radius for a cylindrical pore would be $\sim 17{\cdot}8$ Å, or the width of a parallel-sided slit $\sim 24{\cdot}3$ Å (the exact values depending on the *t*-curve chosen). When a peak in the distribution curve is found slightly above this critical value of r_m, the likelihood that it is an artefact[25] reflecting the tensile strength of the adsorbate must be reckoned with, and the presence of finer pores suspected.

Capillary condensation without hysteresis

It was noted earlier (p. 115) that the upward swing in the Type IV isotherm characteristic of capillary condensation not infrequently commences in the region prior to the lower closure point of the hysteresis loop. This feature can be detected by means of an α_s-plot or a comparison plot (p. 100). Thus Fig. 3.25(*a*) shows the nitrogen isotherm and Fig. 3.25(*b*) the α_s-plot for a particular silica gel:[32] the isotherm is clearly of Type IV and the closure point is situated around $0{\cdot}4p^\circ$; the α_s-plot shows an upward swing commencing at $\alpha = 0{\cdot}73$, corresponding to relative pressures of 0·13 and therefore well below the closure point.

The curves in Fig. 3.25(*c*) and (*d*) refer to nitrogen adsorbed on a chromia gel.[73] The upward swing in the α_s-plot (Fig. 3.25(*d*)) commences at $\alpha_s = 0{\cdot}75$, corresponding to a relative pressure of 0·16, much below the lower closure point ($p/p^\circ \sim 0{\cdot}40$) of the hysteresis loop in the isotherm (Fig. 3.25(*c*)).

Figure 3.26(*a*) and (*b*) gives results for nitrogen on a compact of silica.[8] Curve (*a*) is a comparison plot in which the adsorption on the compact (ordinates) is plotted against that on the uncompacted powder (abscissae); there is a clear break followed by an increased slope, denoting enhanced adsorption on the compact, at $p/p^\circ = 0{\cdot}15$, far below the lower closure point ($\sim 0{\cdot}42$) of the hysteresis loop in the isotherm (curve (*b*)). A second compact, prepared at 64 ton in^{-2} rather than 130 ton in^{-2}, showed a break, not quite so sharp, at $p/p^\circ = 0{\cdot}35$.

A final example appears in Fig. 3.26(*c*) and (*d*) where the experimental substance was a magnesium oxide[56] prepared by hydrolysis of magnesium methylate followed by calcination at 500°C. Curve (*c*) gives a comparison plot of adsorption on a compact against the adsorption on the

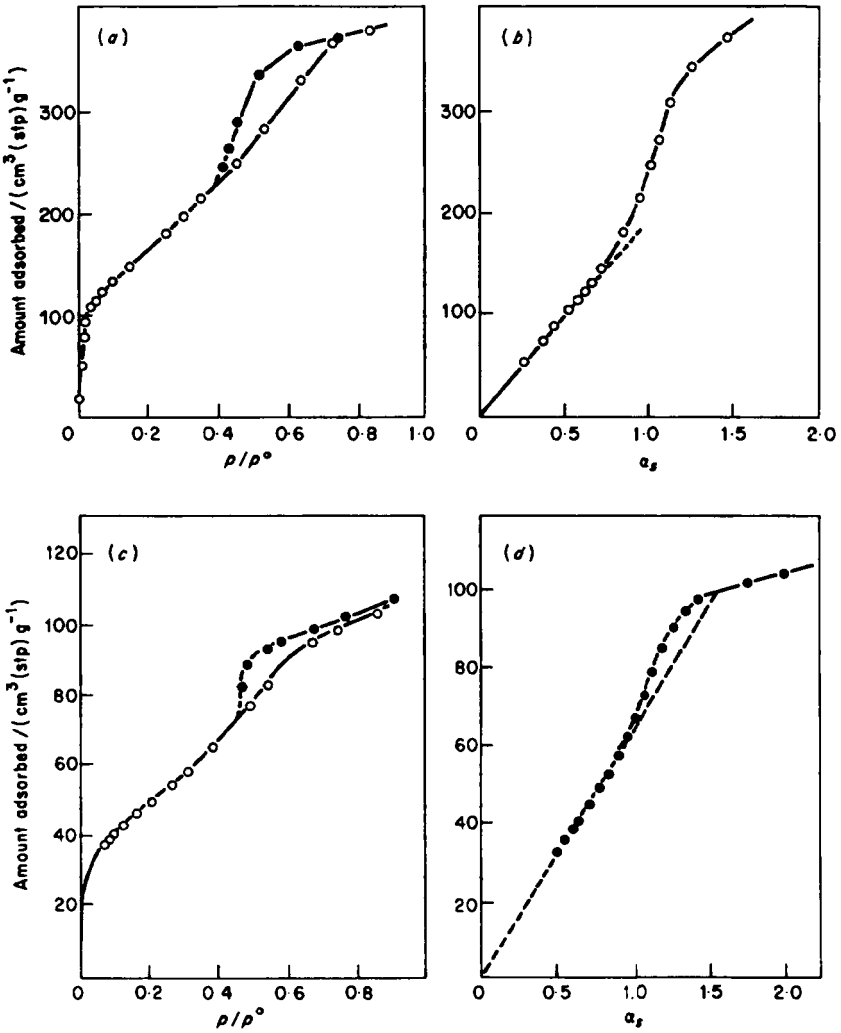

Fig. 3.25 (*a*) Nitrogen adsorption isotherm and (*b*) α_s-plot for mesoporous silica gel[32] F. The α_s-plot is based on the α_s-data given in Table 2.14. (*c*) Nitrogen adsorption isotherm and (*d*) α_s-plot for chromium oxide gel B2 heated in air at 280°C for 27 h.[73] The reference substance for the α_s-plot was a chromium oxide gel which had been heated at 880°C and aged.

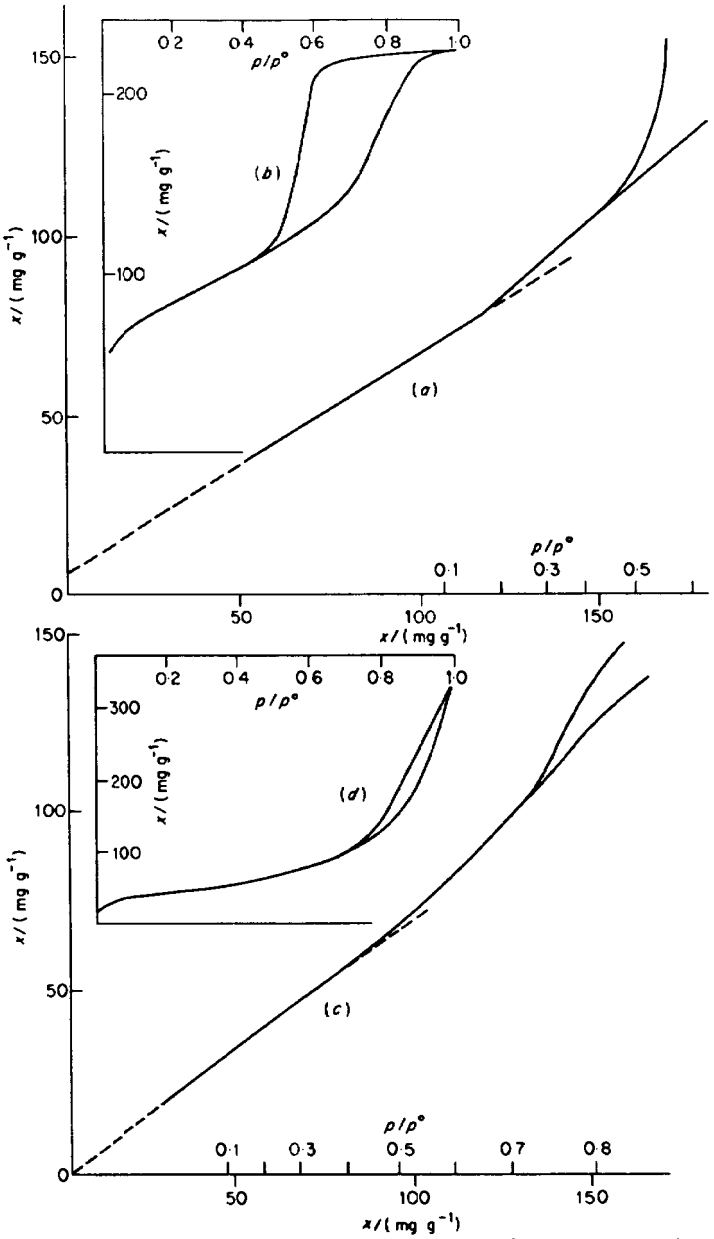

Fig. 3.26 Comparison plots for compacts of silica[8] and magnesia.[56] In each case the adsorption of nitrogen at 78 K on the compact is plotted against that on the uncompacted powder. (*a*) and (*b*), comparison plot and adsorption isotherm for silica powder compacted at 130 ton in^{-2}; (*c*) and (*d*), comparison plot and adsorption isotherm for precipitated magnesia compacted at 10 ton in^{-2}. Note that the upward sweep of the comparison plot commences at a relative pressure below the inception of the loop.

uncompacted material. Again there is an upward deviation commencing at a relative pressure of 0·20, whereas the hysteresis loop does not extend below ~0·40 (curve (*d*)).

In formulating an explanation of this enhanced adsorption, there are several features to be accounted for: the increase in adsorption occurs without hysteresis; the amount of adsorbate involved is relatively small; the Kelvin r_m-values are also small (e.g. for nitrogen, less than ~17 Å); and the effect is found in a region of relative pressures where, according to the simple tensile strength hypothesis, capillary condensate should be incapable of existence.

A possible explanation may be formulated along the following lines. The enhancement is occurring in pores narrow enough for the whole of the adsorbate to be within range of the surface forces emanating from the solid surface. The figure of 17 Å, for example, corresponds to about four molecular diameters; and the work of Prenzlow and Halsey[74] indicates that at this kind of distance the influence of the surface has not completely vanished. The capillary condensed liquid in such pores will therefore have modified properties, and the Kelvin equation will need the addition of a term ψ to allow for the effect of the surface forces on the chemical potential of the condensate. For any given point X on the meniscus, the modified equation may be written

$$RT\ln(p/p^\circ) = -\frac{2\gamma V_L}{r_m} + \psi \tag{3.65}$$

Here ψ is the interaction potential of a molecule at X, and therefore in the presence of its neighbours, ψ is related to, but not identical with, ϕ of Chapter 1 (p. 6).

Since the value of ψ depends on the location of X relative to the surface, the value of r_m—and therefore the local curvature of the meniscus ($=2/r_m$)—will be similarly dependent.

Now by equation (3.58) the tension τ within a capillary-condensed liquid is given by $\tau = 2\gamma/r_m$, consequently Equation (3.65) can be transformed into

$$RT\ln(p/p^\circ) = -\tau V_L + \psi \tag{3.66}$$

or

$$\tau = \frac{RT}{V_L}\ln(p^\circ/p) + \frac{\psi}{V_L} \tag{3.67}$$

Since ψ is necessarily negative (attraction), the magnitude of τ at X will be less than at points beyond the range of the surface forces, and it will vary in magnitude according to the location of X (cf. Fig. 3.10). The general effect of the surface forces is therefore to favour the persistence of capillary condensate.

The pores in question can represent only a small fraction of the pore system since the amount of enhanced adsorption is invariably small. Plausible models are solids composed of packed spheres, or of plate-like particles. In the former model, pendulate rings of liquid remain around points of contact of the spheres after evaporation of the majority of the condensate; if the spheres are small enough this liquid will lie wholly within the range of the surface forces of the solid. In wedge-shaped pores, which are associated with plate-like particles, the residual liquid held in the apex of the wedge will also be under the influence of surface forces.

It is hardly necessary to stress that this picture is merely semi-quantitative in nature; in very narrow pores the surface tension and the density of the adsorbate must both differ appreciably from their bulk values, and the very concept of a meniscus is beginning to lose its meaning. The picture is further complicated by the fact that the tension τ is not constant throughout the liquid, so that the tensile strength is exceeded in some parts before others. Even so, the general sense of the effect of the proximity of the surface is not in doubt and could account for an enhanced adsorption, closely analogous to capillary condensation, in the region immediately prior to the closure point of the loop. At its lower end, this region of increased adsorption merges into the micropore range, which is the subject of Chapter 4.

The upper end of the pore size range

At the upper end of the pore size range there is no *theoretical* limit to the applicability of the Kelvin equation to adsorption isotherms so long as $\theta < 90°$. There is however a *practical* limitation, the nature of which may be gathered from Table 3.8 which gives the relative pressures corresponding to

TABLE 3.8

Values of p/p° for nitrogen at 77·35 K for different values of r_m

r_m/Å	r_m/μm	p/p°
200	0·02	0·9532
500	0·05	0·9810
1000	0·1	0·9904
2000	0·2	0·9952
10000	1·0	0·9990
50000	5·0	0·9998

$V_L = 34{\cdot}68\ \text{cm}^3\ \text{mol}^{-1}$ $\gamma = 8{\cdot}88\ \text{mN m}^{-1}$
$T = 77{\cdot}35$ K.

$$\log_{10}\left(\frac{p}{p^\circ}\right) = \frac{-4{\cdot}16}{r_m/\text{Å}}.$$

some pore sizes, commencing at the upper end of the mesopore range for the case of nitrogen. The relative pressures are bunched so closely together that the isotherm of an adsorbent having a pore system in this size range would be far too steep to measure by any of the standard procedures. Moreover, since p/p° is so close to unity in this region, a small uncertainty in the temperature of the sample has a disproportionately large effect on the calculated value of r_m. This factor is especially important with an adsorptive such as nitrogen, which is used at a temperature far below ambient, where a thermal leak from the surroundings can cause the temperature of the sample to be slightly above that of the bath.[75,76] The magnitude of the resultant error may be judged from Table 3.9, based on a hypothetical isotherm of nitrogen supposedly measured at 77·35 K (the normal boiling point of nitrogen) but where the actual temperature of the sample is 0·05 K higher. At the lower end of the mesopore range ($r_m \sim 20$ Å) the error is scarcely detectable, but when r_m has risen to 200 Å the apparent value of r_m is only 90 per cent of its true value, and at $r_m = 1000$ Å (which is not very far into the macropore range) the apparent value of r_m has already fallen to 65 per cent of its true value.

It is these kinds of uncertainties that have led to the development of mercury porosimetry, in which, since the meniscus is convex, the mercury has to be forced into the pores under pressure. Mercury porosimetry is the subject of Section 3.9.

TABLE 3.9

Effect of an error of 0·05 K in temperature of the solid on the value of r_m calculated from the Kelvin equation

r_m(true)/Å	r_m(app)/Å	r_m(app)/r_m(true)
20	19·8	0·99
100	94·7	0·95
200	180	0·90
500	393	0·79
1000	646	0·65

p° at 77·35 K (b.p.) = 760 Torr p° at 77·40 K = 764 Torr

* $\log_{10}(p^\circ/p) = \dfrac{4{\cdot}16}{r_m/\text{Å}}$

Insert r_m(true) into (*) to obtain $(p^\circ/p)_t$.

Reinsert $(p^\circ/p)_t \times \dfrac{764}{760}$ into (*) to obtain r_m(apparent).

Adsorptives other than nitrogen

The evaluation of pore size distribution by application of the Kelvin equation to Type IV isotherms has hitherto been almost entirely restricted to nitrogen as adsorptive. This is largely a reflection of the widespread use of nitrogen for surface area determination, which has meant that both the pore size distribution and the specific surface can be derived from the same isotherm.

It would clearly be desirable to extend the scope of the Kelvin method to include a range of adsorptives having varied physical properties, especially surface tension, molar volume, molecular shape and size. This would enable the validity of the method and its attendant assumptions to be tested more adequately, and would also allow a variation in experimental technique, for example by permitting measurements at 298 K rather than 77 K.

In principle, the use of a suitable adsorptive should also make it possible, as Karnaukhov[33] has pointed out, to reduce the magnitude of the t-correction, which is always a source of some uncertainty. From the Kelvin equation

$$\ln(p/p^\circ) = -\frac{2\gamma V_L}{RT}\frac{1}{r_m} \tag{3.1}$$

it follows that the higher the value of $\gamma V_L/RT$, the lower is the relative pressure at which condensation will occur in a pore of given radius r_m; and since the value of t decreases as p/p° decreases (p. 135), it would seem at first glance that changing from nitrogen to an adsorptive having a higher value of $\gamma V_L/T$ (Table 3.10) would automatically reduce the value of the t-correction throughout the whole range of pore sizes. In this way it might have been hoped to extend the scope of the Kelvin method to mesopore sizes beyond the practical limit set by nitrogen ($\sim$250 Å). In fact, however, t is given by $t = \theta\sigma$, where θ is the number of statistical molecular layers and σ is the

TABLE 3.10

Values of $\gamma V_L/T$ for typical adsorptives

Adsorptive	T / K	γ / mN m^{-1}	V_L / 10^{-6} m^3 mol^{-1}	$\gamma V_L/T$ / 10^{-6} m^2 mN mol^{-1} T^{-1}
Nitrogen	78	8·88	34·7	3·95
Argon	87·5	13·20	28·53	4·30
Methanol	293	22·60	40·42	3·12
Carbon tetrachloride	293	26·75	96·54	8·72
Benzene	293	28·88	88·56	8·76

effective thickness of each layer; and θ itself is a function not only of p/p° but also of the net heat of adsorption (p. 17), whilst σ depends on the size and orientation of the molecule. Thus it comes about that the beneficial effect of a high value of $\gamma V_L/T$ can be partially or completely nullified if the adsorptive has a high heat of adsorption and a large molecular size.

The point is illustrated by the figures in Table 3.11 for hexane and nitrogen (adsorbed on carbon black). Though the value of $\gamma V_L/T$ is almost twice as high for hexane as for nitrogen, the corresponding values of t for hexane are

TABLE 3.11

Values of t for nitrogen, n-hexane and carbon tetrachloride for different values of r^p

r^p/Å	p/p°			t/Å		
	N_2	C_6H_{14}	CCl_4	N_2	C_6H_{14}	CCl_4
20	0·51	0·26	0·32	6·0	5·5	2·4
30	0·67	0·42	0·465	7·0	7·1	3·7
50	0·80	0·605	0·64	8·6	9·8	5·5
100	0·90	0·795	0·815	~12·5	15·2	8·4

only slightly less, and indeed for the 100 Å pore the value of t is actually greater, than for nitrogen. With carbon tetrachloride (on silica), where $\gamma V_L/T$ is again approximately twice that for nitrogen, the values of t are much below those for nitrogen in the finer pores. This is because the isotherm of CCl_4 is of Type III (with $c = 2$, cf. Chapter 5) so that the uptake is small at low relative pressures; it rises steeply at high relative pressure, however, and the value of t moves closer to that for nitrogen.

A factor militating against the use of other adsorptives for pore size determination at the present time is the lack of reliable t-curves. The number of published isotherms of vapours such as benzene, carbon tetrachloride or the lower alkanes, or even such simple inorganic substances as carbon dioxide, on a reasonable number of well-defined non-porous adsorbents, is very small.

If and when these difficulties can be overcome, the way will be opened to the employment of adsorptives which have a vapour pressure high enough to enable their isotherms to be measured at temperatures close to ambient. This would substantially reduce the effect of thermal leakage and with it the distortion of the isotherm in the region near saturation.

3.8 Evaluation of specific surface from the Type IV isotherm

Application of the BET procedure

In the compaction studies described in Section 3.1, it was found that the Type IV isotherm obtained with the compact was almost coincident, in the pre-hysteresis region, with the Type II isotherm of the uncompacted powder. It follows that the BET area will likewise be unchanged by compaction, for it is this region which gives rise to the BET plot. In the experiments of Fig. 3.4, for example, the BET area of the alumina was still 96 $m^2 g^{-1}$ after compaction at 1480 GN m^{-2} (96 ton in^{-2}) as compared with the value 98 $m^2 g^{-1}$ for the loose powder—a very small reduction, readily explicable in terms of slight loss of area and accessibility around points of contact of neighbouring spheres. (With softer materials such as silica, the specific surface is reduced significantly at sufficiently high compaction pressures.)

It follows therefore that the specific surface of a mesoporous solid can be determined by the BET method (or from Point B) in just the same way as that of a non-porous solid. It is interesting, though not really surprising, that monolayer formation occurs by the same mechanism whether the surface is wholly external (Type II isotherm) or is largely located on the walls of mesopores (Type IV isotherm). Since the adsorption field falls off fairly rapidly with distance from the surface, the building up of the monolayer should not be affected by the presence of a neighbouring surface which, as in a mesopore, is situated at a distance large compared with the size of a molecule.

Striking confirmation of the conclusion that the BET area derived from a Type IV isotherm is indeed equal to the specific surface is afforded by a recent study of a mesoporous silica, Gasil I, undertaken by Havard and Wilson.[47] This material, having been extensively characterized, had already been adopted as a standard adsorbent for surface area determination (cf. Section 2.12). The nitrogen isotherm was of Type IV with a well defined hysteresis loop, which closed at a point below saturation (cf. F, in Fig. 3.1). The BET area calculated from it was $290{\cdot}5 \pm 0{\cdot}9$ $m^2 g^{-1}$, in excellent agreement with the value 291 $m^2 g^{-1}$ obtained from the slope of the initial region of the α_s-plot (based on silica TK800 as reference cf. p. 93).

Electron microscopy revealed that Gasil I is made up of irregularly shaped aggregates, composed of globules of nearly uniform size. It proved possible to break up these aggregates by "rubbing out" an ethanol paste of the material, followed by ultrasonic treatment. The specific surface, calculated from the globular size distribution obtained from the micrographs, was $303{\cdot}7$ $m^2 g^{-1}$, in good agreement with the BET area of the undispersed material. The 4 per cent smaller area in the silica aggregates can again be attributed to the area of

contact between the globules, which could be greater than in the case of alumina since silica is a softer material.

Cumulative surface area from pore size distribution

Each of the procedures described in Section 3.6 for the calculation of pore size distribution involves a value of the pore area δA_i^p for each successive group of pores. In the Roberts procedure δA_i^p can be immediately obtained from the corresponding pore volume and pore radius as $\delta A_i^p = \delta v_i^p / \bar{r}_i^p$ (for cylindrical pores); and in the remaining three methods δA_i^p appears as an essential feature of the calculation. Thus by summing the values of δA_i^p over the whole pore system a value of the *cumulative surface area* $\sum(\delta A_i^p)$ is obtained. If the pore model chosen were a perfect representation of the actual pore system, $\sum(\delta A_i^p)$ should be equal to the BET surface area A(BET). In practice the agreement between the two quantities is rarely within experimental error,[77] and a difference of $\pm 20\%$ between them is quite common. The discrepancy may sometimes be due to the presence of micropores which will lead to an erroneously high value of the BET area (cf. Section 2.14 and Chapter 4). Indeed a value of A(BET) which is significantly higher than $\sum(\delta A_i^p)$ is often taken as evidence that the solid contains micropores. However, in view of the dependence of the value of the cumulative surface area on the necessarily somewhat unrealistic pore model, such evidence for the presence of microporosity must be regarded at most as providing some confirmation of a conclusion reached by other, more reliable, means (cf. Chapter 4).

The Kiselev method[11,43]

At the point where capillary condensation commences in the finest mesopores, the walls of the whole mesopore system are already coated with an adsorbed film of area A^k, say. The quantity A^k comprises the area of the core walls and is less than the specific surface A (unless the pores happen to be parallel-sided slits). When capillary condensation takes place within a pore, the film–gas interface in that pore is destroyed, and when the pore system is completely filled with capillary condensate (e.g. at F in Fig. 3.1) the whole of the film–gas interface will have disappeared. It should therefore be possible to determine the area A^k by suitable treatment of the adsorption data for the region of the isotherm where capillary condensation is occurring.

Picture the transfer, under equilibrium conditions, of dn mole of adsorptive from the bulk liquid where its chemical potential is μ°, to a

mesopore, where its chemical potential is μ^a. The free energy change dG_1 is

$$dG_1 = (\mu^a - \mu^0)\,dn \tag{3.68}$$

If the resultant increase in area of the solid–liquid (*sl*) interface is dA^k, the film–gas (*fg*) interface must diminish by the same amount dA^k (Fig. 3.27); and if the increase in the liquid–gas (*lg*) interface is dA^{lg}, the resulting change dG_2 in free energy is

$$dG_2 = \gamma^{sl}\,dA^k - \gamma^{fg}\,dA^k + \gamma^{lg}\,dA^{lg} \tag{3.69}$$

Now by the Young–Dupré equation

$$\gamma^{fg} - \gamma^{sl} = \gamma^{lg}\cos\theta \tag{3.70}$$

so that insertion of (3.70) into (3.69) gives

$$dG_2 = \gamma^{lg}(dA^{lg} - dA^k\cos\theta) \tag{3.71}$$

If now the contact angle θ is zero, and if (and *only* if) dA^{lg} is also zero, i.e. if the pore does not taper, then Equation (3.71) reduces to

$$dG_2 = \gamma\,dA^k \tag{3.72}$$

where γ^{lg}, being the surface tension of the liquid, has been replaced by the usual symbol γ. Since the system is at equilibrium, the total change in free energy is zero, i.e. $dG_1 + dG_2 = 0$, so that from (3.68) and (3.72) we have†

$$(\mu^a - \mu^0)\,dn = \gamma\,dA^k \tag{3.73}$$

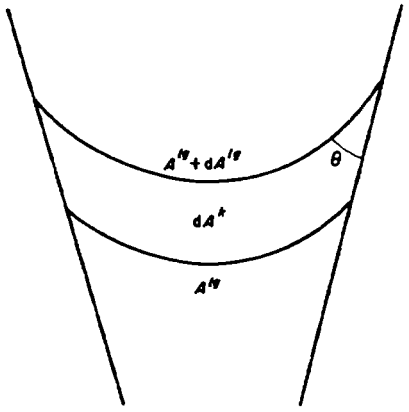

Fig. 3.27 Diagrammatic representation of a meniscus in a tapering capillary.

† Note the difference in sign from Equation (3.50), where dA^k is the area exposed by the *desorption* of dn moles.

Equation (3.73) is the basis of the method proposed by Kiselev for the evaluation of surface area from the Type IV isotherm. If perfect gas behaviour is assumed it becomes

$$RT\ln(p/p^\circ)\,\mathrm{d}n = \gamma\,\mathrm{d}A^k \tag{3.74}$$

and integration between the limits $n = n_c$, and $n = n_s$ (corresponding to the relative pressures at the beginning and end of the capillary condensation process) gives

$$\int_{A^k}^{0} \mathrm{d}A^k = \frac{RT}{\gamma}\int_{n_c}^{n_s} \ln(p/p^\circ)\,\mathrm{d}n \tag{3.75}$$

i.e.

$$A^k = \frac{RT}{\gamma}\int_{n_c}^{n_s} \ln(p^\circ/p)\,\mathrm{d}n \tag{3.76}$$

(Note that $A^k = 0$ when capillary condensation is complete.) Integration by measurement of the area under the curve of $\ln(p^\circ/p)$ against n between the stated limits therefore gives the value of A^k, which is the area of the walls of the *cores*, not of the pores (cf. Fig. 3.28).

To convert the core area into the pore area (=specific surface, if the external area is negligible) necessitates the use of a conversion factor $\boldsymbol{R}$ which is a function not only of the pore model but also of both r^k and t (cf. p. 148). Thus, successive increments of the area under the curve have to be corrected, each with its appropriate value of $\boldsymbol{R}$. For the commonly used cylindrical model,

$$\boldsymbol{R}_i = v_i^p/r_i^k = (r_i^k + t_i)/r_i^k$$

so that in turn $\boldsymbol{R}_i = \sqrt{Q_{ii}}$ of Table 3.5. Since in general, $\boldsymbol{R}_i$ and $\sqrt{Q_{ii}}$ diminish as r^p increases, the discrepancy between A^k and the specific surface should become smaller as the hysteresis loop moves towards higher relative pressures.

A difficulty in using the method is that of identifying the point P_c where capillary condensation commences.[48] This is usually taken as the lower closure point of the loop; but as was pointed out in Section 3.5, capillary condensation can occur without hysteresis if the pores are of an appropriate shape—such as wedge-like—before the irreversible condensation responsible for the hysteresis loop sets in. The uncertainty arising from this cause is considerable, since the curve of $\ln(p^\circ/p)$ is very steep in this region (cf. Fig. 3.28).

The need to assume that the pores are of constant cross-section introduces

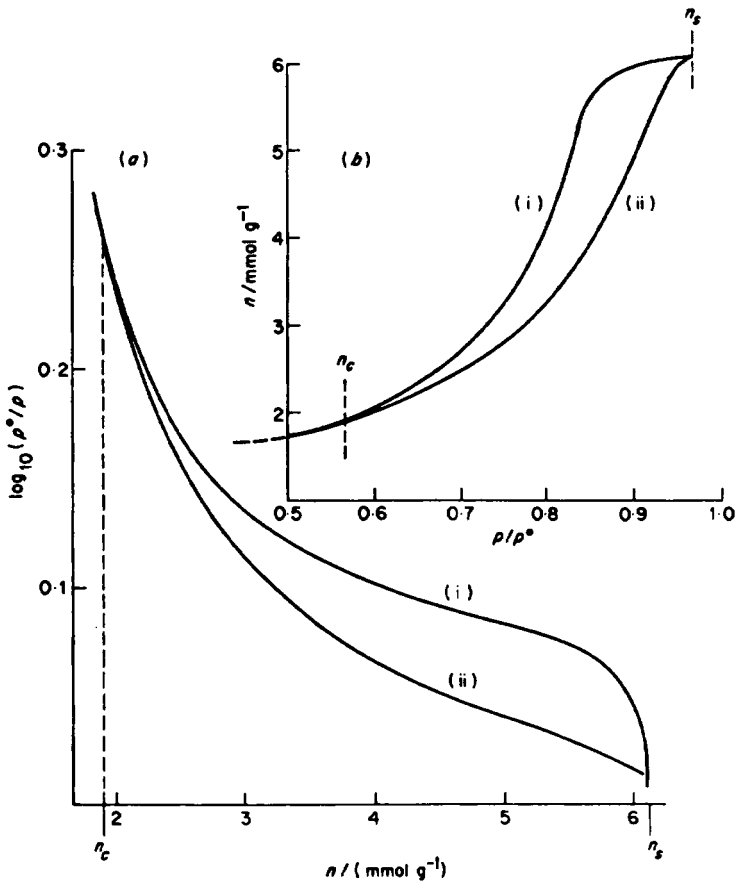

Fig. 3.28 The Kiselev method for calculation of specific surface from the Type IV isotherm of a compact[8] of alumina powder prepared at 64 ton in^{-2}. (*a*) Plot of $\log_{10}(p^\circ/p)$ against n (showing the upper (n_s) and lower (n_c) limits of the hysteresis loop) for (i) the desorption branch, and (ii) the adsorption branch of the loop. Values of A(des) and A(ads) are obtained from the area under curves (i) or (ii) respectively, between the limits n_c and n_s. (*b*) The relevant part of the isotherm.

a further limitation, for if the pore tapers to a significant degree either outwards or inwards the quantity dA^{lg} neglected in arriving at Equation (3.76) can be of first-order importance.[21,48]

Perhaps the most serious limitation, however, arises from the fact neither branch of the hysteresis loop corresponds to thermodynamic reversibility. The value of the integral $\int \ln(p^\circ/p)\,dn = I$, say, differs considerably for the two branches of the loop. In fact

$$\frac{RT}{\gamma} I^{ads} < A^k < \frac{RT}{\gamma} I^{des}$$

and Kiselev has suggested that the mean of the two extremes may be taken as a useful approximation to the core area. In view of all these limitations, added to the possible complications from network effects, close agreement between the specific surface and the BET area cannot in general be expected. The results in Table 3.12 illustrate the kind of divergences which are liable to be encountered; they are based on the isotherms obtained with the compacts of silica and alumina.[8] As expected, the value of the area for a given sample, whether the core area or the pore area, depends markedly on whether it was calculated from the adsorption or the desorption branch. In addition, the average of the adsorption and desorption values is always below the BET area. The pore wall area, though closer to the BET area, still remains distinctly below it in most cases.

The discrepancy between the pore area or the core area on the one hand and the BET area on the other is proportionately larger with silica than with alumina, particularly at the higher degrees of compaction. The fact that silica is a softer material than alumina, and the marked reduction in the BET area of the compact as compared with that of the loose material, indicates a considerable distortion of the particles, with consequent departure of the pore shape from the ideal of interstices between spheres. The factor R for cylinders (p. 171), used in the conversion to pore area in the absence of a better alternative, is therefore at best a crude approximation.

One is obliged to conclude that this method, like those which derive the cumulative surface area from pore size calculations,[77] can be regarded as no more than ancillary to the BET or Point B methods. The few cases where reasonable agreement with the BET area is obtained are probably to be explained by compensation of opposing effects.

3.9 Mercury porosimetry[21,78]

Mercury porosimetry is a technique which was originally developed to enable pore sizes to be determined in the macropore range where, as pointed out in

TABLE 3.12

Evaluation of specific surface from Type IV isotherms of nitrogen, from the area under the curve of $\log(p^\circ/p)$ against n

Adsorbent	"Core" wall area from		"Pore" wall area from			BET area
	Adsorp. Branch $A^A/(m^2\,g^{-1})$	Desorp. Branch $A^A/(m^2\,g^{-1})$	Adsorp. Branch	Desorp. Branch $A^P/(m^2\,g^{-1})$	Average	$A(N_2)/(m^2\,g^{-1})$
Alumina compacts[8] prepared at:						
(1) 32 ton in^{-2}	60	73	83	98	91	100
(2) 64 ton in^{-2}	52	74	63	89	76	97
(3) 96 ton in^{-2}	54	80	66	96	81	98
Silica compacts[8] prepared at						
(4) 16 ton in^{-2}	187	228	233	298	266	351
(5) Silica gel[36] (GS50)	304	361	373	491	432	683
(6) Silica gel[36] (GS80)	348	430	426	513	470	473

All values rounded to nearest unit. (1 ton in^{-2} = 15·4 MN m^{-2}).

Section 3.7, the gas adsorption method breaks down for practical reasons. Since the angle of contact of mercury with solids is ~140° (see later), and therefore more than 90°, an excess pressure Δp is required to force liquid mercury into the pores of a solid. The idea of using mercury intrusion to measure pore size appears to have been first suggested by Washburn[79] who put forward the basic equation

$$r^p = -\frac{2\gamma \cos\theta}{\Delta p} \tag{3.77}$$

(often termed the Washburn equation), where r^p is the radius of the pore, assumed to be cylindrical. Equation (3.77) is a special case of the Young–Laplace equation (3.5), which in the present context may be written as

$$p^{Hg} - p^g = -\gamma\left(\frac{1}{r_1} + \frac{1}{r_2}\right) \tag{3.78}$$

where p^{Hg} is of course the pressure in the liquid mercury phase and p^g that in the gaseous phase. Since the meniscus is a segment of a sphere,

$$r_1 = r_2 = r^p \cos\theta$$

(cf. Fig. 3.29) and

$$p^{Hg} - p^g = \Delta p$$

is the pressure which must be exerted on the mercury to force it into a cylindrical pore of radius r^p. These insertions into Equation (3.78), with slight rearrangement, lead directly to the Washburn equation (3.77).

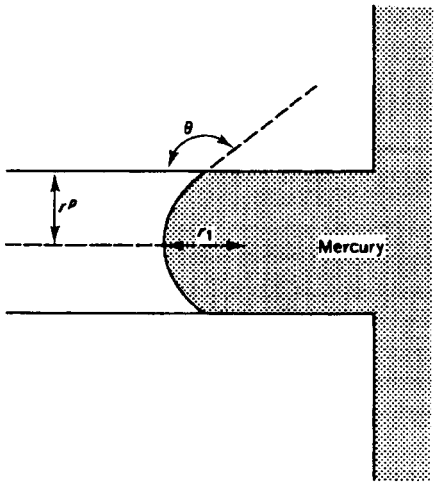

Fig. 3.29 Mercury penetrating a cylindrical pore.

The technique of mercury porosimetry consists essentially in measuring the extent of mercury penetration into an evacuated solid as a function of the applied hydrostatic pressure. The full scope of the method first became apparent in 1945 when Ritter and Drake[80] developed a technique for making measurements at high pressures. The method has enjoyed increasing popularity with the passing of years, and automatic porosimeters are now in use for the routine examination of the pore structure of catalysts, cements and other porous materials. The range of such porosimeters extends from $r^p \sim 35$ Å (corresponding to the usual maximum pressure ~ 2000 bar) to $r^p \sim 7{\cdot}5\ \mu$m, the size of pore penetrated at atmospheric pressure. In some designs the pore size range is extended at the lower end to ~ 15 Å by increasing the maximum applied pressure to ~ 5000 bar, and at the upper end by reducing the applied pressure below atmospheric. There is thus a considerable overlap with the gas adsorption method, but the two methods are best regarded as complementary, for each becomes increasingly uncertain as its scope is extended: gas adsorption at the upper end of the mesopore range (cf. Section 3.7) and mercury porosimetry at the lower end, as will appear later.

Surface tension and the angle of contact

Mercury is unusually prone to contamination, and this probably accounts for the lack of reproducibility to be found in the values of *surface tension* in the earlier literature. Table 3.13 provides a selection of the data reported

TABLE 3.13

The surface tension γ of mercury *in vacuo*

Temperature T/°C	Surface tension γ/mN m^{-1}	Method used	Ref.
25	484 ± 1·5	Sessile drop	81
25	484 ± 1·8	Sessile drop	82
20	485 ± 1·0	Drop pressure	83
25	483·5 ± 1·0	Sessile drop	84
25	485·1	Sessile drop	85
16·5	487·3	Pendant drop	86
25	485·4 ± 1·2		
20	484·6 ± 1·3	Pendant drop	87
20	482·5 ± 3·0	Bubble pressure	88

1 mN m^{-1} = 1 dyn cm^{-1}

since 1945 for the surface tension *in vacuo*. The agreement, within ~1 per cent, must be reckoned as reasonably good in view of the ease of contamination, and it is fortunate that the temperature coefficient is very small. The figure of $\gamma = 480$ mN m^{-2} adopted by Ritter and Drake[80] in their pioneer work still remains the recommended value for routine determinations. Judging by Table 3.13 this may be too low by 1 per cent but in the context of routine determinations the difference is of little account.

The *contact angle* of mercury, like that of other liquids, depends not only on whether the mercury is advancing over, or receding from, the solid surface, but also on the physical and chemical state of the surface itself; values in the literature show a considerable variation. Table 3.14 indicates the range of values obtained by what is perhaps the most popular method, measurement of the height of the sessile drop. The tilting plate method has given values of 139° for mercury on glass and 149° on paraffin wax,[93] whilst other direct measurements with polished surfaces of glass quartz, stainless steel, Teflon and tungsten have yielded equilibrium values[94] of $\theta = 134 \pm 4°$ at 25°C.

TABLE 3.14

Values of the contact angle θ of mercury at room temperature on various solid surfaces

Solid surface	Contact angle	Reference
Glass	140°	89
Glass	135°	90
Glass	139°	91
Glass and steel	150°	92
Coal leaflets	142°	91

Method used: height of sessile drop.

Thus one may conclude that the contact angle of mercury normally lies between 135° and 150°, the exact value depending on the purity and structure of the solid surface.[95] Most workers in the field, however, have followed Ritter and Drake in assuming that $\theta = 140°$ is valid for all solids. The uncertainty of the calculated value of r^p arising from this source is considerable, as may be judged from Table 3.15: the values of r^p corresponding respectively to the three values of θ, 130°, 140° and 150°, for a given applied pressure, differ amongst themselves by many per cent.

TABLE 3.15

Effect of the value of the contact angle θ of mercury on the calculated value of pore radius at different values of applied pressure P

Pressure / atm	Pore radius/Å		
	$\theta = 130°$	$\theta = 140°$	$\theta = 150°$
1	$60{\cdot}9 \times 10^3$	$72{\cdot}6 \times 10^3$	$82{\cdot}1 \times 10^3$
2	$30{\cdot}5 \times 10^3$	$36{\cdot}3 \times 10^3$	$41{\cdot}0 \times 10^3$
10	6090	7260	8210
100	609	726	821
200	305	363	410
500	122	145	164
1000	61	73	82
2000	30	36	41
5000	12	15	16

$$r^p/\text{Å} = \frac{9{\cdot}60 \times 10^3}{P/(\text{MN m}^{-2})} \cos\theta$$

1 atm = 0·1013 MN m^{-2}

Pore size distribution—comparison of results by mercury porosimetry and by adsorption of nitrogen

In mercury porosimetry the volume v(Hg) of mercury taken up by the solid is measured as the applied pressure P (i.e. $p^{Hg} - p^g$) is gradually increased. The value v_i(Hg) at any value of applied pressure P_i, therefore gives the volume of all pores having a radius equal to or *greater than* r_i^p; and is termed the cumulative pore volume. This designation is the converse of that in gas adsorption porosimetry (Section 3.6) where the cumulative pore volume $\sum(\delta v_i^p)$ is the volume of all those pores of radius equal to or *less than* r_i^p. Thus in mercury porosimetry the cumulative pore volume v(Hg) decreases as r^p increases, whereas in gas adsorption $\sum(\delta v_i^p)$ of course increases with increasing r^p. In both techniques, however, the pore size distribution curves are obtained by differentiation of the curves of cumulative volume against r^p, giving curves of dv^p/dr^p against r^p.

Since in practice the lower limit of mercury porosimetry is around 35 Å, and the upper limit of the gas adsorption method is in the region 100–200 Å (cf. p. 133) the two methods need to be used in conjunction if the complete curve of total pore volume against pore radius is to be obtained.

To bring the two curves into correspondence it is necessary to choose some reference point on the mercury intrusion curve, not too close to the lower

limit of the mercury method (Joyner[96] took $r^p = 40$ Å) and then to assume that the *total* pore volume at that point is given by the cumulative volume from the gas adsorption method. The curves of total pore volume against r^p from the respective methods can then be compared over the range, often fairly wide, where they overlap. In this way, Joyner found agreement over the rather wide range 35 to 300 Å with a number of catalysts. Agreement of this kind means that the two methods are supporting each other as far as pore size *distribution* is concerned, but the agreement of total volumes themselves is merely a consequence of the mode of normalization. Agreement of a similar order was found by Dubinin[97] in his comparison of the cumulative volume curves for a porous carbon AY4 obtained by benzene adsorption and mercury intrusion, where the reference point (from internal evidence) appears to have been 80 Å (Fig. 3.30(*a*)). With another carbon AY8 there was a large discrepancy between the two curves, the mercury curve lying far above the curve for benzene adsorption (Fig. 3.30(*b*)). This was plausably explained in terms of macropores being reached through entrances having radii in the mesopore range; since the pressure required for intrusion of mercury into a macropore is governed by the radius r_a^p of the pore *entrance*, the volume of the whole macropore would be registered as if it were a mesopore of radius r^p.

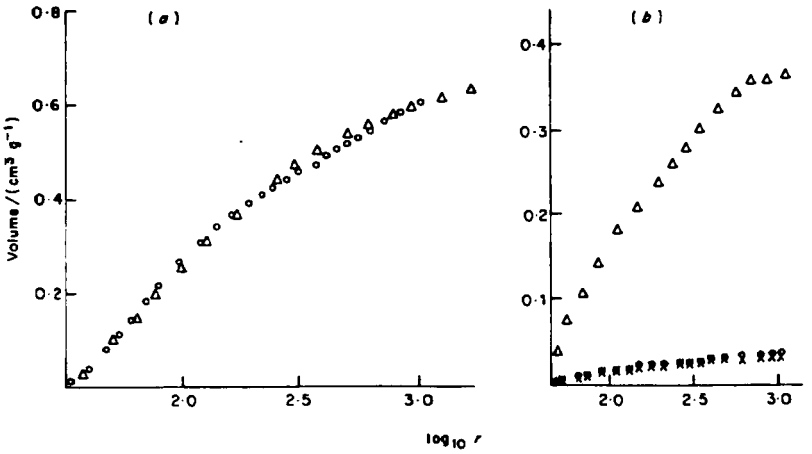

Fig. 3.30 Plot of cumulative pore volume[97] against logarithm of r the effective pore radius. (*a*) For charcoal AY4: △ by mercury intrusion; ○ by capillary condensation of benzene. (*b*) For zinc chloride carbon AY8: △ by mercury intrusion; ○ by capillary condensation of benzene; × by capillary condensation of benzene, after mercury intrusion followed by distillation of mercury under vacuum at temperature rising to 350°C. (Courtesy Dubinin.)

In benzene adsorption however the macropore becomes filled by capillary condensation at the relative pressure $(p/p^\circ)_w$ corresponding to the radius r_w^p of the *body* of the pore; since r_w^p is large, $(p/p^\circ)_w$ is close to saturation (e.g. $(p/p^\circ)_w$ is 0·98 for $r_w^p = 1000$ Å, and 0·998 for $r^p = 10000$ Å) and is beyond the scope of the benzene measurements.

Whereas at the lower end of its range mercury porosimetry overlaps with the gas adsorption method, at its upper end it overlaps with photomicrography. An instructive example is provided by the work of Dullien and his associates on samples of sandstone.[98] By stereological measurements they were able to arrive at a curve of pore size distribution, which was extremely broad and extended to very coarse macropores; the size distribution from mercury porosimetry on the other hand was quite narrow and showed a sharp peak at a much lower figure, ~10 μm (Fig. 3.31). The apparent contradiction is readily explained in terms of wide cavities which are revealed by photomicrography, and are entered through narrower constrictions which are shown up by mercury porosimetry.

An interesting development of the intrusion technique is the use of a fusible alloy in place of mercury. In a further study[99] Dullien and Dhawan injected Wood's metal (at ~110°C) into a set of evacuated core plugs of sandstone, at a different pre-determined pressure for each plug. The plug was then examined by photomicrography after it had cooled down and the metal had solidified, and the amount of injected metal was determined by weighing. The curve for cumulative volume of Wood's metal was in remarkably good agreement with that from mercury porosimetry, indicating that the values of $\gamma \cos\theta$ for the two metals must be—fortuitously—quite close to one another.

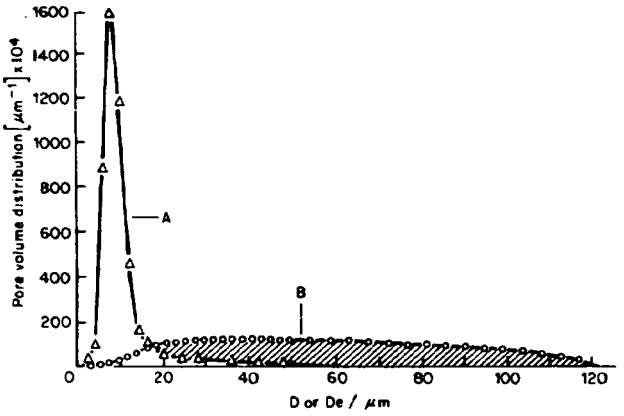

Fig. 3.31 Comparison of pore volume size distributions for Clear Creek sandstone[98] (courtesy Dullien.) Curve (A), from mercury porosimetry; curve (B), from photomicrography (sphere model).

In these studies the value assumed for the contact angle was 140°. In their comparative study referred to earlier, however, Joyner and co-workers[96] found that marginally better agreement between the curves from mercury penetration and gas adsorption could be achieved with $\theta = 130°$. Winslow and Diamond[100] have attempted a more direct evaluation of the effective contact angle by measuring the pressure required to force mercury through carefully drilled, cylindrical holes of known diameter (190–210 μm) in a disc of aged cement paste, dried under standardized conditions. Intrusion of mercury occurred over a narrow range of pressure, and since the mercury spontaneously flowed out again when the pressure was reduced, it was possible to make repeat measurements, which showed excellent reproducibility. The value θ calculated by Equation (3.77) was only 105° for oven-dried paste and 117° for paste dried over $Mg(ClO_4)_2$. The value $\theta = 117°$ was adopted in their subsequent studies on cement pastes, and it results in values of r^p only 60 per cent of those obtained by use of the conventional value $\theta = 140°$.

Effect of pressure on pore structure

The pressures involved in porosimetry are so high (e.g. 1000 atm $= 6{\cdot}6$ ton in^{-2}) that the question as to whether the pore structure is damaged by mercury intrusion naturally arises. This possibility was recognized by Drake,[80] but as a result of several intrusion–extrusion runs at pressures up to ~4000 atm on a number of porous catalysts Drake concluded that any deformation caused by compression was elastic and therefore not permanent.

Similarly, Johula and Wiig[101] in three successive experiments on the same sample of charcoal which was "soft and susceptible to crushing" found that the three penetration curves agreed closely, indicating that the pore structure had suffered no permanent damage.

More recent work has indicated, however, that some pore structures can undergo change if the applied pressure is high enough. Pinote and co-workers,[102] for example, studying a series of graphitized cokes, found that the volume penetrated by mercury at 1000 atm actually exceeded the volume accessible to helium, showing that the mercury had opened up the structure. Similar results were obtained, with various synthetic graphites, by Dickinson and Shore,[103] who found reasonable agreement between the volumes penetrated by mercury and helium, provided that the applied pressure had not exceeded 200 atm, but that any increase beyond that figure resulted in further penetration by mercury till at 1000 atm the intruded volume had increased two-fold.

The increase in pore volume brought about by high intrusion pressures may be caused by fracture of the pore walls that gives access to pores

previously closed, and is characterized by an irreversible change in the cumulative volume curve; or it may result from elastic deformation which opens up cracks and passageways, and then is compatible with the reproducibility of successive runs. An additional possibility is that the applied pressure may, conversely, have a compacting effect in which some pore entrances are narrowed down or actually closed completely. The degree of compaction will depend on the nature of the solid: silica gels for example, are more easily compressed than zeolites.

This compaction effect has been studied by Brown and Lard,[104] who point out that the pore size distribution curves from mercury intrusion and nitrogen adsorption agree reasonably well so long as the pore volume is not too high ($\leqslant 0{\cdot}8\ cm^3\ g^{-1}$ for inorganic oxide xerogels) but that marked discrepancies appear if the pore volume is large ($\sim 1{\cdot}2\ cm^3\ g^{-1}$). A permanent change in the pore structure was demonstrated by heating the sample under reduced pressure (20 Torr at 540°C) to drive off nearly all the mercury, and repeating the mercury porosimetric and gas adsorption determinations. In each case the total pore volume diminished substantially (sometimes by more than half), but the BET area was little affected and the agreement between the two cumulative volume curves improved. It seems that the applied pressure had reduced the size of the macropores by forcing the particles closer together.

In Unger and Fischer's study[105] of the effect of mercury intrusion on structure, three samples of porous silica were specially prepared from spherical particles 100–200 μm in diameter so as to provide a wide range of porosity (Table 3.16). The initial pore volume v^p(EtOH) was determined by "ethanol titration" (see next paragraph). The pore volume v^p(Hg, i) obtained from the first penetration of mercury agreed moderately well with v^p(EtOH),

TABLE 3.16

Values of pore volume of samples of porous silica, determined by ethanol titration (v^p(EtOH)) and by mercury porosimetry (v^p(Hg, i) and v^p(Hg, ii))[105]

	Pore volume/($cm^3\ g^{-1}$)		
Sample	v^p(EtOH)	v^p(Hg, i)†	v^p(Hg, ii)†
1	0·68	0·55	0·31
2	1·50	1·43	0·49
3	2·42	2·40	0·91

† v^p(Hg, i) obtained from first penetration of mercury. v^p(Hg, ii) obtained from second penetration, following retraction and removal of mercury from the first penetration.

but the value v^p(Hg, ii) from the second penetration was markedly lower, the difference v^p(Hg, i) − v^p(Hg, ii) being greater for samples 2 and 3 which had higher initial pore volumes. The pore size distribution curves indicated the preferential removal of the larger pores in all the samples, especially in No. 3 which had the highest initial pore volume; scanning electron microscopy showed that the particle size had not changed, but there was evidence of wall damage. Thus the effect of the mercury intrusion had been to push the spherical particles into a tighter packing.

In the liquid titration method (due to Innes[106]), water or an organic liquid is added slowly from a microburette, with vigorous stirring, to a powder sample of the adsorbent, until "caking" occurs. When the pores are full, the next increment of liquid forms a film on the outside of the particles, which by virtue of its surface tension draws the particles together. The end point is somewhat subjective and is also dependent on the surface tension of the liquid, especially if the solid is highly porous. According to McDaniel and Hottovy,[107] more consistent results can be obtained, at any rate with silica, by soaking the sample in the liquid and centrifuging off the excess liquid, the sample being weighed before and after to determine the amount of liquid retained.

Hysteresis

In their original work Drake and Ritter[80] found that the curves of volume against pressure for the penetration and withdrawal did not coincide. Numerous investigations since then have confirmed that hysteresis is a general feature of mercury porosimetry.

A typical example, from the extensive study by Kamakin[108] on an alumina–silica gel, is shown in Fig. 3.32. When the mercury pressure was reduced to 1 atm at the end of the first cycle, 27 per cent of the intruded mercury was retained by the sample; a second intrusion run followed a different path from the first, whereas the second *extrusion* curve agreed closely with the first. Change in pore structure of the kind described above could perhaps account for the difference between the two intrusion curves, but could not explain the reproducibility of the remainder of the loop. There is no doubt that hysteresis can exist in the absence of structural change.

Perhaps the best known explanation of reproducible hysteresis in mercury porosimetry is based on the "ink bottle" model already discussed in connection with capillary condensation (p. 128). The pressure required to force mercury with a pore having a narrow (cylindrical) neck of radius r_n will be

$$P_n = -\frac{2\gamma \cos\theta}{r_n} \tag{3.79}$$

whereas mercury cannot leave the body of the pore (radius r_w) until the

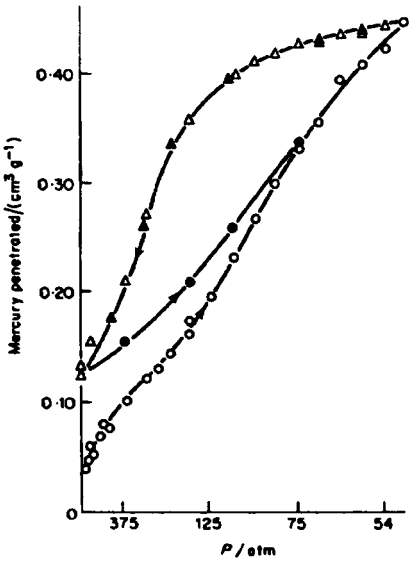

Fig. 3.32 Mercury penetration in alumina–silica gel (Kamakin[108]). ○, penetration; △, retraction; ●, re-penetration; ▲, renewed retraction. (After Scholten[95].)

pressure has fallen to P_w given by

$$P_w = -\frac{2\gamma \cos\theta}{r_w}. \tag{3.80}$$

Since by definition r_n is less than r_w, the pressure P_n for intrusion will be greater than that for extrusion, P_w, and there will be hysteresis.

A method for calculating the dimensions of the cavities and narrow necks from the intrusion–extrusion curves has been proposed by Reverberi.[109,110] The method is essentially as follows: the ascending curve (penetration) branch is measured in the usual way, but the descending curve is mapped out from a series of steps; each step commences at the same maximum pressure, P_{max}, proceeds to a pre-determined minimum pressure which is different for each step, and finally returns to P_{max} in a series of small stages. Two such steps are shown in Fig. 3.33. The pressure is first taken to the maximum value P_{max} at Point O, and is then decreased along OYA to the value P_2 at Point A; pores having *body* radius less than r_2 have now been emptied. Next the pressure is increased to P_3, and the curve mapped out (AA′) is determined by the radii of the necks, lying in the range r_2 to r_3. After completion of the first cycle by increasing the pressure to P_{max} again, the pressure is reduced to P_1,

along OYB, and is then increased again through P_2 and P_3 to P_{max}. The difference between the two volumes intruded between the pressures P_2 and P_3, viz $[(V''_B - V'_B) - (V'_A - V_A)]$ (see Fig. 3.33) gives the volume of ink-bottle pores having neck radii between r_2 and r_3.

The packed sphere model, also referred to in connection with capillary condensation (p. 149) has likewise been adapted to mercury porosimetry. In an early mathematical treatment, Kruyer[92] pointed out that when a liquid such as mercury having a contact angle in excess of 90° penetrates into a bed of spherical particles, there will be toroidal spaces, or "pendular rings", around points of interparticulate contact, which remain unfilled—the converse of the behaviour in capillary condensation where it is these spaces which are filled first of all. When the applied pressure is gradually decreased again the toroidal spaces within an interstice grow in size until separate segments merge; the interstice will then empty completely at the pressure determined by the radius of the sphere inscribed in the interstice. The pressure required for intrusion into the interstice on the other hand will be determined by the size of the opening—the foramen—into the interstice. The pressures for intrusion and extrusion are therefore different and hysteresis will result. A refined theoretical treatment of the behaviour of the model has been given by Frevel and Kressley[111] and others.[112]

As remarked earlier, however (p. 129) it is now recognized that the ink-bottle and similar models are over-simplified and that in the great majority of

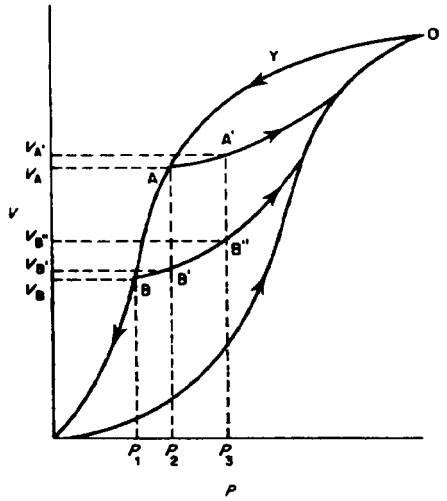

Fig. 3.33 Calculation of pore size distribution in "ink-bottle" pores, from mercury intrusion–extrusion experiment.[110] (After Reverberi.[109])

real solids the pores are connected into a network. A more realistic model of a porous solid is a three-dimensional array of cavities interconnected by narrow channels or "necks"; if the sizes of the cavities and the necks are distributed about mean values the properties of the network will be strongly dependent on the mode of interconnection.[21,45,48,49] The inflow of mercury into a particular group of pores having a given intrusion pressure may be accessible only through pores having a higher entry pressure. The withdrawal of mercury will in general be associated with a different group of pores, so that threads of mercury tend to break and to leave globules trapped in many of the cavities.

A theoretical model of a network has been developed by Androutsopoulos and Mann,[113,114] composed of cylindrical pore segments of equal length formed into a square network so that each segment is connected to six neighbouring segments; all the segments in the network are assigned pore dimensions according to the normal distribution function (other distribution functions could be used if desired). By application of the Washburn equation it was possible to show that trapping of mercury, and therefore hysteresis, should occur (cf. Fig. 3.34). The theoretical penetration and retraction curves calculated from the model were found to reproduce the general form of the experimental curves obtained with an actual solid (a Co/Mo catalyst).

One other cause of hysteresis remains to be mentioned. As was pointed out earlier (p. 177) the contact angle may be different as the mercury is advancing over or receding from a solid surface, and it depends also on the chemical and physical state of the surface; the mercury may even react with the surface layer of the solid to form an amalgam. A change in θ of only a few degrees has a significant effect on the calculated value of pore radius (cf. Table 3.15).

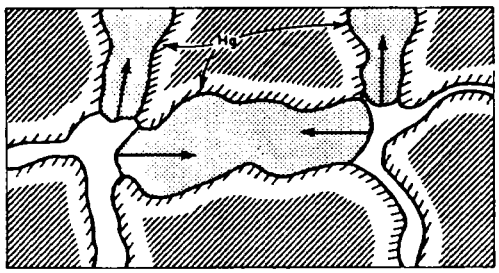

Fig. 3.34 Entrapment of mercury in a pore network. (Courtesy Androutsopoulos and Mann.[113])

Evaluation of pore volume by displacement of mercury and another fluid

The simple expression $1/\rho(\text{Hg}) - 1/\rho(\text{F})$ where $\rho(\text{Hg})$ and $\rho(\text{F})$ are the respective densities of a solid obtained by immersion at atmospheric pressure in mercury and in another suitable fluid F, gives a value of the total pore volume of the solid.[120] Since, by the Washburn equation (3.77), mercury at atmospheric pressure cannot enter pores of radius below $\sim 7{\cdot}5\ \mu\text{m}$ (p. 176), $1/\rho(\text{Hg})$ gives the volume of the solid itself plus that of virtually the whole of the pore system; fluid F on the other hand can enter all pores of diameter greater than σ (σ = molecular diameter of F). $1/\rho(\text{F})$ will therefore give the true volume of the solid plus that of all pores of diameter less than σ, provided that if F is a liquid it wets the solid ($\theta = 0$) and that if F is a gas its adsorption is negligible. If the adsorption is not negligible $\rho(\text{F})$ will be too high. For the best results helium is used as the immersing fluid;[115] its molecule is small ($\sigma = 3{\cdot}0\ \text{Å}$) and its adsorption per unit area at room temperature is the lowest of any gas. Even so, if the specific surface area of the solid is large (hundreds of square metres per gram), then $\rho(\text{Hg})$ will be too high by several per cent.[116] Where high precision is not required, the use of liquids such as carbon tetrachloride or heptane rather than gaseous helium may be preferred on grounds of experimental convenience.

Surface area from mercury porosimetry

By relating the work required to force a volume dv^p of mercury into the pore of a solid to the work required to form an element dA of mercury–solid interface, and making use of the Young-Dupré equation (3.70) one arrives at the expression

$$\gamma \cos\theta \, dA = -p \, dv^p \tag{3.81}$$

Like the analogous equation for capillary condensation (Equation (3.74) Equation (3.81) is based on the tacit assumption that the pore is of constant cross-section. Integration of Equation (3.81) over the range of the mercury penetration curve gives an expression for the surface area $A(\text{Hg})$ of the walls of all the pores which have been penetrated by the mercury:

$$A(\text{Hg}) = -\frac{1}{\gamma \cos\theta} \int_0^{p_{max}} p \, dv^p \tag{3.82}$$

The method has been applied by Rootare and Prenzlow[117] to the determination of the surface area of twenty different powders having BET areas in the range 0·1 to 110 $\text{m}^2\,\text{g}^{-1}$, where the "pores" would be mainly or entirely in the form of the interstices between the particles. The value

TABLE 3.17

Comparison of surface areas determined by mercury porosimetry and by nitrogen adsorption[117]

Sample	Surface area/($m^2 g^{-1}$)	
	By mercury porosimetry	By nitrogen adsorption
Tungsten powder	0·11	0·10
Iron powder	0·20	0·30
Zinc dust	0·34	0·32
Copper powder	0·34	0·49
Silver iodide	0·48	0·53
Aluminium dust	1·35	1·14
Fluorspar	2·48	2·12
Iron oxide	14·3	13·3
Anatase	15·1	10·3
Graphitised carbon black	15·7	12·3
Boron nitride	19·6	20·0
Hydroxyapatite	55·2	55·0
Carbon black, Spheron-6	107·8	110·0

$\theta = 130°$ was assumed throughout. The selection of results given in Table 3.17 serves to illustrate the level of agreement between the surface areas determined by mercury intrusion and by nitrogen adsorption. In view of the assumptions made and the uncertainties involved in both methods, the overall agreement must be reckoned satisfactory. It should be noted, however, that the areas calculated from the mercury *extrusion* data did not agree with the BET values.

A(Hg) will not include any contribution from the finer mesopores, which are not penetrated by the mercury, nor from any micropores which are present (cf. Chapter 4). The importance of these qualifications is demonstrated by the results of a recent study by Sing and his co-workers.[118] A series of alumina gels was prepared by passage of gaseous ammonia into solutions of aluminium nitrate nonohydrate in various alcohols. Their pore structure, as revealed by both nitrogen adsorption and by mercury porosimetry, varied markedly according to the particular alcohol and the concentration of the solution. A selection of mercury intrusion–extrusion plots is shown in Fig. 3.35; curves A, B and C show no tendency to approach a plateau even at the highest pressure, indicating incomplete filling of pores and the presence of a substantial proportion of pores of $r^p < 35$ Å; in curves D and E, on the other hand, the intruded volume tends to a

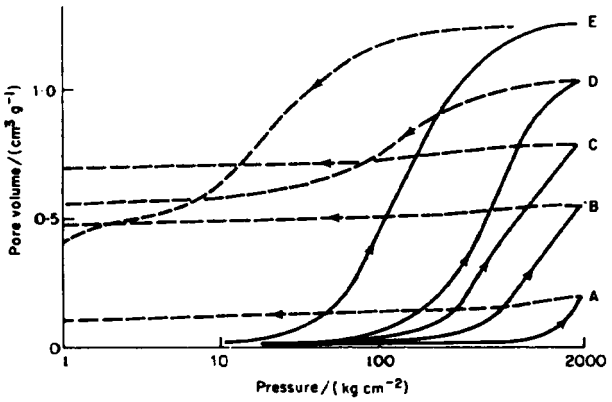

Fig. 3.35 Mercury porosimetry intrusion–extrusion plots[118] of alumina gels prepared from solutions of aluminium monohydrate in: A, propan-2-ol (2·5 w/v%); B, propan-2-ol (4·9 w/v%); C, 2-methylpropan-2-ol (4·9 w/v%); D, 2-methylpropan-2-ol (9·5 w/v%); E, butan-2-ol (9·5 w/v%). ——, ascending, intrusion curve; – – – –, descending, extrusion curve.

maximum suggesting that pores of $r^p < 35$ Å are relatively few. As is seen from the Table 3.18 the agreement between A(Hg) and $A(N_2)$ is good in the case of sample D, but becomes progressively worse in the order C, B, A. The approximate upper limit of r^p as detected by mercury porosimetry corresponds to the pressure at which penetration begins to increase rapidly. In C, B and A this upper limit moves towards finer pores and in (a) has fallen to ~40 Å.

TABLE 3.18

Values of specific surface of alumina gels determined by nitrogen adsorption and by mercury porosimetry[118]

Sample†	Specific surface	
	$A(N_2)/(m^2\,g^{-1})$	A(Hg)/(m² g⁻¹)
A	393	68
B	306	135
C	261	157
D	153	157
E	—	70

† Cf. Fig. 3.35.

Conclusions

Mercury porosimetry is generally regarded as the best method available for the routine determination of pore size in the macropore and upper mesopore range. The apparatus is relatively simple in principle (though not inexpensive) and the experimental procedure is less demanding than gas adsorption measurements, in either time or skill. Perhaps on account of the simplicity of the method there is some temptation to overlook the assumptions, often tacit, that are involved, and also the potential sources of error.

Thus, whilst it is usual† to assume that $\theta = 140°$, the actual value almost certainly depends on the nature of the surface as well as on whether the mercury is penetrating or withdrawing, and an uncertainty up to 20 per cent must be reckoned with (cf. Table 3.14). Again, the surface tension of mercury is sensitive to contamination and it probably depends on the nature of the surface, whilst in extreme cases actual amalgamation can occur. The error in pore size arising from use of the conventional value $\gamma = 480\ \text{mN m}^{-2}$ is very difficult to assess quantitatively; it probably varies from negligible to very large, depending on the nature of the solid and the care taken in the experimentation.

Hysteresis, which is invariably present, adds to the complications: its interpretation is, if anything more complex than with capillary condensation, inasmuch as it can depend not only on the pore structure of the solid but also on the magnitude of the applied pressure.

In a pore system composed of isolated pores of ink-bottle shape, the intrusion curve leads to the size distribution of the necks and the extrusion curve to the size distribution of the bodies of the pores. In the majority of solids, however, the pores are present as a network, and the interpretation of the mercury porosimetry results is complicated by pore blocking effects.

Despite these various limitations, mercury porosimetry constitutes an indispensable tool for the quantitative study of pore structure, but it needs to be supplemented by other techniques, if a reliable picture of the pore system is to be built up.

† In recent years, some workers[119] have preferred the value $\theta = 130°$.

References

1. J. M. van Bemmelen, *Rec. Trans. Chim.* **7**, 37 (1888); "Die Adsorption" (1910).
2. A. Zsigmondy, *Z. Anorg. Chem.* **71**, 356 (1911).
3. W. T. Thomson, *Phil. Mag.* **42**, 448 (1871).
4. J. S. Anderson, *Z. Phys. Chem.* **88**, 191 (1914).
5. L. Gurvitsch, *J. Phys. Chem. Soc. Russ.* **47**, 805 (1915).

6. D. W. Broad and A. G. Foster, *J. Chem. Soc.* 447 (1946).
7. P. H. Emmett and M. Cines, *J. Phys. Chem.* **56**, 735 (1947).
8. S. J. Gregg and J. F. Langford, *J. Chem. Soc. Faraday Trans.* **I, 73**, 747 (1977); J. F. Langford, Ph.D. Thesis, Exeter University (1967).
9. P. C. Carman and F. A. Raal, *Proc. Roy. Soc.* **209A**, 59 (1951).
10. P. Zwietering, Proc. Int. Symp. Reactivity Solids, III, (1956).
11. A. V. Kiselev, *in* "The Structure and Properties of Porous Materials" (eds. D. H. Everett and F. S. Stone), p. 195, Butterworths, London (1958).
12. J. H. de Boer, *in* "The Structure and Properties of Porous Materials" (eds. D. H. Everett and F. S. Stone), p. 68, Butterworths, London (1958).
13. T. Young, "Miscellaneous Works" (ed. Peacock), Vol. 1, p. 418, Murray, London (1855).
14. P. S. Laplace, "Mécanique Céleste", Suppl. Book 10 (1806).
15. R. Defay, I. Prigogine, A. Bellemans and D. H. Everett, "Surface Tension and Adsorption", p. 218, Longmans, London (1966).
16. S. Brunauer, *in* "Surface Area Determination" (eds. D. H. Everett and R. H. Ottewill), p. 63, Butterworths, London (1970).
17. T. Young, *Phil. Trans. Roy. Soc.* **95**, 65 (1805).
18. Dupré, "Théorie Mechanique de la Chaleur", p. 339 (1869).
19. B. V. Derjaguin, *in* "Proceedings of the Second International Congress on Surface Activity, II, p. 154, Butterworths, London (1957).
20. L. R. White, *J. Chem. Soc., Faraday Trans.* **I, 73**, 390 (1977).
21. D. H. Everett and J. M. Haynes, "Colloid Science", Vol. I, p. 123, Specialist Periodical Reports, Chemical Society, London (1973).
22. J. C. P. Broekhoff and J. H. de Boer, *J. Catalysis* **10**, 368 (1968).
23. L. H. Cohan, *J. Amer. Chem. Soc.* **60**, 433 (1938).
24. M. B. Coelingh, Thesis, Utrecht University (1938).
25. J. C. P. Broeckhoff and W. P. van Beek, *J. Chem. Soc., Faraday Trans.* **I, 75**, 42 (1979).
26. E. O. Kraemer, *in* H. S. Taylor's "A Treatise of Physical Chemistry", p. 1661, Macmillan, New York (1931); J. W. McBain, *J. Amer. Chem. Soc.* **57**, 699 (1935); K. S. Rao, *J. Phys. Chem.* **45**, 506, 517 (1941); S. M. Katz, *J. Phys. Chem.* **53**, 1166 (1949).
27. D. H. Everett, *in* "The Solid–Gas Interface" (ed. E. A. Flood), Vol. 2, p. 1055, Dekker, New York (1967).
28. R. M. Barrer and D. M. MacLeod, *Trans. Faraday Soc.* **50**, 980 (1954); R. M. Barrer, N. McKenzie and J. S. S. Reay, *J. Colloid Sci.* 11, 479 (1956).
29. "Contact Angle, Wettability and Adhesion", *Adv. Chem. Series* No. 43, *Amer. Chem. Soc.* (1964).
30. A. G. Foster, *Trans. Faraday Soc.* **28**, 645 (1932).
31. S. Brunauer, R. Sh. Mikhail and E. E. Bodor, *J. Colloid Interface Sci.* **24**, 451 (1967); S. Brunauer, *in* "Surface Area Determination" (eds. D. H. Everett and R. H. Ottewill), p. 63, Butterworths, London (1970).
32. M. R. Bhamhhani, P. A. Cutting, K. S. W. Sing and D. H. Turk, *J. Colloid Interface Sci.* **38**, 109 (1972).
33. A. P. Karnaukhov, *Kinet. Kataliz* **8**, 172 (1967); K. G. Ione, A. P. Karnaukhov and E. E. Kuon, *Kinet. Kataliz* 12, 457 (1971).
34. C. Pierce, *J. Phys. Chem.* **57**, 149 (1953).
35. C. Orr and J. M. DallaValle, "Fine Particle Measurement", p. 271, Macmillan, New York (1959).

36. C. H. Giles, D. C. Havard, W. McMillan, T. Smith and R. Wilson, *in* "Characterisation of Porous Solids" (eds. S. J. Gregg, K. S. W. Sing and H. F. Stoeckli), p. 229, Soc. Chem. Ind., London (1979).
37. A. Wheeler, *in* "Catalysis", Vol. II, p. 118, Reinhold, New York (1955).
38. C. G. Shull, *J. Amer. Chem. Soc.* **70**, 1410 (1948).
39. E. P. Barrett, L. G. Joyner and P. H. Halenda, *J. Amer. Chem. Soc.* **73**, 373 (1951).
40. R. W. Cranston and F. A. Inkley, "Advances in Catalysis" **9**, 143, Academic Press, New York and London (1957).
41. D. Dollimore and G. R. Heal, *J. Applied Chem.* **14**, 109 (1964); *J. Colloid Interface Sci.* **33**, 508 (1970).
42. B. F. Roberts, *J. Colloid Interface Sci.* **23**, 266 (1967).
43. A. V. Kiselev, *Usp. Khim.* **14**, 367 (1945); Proceedings Second International Congress on Surface Activity, **II**, 189 Butterworths, London (1957).
44. W. de Vleesschauwer, *in* "Surface Area Determination" (eds. D. H. Everett and R. H. Ottewill), p. 82, Butterworths, London (1970).
45. J. M. Haynes, *in* "Colloid Science" (ed. D. H. Everett), Vol. 2, p. 101, Chemical Society, London (1975).
46. D. Dollimore and G. R. Heal, *J. Colloid Interface Sci.* **42**, 233 (1973).
47. D. C. Havard and R. Wilson, *J. Colloid Interface Sci.* **57**, 276 (1976).
48. D. H. Everett, *in* "Characterisation of Porous Solids" (eds. S. J. Gregg, K. S. W. Sing and H. F. Stoeckli), p. 229, Soc. Chem. Ind., London (1979).
49. P. H. Doe and J. M. Haynes, *in* "Characterization of Porous Solids" (eds. S. J. Gregg, K. S. W. Sing and H. F. Stoeckli), p. 253, Soc. Chem. Ind., London (1979).
50. E. A. Guggenheim, *Trans. Faraday Soc.* **36**, 407 (1940).
51. J. C. Melrose, *Amer. Inst. Chem. Eng. J.* **12**, 986 (1966).
52. J. W. Gibbs, "Scientific Papers", Vol. 1, p. 219, Longmans, London (1906).
53. W. S. Ahn, M. S. Jhou, H. Pak and S. Chang, *J. Colloid Interface Sci.* **38**, 605 (1972).
54. M. R. Harris, *Chem. and Ind.* 269 (1965).
55. R. G. Avery and J. D. F. Ramsay, *J. Colloid Interface Sci.* **42**, 597 (1973).
56. M. M. Tayyab, Ph.D. Thesis, Brunel University (1971).
57. M. M. Dubinin, *Russ. J. Phys. Chem.* **34**, 959 (1960).
58. D. H. Everett and W. I. Whitton, *Proc. Roy. Soc.* **A230**, 91 (1955).
59. S. J. Gregg and K. H. Wheatley, *in* "Proceedings Second International Congress on Surface Activity" **II**, p. 102, Butterworths, London (1957); K. H. Wheatley, Ph.D. Thesis, London University (1953).
60. S. J. Gregg and M. I. Pope, *J. Chem. Soc.* 1252 (1961); M. I. Pope, Ph.D. Thesis, Exeter University (1957).
61. R. C. Asher and S. J. Gregg, *J. Chem. Soc.* 5057 (1960); R. C. Asher, Ph.D. Thesis, London University (1955).
62. R. Stock, Ph.D. Thesis, London University (1955).
63. E. G. J. Willing, Ph.D. Thesis, London University (1952).
64. K. J. Hill, Ph.D. Thesis, London University (1950).
65. R. K. Packer, Ph.D. Thesis, London University (1952).
66. S. J. Gregg and M. M. Tayyab, *J. Chem. Soc. Faraday Trans.* **I**, **74**, 348 (1978).
67. J. Hickman, Ph.D. Thesis, Exeter University (1958).
68. S. J. Gregg and J. Hickman, *in* Proceedings of the Third Conference on "Industrial Carbon and Graphite", Soc. Chem. Ind., p. 146, Academic Press, London and New York (1970).

69. R. K. Schofield, *Disc Faraday Soc.* No. 3, 105 (1948).
70. O. Kadlec and M. M. Dubinin, *J. Colloid Interface Sci.* **31**, 479 (1969).
71. E. A. Flood, *in* "The Solid–Gas Interface" (ed. E. A. Flood), Vol. 1, p. 54, Dekker, New York (1967).
72. C. G. V. Burgess and D. H. Everett, *J. Colloid Interface Sci.* **33**, 611 (1970).
73. F. S. Baker, J. D. Carruthers, R. E. Day, K. S. W. Sing and L. J. Stryker, *Disc. Faraday Soc.* No. **52**, 173 (1971).
74. C. F. Prenzlow and G. D. Halsey, *J. Phys. Chem.* **61**, 1158 (1957).
75. P. A. Cutting, *in* "Vacuum Microbalance Techniques" **7**, 51, Plenum Press, New York (1970).
76. G. A. Nicolaon and S. J. Teichner, *J. Chim. Phys.* **65**, 871 (1968).
77. J. C. P. Broekhoff, *in* "Preparation of Catalysts II" (eds. B. Delmon, P. Grange, P. Jacobs and G. Poncelet), p. 663, Elsevier, Amsterdam (1979).
78. E. A. Boucher, *J. Mater. Sci.* **11**, 1734 (1976); F. A. L. Dullien and V. K. Batra, *Ind. Eng. Chem.* **62**, 25 (1970); A. A. Liabastre and C. Orr, *J. Colloid Interface Sci.* **64**, 1 (1978).
79. E. W. Washburn, *Proc. Nat. Acad. Sci. U.S.A.* **7**, 115 (1921).
80. H. L. Ritter and L. C. Drake, *Ind. Eng. Chem. Analyt. Ed.* **17**, 782 (1945); L. C. Drake, *Ind. Eng. Chem.* **41**, 780 (1949).
81. C. Kemball, *Trans. Faraday Soc.* **42**, 526 (1946).
82. "Handbook of Chemistry and Physics", 58th edn. F-30, CRC Press, Florida (1978); Ziesing, *Austral. J. Phys.* **6**, 86 (1953).
83. B. P. Bering and K. A. Ioileva, *Dokl. Akad. Nauk, SSSR*, **93**, 85 (1953).
84. F. H. Norton and W. D. Kingery, AEC—Prog. Rep. NYO 4632 (1955).
85. L. L. Olson and J. A. Johnson, *J. Phys. Chem.* **67**, 2529 (1963).
86. H. K. Roberts, *J. Chem. Soc.* 1907 (1964).
87. V. I. Melik-Gaikazyan, V. V. Voronchikhina and E. A. Zakharova, *Elektrokhim.* **4**, 1420 (1968).
88. A. E. Schwancke, W. L. Falke and V. R. Miller, *US-Bur. Min., Inv. Rep.* No. 7340 (1970).
89. T. F. Young quoted by N. K. Adam, "Physics and Chemistry of Surfaces", p. 185, Oxford University Press, London (1941).
90. T. Bate, *Phil. Mag.* **28**, 252 (1939).
91. T. C. Platschenov, V. A. Alexandrov and G. M. Belozerkovski, *in* "Methoden der Strukturuntersuchung au hochdispersen und porösen Stoffen" (trans.), p. 88, Akademic-Verlag, Berlin (1961).
92. S. Kruyer, *Trans. Faraday Soc.* **54**, 1758 (1958).
93. G. Macdougal and C. Ockrent, *Proc. Roy. Soc.* **180**, 151 (1942).
94. A. H. Ellison, R. B. Klemm, A. M. Schwartz, L. S. Grubb and D. A. Petrash, *J. Chem. Eng. Data* **12**, 607 (1967).
95. J. J. F. Scholten, *in* "Porous Carbon Solids" (ed. R. L. Bond), p. 225, Academic Press, London and New York (1967); L. A. DeWit and J. J. F. Scholten, *J. Catalysis* **36**, 36 (1975).
96. L. G. Joyner, E. P. Barrett and R. Skold, *J. Amer. Chem. Soc.* **73**, 3155 (1951).
97. M. M. Dubinin, *in* "Chemistry and Physics of Carbon" (ed. P. L. Walker), Vol. 2, p. 83, Dekker, New York (1966).
98. F. A. L. Dullien and G. K. Dhawan, *J. Colloid Interface Sci.* **47**, 337 (1974).
99. F. A. L. Dullien and G. K. Dhawan, *J. Colloid Interface Sci.* **52**, 129 (1975).
100. D. N. Winslow and S. Diamond, *J. Mater.* **5**, 564 (1970).
101. A. J. Juhola and O. Wiig, *J. Amer. Chem. Soc.* **71**, 2078 (1949).

102. R. Sibut Pinote, P. Cournnault and F. Du Chaffant, *J. Chim. Phys.* **65**, 1188 (1968).
103. J. M. Dickinson and J. W. Shore, *Carbon* **6**, 937 (1968).
104. S. M. Brown and E. W. Lard, *Powder Tech.* **9**, 187 (1974).
105. K. Unger and H. Fischer, *in* "Proceedings of RILEM/IUPAC International Symposium on Pore Structure and Properties of Materials" (eds. S. Modry and M. Svata), Vol. 5, D-127, Academia, Prague (1974).
106. W. B. Innes, *Anal. Chem.* **23**, 759 (1951); **28**, 332 (1956); A. Y. Mottlan and N. E. Fisher, *Anal. Chem.* **34**, 714 (1962).
107. M. P. McDaniel and T. D. Hottovy, *J. Colloid Interface Sci.* **78**, 31 (1980).
108. N. N. Kamakin, *in* "Methoden der Strukturuntersuchung an Hochdispersen und Porösen Stoffen" (trans.), p. 73, Akademie-Verlag, Berlin (1961).
109. A. Reverberi, G. Feraiolo and A. Peloso, *Ann. Chim. (Italy)*, **56**, 1552 (1966).
110. M. Svata, *Powder Technol.* **5**, 345 (1971/72).
111. L. K. Frevel and L. J. Kressley, *Anal. Chem.* **35**, 1492 (1963).
112. R. P. Mayer and R. A. Stowe, *J. Phys. Chem.* **70**, 3867 (1966); J. M. Haynes, *in* "Colloid Science", Vol. 2, p. 101, Specialist Periodical Reports, Chemical Society, London (1975).
113. G. P. Androutsopoulos and R. Mann, *Chem. Eng. Sci.* **34**, 1203 (1979).
114. R. Mann, G. P. Androutsopoulos and H. Golshan, *Chem. Eng. Sci.* **36**, 337 (1981).
115. D. H. T. Spencer, *in* "Porous Carbon Solids" (ed. R. L. Bond), p. 87, Academic Press, London (1967); D. H. T. Spencer and J. Wilson, *Fuel* **55**, 291 (1976).
116. F. A. P. Maggs, *Nature* **186**, 956 (1960).
117. H. M. Rootare and C. F. Prenzlow, *J. Phys. Chem.* **71**, 2733 (1967).
118. B. Cormack, J. J. Freeman and K. S. W. Sing, *J. Chem. Tech. Biotechnol.* **31**, 367 (1980).
119. A. A. Liabastre and C. Orr, *J. Colloid Interface Sci.* **64**, 1 (1978).
120. K. K. Unger, St. Doeller and K. F. Krebs, *in* "Characterisation of Porous Solids" (eds. S. J. Gregg, K. S. W. Sing and H. F. Stoeckli), p. 291, Soc. Chem. Ind., London (1979).

4

The Physical Adsorption of Gases by Microporous Solids: The Type I Isotherm

4.1 Introduction

If a solid contains micropores—pores which are no more than a few molecular diameters in width—the potential fields from neighbouring walls will overlap and the interaction energy of the solid with a gas molecule will be correspondingly enhanced. This will result in a distortion of the isotherm, especially at low relative pressures, in the direction of increased adsorption; there is indeed considerable evidence that the interaction may be strong enough to bring about a complete filling of the pores at a quite low relative pressure.

In the simplest case, adsorption in a microporous solid leads to an isotherm of Type I; consequently it is convenient to approach the subject by a discussion, from a "classical" standpoint, of Type I isotherms.

4.2 Type I isotherms

Type I isotherms are characterized by a plateau which is nearly or quite horizontal, and which may cut the $p/p^\circ = 1$ axis sharply or may show a "tail" as saturation pressure is approached (Fig. 4.1). The incidence of hysteresis varies: many Type I isotherms exhibit no hysteresis at all (Fig. 4.1), others display a definite loop, and in others there is hysteresis which may or may not persist to the lowest pressures ("low-pressure hysteresis") (Fig. 4.2). Type I isotherms are quite common, and are no longer restricted, as seemed at one time to be the case, to charcoals. Many solids, if suitably prepared, will yield Type I isotherms: the xerogels of silica, titania, alumina

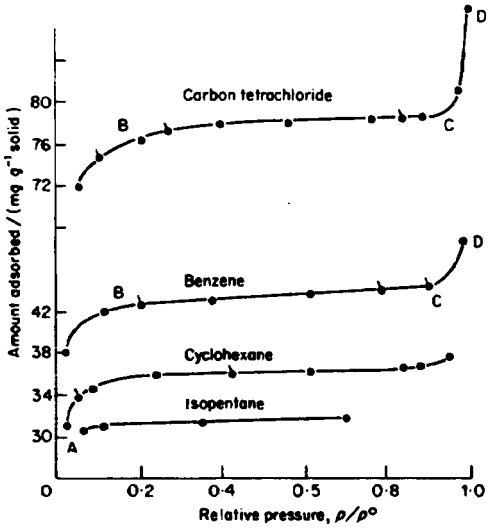

Fig. 4.1 Adsorption isotherms of some organic vapours on ammonium phosphomolybdate[1] outgassed at 180°C. The isotherm temperatures (reading downwards) were 25°C, 25°C, 25°C, 0°C.

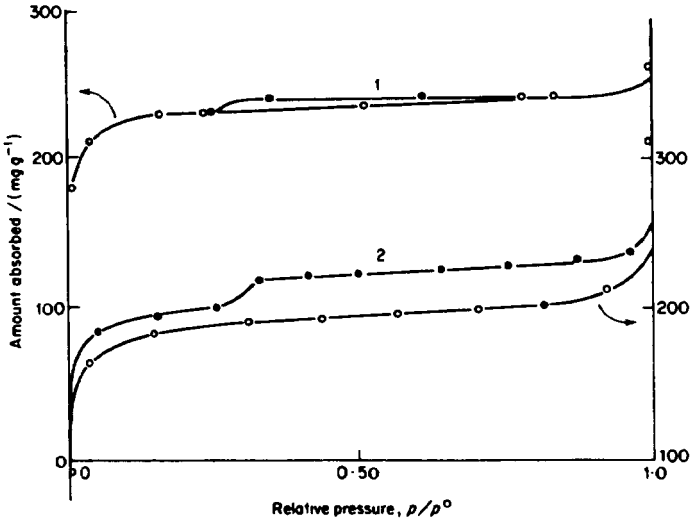

Fig. 4.2 Adsorption isotherms of benzene at 25°C on (1) a charcoal from anthracite coal, activated to 56% yield; (2) an activated coconut charcoal.[2] (After Cadenhead and Everett.)

or stannic oxide, for example, or even certain salts of the heteropolyacids such as ammonium molybdates. Particularly well defined Type I isotherms are given by the molecular sieve zeolites.

The classical interpretation

Any interpretation of the Type I isotherm must account for the fact that the uptake does not increase continuously as in the Type II isotherm, but comes to a limiting value manifested in the plateau BC (Fig. 4.1). According to the earlier, classical view,[3] this limit exists because the pores are so narrow that they cannot accommodate more than a single molecular layer on their walls; the plateau thus corresponds to the completion of the monolayer. The shape of the isotherm was explained in terms of the Langmuir model,[3] even though this had initially been set up for an open surface, i.e. a non-porous solid. The Type I isotherm was therefore assumed to conform to the Langmuir equation already referred to, viz.

$$\frac{n}{n_m} = \frac{Bp}{1 + Bp} \tag{4.1}$$

If relative pressure rather than pressure itself is used, the equation becomes

$$\frac{n}{n_m} = \frac{c(p/p^\circ)}{1 + c(p/p^\circ)} \tag{4.2}$$

which can be immediately derived from the BET equation for restricted adsorption (Equation (2.18)) by putting the maximum number of layers, $N = 1$.

In order to test the Langmuir isotherm against experimental data, Equation (4.1) may be rewritten in the form

$$\frac{p}{n} = \frac{1}{Bn_m} + \frac{p}{n_m} \tag{4.3}$$

and Equation (4.2) as

$$\frac{p/p^\circ}{n} = \frac{1}{cn_m} + \frac{p/p^\circ}{n_m} \tag{4.4}$$

The plot of p/n against p, or of $(p/p^\circ)/n$ against p/p° should therefore yield a straight line of slope $1/n_m$.

Alternatively one may note (with Barrer[4]) that, from Equation (4.1) with substitution of $n/n_m = \theta$, we have

$$\frac{\theta}{1 - \theta} \cdot \frac{1}{p} = B \tag{4.5}$$

or from Equation (4.2)

$$\frac{\theta}{1-\theta}\cdot\frac{1}{p/p^\circ} = c \tag{4.6}$$

so that the quotients on the left-hand sides of these equations should be independent of θ and of p (or p/p°). To apply this second test a value of n_m is needed; if the plateau of the isotherm is nearly or quite horizontal, n_m may be taken as identical with the uptake at saturation pressure.

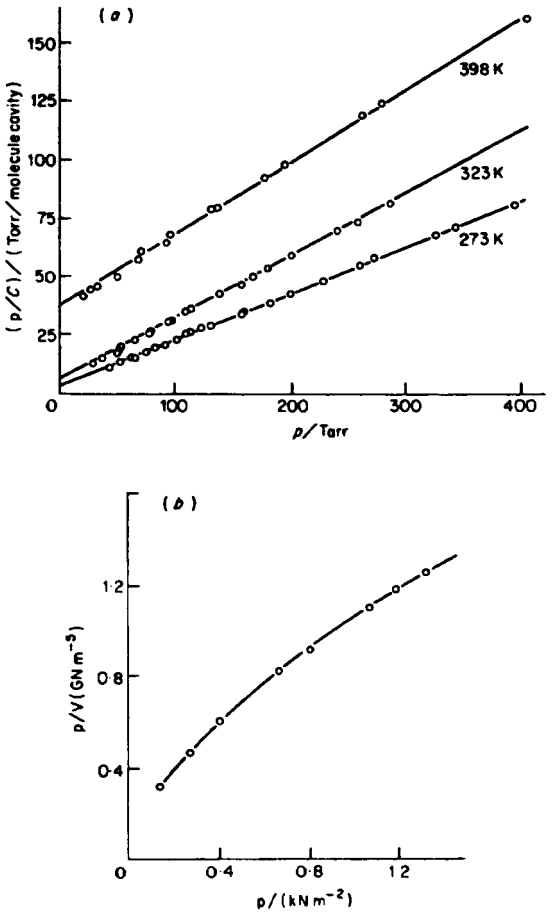

Fig. 4.3 Langmuir plots (*a*) for propane on 5A zeolite[5] (courtesy Ruthven); (*b*) for carbon monoxide on zeolite CaY-54[6] (courtesy Stone). In (*a*) the adsorption is expressed in terms of number C of molecules of adsorbate per cavity; in (*b*), as m^3 (stp).

In practice, the degree of conformity to the Langmuir equation varies considerably. In some cases a good straight line is obtained on plotting p/n against p (or $(p/p^\circ)/n$ against p/p°) (cf. Fig. 4.3(*a*), but in others the line is distinctly curved (cf. Fig. 4.3(*b*)). Likewise the quotients of Equation (4.5) or (4.6) are sometimes almost independent of θ, but sometimes show a strong dependence on θ. Thus on H-chabazite (a zeolite) the plot of $\theta/p(1-\theta)$ against θ is almost horizontal for Ar adsorbed at a number of temperatures, whereas with CO_2 the plot shows the Langmuir quotient to be far from constant at the lower temperatures (Fig. 4.4(*a*) and (*b*)).

The Langmuir equation is based on the assumption that the heat of adsorption does not vary with the coverage θ; it is interesting that in the systems just quoted, the heat of adsorption varies with the amount adsorbed in the case of CO_2, but is virtually constant in the case of Ar.

Conformity to the Langmuir equation, where it occurs, does not constitute proof of the correctness of the mechanism, since both B (or c) and n_m are disposable constants; the quantities v_1 and E_1 (cf. Equation (2.7)) are incapable of *a priori* evaluation. In the present context, however, a point of major interest is the quantity n_m whether derived from the Langmuir plot (Equations (4.3) or (4.4)) or from the plateau level.

According to the classical Langmuir model, n_m is actually equal to the monolayer capacity, and can be converted into the specific surface A of the solid by the standard relation $A = n_m a_m L$ (cf. Equation (2.1)). A number of lines of argument would suggest, however, that this interpretation is invalid, and that the value of A arrived at does not represent a true specific surface.

In the first place, the calculated values of specific surface are often improbably high. A particular Saran char,[7] for example, had a calculated area of $\sim 3000\,m^2\,g^{-1}$. This figure is actually slightly greater than the area

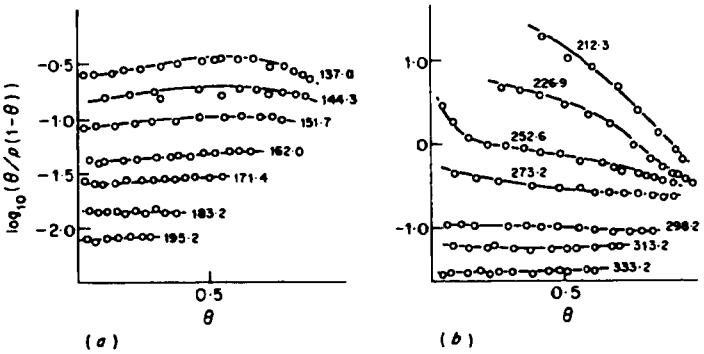

Fig. 4.4 Plot of the logarithm of the Langmuir quotient $\theta/p(1-\theta)$ against θ for adsorption on H-chabasite at various temperatures.[4] (*a*) Argon; (*b*) carbon dioxide. (After Barrer and Davies.)

($2630\ m^2\ g^{-1}$)[8] which could be provided by 1 g of carbon if it were present as layers of graphite only one atom thick and accessible to gas on both sides. A tenuous structure of this kind is very difficult to reconcile with the mechanical strength of the material.

Further evidence pointing in the same direction was provided by Pierce, Wiley and Smith,[9] who found that on steam activation of a particular char at 900°C the saturation uptake increased three-fold, yet the isotherm was still of Type I. They argued that even if the width of the pores was only two molecular diameters before activation, it would increase, by removal of oxides, during the activation so that the second Type I isotherm would correspond to pores more than two molecular diameters wide. (The alternative explanation, that activation produced new pores of the same width as the old, seems unlikely.)

Evidence of a different kind is furnished by the fact that the Gurvitsch rule (p. 113) is often obeyed by systems showing Type I isotherms:[1,11,12] the amounts of different adsorptives taken up by a given adsorbent, when expressed as a volume of liquid, agree within a few per cent. The order of agreement is illustrated by the typical examples in Table 4.1 for the adsorption of *n*-alkanes on ammonium phosphomolybdate,[1,10] and in Table 4.2 which refers to a variety of adsorptives on a silica gel. It must be admitted, however, that there are cases where considerable deviations from the Gurvitsch rule are found, even though the isotherms are of Type I. Thus, in Table 4.3 the variation in values of the saturation uptake is far outside

TABLE 4.1

The Gurvitsch rule for ammonium phosphomolybdate[1,10]. Quantity adsorbed at a relative pressure of 0·9†, calculated as a volume of liquid

Adsorbate	Temperature T/°C	Volume adsorbed v_a/($cm^3\ g^{-1}$)
Methane	−183	0·0508
Ethane	−100	0·0546
Propane	−64	0·0515
n-Butane	−23	0·0490
n-Pentane	0	0·0508
n-Hexane	25	0·0542
n-Heptane	25	0·0526
n-Octane	25	0·0530
n-Nonane	26·3	0·0522
Water	25	0·0555

† On the flat portion of the isotherm, just before the final upward turn.

experimental error. However, since the very low values are found with the larger molecules, the deviations may well be explicable in terms of the molecular sieve effects.

The conformity to the Gurvitsch rule shown by systems giving Type I isotherms is sufficiently general to suggest that the adsorbate is condensed in the pores in a form having a density close to that of the bulk liquid

TABLE 4.2

The Gurvitsch rule for silica gel B.[11] Quantity adsorbed at saturation, calculated as a volume of liquid (v_s) at 25°C

Adsorbate	$v_s/(cm^3\,g^{-1})$
n-C_4H_9OH	0·360
CCl_4	0·344
Dioxan	0·354
C_2H_5OH	0·385
HCN	0·363
CH_3OH	0·384
n-C_3H_7OH	0·351
iso-C_3H_7OH	0·362
$N(C_2H_5)_3$	0·358
H_2O	0·351

TABLE 4.3

The Gurvitsch rule for silica gel J.[13] Quantity adsorbed close to saturation (p/p^*), calculated as a volume of liquid (v_s)

Adsorbate	Temperature T/K	$v_s/(cm^3\,g^{-1})$
Carbon dioxide	195	0·205
Nitrogen	77	0·187
Carbon monoxide	77	0·186
Nitrous oxide	195	0·184
Methane	90	0·160
Ethane	195	0·157
Cyclopropane	195	0·154
Propane	195	0·146
Argon	77	0·142
Benzene	298	0·128
Butane	273	0·125
Carbon tetrachloride	298	0·074
Neopentane	273	0·064

adsorptive. This in turn suggests that the pore has a width in excess of two molecular diameters, since the individual characteristics, of size and shape, of the different molecules would be bound to influence the way in which they would pack into such a narrow capillary. A width of several molecular diameters would be required to ensure the smoothing out of such effects and enable the packing to simulate that in a bulk liquid.

That the uptake n_s at saturation does indeed approximate to the pore volume of the adsorbent is confirmed by the agreement, frequently obtained, between the quantity $n_s V_L$ and the pore volume calculated from the apparent densities ρ(Hg) and ρ(F) of the adsorbent, measured by immersion in mercury and some other suitable fluid respectively. Since (p. 176) mercury at atmospheric pressure cannot enter pores of diameter below $\sim 14\,\mu m$, $1/\rho$(Hg) is equal to the volume of the solid material itself together with nearly all its pores. The other fluid F, which may be either gaseous helium—assumed to be unadsorbed—or a liquid such as benzene, will enter all pores except those with entrances narrower than a single molecular diameter of F. Thus $1/\rho$(F) will be equal to the volume of the solid material plus any sub-molecular pores which are present. Consequently $1/\rho$(Hg) $- 1/\rho$(F) should be virtually equal to the pore volume of the sample and therefore in turn to the Gurvitsch volume.

As emphasized in Chapter 3 (p. 113), however, the uptake at saturation must have a definite value—the isotherm must cut the $p/p^\circ = 1$ axis at a sharp angle, preferably $\sim 90°$—if the test is to be valid. Some typical examples are given in Table 4.4. The agreement between the two measures of pore volume is reasonably good; the fact that the values for the charcoals obtained from the densities are somewhat higher than the "Gurvitsch" values is readily understood inasmuch as the molecules of helium are small enough to enter pores inaccessible to nitrogen or ethyl chloride.

These various considerations led Pierce, Wiley and Smith[9] in 1949, and independently, Dubinin,[15] to postulate that in very fine pores the mechanism of adsorption is pore filling rather than surface coverage. Thus the plateau of the Type I isotherm represents the filling up of the pores with adsorbate by a process similar to but not identical with capillary condensation, rather than a layer-by-layer building up of a film on the pore walls.

Experimental findings in the intervening years have tended to support and extend this concept. The results obtained by Ramsay and Avery[16] in their studies of the effect of compaction on the nitrogen isotherms of two finely divided powders, one of zirconia and the other of silica, are especially instructive in the present context. As in earlier studies (cf. Chapter 3) the isotherm on the original powder was of Type II, but on compaction it first became Type IV with a well defined hysteresis loop, which moved

TABLE 4.4

Comparison of the pore volume obtained (*a*) by the Gurvitsch rule and (*b*) from the densities in mercury and in another fluid

Solid	By Gurvitsch Rule: Pore volume v $(cm^3\ g^{-1}) = x/\rho_L$	Adsorbate†	By densities in Hg and in fluid F: Pore volume $\frac{(1/\rho_{Hg} - 1/\rho_F)}{(cm^3\ g^{-1})}$	Fluid F	Ref.
Charcoal SCO	0·464	Nitrogen	0·473	Helium	7
	0·445	Ethyl chloride			
Charcoal SC33	0·603	Nitrogen	0·612	Helium	7
	0·582	Ethyl chloride			
Charcoal SC70	0·866	Nitrogen	0·873	Helium	7
	0·856	Ethyl chloride			
Stannic oxide heated to 200°C	0·088	Carbon tetrachloride	0·085	Carbon tetrachloride	14
Stannic oxide heated to 300°C	0·094	Carbon tetrachloride	0·098	Carbon tetrachloride	14

† The isotherms were of Type I.

increasingly towards lower relative pressures as the compacting pressure increased (cf. Curves B, C and D of Fig. 4.5, which refers to ZrO_2; results for SiO_2 were similar). The new feature however is that at the highest pressures, 70 and 100 ton in^{-2}, the hysteresis loop disappeared and the isotherm changed to Type I (Curves E and F). Isotherms E and F clearly represent the final stages in a continuous process in which the size of the pores is progressively reduced until it falls below the mesopore range. The uptake at saturation pressure ($p/p^\circ = 1$) with the Type I isotherms E and F thus represents a total pore volume, just as with the Type IV isotherms B, C and D.

Some insight into the special nature of adsorption in systems giving rise to Type I isotherms can be gained by comparing the (Type II) isotherm of an adsorbate on a nonporous sample of a solid, with the Type I isotherm of the same adsorbate on a porous sample of the same chemical substance. A case in point is carbon black as compared with an active carbon. In Table 4.5 due to Dubinin[17] the adsorption of benzene on these two carbons (relative to the adsorption at $p/p^\circ = 0{\cdot}175$, arbitrarily taken as unity) are compared at a number of relative pressures in the low-pressure region. The isotherm on the active carbon is obviously distorted upwards, and this implies that the heat of adsorption is higher than on the "open" surface of carbon black. Curves for the net heat of adsorption against amount adsorbed for a similar pair of carbons, shown in Fig. 4.6, confirm this. A similar kind of distortion of the isotherm of benzene adsorbed on a fine-pored silica relative to that on a nonporous silica, was noted by Kiselev.[18] More recently Sing and his co-workers[19] demonstrated that the isosteric heat of adsorption of nitrogen,

TABLE 4.5

Amount of benzene adsorbed at 20°C on carbon black and on active carbons at low pressures, relative to the amount adsorbed at $p/p^\circ = 0{\cdot}175$

p/p°	On carbon black	On active carbons	
		AC-1	AC-2
1×10^{-5}	0·02	0·12	0·44
1×10^{-4}	0·06	0·16	0·57
1×10^{-3}	0·14	0·46	0·73
1×10^{-2}	0·33	0·71	0·87
1×10^{-1}	0·81	0·92	0·96
0·175	1·00	1·00	1·00

Courtesy of Dubinin[17]

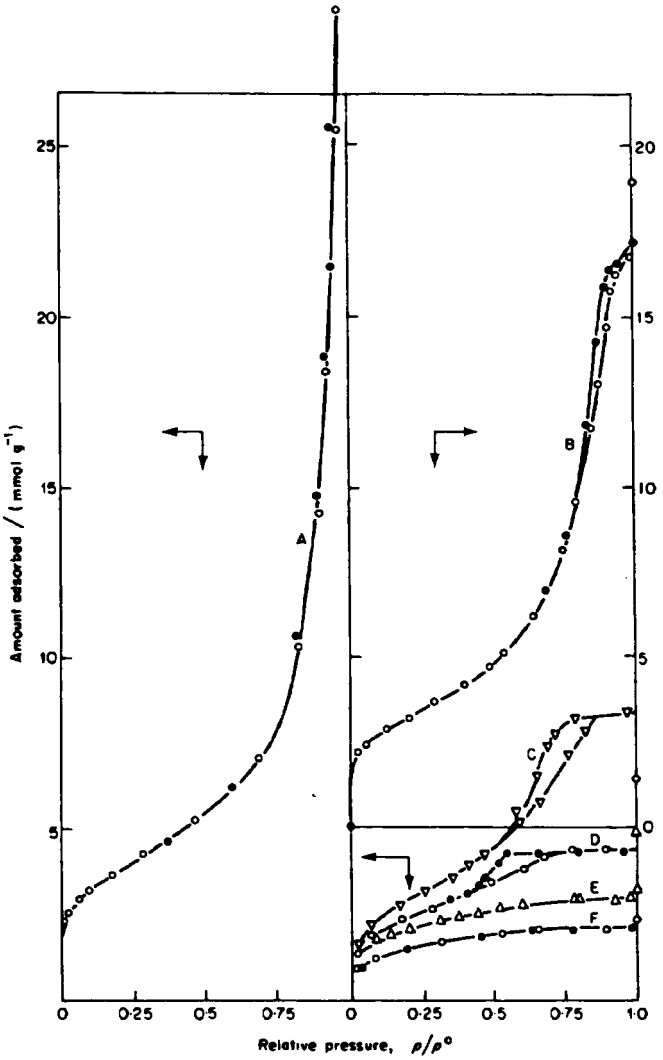

Fig. 4.5 Adsorption isotherms of nitrogen at 77 K on zirconia powder and its compacts.[16] (A) uncompressed; (B) compressed at 3 ton in^{-2}; (C) 10 ton in^{-2}; (D) 30 ton in^{-2}; (E) 70 ton in^{-2}; (F) 100 ton in^{-2}. Open symbols denote adsorption, solid symbols desoprtion. (Courtesy Avery and Ramsay.)

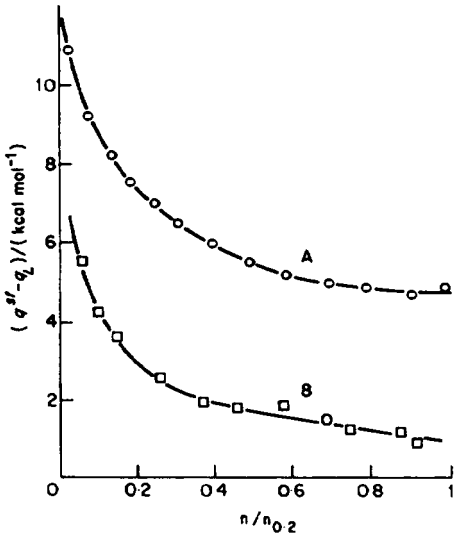

Fig. 4.6 Plot[17] of the net differential heat of adsorption ($q^{st} - q_L$) against the relative adsorption $n/n_{0\cdot2}$, where $n_{0\cdot2}$ is the adsorption at $p/p^\circ = 0\cdot2$. (A) active carbon; (B) carbon black. (After Dubinin.)

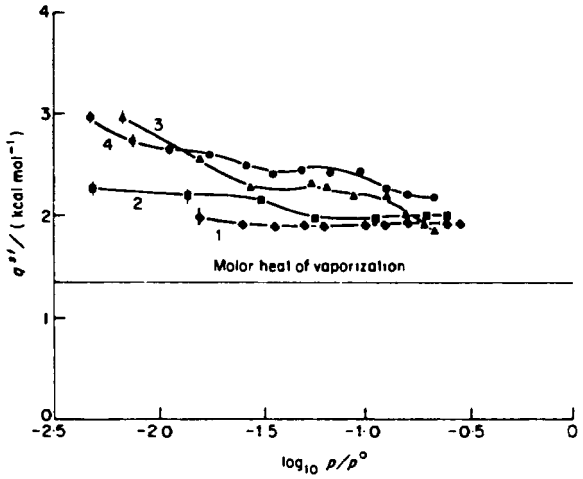

Fig. 4.7 Isosteric heat of adsorption q^{st} of nitrogen adsorbed at 77 K on non-porous and porous silica.[19] (1) ◆, "Fransil", non-porous; (2) ■ gel A, mesoporous; (3) ▲ gel B, mesoporous and microporous; (4) ● gel D, microporous.

calculated from its Type I isotherms on microporous silica, was consistently higher than that from the Type II isotherms on a nonporous silica (Fig. 4.7). The enhancement of the heat of adsorption in very fine pores is only to be expected, as a consequence of the overlap of the adsorption field from neighbouring walls. The likelihood of an intensification of this kind was recognized half a century ago,[20] and more recently a number of attempts have been made at the difficult task of calculating the theoretical interaction energy of an adsorbate molecule with the walls of a micropore.[21] The nature of the treatment will be briefly indicated in the section following.

4.3 The force field in very fine pores

Calculations of the interaction energy in very fine pores are based on one or other of the standard expressions for the pair-wise interaction between atoms, already dealt with in Chapter 1. Anderson and Horlock,[22] for example, used the Kirkwood–Müller formulation in their calculations for argon adsorbed in slit-shaped pores of active magnesium oxide. They found that maximum enhancement of potential occurred in a pore of width 4·4 Å, where its numerical value was 3·2 kcal mol^{-1}, as compared with 1·12, 1·0 and 1·07 kcal mol^{-1} for positions over a cation, an anion and the centre of a lattice cell, respectively, on a freely exposed (100) surface of magnesium oxide.

A more detailed treatment has been given by Gurfein and his associates[23] who chose as their pore model a cylinder with walls only one molecule thick. A few years later, Everett and Powl[8] extended the range of models to include not only a slit-shaped pore with walls one molecule thick, but also a cylinder tunnelled from an infinite slab of solid and a slit formed from parallel slabs of solid.

It emerged from the treatments of both sets of authors that the critical parameter is not the pore size itself (width of slit or radius of cylinder), but rather the ratio of the size of the pore to that of the adsorbate molecule. This is brought out in Fig. 4.8, where (*a*), (*b*) and (*c*) refer to different values of the ratio d/r_0 for the slit model with thick walls; d is the half-width of the slit and r_0 is the collision radius of the molecule. The curves show the variation of the interaction potential ϕ of an adsorbate molecule with its distance z from the middle plane of the slit, and they are plotted in the dimensionless form as ϕ/ϕ^* against z/r_0; here ϕ^* is the interaction potential of a molecule with a freely exposed plane surface, and it corresponds to the minimum in Fig. 1.2. For larger values of d/r_0, there are two minima in the potential (curve (*a*)) but as d diminishes the minima merge to give a single minimum of increasing depth (curves (*b*) and (*c*)).

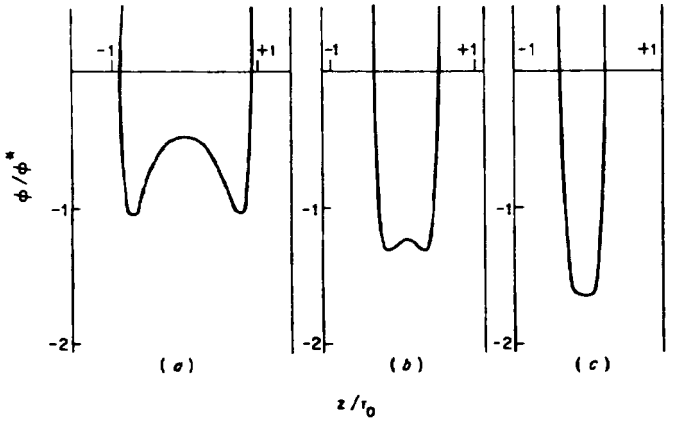

Fig. 4.8 Enhancement of interaction potential in a slit-shaped pore between parallel slabs of solid. Plot of ϕ/ϕ^* against z/r_0 for various values of d/r_0 or R/r_0 (see text). (Reduced from a diagram of Everett and Powl.[8])

The ratio ϕ/ϕ^* is thus a measure of the enhancement of the energy of adsorption in a micropore as compared with that on an open surface. In curve (i) of Fig. 4.9 this ratio is plotted as a function of d/r_0 and, as is seen, the enhancement is still appreciable when $d = 1{\cdot}5r_0$, but has almost disappeared when $d = 2r_0$, i.e. when the slit is only two molecular diameters wide. Even when $d/r_0 = 1$, which corresponds to a single molecule tightly packed into the width of the slit, the enhancement is only 1·6-fold. The effect

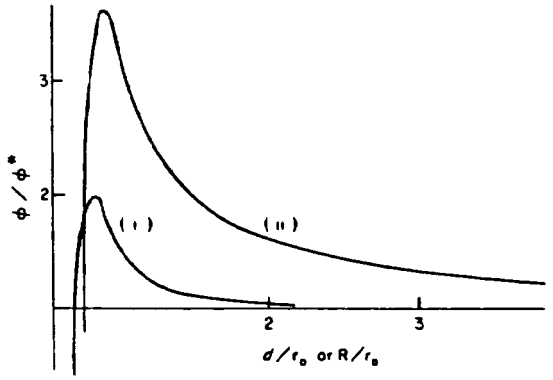

Fig. 4.9 Enhancement of interaction potential in (i) a slit-shaped pore between parallel slabs of solid, (ii) a cylindrical pore in a block of solid. ϕ/ϕ^* is plotted against d/r_0 (see text). (Reduced from a diagram of Everett and Powl.[8])

on the adsorption isotherm could, however, be rather larger than this figure would suggest, on account of possible cooperative effects: the increase in residence time consequent on the enhancement of ϕ would increase the probability of further molecules becoming adsorbed on neighbouring sites within the slit.

As would be expected, the enhancement of potential in cylindrical pores turns out to be considerably greater than in slits, as curve (ii) of Fig. 4.9 clearly demonstrates. At $R/r_0 = 2$ the enhancement is more than 50 per cent, and it is still appreciable when $R/r_0 = 3$ (R = radius of cylinder). The calculations show that at radii in excess of $R = 1{\cdot}086r_0$, the single minimum (comparable with Fig. 4.8(c)) develops into a ring minimum (i.e. two minima are present in any axial plane, cf. Fig. 4.8(a)).

These calculations lend theoretical support to the view arrived at earlier on phenomenological grounds, that adsorption in pores of molecular dimensions is sufficiently different from that in coarser pores to justify their assignment to a separate category as micropores. The calculations further indicate that the upper limit of size at which a pore begins to function as a micropore depends on the diameter σ of the adsorbate molecule; for slit-like pores this limit will lie at a width around $1{\cdot}5\sigma$, but for pores which approximate to the cylindrical model it lies at a pore diameter around $2{\cdot}5\sigma$. The exact value of the limit will of course depend on the actual shape of the pore, and may well be raised by cooperative effects.

4.4 Evaluation of microporosity

If the isotherm is of Type I with a sharp knee and a plateau which is horizontal (cf. Fig. 4.10) the uptake n_s at a point close to saturation, say $p/p^\circ = 0{\cdot}95$, is then a measure of the micropore volume; when converted to a liquid volume (by use of the density of the liquid adsorptive), it may be taken as actually equal to the micropore volume.

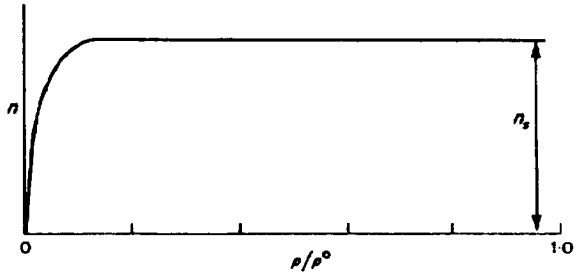

Fig. 4.10 A Type I isotherm.

More often, however, microporosity is associated with an appreciable external surface, or with mesoporosity, or with both.[24] The effect of microporosity on the isotherm will be seen from Fig. 4.11(*a*) and Fig. 4.12(*a*). In Fig. 4.11(*a*) curve (i) refers to a powder made up of nonporous particles and curve (ii) to a solid which is wholly microporous. However, if the particles of the powder are microporous (the total micropore volume being given by the plateau of curve (ii)), the isotherm will assume the form of curve (iii), obtained by summing curves (i) and (ii). Like isotherm (i), the composite isotherm is of Type II, but because of the contribution from the Type I isotherm, it has a steep initial portion; the relative enhancement of adsorption in the low-pressure region will be reflected in a significantly increased value of the BET *c*-constant and a shortened linear branch of the BET plot.

Figure 4.12(*a*) refers to the case where micropores are present along with mesopores. The composite isotherm (iii), like the isotherm (ii) of the mesoporous substance itself, is of Type IV, and again has a steep initial branch with an increased value of *c*.

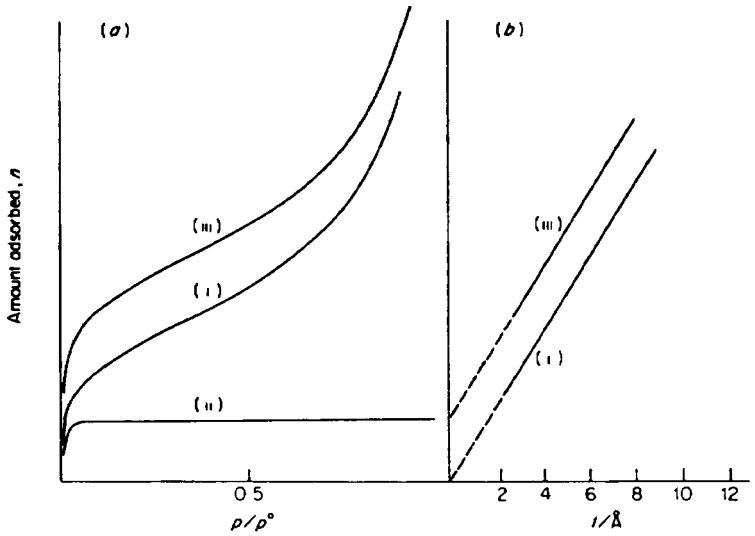

Fig. 4.11 (*a*) Adsorption isotherm for (i) a powder made up of nonporous particles; (ii) a solid which is wholly microporous; (iii) a powder with the same external surface as in (i) but made up of microporous particles having a total micropore volume given by the plateau of isotherm (ii). The adsorption is expressed in arbitrary units. (*b*) *t*-Plots corresponding to isotherms (i) and (iii). The α_s-plots are similar, except for the scale of abscissae.

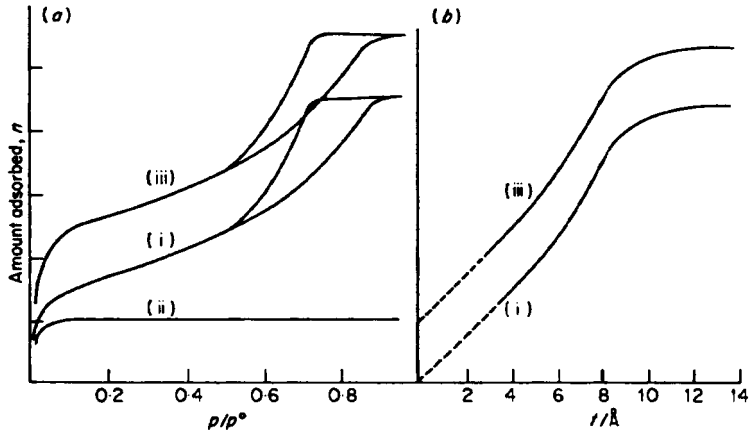

Fig. 4.12 (*a*) Adsorption isotherm for (i) a solid made up of mesoporous grains; (ii) a solid which is wholly microporous; (iii) a granular solid with the same mesoporous system as in (i) but containing also micropores having a total micropore volume given by the plateau of isotherm (ii). The adsorption is expressed in arbitrary units. (*b*) *t*-plots corresponding to isotherms (i) and (iii). The α_s-plots are similar except for the scale of abscissae.

Thus, whilst a powder composed of nonporous particles gives rise to an isotherm of Type II, the converse is not necessarily true: if a solid yields a Type II isotherm, it is not necessarily free of micropores. Similarly, though a Type IV isotherm signifies the presence of mesoporosity, it does not prove the absence of microporosity.[19,24,25]

A high value of the BET constant c is a useful preliminary indication of the presence of microporosity, but it does not enable one to estimate the micropore volume itself, that is in effect to break down the composite isotherm (iii) into its components (i) and (ii).

A number of methods which have been proposed for the evaluation of microporosity from Type II and Type IV isotherms will now be described.

Pre-adsorption

Perhaps the most direct method of evaluating microporosity is to fill up the micropores with some suitable adsorbate whilst leaving the mesopores, macropores and external surface free. The use of *n-nonane* as a pre-adsorbate was proposed by Gregg and Langford[26] on the basis of earlier work[1] on the adsorption of *n*-alkanes C_1 to C_9 on ammonium phosphomolybdate, a microporous solid. This work had shown that the rate at

which the longer chain members could be removed by pumping at room temperature was exceedingly slow; with *n*-nonane, indeed, complete removal required more than 10 hours of pumping at the elevated temperature of 450 K. Thus it was safe to assume that nonane would be wholly retained in micropores during the hour or so of outgassing at room temperature which should be ample for its complete removal from the external surface or from the mesopores of a solid (p° for *n*-nonane at 298 K = 4·7 Torr).

To test the feasibility of the idea, the solid chosen was a carbon black, composed of spherical particles which had been rendered microporous by controlled oxidation at 770 K. Since the particles were reasonably uniform in size, the external surface could be estimated by electron microscopy. The nitrogen isotherm was determined first when the micropores had been filled with nonane, and then after they had been progressively emptied by pumping at elevated temperatures, until finally they were completely empty (Table 4.6). The *modus operandi* was to expose the outgassed solid at 77 K to the vapour of *n*-nonane (from a reservoir of the liquid at room temperature), then allow the solid to warm up to room temperature, and finally to open up to the pumps to remove all adsorbate from the external surface. The nitrogen isotherm of this final sample is shown in curve A of Fig. 4.13, along with curves B, C and D which refer to successive stages in the removal of the *n*-nonane from the micropores by outgassing at successively higher temperatures (cf. Table 4.6). Isotherm E was obtained on the fully outgassed sample.

TABLE 4.6

Adsorption of nitrogen at 77 K on a microporous carbon after pre-adsorption of *n*-nonane[26] (cf. Fig. 4.13)

	Isotherm				
	A	B	C	D	E
T/K	293	408	453	497	723
n_m/(mmol g^{-1})	1·16	1·27	1·74	2·48	3·67
$A(N_2)$/(m^2 g^{-1})	114	124	170	243	360
c(BET)	59	176	410	1200	1940

T = temperature of outgassing of the nonane-charged sample.

n_m = monolayer capacity calculated from the BET plot.

$A(N_2)$ = specific surface calculated from n_m with $a_m(N_2) = 16{\cdot}2$ Å^2.

The specific surface estimated from particle size determined by electron microscopy was 110 m^2 g^{-1}.

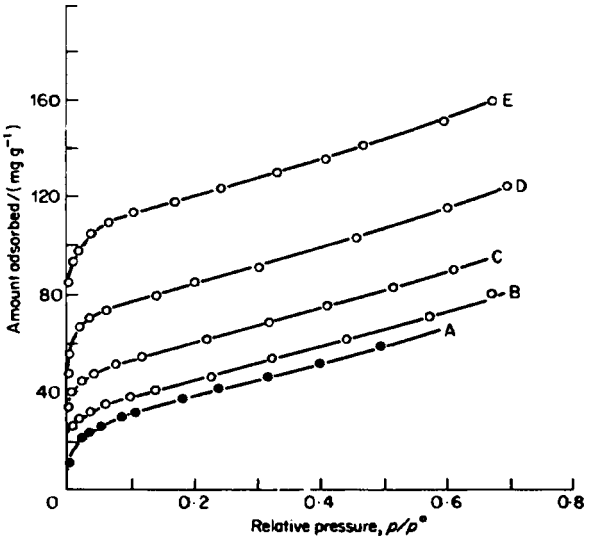

Fig. 4.13 The pre-adsorption method: (*a*) adsorption isotherms of nitrogen at 77 K on a sample of Mogul I carbon black charged with different amounts x of pre-adsorbed nonane.[26] Values of x (mg g^{-1}): (A) 63; (B) 48; (C) 29; (D) 16; (E) 0. (See Table 4.6.) (Some points at low pressures omitted for the sake of clarity.)

Curve A is a typical Type II isotherm, having a value of c around 60 and a clear Point B. The value of specific surface calculated from it, $A = 114\,m^2\,g^{-1}$, agreed well with the geometrical area from the electron micrographs, $110\,m^2\,g^{-1}$. Isotherm E, for the fully outgassed sample, is parallel to isotherm A in the multilayer region, and it seems quite evident that the increased adsorption in isotherm E is solely due to the micropores. Thus the vertical separation of the parallel branches represents the micropore volume and when converted to a liquid volume (by use of the liquid density) should give the micropore volume itself. The other isotherms, B, C, and D, which are likewise parallel to A in the multilayer region, correspond to successive stages in the progressive emptying of the micropores.

All the isotherms give rise to BET plots which are linear over a limited range (e.g. for isotherm E, $0{\cdot}01 < p/p^\circ < 0{\cdot}10$) so that it is possible to calculate both c and the apparent surface area A(app) from each isotherm. The increase in the value of c with the progressive removal of nonane (Table 4.6) is a mathematical consequence of the increasing contribution from the

Type I component; it does not denote any change in the heat of adsorption on the external surface, which remains constant in nature and extent throughout.

The table convincingly demonstrates how the unsuspected presence of micropores can lead to an erroneous value of the specific surface calculated from a Type II isotherm by application of the standard BET procedure. According to the foregoing analysis, the external specific surface of the solid is $114\,m^2\,g^{-1}$; the micropore volume (from the vertical separation of isotherms A and E) is $105\,mm^3\,g^{-1}$, but since the average pore width is not precisely known, the area of the micropore walls cannot be calculated. Thus the BET figure of $360\,m^2\,g^{-1}$ calculated from isotherm E represents merely an apparent and not a true surface area.

It would clearly be of interest to discover how far the nonane method can be used with adsorbates other than nitrogen. A study along these lines has been carried out by Tayyab,[27] but a discussion of his rather unexpected results is best deferred until the role of fine constrictions has been considered (p. 228). Meanwhile it may be noted that the applicability of the technique seems to be limited to adsorptives such as nitrogen or argon which have negligible solubility in solid or supercooled liquid *n*-nonane.

t and α_s-plots

The *t* and α_s-methods, the nature of which was explained in Chapter 2, may be used to arrive at a value of the micropore volume. If the surface of the solid has standard properties, the *t*-plot (or α_s-plot) corresponding to the isotherm of the nonporous powder in Fig. 4.11(*a*) will be a straight line passing through the origin (cf. curve (i) of Fig. 4.11(*b*)) and having a slope proportional to the specific surface of the powder. For the microporous powder which yields the isotherm (iii) of Fig. 4.11(*a*), the *t*-plot (or α_s-plot) will have the form of curve (iii) of Fig. 4.11(*b*); the linear branch of this curve will be parallel to curve (i), since it corresponds to the area of the outside of the particles which is identical with that of the nonporous parent particles.

The intercept on the adsorption axis of the extrapolated linear branch gives the micropore contribution,[24] and when converted to a liquid volume may be taken as equal to the micropore volume itself. It is sometimes convenient indeed to convert all the uptakes into liquid volumes (by use of the liquid density) before drawing the *t*-plots or the α_s-plots. If mesopores are present (in addition to micropores) the plots will show an upward deviation at high relative pressures corresponding to the occurrence of capillary condensation (Fig. 4.12(*b*)). The slope of the linear branch will then be proportional to the area of the mesopore walls together with the

external surface. The micropore contribution will still be given by the intercept on the adsorption axis. (The situation is more complicated if the micropore and mesopore ranges should happen to overlap.)

When using t or α_s-plots for the study of microporosity, the choice of the correct t or α_s-curve is of basic importance. There are two opposing schools of thought on this question. Sing[24] and others[28] argue that the t or α_s-curve must be based on the isotherm determined on a nonporous reference substance which is chemically similar to the material undergoing examination; but Brunauer and his associates,[29,30] and more recently Lecloux,[31] suggest the use of a reference isotherm that gives the same BET c-constant as the solid under test, independent of any similarity or otherwise in the chemical nature of the two substances. The results of an investigation carried out by Parfitt, Sing and Urwin[32] lend strong support to the first of these views.

The experimental material was a sample of rutile on which a layer of microcrystalline titania had been deposited. Isotherms of nitrogen were determined on the original material outgassed at 150°C and on samples that had been outgassed at 25°, 150° or 250°C respectively after being charged with *n*-nonane.

The corresponding α_s-plots, based on a standard α_s-curve for rutile[33] are shown in Fig. 4.14, and are parallel to one another in the multilayer region.

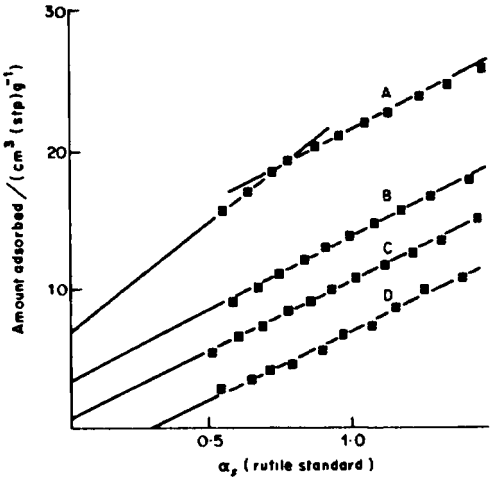

Fig. 4.14 α_s-plots for the adsorption of nitrogen at 77 K on a sample of microporous titania, before and after nonane treatment.[32] Curve (A), before nonane pre-adsorption; curves (B), (C), (D), after nonane pre-adsorption, followed by outgassing at (B) 250°C; (C) 150°C; (D) 25°C. These α_s-plots were based on the standard α_s-curve for rutile.

The intercept on the adsorption axis, and also the value of c, diminishes as the amount of retained nonane increases (Table 4.7). The very high value of c ($>10^3$) for the starting material could in principle be explained by adsorption either in micropores or on active sites such as exposed Ti^{4+} cations produced by dehydration; but, as shown in earlier work,[33] the latter kind of adsorption would result in isotherms of quite different shape, and can be ruled out. The negative intercept obtained with the 25°C-outgassed sample (Fig. 4.14 curve (D)) is a mathematical consequence of the reduced adsorption at low relative pressure which in expressed in the low c-value ($c = 13$). It is most probably accounted for by the presence of adsorbed nonane on the external surface which was not removed at 25°C but only at 150°C. (The Frenkel–Halsey–Hill exponent (p. 90) for the multilayer region of the 25°C-outgassed sample was only 1·9 as compared with 2·61 for the standard rutile, and 2·38 for the 150°C-outgassed sample).

The values of external specific surface A(ext) calculated from the slopes of the parallel branches of the α_s-plots are in close agreement (cf. Table 4.8, column 4) and the whole picture is therefore internally consistent: the four isotherms represent different degrees of filling of the micropores with nonane, leaving the external surface unaffected.

To test the Brunauer approach, it was necessary to use standard isotherms of nitrogen having the same c-constants as the experimental isotherms of Table 4.7. Since nitrogen isotherms with $c > 10^3$ have not been reported in the literature, theoretical isotherms corresponding to the c-values of Table 4.6 were calculated by Brunauer's modification[34] of Anderson's equation,[35] and standard α_s-curves were constructed from them. The corresponding α_s-plots appear in Fig. 4.15; they are no longer parallel

TABLE 4.7

Adsorption of nitrogen at 77 K on rutile before and after pre-adsorption of nonane[32]

Sample	Outgassing temperature/°C	BET parameters			Nonane content ($mg\,g^{-1}$)
		$A(N_2)$ ($m^2\,g^{-1}$)	c	Range† of p/p°	
As received	150	65·0	10^3	0·02–0·25	0
Nonane pre-adsorbed	25	19·1	13	0·10–0·35	20
Nonane pre-adsorbed	150	28·9	101	0·02–0·35	11
Nonane pre-adsorbed	250	38·2	230	0·02–0·30	6

† Range of linearity of BET plot (Equation (2.13)).

TABLE 4.8

Use of α_s-plots[32] to calculate the apparent specific surface A† and the external specific surface A(ext) of the samples of Table 4.7

Sample	Outgassing Temp./°C	α_s-curve based on rutile (Sing)		α_s-curve based on c-value (Brunauer)		
		A ($m^2 g^{-1}$)	A(ext) ($m^2 g^{-1}$)	A ($m^2 g^{-1}$)	A(ext) ($m^2 g^{-1}$)	A(BET) ($m^2 g^{-1}$)
As received	150	69·0	21·1	58·5	21·8	65·0
Nonane pre-adsorbed	25	12·6	21·9	18·6	18·6	19·1
Nonane pre-adsorbed	150	28·2	21·2	25·4	25·4	28·9
Nonane pre-adsorbed	250	37·9	22·0	32·5	32·5	38·3

† The apparent specific surface A was calculated from the BET plot.

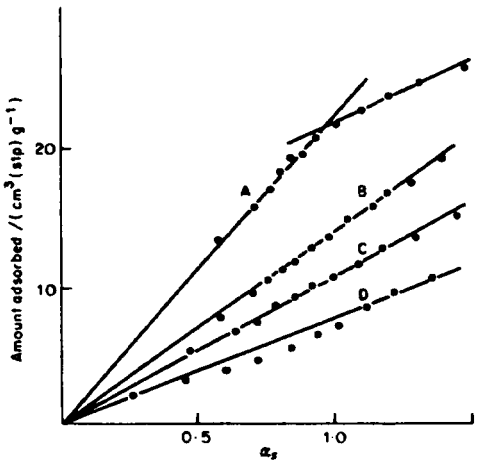

Fig. 4.15 α_s-plots for the adsorption of nitrogen on a sample of microporous titania, before and after nonane treatment. Curve (A), before nonane pre-adsorption; curves (B), (C), (D) after nonane pre-adsorption, followed by outgassing at (B) 250°; (C) 150°C; (D) 25°C. The α_s-plots were based on standard nitrogen isotherms having the same c-values as the isotherms of Table 4.7.

to one another, but on extrapolation they all pass through the origin, which would imply—in contradiction to the appearance of the electron micrographs—that the samples are not porous. Moreover, the values of specific surface calculated from the slopes of these plots (cf. Chapter 2) vary widely amongst themselves according to the amount of retained nonane (Table 4.8, columns 2 and 5), but there is no obvious reason why this should be so, nor indeed why any nonane should be retained at all by the 150°C- or 250°C-outgassed samples in the absence of micropores. Separate experiments demonstrate that nonporous rutile does not retain nonane when outgassed at 150°C or above.

In the light of these results there is little doubt that the *t*-curve (or α_s-curve) used in testing for microporosity should be based on the isotherm of a nonporous solid *chemically* similar to the substance under test and *not* on a reference isotherm which happens to have the same value of the *c*-constant.

Comparison plot[36]

The comparison plot (cf. Section 2.10) is a simple plot of the uptake per unit mass of the experimental material against that of a reference sample at the same relative pressure. It may be regarded as an alternative to the α_s-plot, in which the abscissae are actual adsorptions on a sample arbitrarily taken as a standard.

Application of the comparison plot to the detection of microporosity is illustrated by the results obtained by Lee and Newnham[37] in their study of γ-MnO_2 outgassed at a series of temperatures. The comparison plot for nitrogen adsorbed on the sample outgassed at 298 K (taking a synthetic and non-porous sample of MnOOH as reference material) was a straight line passing through the origin (Fig. 4.16, curve A) indicating the absence of microporosity; outgassing at 393 K and 423 K gave straight lines parallel with the first, but having intercepts (curves B and C) which indicate that microporosity had developed. The plot of the 493 K outgassed sample (curve D) had a slightly higher slope (pointing to a small increase in area—probably due to widening of some micropores) and an increased intercept. That the increased intercepts were indeed caused by micropore development was confirmed by the fact that, after pre-adsorption of nonane, the plot for the 493 K sample passed through the origin, just as would be expected if the micropores had become blocked by the nonane (curve E).

The Dubinin–Radushkevitch (DR) plot

The pioneer efforts of Dubinin[15] in advancing our understanding of the

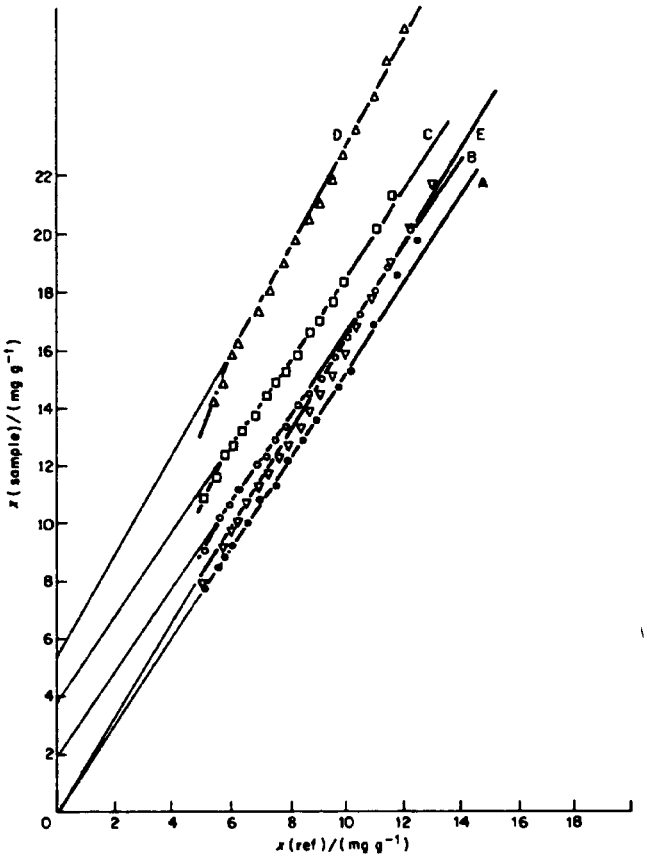

Fig. 4.16 Comparison plots[37] for a microporous sample of γ-MnO_2 after outgassing at various temperatures, also after pre-adsorption of nonane. The adsorption on the sample is plotted against the adsorption on a reference sample of synthetic MnOOH. (Courtesy Lee and Newnham.) Outgassing temperature (K): Curve A, ●, room; B, ○, 393; C, □, 443; D, △, 493 K. Curve E, pre-treated with nonane.

process of adsorption in very fine pores have already been referred to (p. 202). More than thirty years ago Dubinin, in collaboration with Radushkevich,[38] put forward an equation for the estimation of the micropore volume from the low- and medium-pressure parts of the adsorption isotherm. Their treatment represents an adaptation of the earlier Polanyi theory of adsorption,[39] an essential parameter of which is the quantity $\mathcal{A}$

defined by the expression

$$\mathscr{A} = RT\ln(p^\circ/p) \tag{4.7}$$

$\mathscr{A}$ was originally termed by Polanyi the adsorption potential, but Dubinin prefers the designation differential molar work of adsorption. Clearly, $\mathscr{A} = -\Delta G$ (where ΔG is the differential free energy of adsorption) and is, of course, quite distinct from the interaction potential of Chapter 1 and of Section 4.3.

According to Dubinin's ideas, the process involved is volume filling of the micropores rather than layer-by-layer adsorption on the pore walls. A second parameter is therefore the degree of filling of the micropores, defined by

$$\theta = W/W_0 \tag{4.8}$$

where W_0 is the total volume of the micropore system and W the volume that has been filled when the relative pressure is p/p°. A fundamental postulate is that θ is a function of $\mathscr{A}$:

$$\theta = \phi(\mathscr{A}/\beta) \tag{4.9}$$

where β is a scaling factor (similarity constant) which brings the "characteristic curves" of θ against $\mathscr{A}$ for different adsorptives into coincidence with the curve for some particular adsorbate taken as an arbitrary standard (Dubinin chose benzene): for the standard adsorbate, therefore, $\beta = 1$. An additional assumption, based on supporting evidence, is that the ratio $\mathscr{A}_1 : \mathscr{A}_2$ for any pair of adsorbates is independent of θ, from which it follows that β will be a constant characteristic of the adsorbate.

On the assumption that the pore size distribution is Gaussian, Dubinin and Radushkevich arrived at the expression

$$\theta = \exp\left[-k\left(\frac{\mathscr{A}}{\beta}\right)^2\right] \tag{4.10}$$

where k is another characteristic parameter. By combining Equations (4.7), (4.8) and (4.10) we obtain

$$W = W_0 \exp\left[-\frac{k}{\beta^2}(RT\ln p^\circ/p)^2\right] \tag{4.11}$$

or

$$\frac{W}{W_0} = \exp\left[-B\left(\frac{T}{\beta}\right)^2 \log_{10}^2(p^\circ/p)\right] \tag{4.12}$$

where

$$B = 2{\cdot}303R^2/k \tag{4.13}$$

For plotting, Equation (4.12) may be transformed into

$$\log_{10} W = \log_{10} W_0 - D \log_{10}^2 (p^\circ/p) \tag{4.14}$$

where

$$D = B\left(\frac{T}{\beta}\right)^2 \tag{4.15}$$

W is simply the amount adsorbed expressed as a liquid volume, and is given by $W = n/\rho^*$ where ρ^* is the density of the adsorbate in the micropores. At temperatures well below the critical point—near the boiling point of the adsorptive, for example—ρ^* may be taken as equal to the ordinary density ρ_L of the bulk liquid adsorptive.

Parameter k of Equation (4.10) is an expression of the breadth of the Gaussian distribution of the cumulative micropore volume W over the normalized work of adsorption $\mathcal{A}/\beta$, and is therefore determined by the pore structure. Thus B also (cf. Equation (4.13)) is characteristic of the pore structure of the adsorbent, and has accordingly been termed the structural constant of the adsorbent.[40]

According to Equation (4.14) the DR plot of $\log_{10} W$ (i.e. of $\log_{10} n/\rho_L$) against $\log_{10}^2(p^\circ/p)$ should be a straight line having an intercept equal to the total micropore volume W_0. From its slope the value of B/β^2 (cf. Equation (4.12)), but not of B and β separately, should be obtainable.

For a substantial number of systems the DR plot is indeed a good straight line. In Fig. 4.17, for example, the linearity of the plots extends over a very

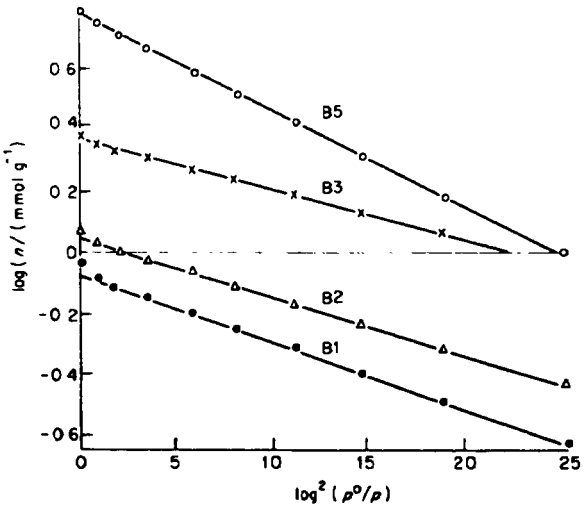

Fig. 4.17 Plot of $\log_{10}(n/(\text{mmol g}^{-1})$ against $\log_{10}^2 (p^\circ/p)$ for the adsorption of benzene at 20°C on a series of progressively activated carbons prepared from sucrose.[41] (Courtesy Dubinin.)

wide range of relative pressures—of some ten thousand-fold in each case—and in Fig. 4.18 the range of reasonable linearity is also extensive. The persistence of linearity up to relative pressures close to unity (as in Fig. 4.17), i.e. into the plateau region of the isotherm, is puzzling: in this region the process is presumably no longer one of micropore filling but rather adsorption on the (small) external surface and in the few mesopores which may be present. It will further be noted that in Fig. 4.18, plots B, C and D refer to samples in which micropores have been generated by thermal decomposition, whereas the points on curve A were obtained with the nonporous starting material (circles) or with a microporous sample in which the pores had been blocked with *n*-nonane. It is evident that straight line plots can be obtained with a material which is free of micropores. We therefore encounter the anomaly that one and the same equation appears to govern quite different processes.

Frequently, however, the DR plot deviates from linearity, and in a number of ways. Sometimes the plot is convex to the $\log^2 (p^\circ/p)$ axis, as in Fig. 4.19(*a*), and sometimes concave, as in Fig. 4.19(*b*). The question then arises as to whether one should extropolate from the low-pressure,

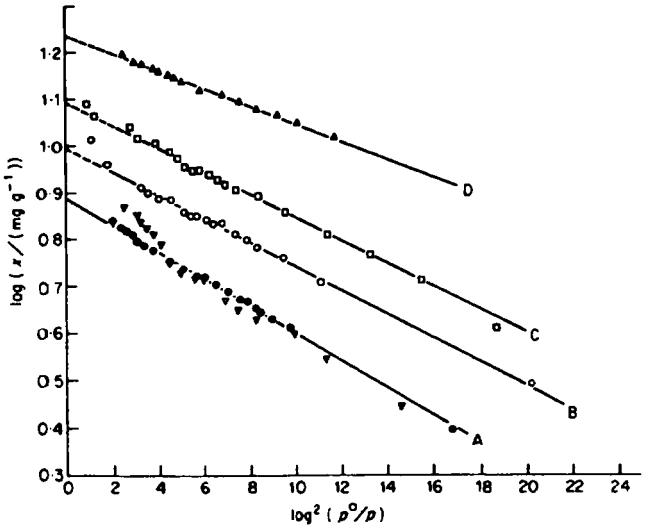

Fig. 4.18 Plot of $\log (x/(\text{mg g}^{-1}))$ against $\log^2 (p^\circ/p)$ for the adsorption of nitrogen at 77 K on the samples of manganese dioxide referred to in Fig. 4.16. Outgassing temperature: (A) room: (B) 393 K; (C) 443 K; (D) 493 K. For the points denoted by ▽ in Curve A, a sample was outgassed at 493 K and charged with nonane before the final outgassing at room temperature.[37] (Courtesy Lee and Newnham.)

reasonably linear part of the isotherm, or merely take the saturation uptake as giving the micropore volume.

Occasionally the DR plot falls into two straight lines (cf. Fig. 4.20), and the question again arises as to the significance of the different values of the uptake at $p^\circ/p = 1$, derived by extrapolation of the respective branches. Quite often, the DR plot displays an upward turn as saturation pressure is approached (Fig. 4.18 and 4.21), a feature which can readily be understood in terms of multilayer adsorption and capillary condensation in mesopores.

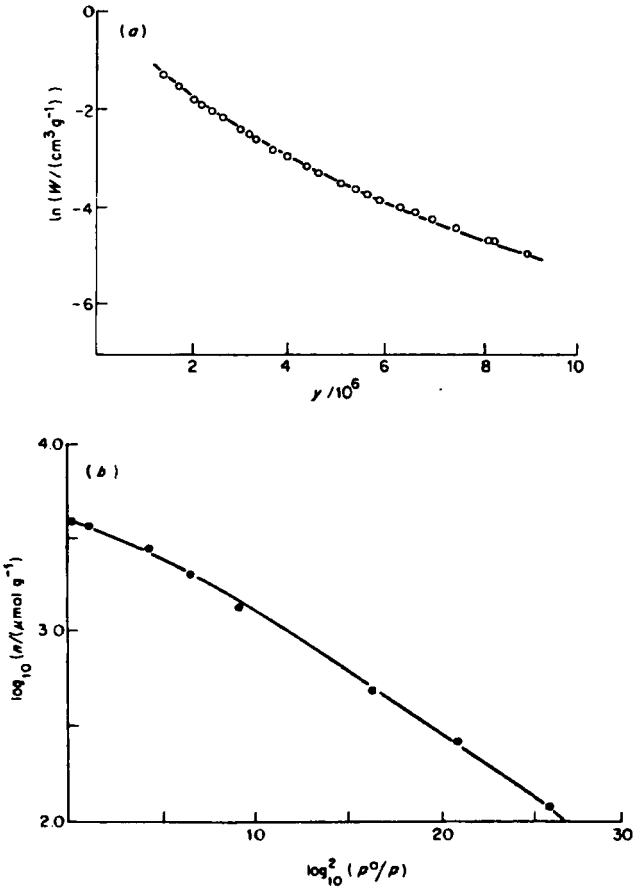

Fig. 4.19 (*a*) Plot of ln $(W/(\text{cm}^3\ \text{g}^{-1}))$ against $(T/\beta)^2 \log^2 (p^\circ/p)$ $(= y)$ for adsorption of nitrous oxide on an activated carbon at 298 K. The amount W adsorbed is expressed as volume of liquid. β is the similarity constant of N_2O (cf. Equation 4.12). (After Stoeckli *et al.*[42]) (*b*) DR plot for sulphur dioxide on an activated sugar charcoal.[43]

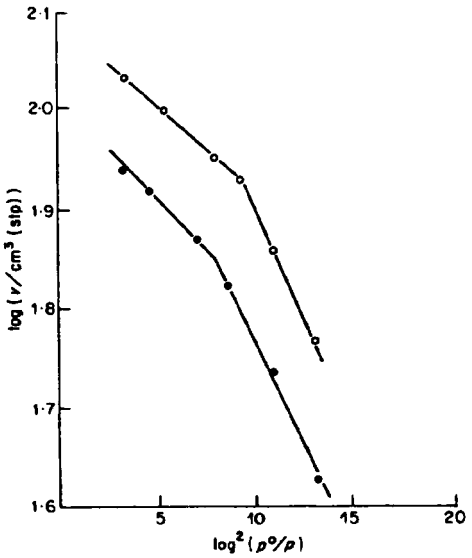

Fig. 4.20 DR plots for carbon dioxide adsorbed at 293 K on Linde molecular sieves. O, powder 5A; ●, powder 4A. (Reduced from the original diagram of Lamond and Marsh.[44])

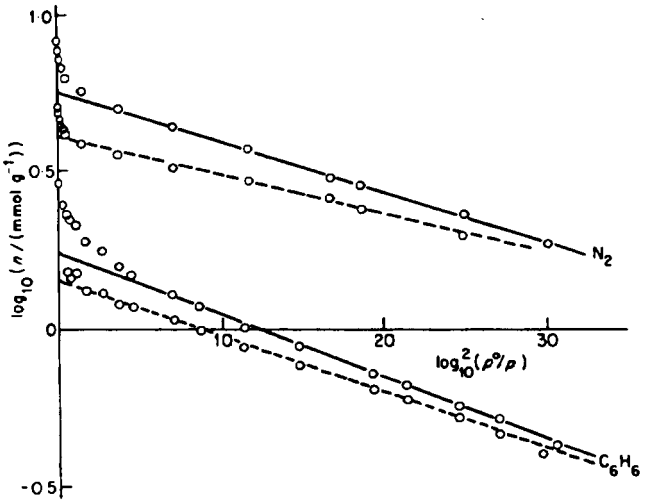

Fig. 4.21 DR plots for the adsorption of benzene at 20°C and nitrogen at −195°C on carbon AYF (continuous lines). The dashed lines are the DR plots corrected for adsorption in mesopores. (Courtesy Dubinin.[45])

The extrapolated value of micropore volume (cf. dashed lines in Fig. 4.21) would then need to be corrected for mesopore adsorption which would have contributed to the uptake at lower relative pressures.

A major difficulty in testing the validity of predictions from the DR equation is that independent estimates of the relevant parameters—the total micropore volume and the pore size distribution—are so often lacking. However, Marsh and Rand[46] compared the extrapolated value for W_0 from DR plots of CO_2 on a series of activated carbons, with the micropore volume estimated by the pre-adsorption of nonane. They found that, except in one case, the value from the DR plot was below, often much below, the nonane figure (Table 4.9).

TABLE 4.9

Micropore volume W_0 in activated carbons[46]

Carbon	Burn-off (%)	Micropore volume/($cm^3\,g^{-1}$)	
		DR plot (carbon dioxide at 273 K)	Nitrogen displaced by nonane
Polyfurfuryl alcohol	0	0·15	0·0
	21	0·25	0·28
	51	0·31	0·42
	71	0·39	0·58
Polyvinylidene chloride	0	0·27	0·38
	21	0·40	0·94
	37	0·54	0·64
	56	0·54	0·72
	82	0·27	0·81

Density of adsorbed phase/($g\,cm^{-3}$): nonane, 0·72; nitrogen, 0·81; carbon dioxide, 1·10.

In the attempt to extend the scope of the DR treatment, Dubinin and Astakhov[47] have put forward a more general equation,

$$\theta = \exp[-(\mathscr{A}/\mathscr{E})^m] \tag{4.16}$$

which is based on a Weibull[48] rather than a Gaussian distribution of pore sizes; m is a small integer, and $\mathscr{E}$ is a characteristic free energy of adsorption, equivalent to the value of $\mathscr{A}$ when $\theta = 1/e = 0{\cdot}368$. Thus, by reference to Equation (4.7) we have

$$\theta = \exp\left[-\left(\frac{RT}{\mathscr{E}}\right)^m \ln^m(p^\circ/p)\right] \tag{4.17}$$

or

$$\log_{10} W = \log_{10} W_0 - D' \log_{10}^m (p^\circ/p) \tag{4.18}$$

where

$$D' = 2{\cdot}303^{m-1}\left(\frac{RT}{\mathscr{E}}\right)^m$$

The original DR equation is thus a special case of the Dubinin–Astakhov equation, with $m = 2$; parameter $\mathscr{E}$ of Equation (4.18) for $m = 2$ is related to the structural constant B of the DR treatment through the simple expression

$$B = (2{\cdot}303R/\mathscr{E})^2$$

An example from Dubinin's paper[17] illustrates the application of the new equation. For benzene at 293 K, the plot of Equation (4.18) with $m = 2$ gave a line concave to the $\log^2(p^\circ/p)$ axis. A revised value of m was therefore required, and was obtained as follows. A provisional value of W_0 ($= 408\ \text{mm}^3\ \text{g}^{-1}$) was estimated from the plateau of the isotherm; the relative pressure $(p/p^\circ)_x$ corresponding to $W/W_0 = 0{\cdot}368$ was then read off, and a first value of $\mathscr{E}$ calculated from

$$\mathscr{E} = 2{\cdot}303RT\log_{10}(p^\circ/p)_x$$

(cf. Equation (4.7)). A single point on the isotherm, W_y, $(p/p^\circ)_y$ say, was selected (in the range $0{\cdot}7 < \theta < 0{\cdot}8$) and a provisional value of m was obtained by means of the equation (cf. Equation (4.14))

$$m = \frac{\log_{10}(2{\cdot}303\log_{10} W_0/W_y)}{\log_{10}(\mathscr{A}_y/\mathscr{E})} \tag{4.19}$$

after calculating $\mathscr{A}_y$ by Equation (4.7). This gave $m = 2{\cdot}96$. The value $m = 3$ was therefore adopted, and $\log W$ plotted against $\log^3(p^\circ p)$ when a reasonably good straight line resulted, whence refined values of $W_0 = 399\ \text{mm}^2\ \text{g}^{-1}$ and $\mathscr{E} = 6{\cdot}61\ \text{kcal mol}^{-1}$ were calculated. Similar results were obtained with cyclohexane, again with $m = 3$ and $\mathscr{E} = 6{\cdot}93\ \text{kcal mol}^{-1}$.

For a second active carbon, AG, the DR plot was convex to the $\log^2_{10}(p^\circ/p)$ axis. This carbon was believed from X-ray results to have a wider distribution of pores. It was found that the isotherms of both benzene and cyclohexane could be interpreted by postulating that the micropore system consisted of two sub-systems each with its own W_0 and $\mathscr{E}$, and with $m = 2$:

$$n = W_{0,1}\rho\exp[-(\mathscr{A}/\mathscr{E}_1)^2] - W_{0,2}\rho\exp[-(\mathscr{A}/\mathscr{E}_2)^2] \tag{4.20}$$

The two adsorbates gave reasonable agreement between the corresponding values of W_0 and of $\mathscr{E}$ for each structure (Table 4.10), and the considerable difference between the values of $\mathscr{E}_1$ and $\mathscr{E}_2$ respectively indicated that the

TABLE 4.10

Micropore structure parameters W_0 and $\mathcal{E}$ of the active carbon AG.[17] (Standard vapour: benzene)

Vapour	First structure		Second structure		
	$W_{0,1}$ / $cm^3\,g^{-1}$	$\mathcal{E}_1$ / kcal mol^{-1}	$W_{0,2}$ / $cm^3\,g^{-1}$	$\mathcal{E}_2$ / kcal mol^{-1}	$W_0 = W_{0,1} + W_{0,2}$ / $cm^3\,g^{-1}$
C_6H_6	0·219	5·49	0·221	3·03	0·440
C_6H_{12}	0·181	5·10	0·232	3·03	0·443

contribution from the second structure is insignificant until high relative pressures are reached. Another generalization of the DR equation has been proposed by Stoeckli,[42,49] who concludes that when a wide range of temperatures is taken into account the original version (4.12) holds only for carbons which have a narrow range of micropore size. For strongly activated carbons with a heterogeneous collection of micropores, the overall isotherm is the sum of the contributions from individual pore groups, each group being characterized by its own W_0 and B_j and obeying the DR equation. The overall isotherm is thus:

$$W = \sum_j W_{0,j} \exp[-B_j(T/\beta)^2 \log_{10}^2(p^\circ/p)] \tag{4.21}$$

For a continuous distribution, summation may be replaced by integration; and by assuming a Gaussian distribution of size, Stoeckli arrives at a somewhat complicated expression (not given here) which enables the total micropore volume W_0, a structural constant B_0 and the spread Δ of size distribution to be obtained from the isotherm. He suggests that B_0 may be related to the radius of gyration $\bar{R}_g$ of the micropores by the expression

$$\bar{R}_g = 62 \times 10^6 B_0 \tag{4.22}$$

These procedures proposed by Dubinin and by Stoeckli[50] are, as yet, in the pioneer stage. Before they can be regarded as established as a means of evaluating pore size distribution, a wide-ranging study is needed, involving model micropore systems contained in a variety of chemical substances. The relationship between the structural constant B and the actual dimensions of the micropores, together with their distribution, would have to be demonstrated. The micropore volume would need to be evaluated independently from the known structure of the solid, or by the nonane preadsorption method, or with the aid of a range of molecular probes.

The DRK equation

In 1959 Kaganer[51] suggested that the DR equation, in modified form, could be used for surface area determination. Kaganer retained the principle of the characteristic curve and the Gaussian distribution of adsorption potential (p. 220), but replaced the concept of micropore filling by that of surface coverage. The fractional filling (W/W_0) of the DR equation was replaced by the surface coverage (n/n_m), but the new equation—often termed the DRK equation—has the same form as the original DR equation and reads

$$\log_{10}(n/n_m) = -D \log^2_{10}(p^\circ/p) \tag{4.23}$$

where n is the amount adsorbed at relative pressure p/p° and n_m is the monolayer capacity, D being a characteristic constant.

According to Equation (4.23), the plot of $\log n$ against $\log^2(p^\circ/p)$ should be a straight line having an intercept $\log n_m$ on the $\log n$ axis.

The results of a comparison between values of n_m estimated by the DRK and BET methods present a confused picture.[52-55] In a number of investigations linear DRK plots have been obtained over restricted ranges of the isotherm, and in some cases reasonable agreement has been reported between the DRK and BET values. Kiselev and his co-workers[56] have pointed out, however, that since the DR and the DRK equations do not reduce to Henry's Law ($n = \text{const} \times p$) as $n \to 0$, they are not readily susceptible of statistical-thermodynamic treatment. Moreover, it is not easy to see how exactly the same form of equation can apply to two quite diverse processes involving entirely different mechanisms. We are obliged to conclude that the significance of the DRK plot is obscure, and its validity for surface area estimation very doubtful.

4.5 Constrictions in micropores

Adsorption is invariably an exothermic process, so that, provided equilibrium has been established, the amount adsorbed at a given relative pressure must diminish as the temperature increases. It not infrequently happens, however, that the isotherm at a given temperature T_2 actually lies *above* the isotherm for a lower temperature T_1. Anomalous behaviour of this kind is characteristic of a system which is not in equilibrium, and represents the combined effects of temperature on the rate of approach to equilibrium and on the position of equilibrium itself. It points to a process which is "activated" in the reaction-kinetic sense and which therefore occurs more rapidly as temperature is increased.

According to the hypothesis advanced by Maggs[57] and independently by

Zwietering and van Krevelen,[58] this activated process is the diffusion of adsorbate molecules through very narrow constrictions into cavities beyond. When the width of a constriction is very close to the diameter of the adsorbate molecules, the molecules will encounter an energy barrier to their passage through the constriction, so that the rate of entry into the cavity will have a positive temperature coefficient. The number of molecules actually entering the cavity during the period of a measurement—and thus the amount adsorbed—will increase with rise in temperature. At sufficiently high temperatures the rate will become fast enough for equilibrium to be attained within the time of the measurement, and the measured uptake will then diminish with rising temperature in the usual way.

Some of the early work on the subject was carried out on coal, and the results illustrate the way in which the "activated entry" effect can complicate the interpretation of Type I isotherms. Table 4.11 gives the uptake (as volume of liquid) of nitrogen at 77 K and 90 K, and of butane at the much higher temperature of 273 K, on a number of coal samples at a pressure slightly below saturation. The increase in uptake with increased temperature is striking, and it is particularly interesting that the adsorption of butane greatly exceeds that of nitrogen, despite its larger molecular size.

Wynne-Jones and Marsh[60] found somewhat similar results with a number of carbons made by pyrolysis of eight organic polymers at a series of temperatures. The isotherms of N_2 at 77 K and of CO_2 at 195 K were measured, and the apparent surface area calculated by the usual BET procedure. (Owing to the microporous nature of the solids, these figures for area will be roughly proportional to the uptake at saturation and therefore

TABLE 4.11

The uptake, expressed as a volume v_s of liquid, of nitrogen and of butane by a number of coal samples, at a pressure slightly below saturation on the Type I isotherms[59]

		Value of $v_s/(mm^3\,g^{-1})$ from		
Sample	%C	N_2 at 77 K	N_2 at 90 K	C_4H_{10} at 273 K
1	94·0	1·7	4·7	15·7
2	91·5	~0	~0	1·0
3	88·5	~0	~0	1·5
4	87·5	0·1	0·7	3·0
5	85·0	0·9	2·3	15·9
6	82·5	7·4	7·7	29·8
7	80·0	38·0	52·1	87·7
8	78·5	43·3	57·8	104·7

to the micropore volume, whatever their significance, if any, in terms of actual surface area.) In all cases, the nitrogen isotherms led to lower, sometimes much lower, values of the apparent area than did the carbon dioxide isotherms (cf. Fig. 4.22). The minimum dimensions[61] of the two adsorptives are not very different (for CO_2, 2·8 Å; for N_2, 3·0 Å), and consequently by far the most important factor in producing the greater uptake of CO_2 is the higher temperature of measurement.

In the experiments of Fig. 4.23 the same adsorbate (*n*-butane) was used at all three temperatures, the adsorbent being a carbon rendered microporous by partial "burn-off" (0·27%) in oxygen. The increase in uptake with increase in temperature is very marked, and the extensive hysteresis provides supporting evidence for the presence of an activated process. In Table 4.12, the results for other degrees of burn-off are given, and the adsorbates included nitrogen and carbon dioxide in addition to butane. The uptake v_s of butane at saturation again showed marked dependence on temperature with all three samples of carbon, but the proportionate increase varied somewhat between the samples, indicating that there is a distribution of constriction width. The value of v_s for CO_2 at 196 K is higher than for butane at the same temperature, as would be expected from the larger size of butane (minimum dimension ~4·9 Å); it is also higher than for nitrogen at 77 K, as a consequence of the difference in the temperatures. Pore widths in the range 3–5 Å seem to be indicated.

Further information as to the width of constrictions can be obtained from measurement of the heat of immersion of the solid in a range of liquids

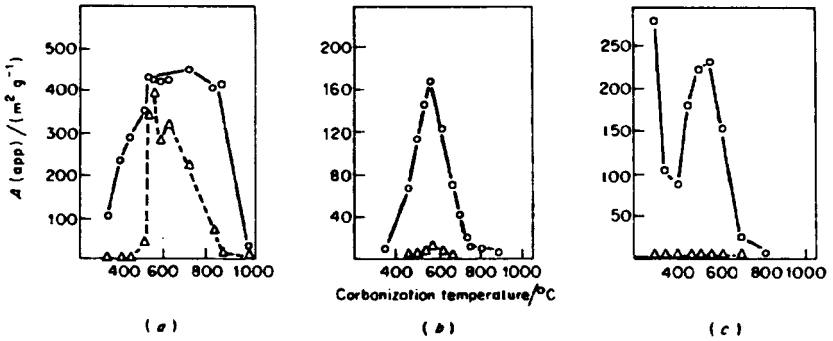

Fig. 4.22 Apparent specific surface A(app) of carbons[60] obtained from the decomposition of polymers, plotted against the carbonization temperature. (*a*) Polyfurfuryl carbons; (*b*) dibenzanthrone carbons; (*c*) polyvinylchloride carbons. O, A(app) estimated from CO_2 isotherm at 195 K ($a_m(CO_2)$ = 17·0 Å^2); Δ, A(app) estimated from N_2 isotherm at 77 K ($a_m(N_2)$ = 16·2 Å^2). (Courtesy Marsh and Wynne Jones.)

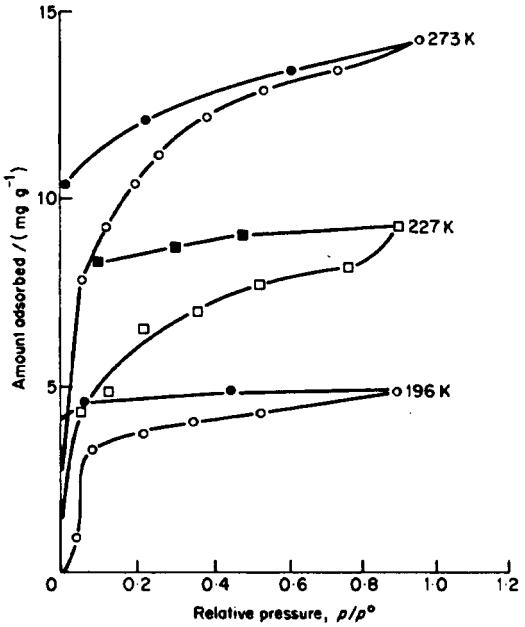

Fig. 4.23 Adsorption isotherms of butane vapour at different temperatures[62] on a sample of carbon (prepared by heating a mixture of coke and pitch at 600°C), burnt off by 0.27%.

TABLE 4.12

Values of the uptake at saturation, of butane, carbon dioxide and nitrogen, by a sample of carbon, expressed as a volume of liquid v_s. The carbon had been "burnt off" to different extents by heating in oxygen at 500°C on a sorption balance[62]

	Values of $v_s/(mm^3\ g^{-1})$				
			from C_4H_{10}		
% Burn-off	from N_2 at 78 K	from CO_2 at 196 K	at 196 K	at 227 K	at 273 K
0	5·5	21	2·4	8	21
0·27	–	22	8·5	15	24
0·42	11·7	22·5	7·2	14·5	24
2·77	22·2	24·5	–	–	17

differing in molecular size. The method is illustrated by the work of Barton, Beswick and Harrison[63] who studied two microporous carbons prepared from Saran polymer A by pyrolysis and by prolonged treatment with KOH respectively. The results for the pyrolysed material are shown in Fig. 4.24 where Points 3, 4, 5 and 6 correspond to immersing liquids which contain respectively zero, one, two and three branch methyl groups. The heat of immersion falls steeply from Point 3 to Point 6, even though the molar volume has increased only slightly. These results show that it is the minimum dimension of the adsorbate molecule, and not the average dimension given by the molar volume (cf. Equation (2.26)), which determines how much surface area will be contacted. Since the heat of immersion in the trimethyl derivative (Point 6) is quite small, it follows that the majority of pores are reached through entrances narrower than the width of three methyl groups—say ~6·2 Å (the kinetic diameter of neopentane). That the heat of immersion in benzene (Point 2) is almost the

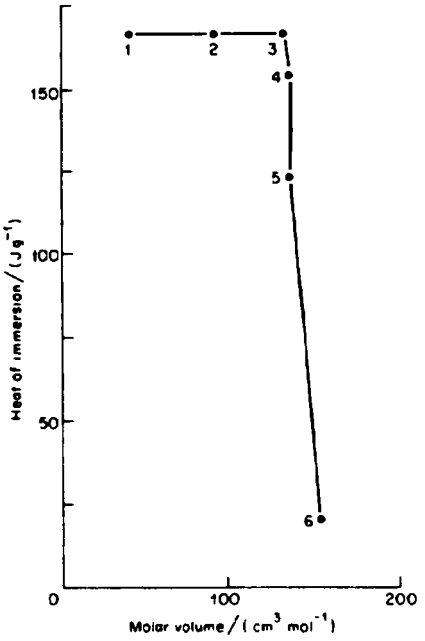

Fig. 4.24 Heat of immersion of a carbon (prepared by pyrolysis of Saran Polymer A) in different liquids at 300 K. The liquids for points 1–6 were: (1) methanol; (2) benzene; (3) n-hexane; (4) 3-methyl benzene; (5) 2,2-dimethyl butane; (6) 2,2,4-trimethyl pentane. The abscissae represent the molar volumes of the liquids. (Redrawn from the original diagram of Barton, Beswick and Harrison.[63])

same as in methanol (Point 1) suggests that the pores are slit-shaped, since the thickness of the "flat" benzene molecule, 3·5 Å, is approximately the same as the diameter of a methyl group.

4.6 Low-pressure hysteresis

It has already been noted (p. 195) that some Type I isotherms exhibit a kind of hysteresis which persists to the lowest pressures (cf. Fig. 4.2); some adsorbate is retained even after prolonged outgassing ($\sim 10^{-4}$ Torr) at the temperature of the isotherm determination, and can only be removed if the pumping is carried out at an elevated temperature. Further examples are shown in Fig. 4.25, as well as in Fig. 4.23.

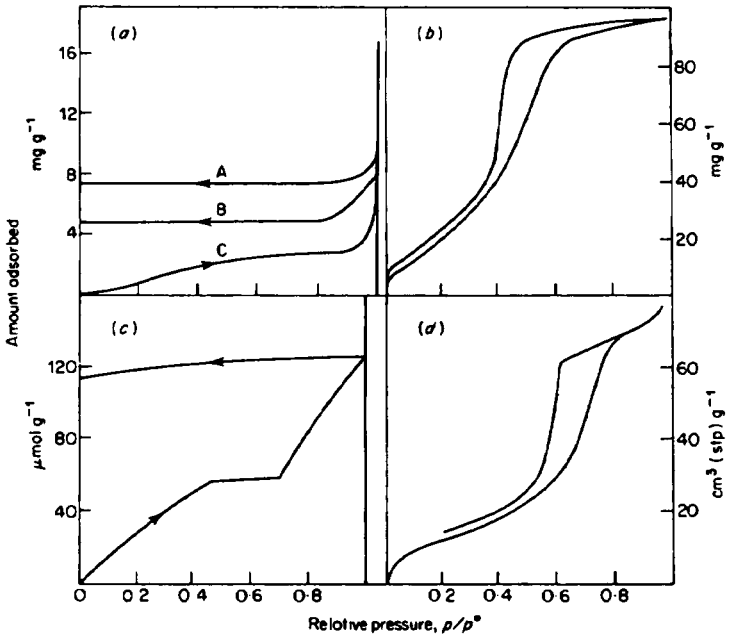

Fig. 4.25 Adsorption isotherms showing low-pressure hysteresis. (*a*) Carbon tetrachloride at 20°C on unactivated polyacrylonitrile carbon: Curves A and B are the desorption branches of the isotherms of the sample after heat treatment at 900°C and 2700°C respectively; Curve C is the common adsorption branch;[64] (*b*) water at 22°C on stannic oxide gel heated to 300°C;[66] (*c*) krypton at 77·4 K on exfoliated graphite;[65] (*d*) ethyl chloride at 6°C on porous glass.[67] (Redrawn from the diagrams in the original papers, with omission of experimental points.)

Low-pressure hysteresis is not confined to Type I isotherms, however, and is frequently superimposed on the conventional hysteresis loop of the Type IV isotherm. In the region below the shoulder of the hysteresis loop the desorption branch runs parallel to the adsorption curve, as in Fig. 4.26, and in Fig. 4.25(*b*) and (*d*). It is usually found that the low-pressure hysteresis does not appear unless the desorption run commences from a relative pressure which is above some threshold value. In the study of butane adsorbed on powdered graphite referred to in Fig. 3.23, for example, the isotherm was reversible so long as the relative pressure was confined to the branch below the shoulder F.

The explanation of low-pressure hysteresis proposed by Arnell and McDermott[69] some thirty years ago was formulated in terms of the swelling of the particles which accompanies adsorption. The swelling distorts the structure, for example by prising apart weak junctions between primary

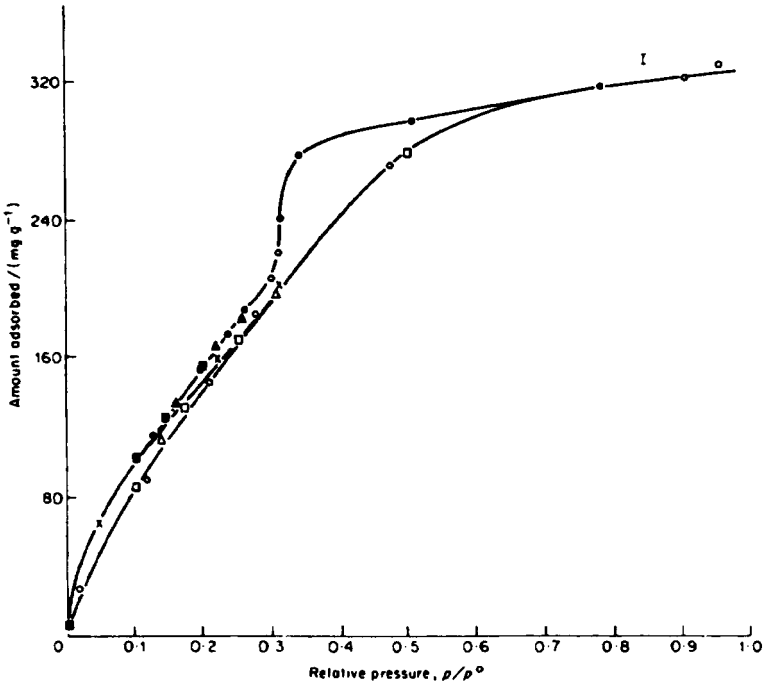

Fig. 4.26 Low-pressure hysteresis in the adsorption isotherm of water at 298 K on a partially dehydroxylated silica gel.[68] ○, first adsorption run (outgassing at 200°C); ●, first desorption; △, second adsorption run (outgassing at 200°C); ▲, second desorption (after reaching $p/p^\circ = 0{\cdot}31$); ×, third adsorption run (outgassing at 25°C).

particles, and opens up cavities which were previously inaccessible to adsorbate molecules. Since the distortion is not perfectly elastic, some molecules become trapped and can escape only very slowly, or possibly not at all, during the desorption run unless the temperature is raised.

The idea has been developed in a comprehensive paper by Everett and his co-workers[70] based on the work of the Bristol school extending over fifteen years or more, with various forms of active carbon as adsorbent. In one study, for example, isotherms of benzene were measured at a series of temperatures on the same sample of carbon (prepared by thermal decomposition of a compacted polyvinylchloride) without intermediate removal of the sample from the apparatus; outgassing was carried out at the end of the run at the isotherm temperature. In Run 1 at 25°C, hysteresis was absent (Table 4.13), but in Run 2 at 35°C some hysteresis was present and in Run 3 at 45°C, even more. A repeat run (Run 5) at 25°C (after Run 4 at 40°C) unlike the original run at this temperature, now displayed hysteresis, some of which still remained after storage for two months and annealing at the elevated temperature of 305°C (Run 7). Thus, the low-pressure hysteresis was associated with a distortion of the structure of the adsorbent which is difficult to reverse and leads to an increase in the saturation uptake. The mechanism proposed by Everett is an irreversible intercalation within pores of molecular dimensions. It is supported by the fact that, with a sample pelleted at 25 000 lb in^{-2}, hysteresis appeared at 25°C in isotherms of *n*-hexane and cyclohexane, but not of benzene which has a slightly thinner molecule; but a sample pelleted at the much higher pressure of 125 000 lb in^{-2}, which would tend to narrow down the crevices, gave hysteresis even with benzene.

TABLE 4.13

Adsorption of benzene by carbon 8P. Height (h) of hysteresis loop at $p/p^* = 0{\cdot}25$, and uptake at saturation (w_s). Runs were carried out in the order given†

Run	T/°C	h(%)	w_s(%)
1	25	0·00	35·5
2	35	0·12	35·5
3	45	0·50	36·3
4	40	0·27	38·2
5	25	0·42	38·2
	Store *in vacuo* for 2 months at room temp.		
6	25	0·37	36·5
	Anneal at 305°C for 80 hr		
7	25	0·10	36·15

† Reduced from the data of Everett and co-workers.[70]

For the experiments referred to in Fig. 4.25(*a*), McEnaney was able to show,[64] on reasonable assumptions, that the stress induced by adsorption swelling should be sufficient to fracture the carbon over short distances. A "memory" effect in the carbon network would lead to trapping of some adsorbed carbon tetrachloride molecules during the desorption run.

The swelling of the adsorbent can be directly demonstrated as in the experiments of Fig. 4.27 where the solid was a compact made from coal powder and the adsorbate was *n*-butane. (Closely similar results were obtained with ethyl chloride.) Simultaneous measurements of linear expansion, amount adsorbed and electrical conductivity were made, and as is seen the three resultant isotherms are very similar: the hysteresis in adsorption in Fig. 4.27(*a*), is associated with a corresponding hysteresis in swelling in (*b*) and in electrical conductivity in (*c*). The decrease in conductivity in (*c*) clearly points to an irreversible opening-up of interparticulate junctions; this would produce narrow gaps which would function as constrictions in micropores and would thus lead to adsorption hysteresis (cf. Section 4.5).

A lamellar solid of especial interest is montmorillonite, a clay mineral.

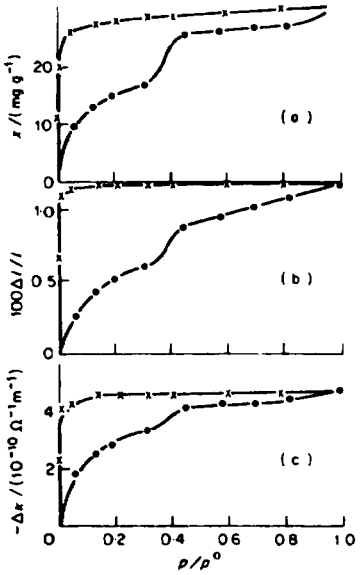

Fig. 4.27 Swelling and low-pressure hysteresis in the adsorption of n-butane on compacts of coal at 273 K.[71] The following are plotted against the relative pressure: (*a*) the amount adsorbed; (*b*) the percentage increase on length; (*c*) the decrease $-\Delta\kappa$ in electrical conductivity. The curves for ethyl chloride were very similar to the above curves.

Extensive intercalation of polar molecules takes place in this substance in an irreversible manner, and marked hysteresis results (Fig. 4.28). The driving force is thought to be the interaction between the polar molecules and the exchange cations present in the montmorillonitic sheets, since non-polar molecules give rise to a simple Type B hysteresis loop with no low-pressure hysteresis.

The degree to which a solid expands during adsorption depends on the overall rigidity of the sample; and, with an agglomerated sample (p. 21) where the rigidity is high, the swelling will be of relatively minor importance and the major cause of low-pressure hysteresis will be the activated passage of molecules through pre-existing constrictions into wider cavities, in the manner outlined in Section 4.5. The hysteresis curves of Fig. 4.23, for the adsorption of butane on active carbon, provide examples.

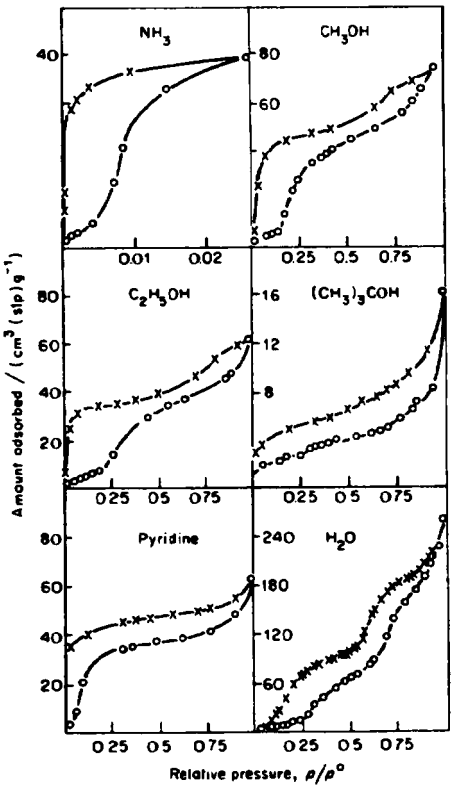

Fig. 4.28 Isotherms for polar adsorbates on natural montmorillonite[72] at 323 K. (Courtesy Barrer.) O, adsorption; ×, desorption.

Water is an adsorbate which is particularly prone to show penetration effects, on account of its small molecular size, its ability to rehydrate or rehydroxylate various oxides, and its capability of dissolving many ionic solids. These factors are responsible for some notable divergences in behaviour between water and conventional adsorptives such as nitrogen. Thus, in an investigation of the properties of a series of chromia gels prepared in several ways, Sing and his collaborators determined the isotherms of water and nitrogen. The water isotherms showed hysteresis throughout the whole range, down to the lowest pressures, whereas the nitrogen isotherms were free of hysteresis. The figures for the $A(N_2)$ and $A(H_2O)$ calculated by the usual BET procedure with $a_m(N_2) = 16{\cdot}2\,Å^2$ and $a_m(H_2O) = 10{\cdot}6\,Å^2$, are given in Table 4.14. For most samples $A(H_2O)$

TABLE 4.14

Adsorption of nitrogen at 77 K and of water at 293 K[73]

Gel	$A(N_2)$† $m^2\,g^{-1}$	$A(H_2O)$† $m^2\,g^{-1}$	$v_s(N_2)$‡ $cm^3\,g^{-1}$	$v_s(H_2O)$‡ $cm^3\,g^{-1}$	Isotherm type N_2	Isotherm type H_2O
A	150	174	–	–	II	II
B	49	172	–	–	II	II
C	1	267	0	0·096		I
D	1	232	0	0·089		I
E	165	94	0·145	0·146	IV	IV

† A = BET specific surface.

‡ v_s = uptake at saturation, calculated as volume of liquid (Gurvitsch volume).

was higher than $A(N_2)$ but the discrepancy is particularly striking in the case of gels C and D. It is evident that water can penetrate into pores (or pore openings) which are too narrow to admit nitrogen molecules; the driving force for the swelling—which would promote further penetration—was believed to be the partial rehydration of the Cr^{3+} ion by the tendency to complete the coordination sphere.[73]

The penetration of water along cleavage cracks of ball-milled calcite—where incipient dissolution probably played some part—was studied by Gregg and Gammage.[74] A high degree of hysteresis extending over the whole range of pressures was found, especially with samples which had been subjected to prolonged milling (Fig. 4.29).

Rehydroxylation as a cause of low-pressure hysteresis is exemplified in the isotherm of Fig. 4.26, where the adsorbent was a partially dehydroxylated

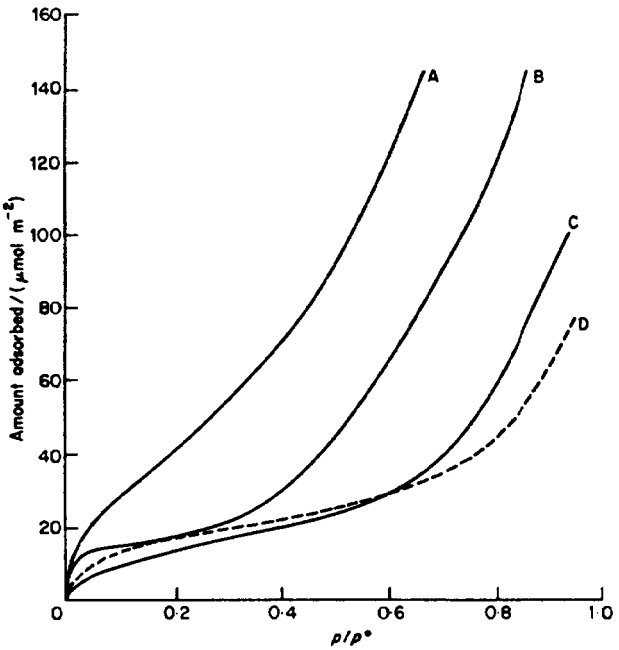

Fig. 4.29 Adsorption isotherms of water vapour on calcite, after being ball-milled for different periods (A, B, C) and on precipitated calcium carbonate (D). Period of milling: (A) 1000 h; (B) 150 h; (C) 22 h; outgassing temperature 25°C. Isotherms A, B and C (but not D) all showed extensive low-pressure hysteresis, but for clarity the desorption branch is omitted. The amount adsorbed is referred to 1 m^2 of BET-nitrogen area.[74]

silica.[68] If the adsorbent is a fully dehydroxylated silica, the hysteresis produced by the rehydroxylation which takes place in the course of the isotherm determination is much intensified, and will be referred to in more detail in Chapter 5.

4.7 Constrictions and the nonane pre-adsorption technique

As remarked on p. 214, the validity of the nonane pre-adsorption method when adsorptives other than nitrogen are employed for determination of the isotherms, has been examined by Tayyab.[27] Two organic adsorptives, *n*-hexane and carbon tetrachloride, which could be used at or near room temperature, were selected; and the adsorbents were the ammonium salts of

the three heteropolyacids, silicomolybdic, phosphomolybdic and phosphotungstic, which by the nonane-nitrogen technique had been shown to be highly microporous. A gravimetric technique[75] was adopted for measurement of the isotherms, and for ease of comparison the isotherms were plotted with the uptake expressed as the volume of liquid.

In some respects the results obtained were as expected and in others were quite unexpected. Thus, the volume adsorbed near saturation (the "Gurvitsch" volume) was consistently lower for the organic adsorptives than for nitrogen, a finding plausibly explained as a molecular sieve effect since the organic substances have larger molecules than nitrogen. After pre-adsorption of nonane, on the other hand, the isotherms of both carbon tetrachloride and hexane were considerably *higher* than the corresponding isotherms of nitrogen. Typical results (selected from 28 individual isotherms) are shown in Figs. 4.30–4.32. The explanation offered is that the nonane is blocking the entrance to cavities, rather like a stopper in the neck of a bottle, and that hexane and carbon tetrachloride are able to diffuse slowly through the stopper to reach the cavity beyond. That such diffusion can occur with the organic adsorptives but not with nitrogen may be attributed to the much higher temperature of measurement and also to the greater solubility of hexane and carbon tetrachloride in *n*-nonane. An additional factor promoting diffusion is that at the temperature of

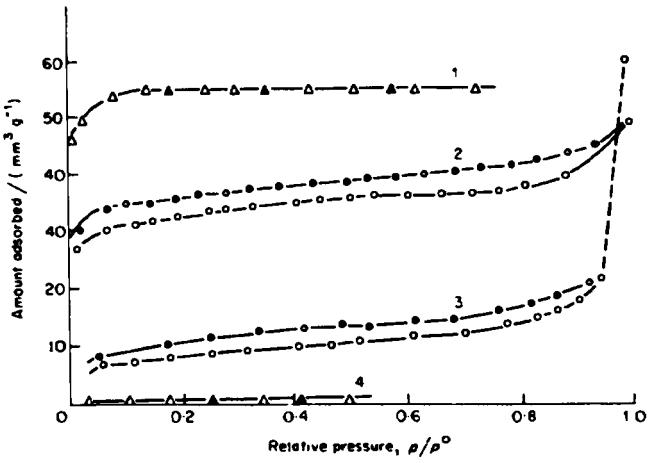

Fig. 4.30 Adsorption isotherms on ammonium silicomolybdate powder.[27] (1), (4), nitrogen at 77 K; (2), (3), *n*-hexane at 298 K. Isotherms 1 and 2 were measured before, and 3 and 4 after, pre-adsorption of n-nonane. Open symbols, adsorption; solid symbols, desorption. (Adsorption is expressed in mm^3 (liquid.)

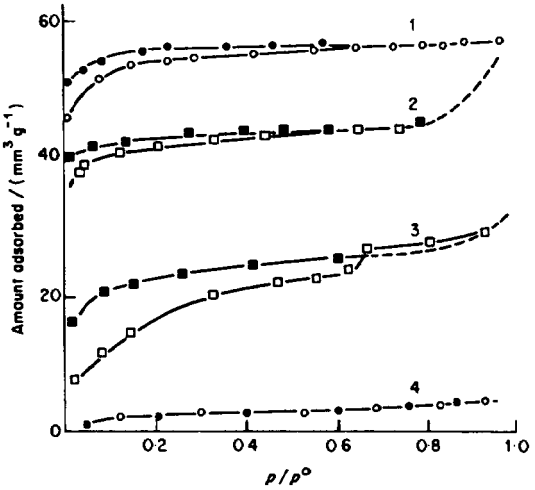

Fig. 4.31 Adsorption isotherms on ammonium phosphomolybdate powder.[27] (1), (2), before pre-adsorption of nonane; (3), (4) after pre-adsorption of nonane. (1), (4), nitrogen (77 K); (2), (3), carbon tetrachloride (298 K). Adsorption is expressed in mm^3(liquid).

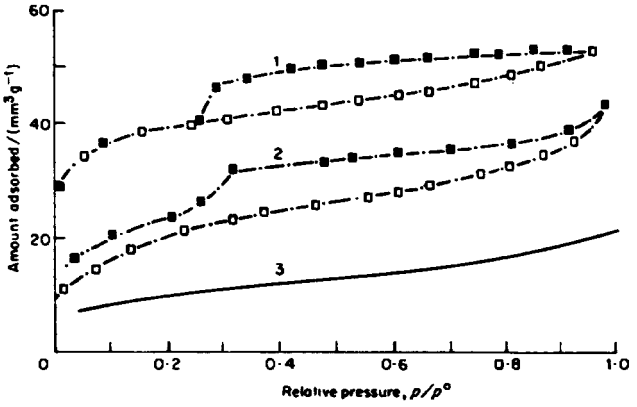

Fig. 4.32 Adsorption isotherms of carbon tetrachloride (at 298 K) on ammonium phosphotungstate compact,[27] (1) before, (2) after pre-adsorption of n-nonane. (3) is the isotherm of nitrogen, after pre-adsorption, for reference. Open symbols, adsorption; solid symbols, desorption.

measurement *n*-nonane is solid in the case of nitrogen (77 K) and liquid in the case of the other two adsorptives (298 K). The penetration hypothesis is supported by the low-pressure hysteresis found with the isotherms of both hexane and carbon tetrachloride on the nonane-treated samples.

It follows that the applicability of the nonane pre-adsorption method for the evaluation of microporosity is restricted to adsorptives such as nitrogen which are used at temperatures far below ambient and which have negligible solubility in solid or liquid nonane.

4.8 Further comments on narrow pores

From knowledge accumulated since the original concept of micropores was formulated, it seems that the micropore region may be subdivided into two sub-regions, distinguished by the different mechanisms involved. In both regions the uptake at a given relative pressure is higher than it would be on a corresponding open surface, and the resultant upward distortion of the isotherm can be detected by the t, α_s or comparison plots.

The lower pressure sub-region is characterized by a considerable enhancement of the interaction potential (Chapter 1) and therefore of the enthalpy of adsorption; consequently the pore becomes completely full at very low relative pressure (sometimes 0·01 or less), so that the isotherm rises steeply from the origin. This behaviour is observed with molecular sieve zeolites, the enhancement of the adsorption energy and the steepness of the isotherm being dependent on the nature of the adsorbent–adsorbate interaction and the polarizability of the adsorbate.[76,77]

In the higher pressure sub-region, which may be extended to relative pressure up to ~0·1 to ~0·2, the enhancement of the interaction energy and of the enthalpy of adsorption is relatively small, and the increased adsorption is now the result of a cooperative effect. The nature of this "secondary" process may be appreciated from the simplified model of a slit in Fig. 4.33. Once a monolayer has been formed on the walls, then if molecules (1) and (2) happen to condense opposite one another, the probability that (3) will condense is increased. The increased residence time of (1), (2) and (3) will promote the condensation of (4) and of still further molecules. Because of the cooperative nature of the mechanism, the separate stages occur in such rapid succession that in effect they constitute a single process. The model is necessarily very crude and the details for any particular pore will depend on the pore geometry.

This second sub-region will give rise to a rounded knee to the isotherm. Thus a purely microporous solid which contains both categories of micropore will give rise to a Type I isotherm, having a very steep initial

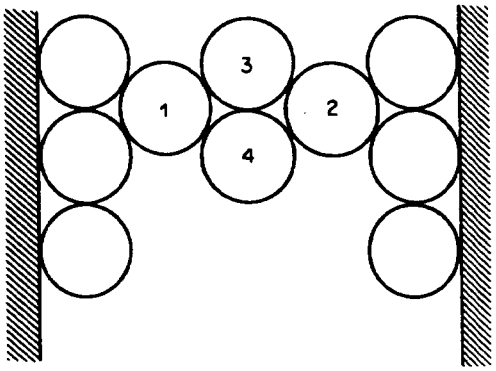

Fig. 4.33 Model of cooperative adsorption in a slit-shaped pore.

branch succeeded by a more gradual approach to the plateau[78] (cf. Fig. 4.34). The increase in the enthalpy of adsorption in this second sub-region of the isotherm will be quite small and may even be below the limits of detection: the major cause of the enhanced adsorption is now an increase in the entropy of adsorption reflecting the importance of configurational factors.

If mesopores are present in addition to micropores, the isotherm will be of Type IV, with the characteristic hysteresis loop; but, as explained in

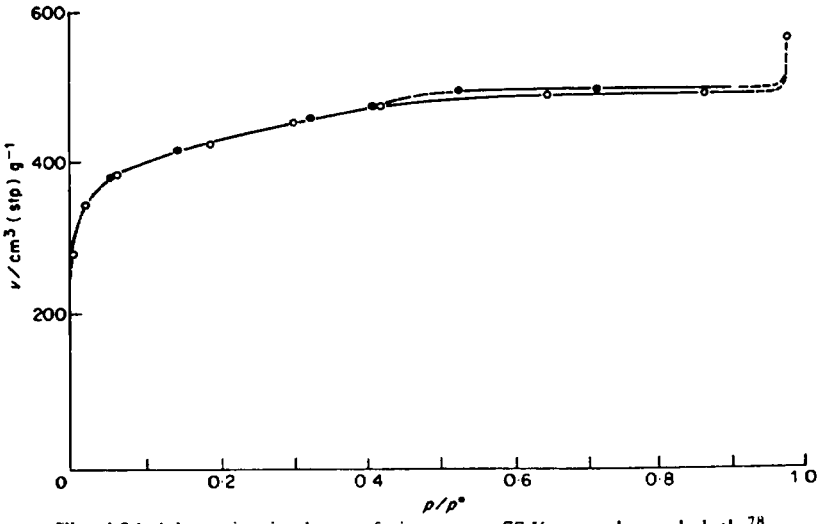

Fig. 4.34 Adsorption isotherm of nitrogen at 77 K on a charcoal cloth.[78]

Chapter 3, there is often a region immediately preceding the lower closure point, in which increased adsorption is brought about by reversible capillary condensation. The meniscus now tends to be somewhat ill defined owing to its small dimensions (p. 153), but the mechanism can still be thought of in Kelvin terms, where the driving force is the pressure difference across an interface.

In general, therefore, there are three processes, prior to the kind of capillary condensation associated with the hysteresis loop of a Type IV isotherm, which may occur in a porous body containing micropores along with mesopores: a primary process taking place in very narrow micropores; a secondary, cooperative process, taking place in wider micropores, succeeded by a tertiary process governed by a modified Kelvin equation.

The limits of pore size corresponding to each process will, of course, depend both on the pore geometry and the size of the adsorbate molecule. For slit-shaped pores the primary process will be expected to be limited to widths below $\sim 2\sigma$, and the secondary to widths between $\sim 2\sigma$ and $\sim 5\sigma$. For more complicated shapes such as interstices between small spheres, the equivalent diameter will be somewhat higher, because of the more effective overlap of adsorption fields from neighbouring parts of the pore walls. The tertiary process—the reversible capillary condensation—will not be able to occur at all in slits if the walls are exactly parallel; in other pores, this condensation will take place in the region between $\sim 5\sigma$ and the inception of the hysteresis loop; and in a pore system containing a variety of pore shapes, reversible capillary condensation occurs in such pores as have a suitable shape alongside the irreversible condensation in the main body of pores.

To provide an approximate quantitative framework, the following limits of width of slit-like pores, for nitrogen at 77 K are suggested for the respective processes:

Primary	Secondary	Tertiary
~ 3 Å to ~ 7 Å	~ 7 Å to ~ 18 Å	$> \sim 18$ Å

The term *supermicropores* has been proposed[79] for the pores in which adsorption occurs by the secondary process; the pores in which the primary process operates would then be termed, simply, micropores (or alternatively ultramicropores,[29,30] or ultrapores[80]).

Much more work will have to be done in this important field, however, before either the concepts or the terminology[81] can be regarded as fully established.

References

1. S. J. Gregg and R. Stock, *Trans. Faraday Soc.* **53**, 1355 (1957).
2. D. A. Cadenhead and D. H. Everett, Conf. on Industrial Carbon and Graphite, p. 272, Society of Chemical Industry (1958).
3. I. Langmuir, *J. Amer. Chem. Soc.* **38**, 2219 (1916); **40**, 1368 (1918).
4. R. M. Barrer, "Zeolites and Clay Minerals", p. 109, Academic Press, London and New York (1978); R. M. Barrer and J. A. Davies, *Proc. Roy. Soc.* **A320**, 289 (1970).
5. D. M. Ruthven and K. F. Loughlin, *J. Chem. Soc., Faraday Trans.* **I, 68**, 690 (1972).
6. T. A. Egerton and F. S. Stone, *Trans. Faraday Soc.* **66**, 2364 (1970).
7. R. U. Culver and N. S. Heath, *Trans. Faraday Soc.* **51**, 1569 (1955).
8. D. H. Everett and J. C. Powl, *J. Chem. Soc., Faraday Trans. I*, **72**, 619 (1976).
9. C. Pierce, J. W. Wiley and R. N. Smith, *J. Phys. Chem.* **53**, 669 (1949).
10. R. Stock, Ph.D. Thesis, London University (1957).
11. D. W. Broad and A. G. Foster, *J. Chem. Soc.* 366 (1945).
12. M. A. Brown and A. G. Foster, *J. Phys. Chem.* **56**, 733 (1952).
13. D. Dollimore and T. Shingles, *J. Appl. Chem.* **19**, 218 (1969).
14. J. F. Goodman, Ph.D. Thesis, London University (1955).
15. M. M. Dubinin and E. D. Zaverina, *Zhur. Fiz. Khim.* **23**, 1129 (1949); M. M. Dubinin, *Quart. Rev. Chem. Soc.* **9**, 101 (1955).
16. R. G. Avery and J. D. F. Ramsay, *J. Colloid Interface Sci.* **42**, 597 (1973).
17. M. M. Dubinin, *in* "Progress in Surface and Membrane Science", (eds. J. F. Danielli, M. D. Rosenberg and D. A. Cadenhead), Vol. 9, p. 1, Academic Press, New York and London (1975).
18. A. V. Kiselev, *in* "The Structure and Properties of Porous Materials" (eds. D. H. Everett and F. S. Stone), p. 51, Butterworths, London (1958).
19. M. R. Bhambhani, P. A. Cutting, K. S. W. Sing and D. H. Turk, *J. Colloid Interface Sci.* **38**, 109 (1972).
20. M. Polanyi, *in* "The Adsorption of Gases on Solids", *Disc. Faraday Soc.* p. 316 (1932); J. H. de Boer and J. F. H. Custers, *Z. Phys. Chem.* **25B**, 225 (1934).
21. K. S. W. Sing, *in* "Colloid Science", Vol. 1 (ed. D. H. Everett), p. 10, Specialist Periodical Report, Chemical Society, London (1973); D. Nicholson and K. S. W. Sing, *in* "Colloid Science" (ed. D. H. Everett), Vol. 3, p. 21, Chemical Society, London (1979).
22. P. J. Anderson and R. F. Horlock, *Trans. Faraday Soc.* **65**, 251 (1969).
23. N. S. Gurfein, D. P. Dobychin and L. S. Koplienko, *Zhur. Fiz. Khim.* **44**, 741 (1970); *Russ. J. Phys. Chem.* **44**, 411 (1970) transl.
24. K. S. W. Sing, *Chem. Ind.* 829 (1967); *Chem. Ind.* 1520 (1968); K. S. W. Sing, *in* "Surface Area Determination" (eds D. H. Everett and R. H. Ottewill), p. 25, Butterworths, London (1970).
25. D. Aldcroft, G. C. Bye, J. G. Robinson and K. S. W. Sing, *J. Appl. Chem.* **18**, 301 (1968); D. Aldcroft, G. C. Bye and G. O. Chigbo, *Trans. Brit. Ceram. Soc.* **70**, 19 (1971).
26. S. J. Gregg and J. F. Langford, *Trans. Faraday Soc.* **65**, 1394 (1969); J. F. Langford, Ph.D. Thesis, Exeter University (1967).
27. S. J. Gregg and M. M. Tayyab, *J. Chem. Soc. Faraday Trans. I*, **74**, 349 (1978); M. M. Tayyab, Ph.D. Thesis, Brunel University (1971).
28. G. A. Nicolaon and S. J. Teichner, *J. Chim. Phys.* **66**, 1816 (1969); G. C. Bye and C. R. Howard, *J. Appl. Chem.* **21**, 324 (1971); R. L. Mieville, *J. Colloid*

Interface Sci. **41**, 37 (1972); H. Jeziorowski, H. Knozinger and W. Meye, *J. Colloid Interface Sci.* **50**, 283 (1975); R. Saez Puche and M. A. Alario Franco in "Characterisation of Porous Solids" (eds. S. J. Gregg, K. S. W. Sing and H. F. Stoeckli), p. 127, Soc. Chem. Ind. London (1979).
29. R. Sh. Mikhail, S. Brunauer and E. E. Bodor, *J. Colloid Interface Sci.* **26**, 45, 54 (1968).
30. S. Brunauer, *in* "Surface Area Determination" (eds. D. H. Everett and R. H. Ottewill), pp. 70, 79, Butterworths, London (1970).
31. A. Lecloux and J. P. Pirard, *J. Colloid Interface Sci.* **70**, 265 (1979).
32. G. D. Parfitt, K. S. W. Sing and D. Urwin, *J. Colloid Interface Sci.* **53**, 187 (1975).
33. G. D. Parfitt, D. Urwin and T. J. Wiseman, *J. Colloid Interface Sci.* **36**, 217 (1971).
34. S. Brunauer, J. Skalny and E. E. Bodor, *J. Colloid Interface Sci.* **30**, 546 (1969).
35. R. B. Anderson, *J. Amer. Chem. Soc.* **68**, 686 (1946).
36. C. E. Brown and P. G. Hall, *Trans. Faraday Soc.* **67**, 3558 (1971).
37. J. A. Lee and C. E. Newnham, *J. Colloid Interface Sci.* **56**, 391 (1976).
38. M. M. Dubinin and L. V. Radushkevich, *Proc. Acad. Sci. USSR.* **55**, 331 (1947); M. M. Dubinin, *Russ. J. Phys. Chem.* **39**, 697 (1965).
39. M. Polanyi, *Verb. Deutsch. Physik. Ges.* **16**, 1012 (1914).
40. M. M. Dubinin, *in* "Chemistry and Physics of Carbon" (ed. P. L. Walker), Vol. 2, p. 51, Marcel Dekker, New York (1966); H. F. Stoeckli, *Chimia* **28**, 727 (1974).
41. M. M. Dubinin, *in* "Proceedings of the Conference on Industrial Carbon and Graphite", p. 219, Soc. Chem. Ind., London (1958).
42. U. Huber, H. F. Stoeckli, J. Ph. Houriet, *J. Colloid Interface Sci.* **67**, 195 (1978).
43. S. J. Gregg, *J. Chem. Soc.* 351 (1943).
44. T. G. Lamond and H. Marsh, *Carbon* **1**, 281, 293 (1964).
45. M. M. Dubinin, *in* "Chemistry and Physics of Carbon" (ed. P. L. Walker), Vol. 2, p. 86, Marcel Dekker, New York (1966).
46. H. Marsh and B. Rand, *in* "Third Conference on Industrial Carbon and Graphite" (Soc. Chem. Ind.), p. 93, Academic Press, London and New York (1970).
47. M. M. Dubinin and V. A. Astakhov, *Adv. Chem. Ser.* No. 102, p. 69 (1971).
48. W. Weibull, *J. Appl. Mech.* **18**, 293 (1951).
49. H. F. Stoeckli, *J. Colloid Interface Sci.* **59**, 184 (1977); H. F. Stoeckli, J. Ph. Houriet, A. Perret and U. Huber, *in* "Characterisation of Porous Solids" (eds. S. J. Gregg, K. S. W. Sing and H. F. Stoeckli), p. 31, Soc. Chem. Ind. London (1979).
50. M. M. Dubinin and H. F. Stoeckli, *J. Colloid Interface Sci.* **75**, 34 (1980).
51. M. G. Kaganer, *Zhur. Fiz. Khim.* **33**, 2202 (1959).
52. D. F. Klemperer, *in* "Surface Area Determination", p. 55, Butterworths, London (1970); B. A. Gottwald, *in* "Surface Area Determination", p. 59, Butterworths, London (1970).
53. A. Granville, P. G. Hall and C. J. Hope, *Chem. and Ind.*, p. 435 (1970).
54. P. L. Walker and R. L. Patel, *Fuel* **49**, 91 (1970).
55. V. D. Pomeshchikov and V. V. Pozdeev, *Kinetika i Kataliz.* **12**, 794 (1971).
56. N. N. Avgul, A. G. Bezus, E. S. Dobrova and A. V. Kiselev, *J. Colloid Interface Sci.* **42**, 486 (1973).
57. F. A. P. Maggs, *Research* **6**, S13 (1953).

58. P. Zwietering and D. W. van Krevelin, *Fuel* **33**, 331 (1954).
59. S. J. Gregg and M. I. Pope, *Fuel* **38**, 501 (1959).
60. H. Marsh and W. F. K. Wynne-Jones, *Carbon* **1**, 281 (1964).
61. R. M. Barrer, *Quart. Rev. Chem. Soc.* **3**, 293 (1949); "Zeolites and Clay Minerals", p. 291, Academic Press, London and New York (1978).
62. S. J. Gregg, R. M. Olds and R. F. S. Tyson, *in* "Third Conference on Industrial Carbon and Graphite" (Soc. Chem. Ind.), p. 184, Academic Press, London and New York (1970).
63. S. S. Barton, F. G. Beswick and B. H. Harrison, *J. Chem. Soc. Faraday Trans.* I, **68**, 1647 (1972).
64. N. G. Dovaston, B. McEnaney and C. J. Weedon, *Carbon* **10**, 277 (1972); B. McEnaney, *J. Chem. Soc. Faraday Trans.* I, **70**, 84 (1974).
65. V. R. Deitz and E. Berlin, *J. Collaid Interface Sci.* **44**, 57 (1973).
66. J. F. Goodman, Ph.D. Thesis, London University (1955).
67. H. W. Quinn and R. McIntosh, *in* "Proceedings of the Second International Congress on Surface Activity", II, p. 122, Butterworths, London (1957).
68. K. S. W. Sing and J. D. Madeley, *J. Appl. Chem.* **4**, 365 (1954).
69. J. C. Arnell and H. L. McDermott, *in* "Proceedings of the Second International Congress on Surface Activity", II, p. 113, Butterworths, London (1957).
70. A. Bailey, D. A. Cadenhead, D. H. Davies, D. H. Everett and A. J. Miles, *Trans. Faraday Soc.* **67**, 231 (1971).
71. M. I. Pope and S. J. Gregg, *Fuel* **39**, 308 (1960).
72. R. M. Barrer and J. S. S. Reay, *in* "Proceedings of the Second International Congress on Surface Activity", II, p. 79, Butterworths, London (1957).
73. F. S. Baker, K. S. W. Sing and L. J. Stryker, *Chem. and Ind.* 718 (1970); F. S. Baker, J. D. Carruthers, R. E. Day, K. S. W. Sing and L. J. Stryker, *Discuss. Faraday Soc.* No. 52, p. 173 (1971).
74. R. B. Gammage and S. J. Gregg, *J. Colloid Interface Sci.* **38**, 118 (1972); R. B. Gammage, Ph.D. Thesis, Exeter University (1964).
75. P. A. Cutting, *in* "Vacuum Microbalance Techniques", Vol. 7, p. 71, Plenum Press, New York (1970).
76. J. L. Soto, P. W. Fisher, A. J. Glessner and A. L. Myers, *J. Chem. Soc., Faraday Trans.* I, **77**, 157 (1981).
77. D. Atkinson and G. Curthoys, *J. Chem. Soc., Faraday Trans.* I, **77**, 897 (1981).
78. A. McLeod and K. S. W. Sing, unpublished work.
79. M. M. Dubinin, *in* "Characterisation of Porous Solids" (eds. S. J. Gregg, K. S. W. Sing and H. F. Stoeckli), p. 1, Soc. Chem. Ind., London (1979).
80. A. V. Kiselev, *Discuss. Faraday Soc.* **52**, 14 (1971).
81. K. S. W. Sing, *in* "Characterisation of Porous Solids", p. 98, Soc. Chem. Ind., London (1979).

5

Type III and Type V Isotherms The Special Behaviour of Water

5.1 Type III isotherms

Both Type III and Type V isotherms are characterized by convexity towards the relative pressure axis, commencing at the origin. In Type III isotherms the convexity persists throughout their course (Fig. 5.1(*a*), whereas in Type V isotherms there is a point of inflection at fairly high relative pressure, often ~0·5 or even higher, so that the isotherm bends over and reaches a plateau DE in the multilayer region of the isotherm (cf. Fig. 5.1(*b*)); sometimes there is a final upward sweep near saturation pressure (see DE′ in Fig. 5.1(*b*)) attributable to adsorption in coarse mesopores and macropores.

Types III and V isotherms are characteristic of weak gas–solid interactions,[1] the Type III isotherm being given by a nonporous or macroporous solid and the Type V isotherm by a mesoporous or microporous solid.

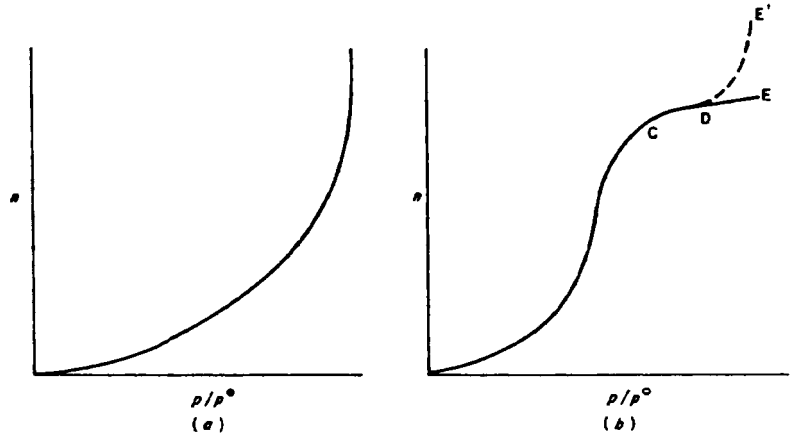

Fig. 5.1 (*a*) Type III isotherm; (*b*) Type V isotherm.

When the BDDT classification was put forward in 1940 such isotherms were rare and although a number of well documented cases of both types have been reported in recent years they must still be regarded as somewhat uncommon.

The weakness of the adsorbent–adsorbate forces will cause the uptake at low relative pressures to be small; but once a molecule has become adsorbed, the adsorbate–adsorbate forces will promote the adsorption of further molecules—a cooperative process—so that the isotherms will become convex to the pressure axis.

Type III (and Type V) isotherms may originate through the adsorption of either nonpolar or polar molecules, always provided that the adsorbent–adsorbate force is relatively weak.

A polar adsorbate of particular interest in this context is water, because the dispersion contribution to its overall interaction energy is unusually small compared with the polar contribution. Barrer[2] has calculated that the dispersion interaction energy of water with an H-chabasite at 298 K is only 2·65 kcal mol^{-1}, much smaller than the molar enthalpy of condensation, 10·6 kcal mol^{-1}, which of course includes the contributions from the four hydrogen bonds linking each molecule to its immediate neighbours. Not surprisingly, water provides many examples of Type III isotherms (cf. p. 262).

The way in which these factors operate to produce Type III isotherms is best appreciated by reference to actual examples. Perhaps the most straightforward case is given by organic high polymers (e.g. polytetrafluoroethylene, polyethylene, polymethylmethacrylate or polyacrylonitrile) which give rise to well defined Type III isotherms with water or with alkanes, in consequence of the weak dispersion interactions (Fig. 5.2). In some cases the isotherms have been measured at several temperatures so that q^{st} could be calculated; in Fig. 5.2(*c*) the value is initially somewhat below the molar enthalpy of condensation q_L and rises to q_L as adsorption proceeds. In Fig. 5.2(*d*) the higher initial values of q^{st} are ascribed to surface heterogeneity.

The strength of dispersion interaction of a solid with a gas molecule is determined not only by the chemical composition of the surface of the solid, but also by the surface density of the force centres.[2] If therefore this surface density can be sufficiently reduced by the pre-adsorption of a suitable substance,[6] the isotherm may be converted from Type II to Type III. An example is rutile, modified by the pre-adsorption of a monolayer of ethanol; the isotherm of pentane, which is of Type II on the unmodified rutile (Fig. 5.3, curve A), changes to Type III on the treated sample (cf. Fig. 5.3 curve B). Similar results were found with hexane-1-ol as pre-adsorbate.[7] Another example is the pre-adsorption of amyl alcohol on a quartz powder

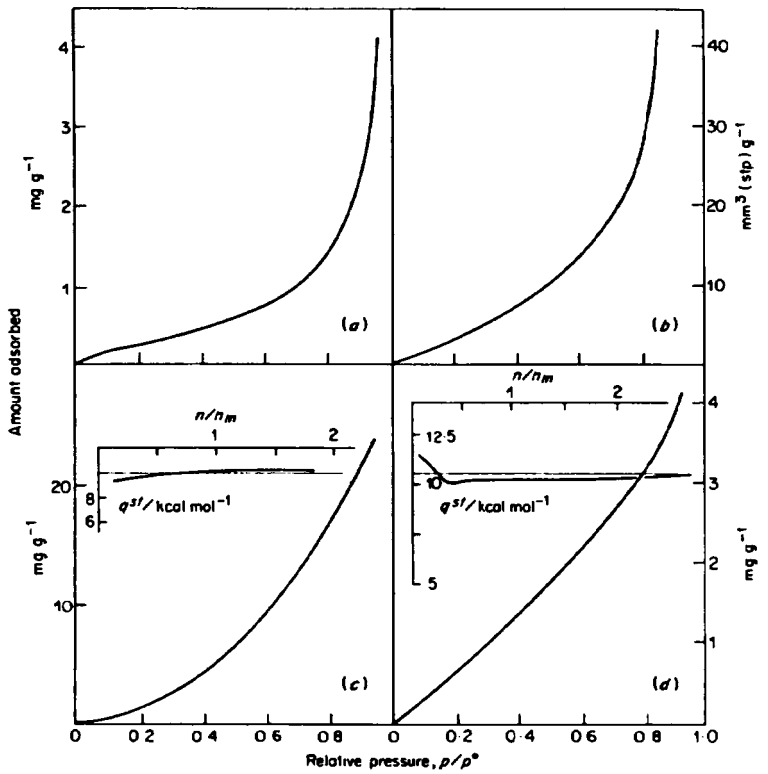

Fig. 5.2 Type III isotherms. (*a*) n-hexane on PTFE[3] at 25°C; (*b*) n-octane on PTFE[4] at 20°C; (*c*) water on polymethylmethacrylate[5] at 20°C; (*d*) water on bis(A-polycarbonate) (Lexan)[5] at 20°C. The insets in (*c*) and (*d*) give the curves of heat of adsorption against fractional coverage; the horizontal line marks the molar heat of liquefaction. (Redrawn from diagrams in the original papers, with omission of experimental points.)

previously ground under liquid water, where both carbon tetrachloride and *n*-octane gave Type III isotherms.[8]

An interesting example of surface modification is found when the original surface is energetically uniform and therefore gives rise to a Type VI, i.e. stepped, isotherm. Pre-adsorption of a suitable involatile monolayer, such as ethylene at 77 K on graphitized carbon, causes the isotherm (e.g. of argon) to assume Type III character in the low-pressure region; thus the first step is displaced towards higher relative pressures and the steps become less clearly defined.[9]

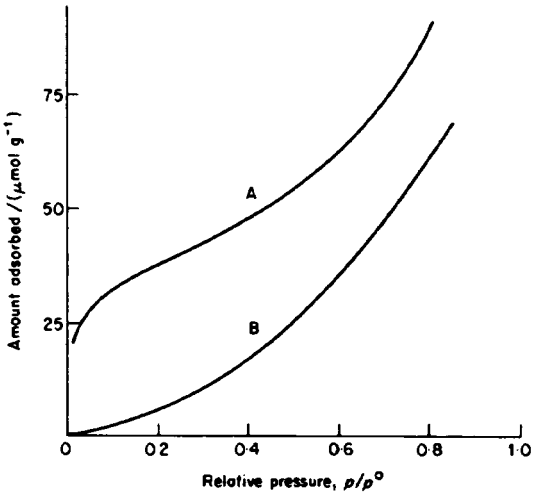

Fig. 5.3 Adsorption of pentane vapour at 273 K on a sample of nonporous rutile before and after modification of the surface by pre-adsorption of ethanol.[7] Curve (A), unmodified surface; curve (B), surface containing 52 μmol g^{-1} of ethanol. (After Parfitt.)

Another way in which the surface may be modified is by actual chemical reaction. Thus in Kiselev's detailed study,[10] a hydroxylated silica was treated with trimethylchlorosilane so as to replace the hydroxyl groups by the nonpolar $Si(CH_3)_3$ groups; this had the effect of weakening both the dispersion and the polar interactions. Kiselev[10] measured the isotherms of benzene on samples of a silica (Aerosil) which had undergone progressive surface modification in this manner. As the surface concentration of the $Si(CH_3)_3$ groups increased the isotherm gradually lost its Type II character until with the completely converted surface, it was of Type III (Fig. 5.4(*a*)). Correspondingly, the curve of the heat of adsorption against amount adsorbed became progressively lower (Fig. 5.4(*b*)) and the final curve corresponding to the Type III isotherm had the expected form of a low initial value gradually climbing to the heat of condensation as the uptake increased.

The results obtained for the adsorption of butane on a ball-milled calcite[11] are also of interest. When the solid was outgassed at 150°C to remove physically adsorbed water, the butane isotherm was of Type II with $c = 26$ (Fig. 5.5, curve (ii)); but outgassing at 25°, which would leave at least a monolayer of molecular water on the surface, resulted in a Type III isotherm (Fig. 5.5, curve (i)). Though butane is nonpolar its polarizability is

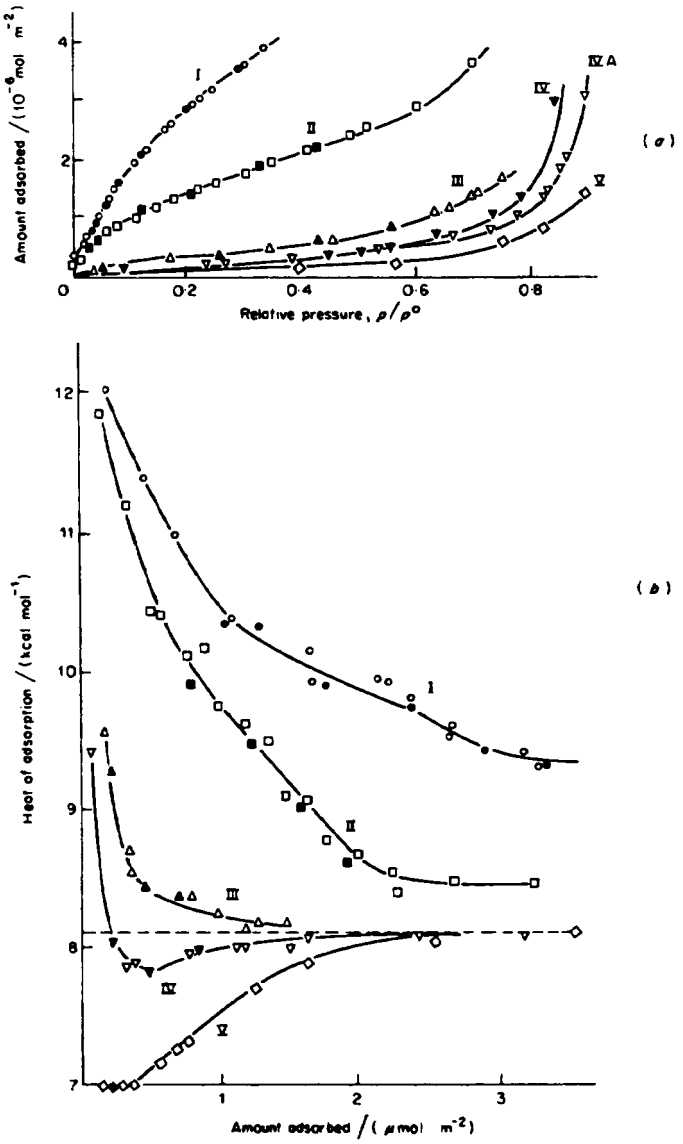

Fig. 5.4 The adsorption of benzene vapour on silica (Aerosil), whose surface has been progressively covered with $Si(CH_3)_3$ groups. The surface concentrations of $Si(CH_3)_3$ are: (I), 0%; (II), 60%; (III), 80%; (IV) and (IVa), 90%; (V), 100%. (*a*) Adsorption isotherms; (*b*) curves of the differential heat of adsorption against the amount adsorbed per unit area. (Courtesy Kiselev.[10])

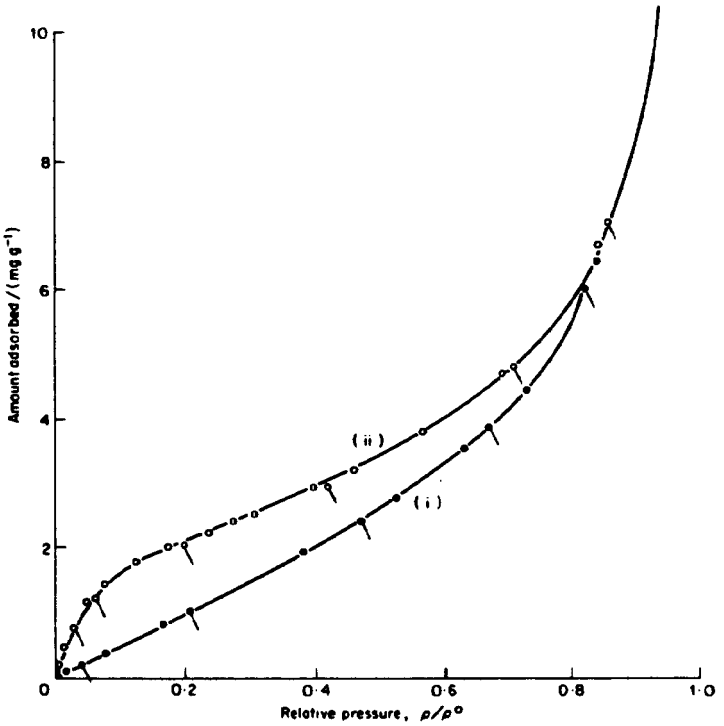

Fig. 5.5 Adsorption isotherms of butane at 0°C on Iceland Spar[11] ground for 1000 h. Curve (i), the solid was outgassed at 25°C. Curve (ii), the solid was outgassed at 150°C. ● ○, adsorption; ◐ ◯, desorption.

relatively high ($82{\cdot}5 \times 10^{-25}$ cm^3 per molecule); consequently its overall energy of interaction with an ionic solid would be comparatively large, producing a Type II isotherm. Once the solid is covered with a layer of adsorbed water, however, the adsorbent–adsorbate interaction energy would be virtually reduced to the weak dispersion energy of water with butane so that a Type III isotherm should result. This explanation is supported by the fact that the adsorption isotherms of the *n*-alkanes on *liquid* water[12] (calculated by the Gibbs adsorption equation from measurements of the surface tension of water in the presence of alkane vapour) were found to be of Type III. Cyclohexane was similarly found to yield a Type III isotherm on block-dried precipitated calcium carbonate.[13] The results obtained by Stock[13] with calcium sulphate and hexane were slightly different inasmuch as the isotherm given by the solid calcined at 280°C and

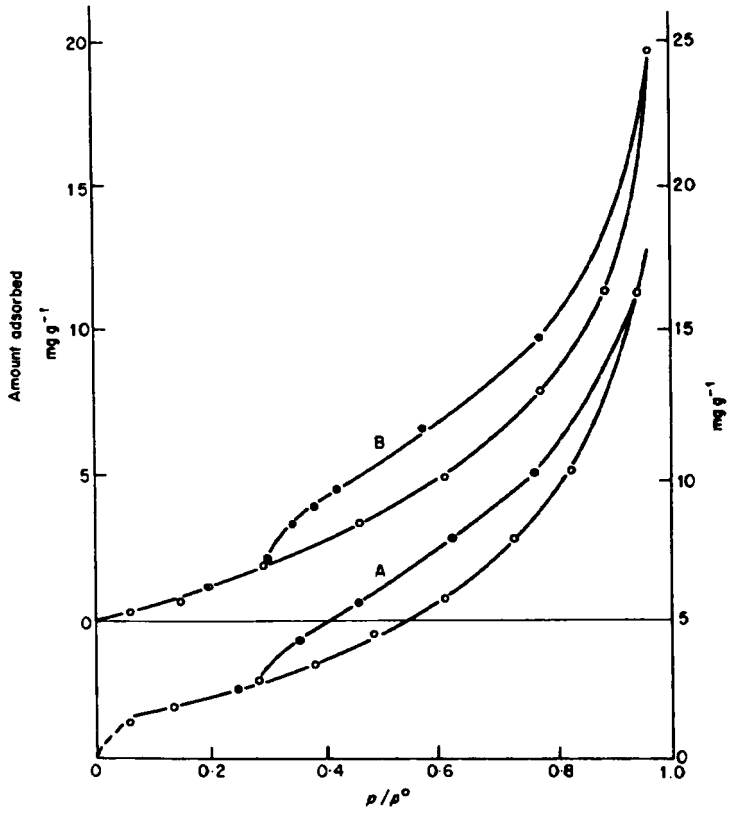

Fig. 5.6 Adsorption isotherms at 25°C of n-hexane on calcium sulphate[13] which had been calcined at 280°C. Curve (A), the solid was outgassed at 120°. Curve (B), the solid was treated with liquid water to produce a composition of $CaSO_4 . O{\cdot}35H_2O$ and was then outgassed at 25°C.

outgassed at 120°C was of Type IV with a rather rounded knee and a Type B hysteresis loop. After the addition of enough water to produce the overall composition $CaSO_4 . 0{\cdot}35H_2O$, the adsorption branch of the hexane isotherm assumed the Type III shape, but the hysteresis loop remained (cf. Fig. 5.6).

5.2 Validity of the BET procedure for Type III isotherms

In the context of the present book, a question of particular interest is how

far the BET procedure for the evaluation of monolayer capacity and specific surface remains valid when the isotherm is of Type III.

As already pointed out, a Type III isotherm results from the BET equation when the value of c is less than 2 (p. 46). For $c = 3$, the isotherm is no longer strictly of Type III, but the point of inflection, at about $0{\cdot}01p^\circ$, is barely perceptible, and at first glance the isotherm appears to be a genuine Type III—a fact of some consequence because the value $c \sim 3$ is relatively common amongst isotherms which are apparently of Type III.

In applying the BET procedure to Type III isotherms, $c = 1$ constitutes a special case: insertion of $c = 1$ into the standard BET equation (2.12) leads to the simplified equation

$$\frac{p/p^\circ}{n(1 - p/p^\circ)} = \frac{1}{n_m} \tag{5.1}$$

so that the usual BET plot of $p/p^\circ/n(1 - p/p^\circ)$ against p/p° will give a horizontal line distant $1/n_m$ from the p/p° axis.

When the value of c exceeds unity, the value of n_m can be derived from the slope and intercept of the BET plot in the usual way; but because of deviations at low relative pressures, it is sometimes more convenient to locate the "BET monolayer point", the relative pressure $(p/p^\circ)_m$ at which $n/n_m = 1$. First, the value of c is found by matching the experimental isotherm against a set of ideal BET isotherms, calculated by insertion of a succession of values of c (1, 2, 3, etc., including nonintegral values if necessary) into the BET equation in the form:

$$\frac{n}{n_m} = \frac{c(p/p^\circ)}{(1 - p/p^\circ)(1 + c - 1\,p/p^\circ)} \tag{5.2}$$

Once c is known, the monolayer point is picked out by use of the relation

$$(p/p^\circ)_m = \frac{-1 \pm \sqrt{c}}{c - 1} \tag{5.3}$$

which can be derived by putting $n/n_m = 1$ in (5.2) and solving for p/p°. Thus, for $c = 2$, $(p/p^\circ)_m = 0{\cdot}41$; for $c = 3$, $(p/p^\circ)_m = 0{\cdot}366$; and for $c = 1$, of course, $(p/p^\circ)_m = 0{\cdot}5$.

When the values of the BET monolayer capacity calculated from Type III isotherms are compared with independent estimates (e.g. from nitrogen adsorption) considerable discrepancies are frequently found. A number of typical examples are collected in Table 5.1. Comparison of the value of the monolayer capacity predicted by the BET equation with the corresponding value determined independently (columns (iv) and (v)) show that occasionally, as in line 6, the two agree reasonably well, but that in the majority

TABLE 5.1

Comparison of monolayer capacity $n_m(X)$ calculated with BET equation from the Type III isotherm of adsorptive X with an independent value of n_m

(i) System	(ii) c	(iii) $(p/p^\circ)_m$	(iv) n_m from $(p/p^\circ)_m$	(v) n_m (independent)†	(vi) $a_m(X)$‡	(vii) Ref.
1. MgO–CCl_4	2·3	0·41	160 mg g^{-1}	80 mg g^{-1}	37 Å^2	14
2. SiO_2–CCl_4	3	0·37	3·1 μmol m^{-2}	4·5 μmol m^{-2}	37 Å^2	15
3. SiO_2–CCl_4	2	0·41	0·46 mmol g^{-1}	0·69 mmol g^{-1}	37 Å^2	16
4. $CaCO_3$–C_4H_{10}	2	0·41	2·25 mg g^{-1}	~1·8 mg g^{-1}	40 Å^2	11
5. $CaCO_3$–C_6H_{12}	~1	~0·50	2·8 mg g^{-1}	6·1 mg g^{-1}	–	13
6. TiO_2 (mod. with C_2H_5OH)–C_5H_{12}	1	0·50	27·6 μmol g^{-1}	27·4 μmol g^{-1}	45 Å^2	7
7. H_2O(liquid)–C_5H_{12}	~2	~0·41	0·85 μmol m^{-2}	3·7 μmol m^{-2}	45 Å^2	12

Notes: (2) SiO_2(Fransil); (3) SiO_2(TK800); (4), (5) $CaCO_3$ modified with monolayer of H_2O; (6) TiO_2 modified with monolayer of C_2H_5OH.

† (1), (2), (3), (4), (6), from $A(N_2)$; (5), from Point B of isotherm of X on the unmodified $CaCO_3$; (7) from Gibbs equation.

‡ Value assumed in calculating n_m(independent) from $A(N_2)$ or Point B.

of cases they diverge widely. Such an outcome is not really surprising in view of the artificial nature of the BET model. As was emphasized in Chapter 2, in order to obtain a sound value of the monolayer capacity from the adsorption isotherm, it is necessary that the building-up of the monolayer shall be virtually complete before the formation of the multilayer commences, so that there is a clearly identifiable point on the isotherm (Point B) corresponding to this condition. In systems which give rise to a Type III isotherm, however, the multilayer is being built up on some parts of the surface whilst the monolayer is still incomplete on other parts.

One must conclude therefore that the BET procedure for evaluation of monolayer capacity is not applicable to a Type III (nor by implication, to a Type V) isotherm.

5.3 Use of the α_s-plot for evaluation of specific surface[17,18] from Type III isotherms

It is, however, possible to use a Type III isotherm of an adsorptive G, say, on a solid S for the evaluation of the specific surface of S, provided a standard sample of the solid is available to enable one to construct a standard α_s-curve of G on S. The area of the standard sample must be known, usually from the nitrogen isotherm.

If the isotherm of G on the solid under test is identical in shape with that on the reference sample, then its α_s-plot will be a straight line passing through the origin, and having a slope equal to the ratio A(test solid)/A(reference solid). Since A(reference solid) is known, the specific surface of the test solid is obtainable at once.

The method is illustrated in a study of four nonporous samples of silica by Sing and his co-workers.[18] The isotherms of nitrogen at 77 K and of carbon tetrachloride at 293 K, were measured for all four, and one sample (a nonporous silica, Fransil) was taken as standard for the construction of the α_s-curve of carbon tetrachloride.[17] The BET specific surface of all samples was calculated from the BET plots of nitrogen with $a_m(CCl_4) = 37$ Å^2. Not surprisingly, there was poor agreement between corresponding values of the BET specific surface by nitrogen and by carbon tetrachloride respectively (Table 5.2, columns (ii) and (iv)). The values of specific surface calculated from the α_s-plots of carbon tetrachloride, on the other hand, showed very satisfactory agreement with the corresponding values of the nitrogen specific surface (cf. columns (ii), (iii) and (v)).

It will be noted that this method avoids any necessity to assume a value for the molecular area of the adsorbate, and it is not even necessary that the

TABLE 5.2

Surface areas[18] of nonporous silicas calculated by the BET and the α_s methods from isotherms of nitrogen (77 K) and carbon tetrachloride (298 K)

Sample	Surface area/($m^2 g^{-1}$)			
	Nitrogen		Carbon tetrachloride	
	A_N(BET)	$A_N(\alpha_s)$	A_c(BET)	$A_c(\alpha_s)$
Fransil	38·7	–	18	–
TK70	36·3	35·6	27	35·8
TK800	154	153	69	153
Aerosil 200	194	193	116	190

The α_s-plots were based on the standard isotherms of N_2 and CCl_4 respectively, on Fransil. For calculation of A_c(BET), the value $a_m(CCl_4) = 37$ Å^2 was assumed.

isotherm shall conform exactly to the BET equation, nor indeed to any simple equation at all. Thus the method is applicable to mesoporous solids and the relevant part of the α_s-plot is then the initial branch which passes through the origin and precedes the upward deviation due to capillary condensation. The α_s-method therefore enables one to combine the secure basis of the nitrogen-BET method with the advantage of using an adsorptive which permits measurement of isotherms at or near room temperature.

5.4 The influence of porosity

Mesoporosity

In Chapter 3, the effect of mesoporosity in converting Type II into Type IV isotherms was discussed by reference to experiments in which nonporous powders were compacted so as to produce mesoporous solids. Analogous experiments demonstrating the conversion of Type III into Type V isotherms are lacking, but other, slightly less direct, evidence is still available. Thus Kiselev[19] has measured the isotherms of *n*-pentane on several varieties of silica. The different isotherms, reduced to a common basis by plotting the adsorption per unit area (as determined, presumably by nitrogen adsorption) are shown in Fig. 5.7. Curve A refers to quartz and pyrex glass which are virtually nonporous, and curve B to silica gel having pore openings of diameter around 100 Å (cf. Chapter 3). The two curves agree excellently up to the point where the hysteresis loop commences for

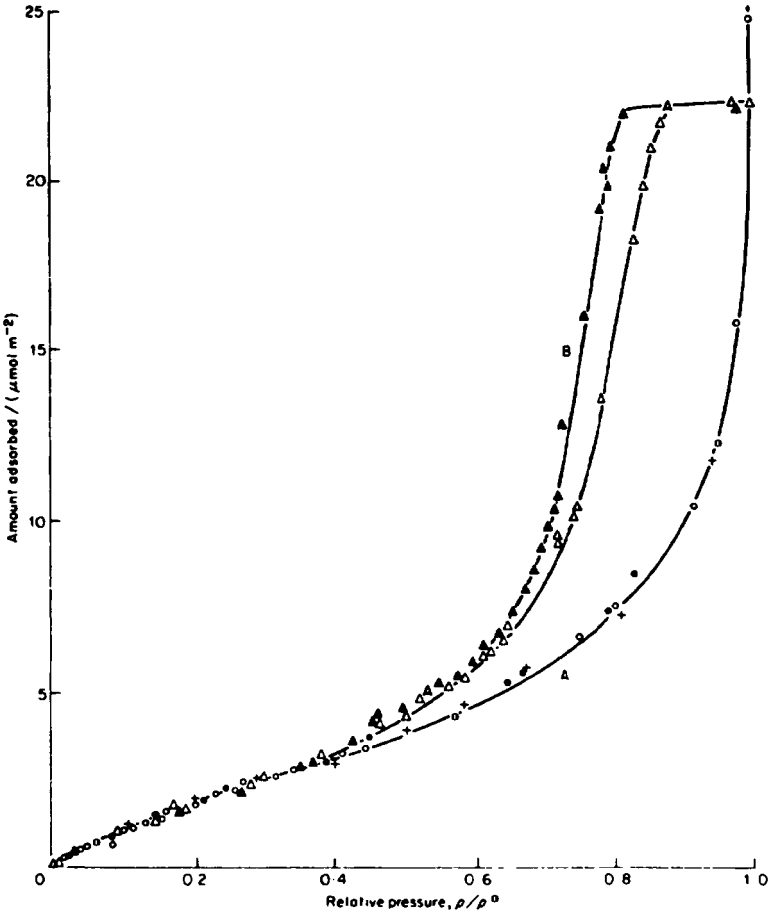

Fig. 5.7 Adsorption isotherms of n-pentane vapour on (A), quartz and pyrex glass; and (B), wide-pored silica gel. ○, ●, quartz; +, pyrex glass; △, ▲ wide-pored silica gel.[19] Solid symbols denote desorption. (Courtesy Kiselev.)

silica gel; the turn-over at the top of the isotherm B clearly arises from the presence of mesopores within the gel, just as in corresponding example where Type II isotherms are converted into Type IV (p. 114). Admittedly the isotherms are not exactly Type III and V, since there is a just detectable point of inflection, in the low-pressure region (comparison with model Type III isotherms show that $c \triangleq 3$, cf. p. 255); but the departure from true Type III or Type V shape is insufficient to detract from the argument. In the isotherms of Fig. 5.8 the mesoporosity of the adsorbent (a silica gel) was evident from the Type IV isotherm of benzene.[13] Cyclohexane, unlike benzene, is not capable of specific adsorption (p. 11) and its isotherm is convex to the pressure axis in the low-pressure region. Otherwise its isotherm is similar to that of benzene, and the hysteresis loop is typical of capillary condensation in a mesopore system; the plateau for each isotherm corresponds to the complete filling of the pores, as was confirmed by the fact that the uptakes at saturation when converted to liquid volumes agreed within experimental limits: 597 $mm^3 g^{-1}$ for benzene and 601 $mm^3 g^{-1}$ for cyclohexane.

Other examples, concerning the water–silica system, are referred to later in the Chapter.

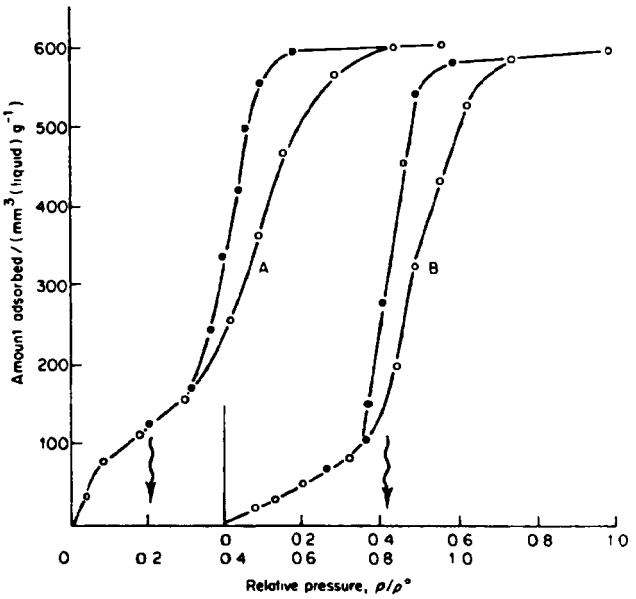

Fig. 5.8 Adsorption isotherms at 25°C of benzene and cyclohexane on a mesoporous silica gel.[13] Curve (A), benzene; curve (B), cyclohexane. Solid symbols denote desorption.

Microporosity

The enhancement of interaction energy in micropores was discussed in some detail in Chapter 4. It was emphasized that the critical pore width d at which the enhancement first appears increases with increasing diameter σ of the adsorbate molecule, since the relevant parameter is the ratio d/σ rather than d itself. The quantity σ is involved because the magnitude of the dispersion interaction increases as the polarizability, and therefore the size, of the molecule increases (cf. p. 5).

A substance having particularly high polarizability is carbon tetrachloride, which should therefore be an especially sensitive probe for the micropore effect ($\alpha(CCl_4) = 10{\cdot}1 \times 10^{-24}$; cf. $\alpha(N_2) = 1{\cdot}73 \times 10^{-24}$ or $\alpha(CO_2) = 2{\cdot}59 \times 10^{-24}$ cm^3 per molecule). Results of Cutting and Sing[15,17] for carbon tetrachloride adsorbed at 20°C on different samples of silica gel, shown in Fig. 5.9, confirm that this is so. On two nonporous samples of silica, Fransil and TK800, the isotherms (Curves A and B) were close to Type III, the value of c being $c = 3$, consistent with the weak interaction between silica and carbon tetrachloride; on a gel characterized by nitrogen adsorption as mesoporous, the isotherm was also of Type III (curve C). However, for the microporous sample (the microporosity had been demonstrated by the α_s-plot of nitrogen), the isotherm had changed to Type

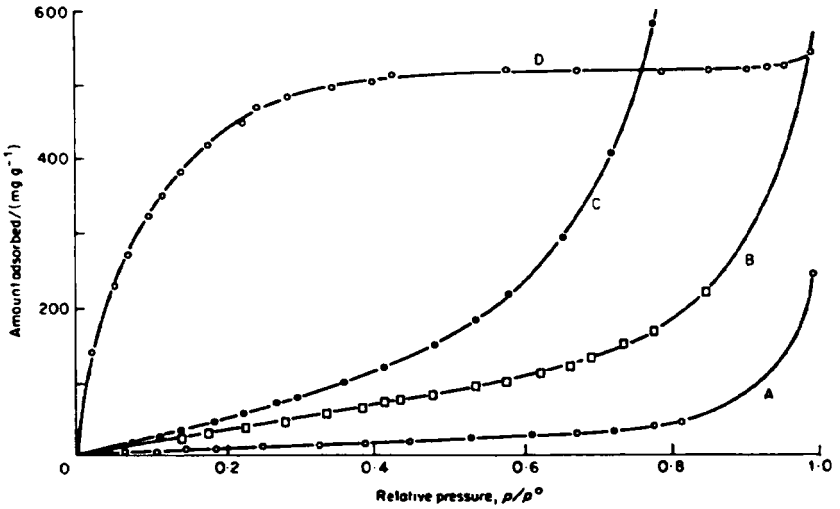

Fig. 5.9 Adsorption isotherms of carbon tetrachloride at 20°C on various samples of silica.[15,17] (A) "Fransil" (nonporous particles); (B) "TK 800" (nonporous particles); (C) a mesoporous gel; (D) a microporous gel.

I (curve D). Thus the micropores had been able to enhance the adsorbent–adsorbate interaction sufficiently to replace monolayer–multilayer formation by micropore filling and thereby change the isotherm from being convex to being concave to the pressure axis.

5.5 The special behaviour of water

On carbon

As already indicated, the interaction energy of water with a nonpolar solid is unusually small. Consequently the adsorption of water by a nonpolar solid is far smaller than that of nonpolar adsorptives having larger and therefore more polarizable molecules where the interaction energy is correspondingly much greater.[48] The contrast in the behaviour of water and hexane towards graphitized carbon black[20] (a nonpolar adsorbent) in Fig. 5.10 is quite striking. Though only dispersion forces are present with both absorbates, they are much stronger in the case of the hydrocarbon because of its long

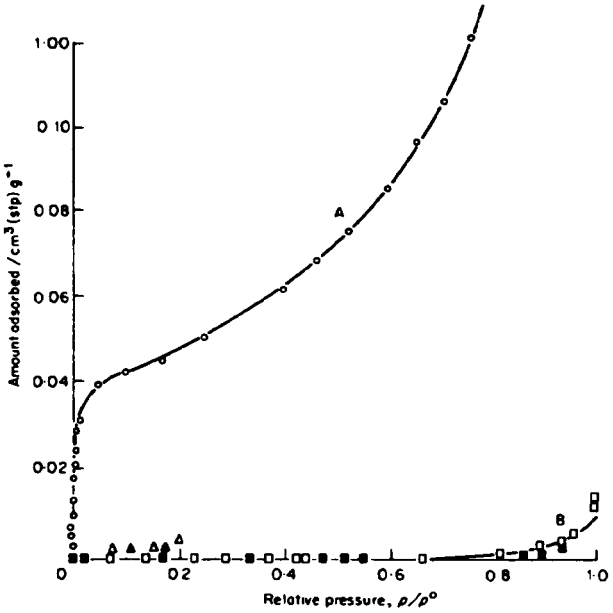

Fig. 5.10 The adsorption isotherms of n-hexane (A) and of water (B) on graphitized carbon black.[20] Solid symbols denote desorption. (After Kiselev.)

chain structure (the chain can lie parallel to the surface), and are indeed strong enough to produce a Type II isotherm.

Because of the hydrogen bonding propensity of the water molecule, the adsorption isotherm of water is especially sensitive to the degree of polarity of the adsorbent surface. This is well illustrated by experiments which show how the removal of polar groups from a surface can lead to a drastic reduction in adsorption and to extreme Type III character in the isotherm. Thus in Fig. 5.11, due to Kiselev,[21] the adsorbent was oxygenated carbon black, from which chemisorbed oxygen (and other polar groups such as OH and COOH) was progressively removed by heating in vacuo or in hydrogen.

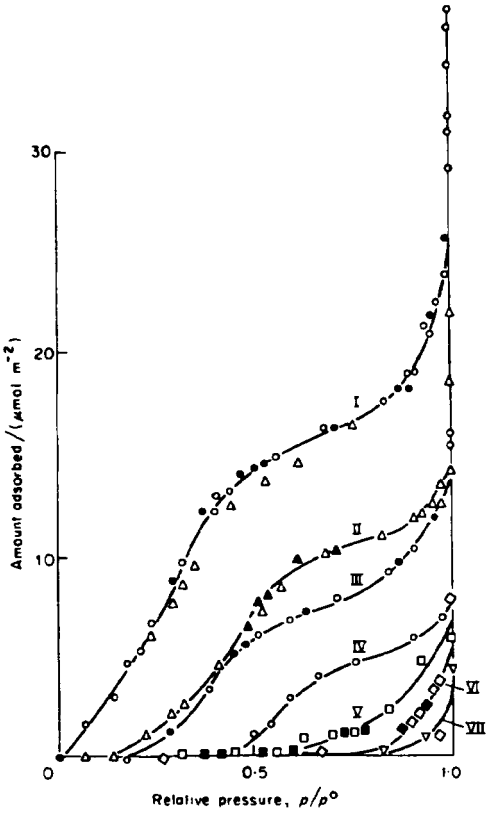

Fig. 5.11 Adsorption of water vapour on oxygenated carbon. (I) heated in vacuo at 200°C; (II) in vacuo at 950°C; (III) in vacuo at 1000°C; (IV) at 1100°C in a hydrogen stream; (V) in hydrogen at 1150°C; (VI) in hydrogen at 1700°C; and (VII) at 3200°C. (Courtesy Kiselev.[21])

The final treatment consisted of heating in hydrogen at 3200°C, which would remove virtually all the polar groups. The progressive lowering of the isotherm is very obvious, and in the last three isotherms the adsorption is barely detectable until relative pressures in excess of 0·5 are reached.

A quantitative relationship between the uptake of water and the amount of chemisorbed oxygen on the surface was established by Walker and Janov[22] in a detailed study on a set of samples of Graphon, a graphitized carbon. Separate batches were first activated in a stream of oxygen at 500°C to produce different burn-offs. From each batch individual samples were then so treated as to obtain different and known contents of chemisorbed oxygen: each sample was first cleaned by outgassing at 950°C, its surface was then saturated by exposure to oxygen at 350°C, and finally it was outgassed at a temperature between 350°C and 950°C to obtain a partially covered surface. The amount of chemisorbed oxygen on each sample was obtained from the loss in weight on further outgassing at 950°C.

On the usual assumption that the oxygen is chemisorbed only on the edge carbons of the crystallites, the average area per chemisorbed oxygen atom was taken to be identical with the average area per edge carbon atom, viz 8·3 Å^2. The "active surface area" A(act) of each sample was then immediately calculable from its content of chemisorbed oxygen. The water isotherms, all of Type III, moved progressively downwards as the oxygen content diminished (Fig. 5.12(*a*)), but when the results were plotted as mg of water per m^2 of active surface area, the points from the separate isotherms fell close to a common curve, except for two divergent points above $p/p^\circ \sim 0{\cdot}5$ (Fig. 5.12(*b*)).

Actually, the nature of the relationship becomes particularly clear if the scale of adsorption is converted to molecules of water adsorbed per atom of chemisorbed oxygen (see right-hand scale of Fig. 5.12(*b*)). It is then immediately obvious that the number of molecules of water adsorbed is commensurate with the number of chemisorbed oxygen atoms.[27] Since, however, the area of an adsorption site is only 8·3 Å^2, whereas the minimum area requirement of an adsorbed water molecule is 10·5 Å^2, any simple picture of the adsorbed film as a multilayer being built up from a close-packed monolayer in which each water molecule is attached to a separate oxygen is untenable. As has already been emphasized (p. 257), in systems giving rise to Type III isotherms the processes of monolayer and multilayer formation are not neatly separated: adsorption proceeds, rather, by some kind of cooperative mechanism (involving, in the case of water, hydrogen bonding) which cannot as yet be formulated in detail.

Even so, it is of interest to calculate the BET monolayer capacity from the composite isotherm of Fig. 5.12(*b*). Though the isotherm did not conform very closely to the BET equation, the isosteric net heat of adsorption was

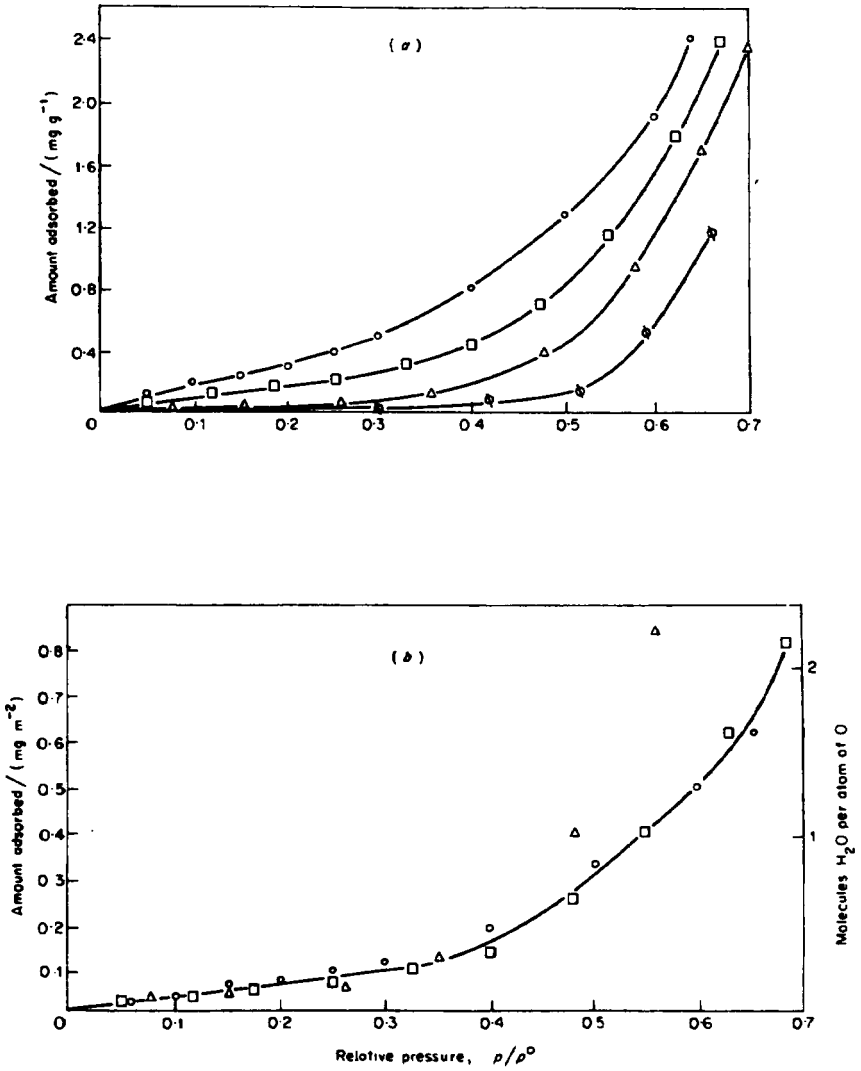

Fig. 5.12 (*a*) Water adsorption isotherms at 20°C on Graphon activated to 24·9% burn-off, where its active surface was covered to varying extents by oxygen complex.[22] (*b*) The results of (*a*) plotted as amount adsorbed per m^2 of "active surface area" (left-hand scale) and also as number of molecules of water per atom of chemisorbed oxygen (right-hand scale). (After Walker.)

found to be effectively zero, so that one may put $c = 1$. The BET monolayer capacity would thus correspond to $p/p^\circ = 0{\cdot}5$ where, according to Fig. 5.12(*b*), the number of molecules of water per atom of oxygen is $\sim 0{\cdot}8$. Thus the monolayer capacity of the chemisorbed oxygen on a graphitized carbon can be approximately evaluated from the water isotherm.

As will be seen shortly, an analogous result is obtained with the silica–water system, where the BET monolayer capacity of water calculated from the water isotherm is roughly equal to the hydroxyl content of the silica surface.

By analogy with carbon tetrachloride on silica it might perhaps be expected that the presence of microporosity in carbon would lead to a Type I isotherm of water if both mesoporosity and external surface area are negligible. Actually this outcome is rarely found: in practice the water isotherm remains convex to the pressure axis in the initial region, and acquires the form of Type V. Figure 5.13 provides excellent examples.[20] The nitrogen isotherms, by their Type I shape, clearly show that the carbons are microporous, but the water isotherms are both of Type V. As is seen, the (liquid) volumes of the two adsorbates taken up on the same adsorbent are almost equal, showing that the Gurvitch rule is obeyed and confirming that the overall process occurring is one of volume filling rather than surface coverage.

Type V isotherms of water on carbon display a considerable variety of detail, as may be gathered from the representative examples collected in Fig. 5.14. Hysteresis is invariably present, but in some cases there are well defined loops (Fig. 5.14(*b*), (*c*), (*d*), (*f*)), and in others the hysteresis extends over the whole range of pressures, some adsorbate being retained on outgassing at the temperature of the isotherm (Fig. 5.14(*e*)); curves similar to Fig. 5.14(*b*) are fairly common. The various explanations of hysteresis in Type V isotherms, to be found in the literature remain somewhat speculative. The steep upward sweep has been ascribed to the coalescence of clusters of molecules which have been nucleated by neighbouring atoms of chemisorbed oxygen;[27] and the steep fall in the desorption branch, as in Fig. 5.14(*a*) or (*b*), has been attributed to the evaporation of capillary-condensed water. Extreme low-pressure hysteresis, as in Fig. 5.14(*e*) is very probably due to penetration effects of the kind discussed in Chapter 4.

An additional complicating factor in many carbons is the presence of ash, which is usually hydrophilic; if present as MgO or CaO resulting from high-temperature treatment of the charcoal, the ash will of course adsorb water chemically as well as physically.

A puzzling feature is that obedience to the Gurvitch rule is by no means universal, the (liquid) volume of water at saturation usually being less than that of the other adsorbate. In Fig. 5.14 for example, the volume of water at

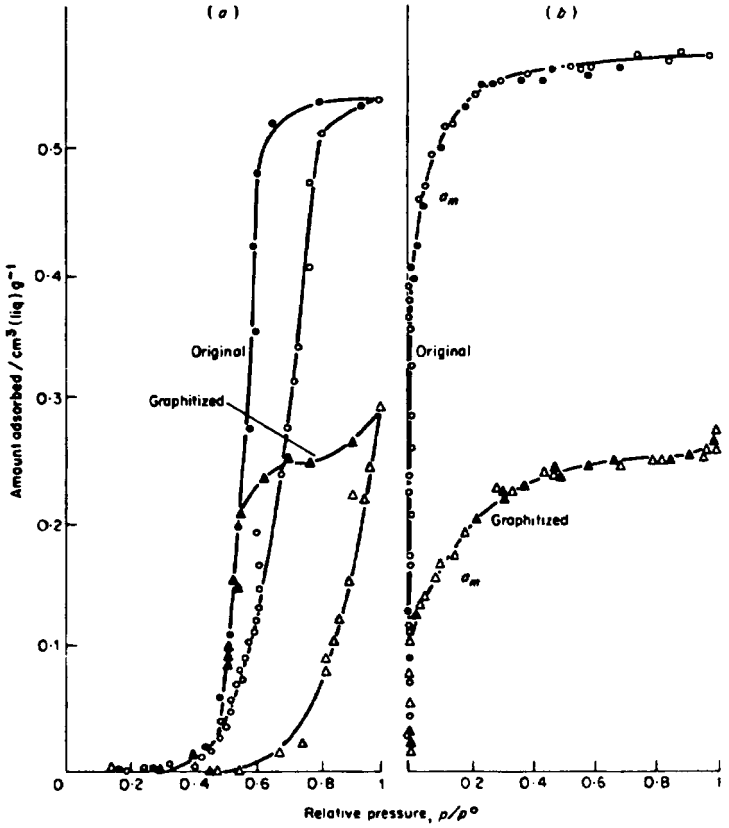

Fig. 5.13 Adsorption isotherms on graphitized and on ungraphitized charcoal. (*a*) Adsorption of water vapour; (*b*) adsorption of nitrogen at −195°C. The adsorption values are expressed in cm^3 of liquid adsorbate per gram of adsorbent. (Courtesy Kiselev.[20])

or near saturation was 670, 490 and 800 $mm^3\ g^{-1}$ for Figures (*a*), (*c*) and (*d*) respectively, whereas the corresponding volumes of nitrogen were 790, 670 and 870 $mm^3\ g^{-1}$ expressed throughout as volumes of liquid. In Fig. 5.14(*b*) the values were 660 $mm^3\ g^{-1}$ for benzene and 600 $mm^3\ g^{-1}$ for water. Such results suggest that the water may be present in a form substantially less dense than ordinary water or even ice, because of a more open structure consequent on hydrogen bonding.

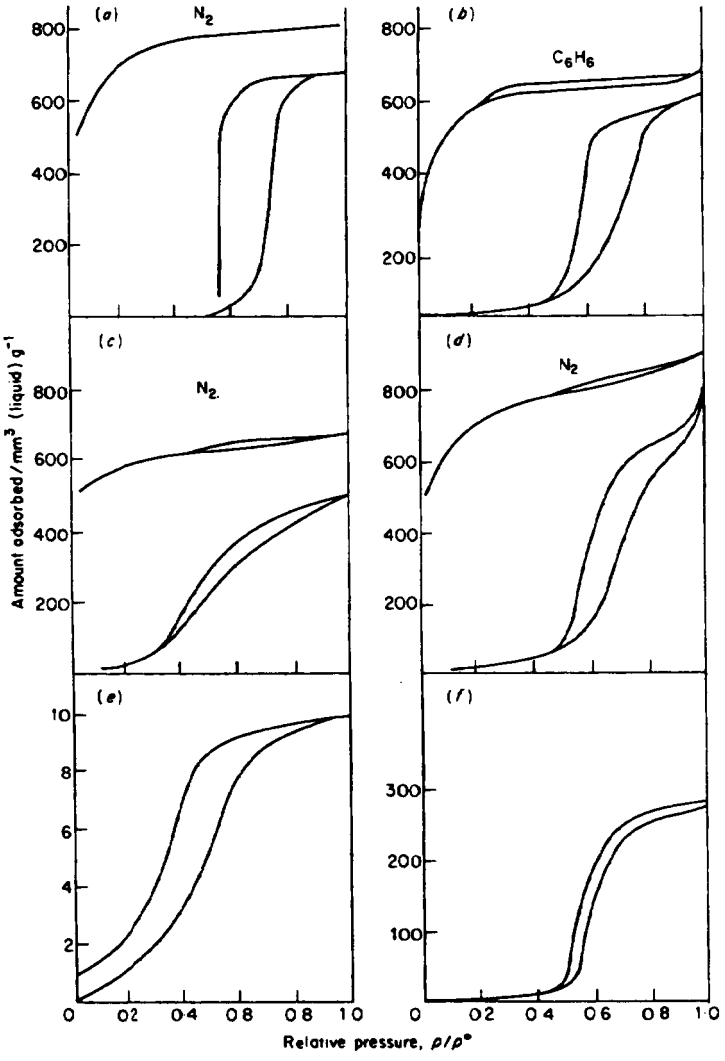

Fig. 5.14 Adsorption isotherms of water on carbon in (*a*) to (*f*) with corresponding isotherms of nitrogen in (*a*), (*c*) and (*d*), and of benzene in (*b*). (*a*) Charcoal C;[23] (*b*) active carbon AY8;[24] (*c*) charcoal A;[23] (*d*) charcoal B;[23] (*e*) a coal tar pitch kilned at 1200°C;[25] (*f*) a charcoal (S600H).[26] (Redrawn from the diagrams in the original papers.)

On silica

An outstanding feature of the adsorption of water vapour on silica is its sensitivity to the course and subsequent treatment of the silica sample, in particular the temperature to which it has been heated.[28] Figure 5.15 shows the strong dependence of the isotherm for a particular silica gel on the temperature of its heat treatment; the isotherm is progressively lowered as the temperature increases, especially above 400°C, and the shape changes from Type II for the lower temperatures to Type III for 600°C, 800°C and 1000°C.

It is now recognized that this kind of behaviour reflects the degree of hydroxylation of the surface, which varies from ~100 per cent for an unheated silica to ~0 per cent after heat treatment at 1100°C. The surface concentration corresponding to a given intermediate temperature of heating can be obtained from the weight loss on further heating at 1100°C, if the specific surface is known from, say, nitrogen adsorption.[28,30] A curve of hydroxyl content (number of OH groups per 100 Å^2) against the temperature of heat treatment is given in Fig. 5.16; the samples had been prepared by flame hydrolysis of silicon tetrachloride, and had been fully hydroxylated by immersion in liquid water prior to the heat treatment.

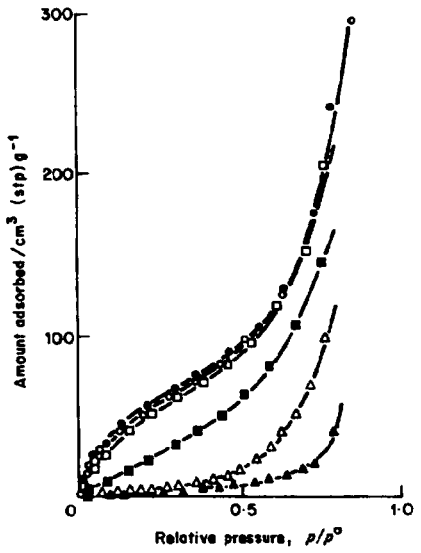

Fig. 5.15 First adsorption isotherms of water vapour at 20°C on silica gel SG pretreated at 25°C (○), 200°C (●), 400°C (□), 600°C (■), 800°C (△), and 1000°C (▲). (Courtesy Naono.[29])

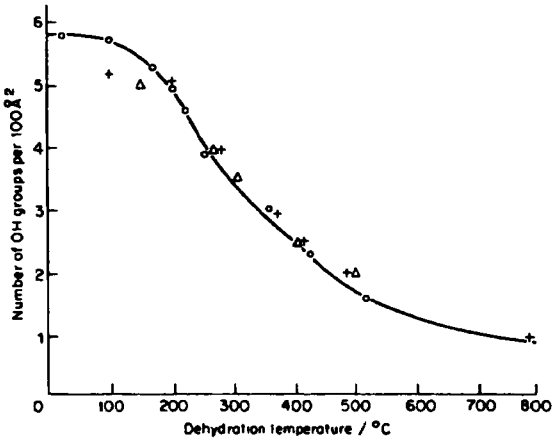

Fig. 5.16 Surface concentration of hydroxyl groups of silica, as a function of the temperature of dehydration. Data are: +, from Fripiat and Uytterhoeven;[31] Δ, from Kiselev and Zhuralev;[32] O, from Taylor[33] (cf. Barby[34]).

On a partially dehydroxylated surface, the hydroxyl groups can be broadly divided into two categories, according as they are, or are not, close enough to their nearest neighbour to undergo hydrogen bonding with it. The former can be sub-divided into "vicinal", where the two interacting hydroxyl groups are attached to adjacent silicon atoms, and "geminal", where the two groups are attached to the same silicon atom. The proportion of the isolated groups increases with increasing temperature of heat treatment, and for temperatures above ~400°C, almost all of the hydroxyl groups are of the isolated variety. Infrared spectroscopy has been invaluable in confirming and refining this general picture.

A completely dehydroxylated surface consists essentially of an array of oxygen atoms: the Si–O linkages are essentially covalent so that the silicon atoms are almost completely screened by the much larger oxygen atoms. Such a surface represents the extreme case and, even on samples ignited at 1100°C, a minute residue of isolated hydroxyl groups will be present.

The adsorption of water on a fully hydroxylated silica involves hydrogen bonding but is essentially physical in nature and is completely reversible in the low pressure range; the isotherm is of Type II on a nonporous sample (Fig. 5.17(*a*)), and of Type IV, with no low-pressure hysteresis, on a porous sample (Fig. 5.18).

When a partially dehydroxylated silica is exposed to water vapour it undergoes slow rehydroxylation. This process will occur during the course

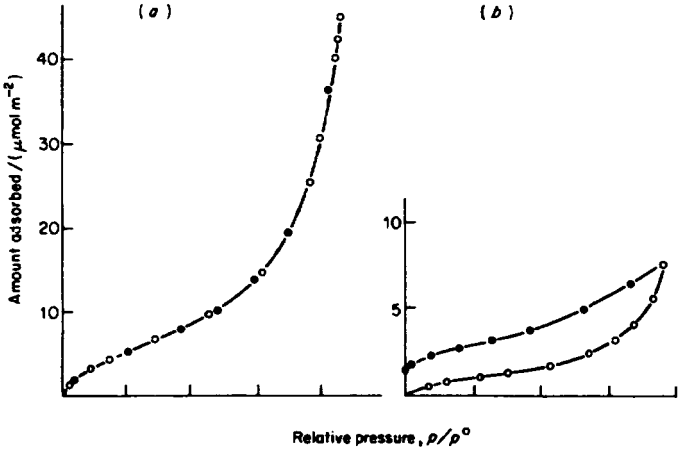

Fig. 5.17 Adsorption of water vapour at 25°C on samples of nonporous silica (TK 800).[35] (*a*) The sample had been exposed to nearly saturated water vapour ($p/p^\circ = 0{\cdot}98$) before determination of the isotherm. (*b*) The sample had been outgassed at 1000°C. (Some points omitted for clarity.)

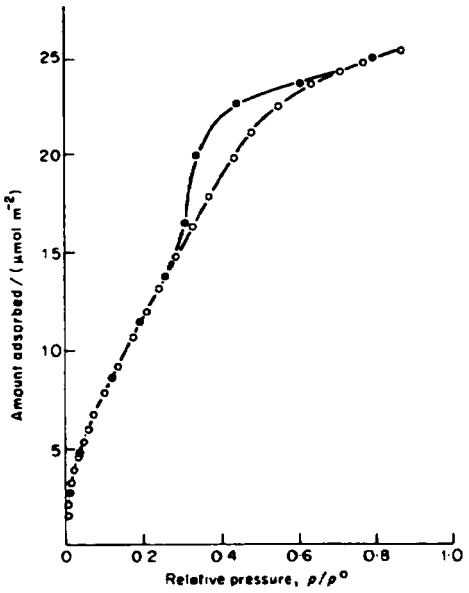

Fig. 5.18 Adsorption isotherm of water vapour[35] at 25°C on microporous silica gel E outgassed at 25°C. ○, Adsorption, ●, desorption.

of an isotherm determination, and because of its limited rate, will produce low-pressure hysteresis. Rehydroxylation probably commences with physical adsorption, initiated by hydrogen bonding of water molecules to any remaining hydroxyl groups in the surface, followed by the growth of clusters of molecules having a rudimentary form of the well known tetrahedral structure of liquid water and ice. When an adsorbed molecule is sufficiently close to a surface oxygen, chemical interaction resulting in two hydroxyl groups can occur; but since this rehydroxylation demands some rearrangement of surface atoms it will be an activated process and will therefore be slow. Owing to their superior ability to promote cluster formation, paired hydroxyl groups will lead to more rapid hydroxylation than will isolated groups, and low-pressure hysteresis will be correspondingly less.

The effect of these factors on the adsorption isotherm may be elucidated by reference to specific examples. In the case of the isotherm of Fig. 5.17(*a*), the nonporous silica had not been re-heated after preparation, but had been exposed to near-saturated water vapour to ensure complete hydroxylation. The isotherm is of Type II and is completely reversible. On the sample outgassed at 1000°C (Fig. 5.17(*b*)) the isotherm is quite different: the adsorption branch is very close to Type III, and there is extrensive hysteresis extending over the whole isotherm, with considerable retention of adsorbate on outgassing at 25°C at the end of the run.

Analogous results are obtained with porous silicas. Figure 5.18 and Fig. 4.26 show the isotherms for a fully hydroxylated and a slightly dehydroxylated silica gel respectively; the presence of slight low-pressure hysteresis in the latter and its absence in the former will be noted. Figure 5.19 refers to a silica gel which had been heated at 900°C. The first adsorption–desorption cycle exhibited much hysteresis which extended over the whole pressure range; the second adsorption branch was quite different from the first, having changed almost to Type IV in place of the original Type V form (with a final upward sweep in both), whereas the second *desorption* branch was coincident with the first. It seems clear that exposure to water vapour during the isotherm determination had brought about almost complete rehydroxylation.

The relationship between the BET monolayer capacity of physically adsorbed water and the hydroxyl content of the surface of silica has been examined by Naono and his co-workers in a systematic study,[29] following the earlier work by Morimoto.[37] Samples of the starting material—a silica gel—were heated for 4 hours in vacuum at a succession of temperatures ranging from 25 to 1000°C, and the surface concentration N_h of hydroxyl groups of each sample was obtained from the further loss on ignition at 1100°C combined with the BET-nitrogen area. Two complete water isotherms were determined at 20°C on each sample, and to ensure complete

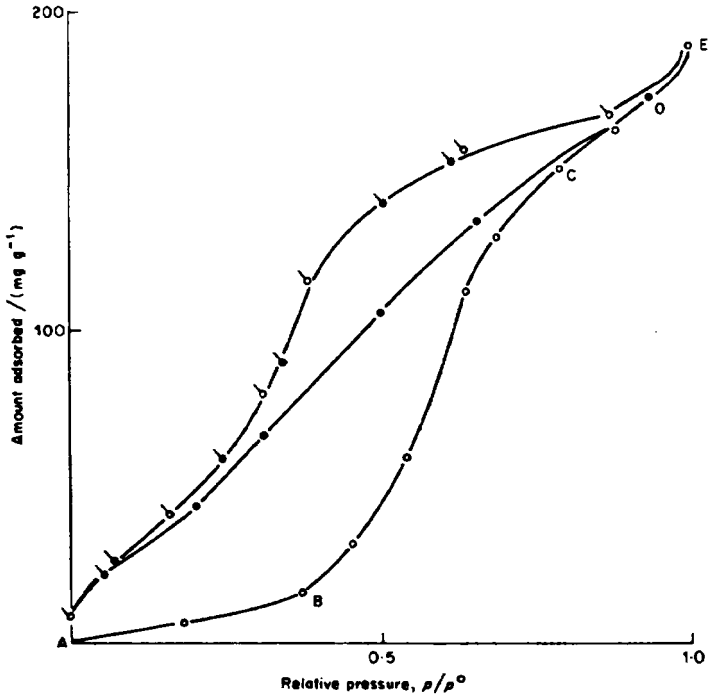

Fig. 5.19 Adsorption of water vapour on a silica gel which had been heated at 900°C. (The water content, calculated from the loss in weight at 1000°C, was 0·2%.)[36] First run: O, adsorption; Ō, desorption. Second run: ●, adsorption; ●̄, desorption.

rehydroxylation, the sample remained exposed to nearly saturated water vapour for 15 hours at the top end of the adsorption branch, before commencing the desorption run. All the isotherms (except that for 25°C) exhibited low-pressure hysteresis and retention of a quantity n_c of adsorbate on outgassing at 25°C, representing water irreversibly taken up during rehydroxylation. The desorption branch of the second isotherm was parallel to, and distant n_c below, the first desorption branch in the monolayer region (0·1–0·3p°) confirming that rehydroxylation was complete. From n_c, the surface concentration N_c of chemisorbed water (i.e. of OH groups formed by rehydroxylation) was obtained. Finally, by application of the BET procedure to the *second* desorption isotherm, the monolayer capacity N_p of physisorbed water on fully hydroxylated surface was evaluated. N_c, N_h and N_p were all referred to 100 Å^2 of surface.

TABLE 5.3

Content of chemisorbed and physisorbed water on a silica gel surface[29]

Pre-treatment temp./°C	$A/(m^2\,g^{-1})$	N_h(OH)	N_c(OH)	$N_h + N_c$	$N_p(H_2O)$
25	358	5·4	0·0	5·4	4·0
200	357	5·2	$0{\cdot}0_6$	$5{\cdot}2_6$	4·1
400	356	4·2	$0{\cdot}9_4$	$5{\cdot}1_4$	4·1
600	355	$1{\cdot}5_0$	2·2	$3{\cdot}7_0$	3·6
800	331	$0{\cdot}4_3$	2·0	$2{\cdot}4_3$	3†
1000	267	$0{\cdot}0_8$	0·9	$0{\cdot}9_8$	–

† Approximate value due to noticeable fluctuation of the BET plot.
N_p, N_c, N_h are all expressed per 100 Å^2.

In Table 5.3, N_p is compared with the total hydroxyl concentration ($N_h + N_c$) of the corresponding fully hydroxylated, sample. The results clearly demonstrate that the physical adsorption is determined by the total hydroxyl content of the surface, showing the adsorption to be localized. It is useful to note that the BET monolayer capacity $n_m(H_2O)$ ($= N_p$) of the water calculated from the water isotherm by the BET procedure corresponds to approximately 1 molecule of water per hydroxyl group, and so provides a convenient means of estimating the hydroxyl concentration on the surface. Since the adsorption is localized,[49] $n_m(H_2O)$ does not, of course, denote a close-packed layer of water molecules. Indeed, the area occupied per molecule of water is determined by the structure of the silica, and is $a_m(H_2O) \simeq 20$ Å^2.

On metal oxides

The hydrophobic character exhibited by dehydroxylated silica is not shared by the metal oxides on which detailed adsorption studies have been made, in particular the oxides of Al, Cr, Fe, Mg, Ti and Zn. With these oxides, the progressive removal of chemisorbed water leads to an increase, rather than a decrease, in the affinity for water. In recent years much attention has been devoted, notably by use of spectroscopic and adsorption techniques, to the elucidation of the mechanism of the physisorption and chemisorption of water by those oxides; the following brief account brings out some of the salient features.

In the pioneering study of rutile by Hollabaugh and Chessick,[38] adsorption isotherms of water were determined after an outgassing at 450°C, and were repeated after evacuation at 90°C at the end of the run. The

two isotherms were found to be parallel over a wide range of relative pressure ($0{\cdot}1 < p/p^\circ < 0{\cdot}6$) and the difference between them was attributed to chemisorption. The monolayer capacities corresponding to chemisorption and physisorption were found to be in the ratio 1:1·8, and therefore not far from 1:2.

Other workers have followed a similar approach: prolonged evacuation at a low temperature, usually 25°C, is assumed to remove physisorbed, but not chemisorbed water, so that the subsequent isotherm can be ascribed to physisorption.

The application of these principles is illustrated by reference to the work of McCaffety and Zettlemoyer[39] on crystalline α-Fe_2O_3. The isotherms in Fig. 5.20 were determined after outgassing (48 h at 10^{-6} Torr) at various temperatures over the range 25–375°C. The initial isotherm for each stated

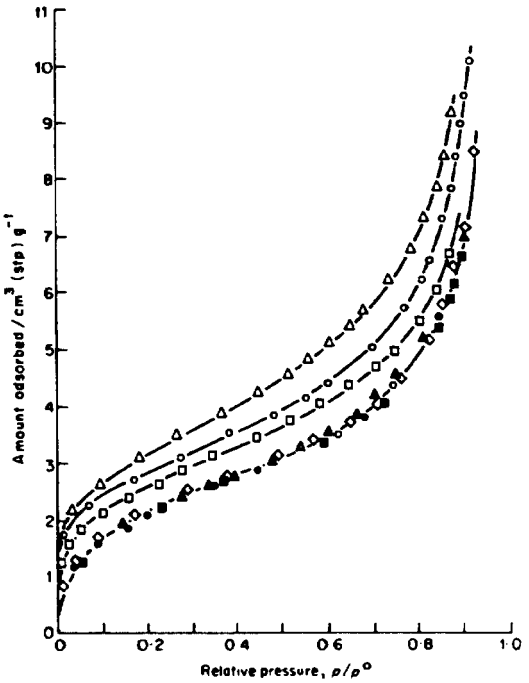

Fig. 5.20 Adsorption isotherms for water vapour on α-Fe_2O_3 at 15°C for various outgassing temperatures.[39] Solid points indicate second isotherm after 25°C evacuation of physically adsorbed water. (Courtesy Zettlemoyer.) Outgassing temperature, ◇, 25°C; □, 100°C; ○, 250°C; △, 375°C.

temperature T was followed by a repeat isotherm, after evacuation at 25°C to remove physisorbed water. All the repeat isotherms fell on, or very close to, the first isotherm for 25°C outgassing, which clearly represents, therefore, the physisorption isotherm for all the samples. The increased uptake on samples outgassed at or above 100°C was thus accounted for by chemisorption, and the extent of hydroxylation was calculated from the difference between the monolayer capacity n_m for T and for 25°C; for the 375°C-outgassed sample n_m corresponded to 5·6OH groups per 100 Å^2, which interestingly is close to the figure, 5·2OH per 100 Å^2, for fully hydroxylated silica. Additional information was provided by measurements of the dielectric constant ε' as a function of surface coverage of adsorbed water. The value of ε' was almost constant in the range up to monolayer completion, consistent with localized adsorption, and believed to be due to hydrogen bonding of each water molecule to two underlying hydroxyl groups; ε' increased sharply at the beginning of multilayer formation, showing that the molecules were able to respond to the a.c. field and were therefore mobile.

A detailed study of the physical and chemical adsorption of water on three xerogels, ferric oxide, alumina and titania, as well as on silica (cf. p. 272) has been carried out by Morimoto and his co-workers.[37] Each sample was outgassed at 600°C for 4 hours, the water isotherm determined at or near 20°C, and a repeat isotherm measured after an outgassing at 30°C. The procedure was repeated on the same sample after it had been evacuated at a

TABLE 5.4

Physisorption and chemisorption of water on alumina, titania and ferric oxide: selection of results (Morimoto *et al.*[37])

Oxide	Outgassing temperature/°C	Adsorption temperature/°C	$N_p(H_2O)$	$N_c(OH)$	$N_h(OH)$	$\frac{N_p}{N_c + N_h}$
Al_2O_3	100	20	6·00	2·20	11·92	0·43
	300	20	6·00	4·89	6·04	0·55
	600	20	6·00	8·34	1·60	0·60
TiO_2	250	18	4·30	5·91	1·65	0·57
	600	18	4·14	6·35	0·10	0·64
α-Fe_2O_3	250	25	3·81	4·57	3·95	0·45
	600	25	4·04	7·91	0·22	0·50

N_p = monolayer capacity of physisorbed water (molecules H_2O per 100 Å^2).

N_c = amount of chemisorbed water formed during isotherm determination (OH groups per 100 Å^2).

N_h = hydroxyl content before isotherm determination (OH groups per 100 Å^2).

series of temperatures ranging from 100° to 500°C. As in the later work of Naono,[29] the number of OH groups per 100 Å^2, N_h, was estimated from the loss on ignition at 1100°C together with the BET-nitrogen area of the samples.

The BET monolayer capacity N_1 calculated from the first water isotherm included both physisorbed and chemisorbed water, whereas that from the second isotherm N_p, included only the physisorbed water. Thus the difference $(N_1 - N_p)$ gave the amount N_c of chemisorbed water taken up as hydroxyl groups during the isotherm determination. $(N_c + N_h)$ was therefore the *total* concentration of hydroxyl groups on the surface when the second water isotherm was being measured.

Representative results are given in Table 5.4. From column 7, it is seen that the ratio $N_p/(N_c + N_h)$ is in the region of 1:2 (in contrast to the 1:1 found with silica) suggesting that each molecule of water in the physisorbed monolayer is bonded to two surface hydroxyl groups.

On titania

The isotherms of water on titania sometimes, but not always, exhibit an unusual feature (Dawson,[40] Parfitt and co-workers[41]) in the form of a second knee X in the $p/p°$ range 0·2 to 0·3, in addition to a rather rounded knee (cf. D in Figs. 5.21 and 5.22) at a lower relative pressure $p/p° \sim 0·05$.

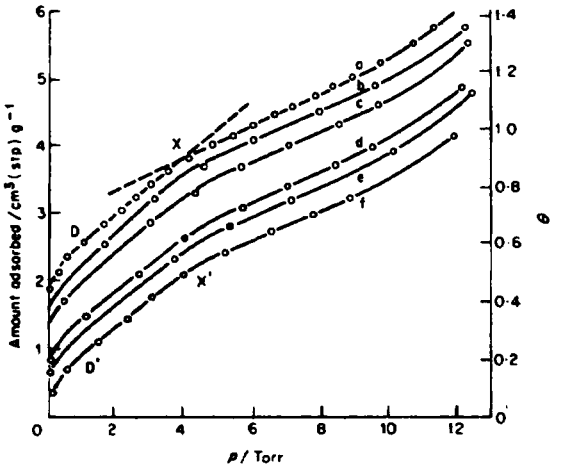

Fig. 5.21 Adsorption isotherms of water at 20°C on rutile A (11·5 m^2 g^{-1}) outgassed at (*a*) 250°C; (*b*) 200°C; (*c*) 150°C; (*d*) 100°C; (*e*) 60°C; (*f*) 20°C. The coverage θ was calculated with $a_m(H_2O) = 10.1$ Å. (Courtesy Dawson.[40])

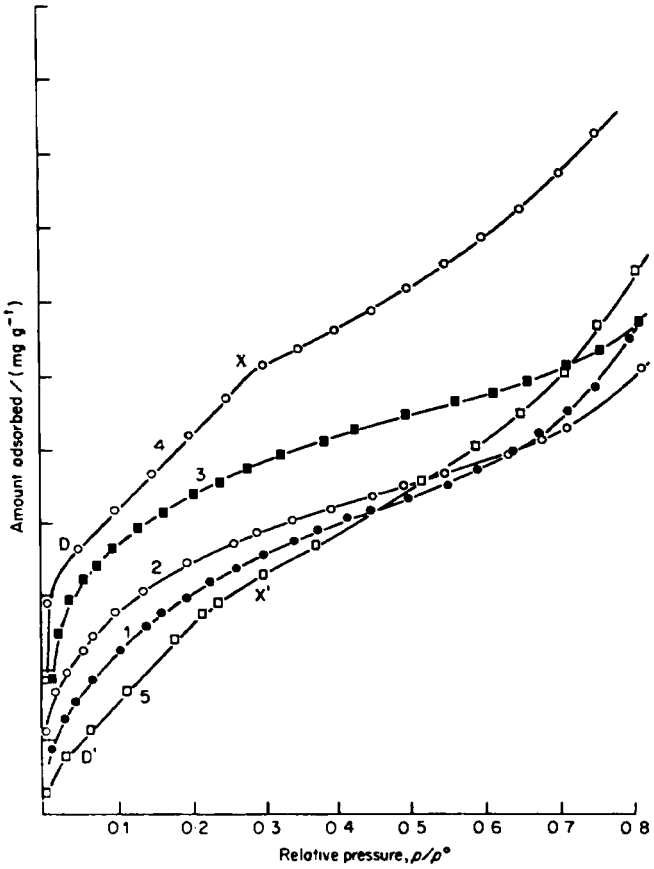

Fig. 5.22 Isotherms of water at 25°C on a sample of rutile,[42] after outgassing in succession at (1) 25°C; (2) 100°C; (3) 150°C; (4) 300°C; (5) 25°C.

In Fig. 5.21, from Dawson's paper, the uptake at X for the 250°C-outgassed sample is close to the calculated value for a monolayer of water with $a_m(H_2O) = 10{\cdot}1$ Å^2. Point X has therefore been ascribed to a close-packed monolayer of water on a hydroxylated surface of rutile. The fact that the differential entropy of adsorption relative to the liquid state (calculated from the isosteric heat of adsorption) changes sharply from negative to positive values in this region with $\Delta_a s \sim 0$ at X was regarded as supporting evidence.[41]

More recent results, however, throw some doubt on this interpretation. The isotherms in Fig. 5.22 were determined after successive outgassings at (1) 25°C, (2) 100°C, (3) 150°C, (4) 300°C, and (5) 25°C, respectively. It will be noted: (a) that only isotherms (4) and (5) exhibit a Point X; and that they are nearly parallel at $p/p^\circ > 0{\cdot}1$; (b) that isotherms (2) and (3) are similarly parallel in the same range; and (c) that isotherms (1) and (5), though both obtained after outgassing at 25°C, are quite different in shape.

In order to interpret these results it is helpful to recall the various ways in which water may interact with titania.[43] The surface of TiO_2 exposes *both* Ti^{4+} ions *and* O^{2-} ions, and—as shown by infrared spectroscopy, temperature programmed desorption and heat of adsorption measurements—water can be chemisorbed on the Ti^{4+} sites in two forms: either as H_2O ligands, or as OH groups (formed by dissociative interaction with the Ti^{4+} and a contiguous O^{2-} ion). Ligand adsorption is rapid, whereas dissociative chemisorption is activated and therefore slow at room temperature; and as shown by Day and Parfitt[41] *isolated* hydroxyl groups do not promote appreciable rehydroxylation at ambient temperature. Finally, water can be physisorbed on the chemisorbed layer. This occurs through hydrogen bonding to the ligand water molecules, to the surface hydroxyl groups, and also—though much more feebly—to the surface oxide ions.

Physisorbed water is removed by prolonged outgassing at temperatures below 100°C; ligand water is progressively removed at temperatures ranging from ~100°C to ~300°C, whilst hydroxyl groups are driven off between ~200°C and ~500°C, isolated groups being retained the longest.

Thus in Fig. 5.22 the first outgassing at 25°C will have removed physisorbed water only, so that curve (1) is the isotherm of physical adsorption on the fully hydroxylated material. The 300°C outgassing, on the other hand, will have removed all the ligand water and the majority of the hydroxyl groups; when isotherm (4) is determined, therefore, the Ti^{4+} ions will chemisorb ligand water at low relative pressure, but the number of hydroxyl groups reformed will be very small.

Physisorption of water will take place on the chemisorbed layer in the manner already indicated, so that isotherm (4) represents the combined result of the chemisorption and the physisorption. The physisorbed, but not the chemisorbed, water is removed by the subsequent 25°C outgassing, and is taken up again during the determination of isotherm (5). Thus the vertical separation of the isotherms beyond points X and X′, ~150 $\mu mol\, g^{-1}$, is equal to the amount of ligand water retained after outgassing at 25°C. The fact that isotherms (1) and (5) follow different courses is a consequence of the change in the nature of the surface, brought about by the removal of hydroxyl groups by the outgassing at elevated temperature.

The earlier interpretation of point X in terms of a close-packed monolayer of water would thus seem untenable. As has been clearly demonstrated, the total uptake at X, 327 μmol g^{-1}, contains a contribution of 150 μmol g^{-1} from chemisorption; thus physisorption accounts for only 177 μmol g^{-1}, which corresponds to 21 $Å^2$ per molecule of water. The fact that the *total* uptake at X corresponds to 11·2 $Å^2$, and is therefore close to the figure 10·5 $Å^2$ for a close-packed monolayer, must be regarded as fortuitous.

The picture is broadly confirmed by the differential energy of adsorption of nitrogen on rutile, obtained in a recent microcalorimetric study.[44] After outgassing at 150°C the values obtained were slightly lower than those for silica under similar conditions of outgassing and surface coverage; but very high values in excess of 20 kJ $mole^{-1}$, were obtained on 20 per cent of the surface after outgassing at 250°C, and on ~40 per cent after outgassing at 400°C, and are readily explained in terms of strong interaction of nitrogen with exposed cations.

The microcalorimetric measurements of Della Gatta and his co-workers[45] in their investigation of the interaction of water vapour with highly dehydroxylated γ-alumina confirm that in this system also, the nondissociative chemisorption of water is nonactivated, whilst the dissociative chemisorption is always activated. Thus the pseudo-equilibrium between the two chemisorbed states is displaced towards dissociative chemisorption as the temperature is increased above ~150°C.

A discussion of the adsorption of water on oxides would be incomplete without some reference to the irreversible effects which are often encountered when samples of oxide, hydroxide or oxide-hydroxide are exposed to the vapour. These effects ("low-temperature ageing"), which manifest themselves in changes in surface area, in pore structure and sometimes in the lattice structure itself, are complex and difficult to reproduce exactly.[46]

Water appears to play a double role in these ageing phenomena.[47] On the one hand, the presence of water ligands at the surface helps to stabilize the system by reducing the surface energy, and thereby retards or even arrests the ageing. If the water is removed, partial collapse of the gel structure ensues; but once all the molecular water has been removed the system again becomes stable, and at room temperature the ageing may be slow enough for reproducible isotherms of nitrogen, argon, etc., to be obtainable over periods of days or even weeks. If, however, the metastable sample is exposed to water vapour, ageing is greatly accelerated because the adsorbed water promotes the movement of ions in the surface layer of the solid.

In view of the complications which may be produced by surface hydration, hydroxylation and ageing, it is essential to check the reproducibility and reversibility of water isotherms if sound conclusions are to be

drawn as to the nature of the adsorption processes involved. Any observed change in the adsorption characteristics with time can, of course, provide valuable information as to the extent and the mechanism of ageing, provided it is amplified by independent data, such as the isotherms of nitrogen or electron micrographs.

References

1. A. V. Kiselev, *J. Colloid Interface Sci.* **28**, 430 (1968).
2. R. M. Barrer, *J. Colloid Interface Sci.* **21**, 415 (1966).
3. J. W. Whalen, *J. Colloid Interface Sci.* **28**, 443 (1968).
4. D. P. Graham, *J. Phys. Chem.* **69**, 4889 (1965).
5. H. H. G. Jellinek, M. D. Luh and V. Nagarajan, *Koll.-Z. u. Polymere* **232**, 758 (1969); T. Iwaki and H. H. G. Jellinek, *J. Colloid Interface Sci.* **69**, 17 (1979).
6. F. P. Shirley and W. H. Wade, *J. Colloid Interface Sci.* **38**, 205 (1972); A. C. Zettlemoyer and H. H. Hsing, *J. Colloid Interface Sci.* **58**, 263 (1977); R. E. Day, G. D. Parfitt and J. Peacock, *J. Colloid Interface Sci.* **70**, 130 (1979).
7. R. E. Day, G. D. Parfitt and J. Peacock, *Disc. Faraday Soc.* No. **52**, 215 (1971); *J. Colloid Interface Sci.* **70**, 130 (1979).
8. J. W. Whalen and P. C. Hu, *J. Colloid Interface Sci.* **65**, 460 (1978).
9. C. F. Prenzlow, H. R. Beard and R. S. Brundage, *J. Phys. Chem.* **73**, 969 (1969); C. F. Prenzlow, *J. Colloid Interface Sci.* **37**, 849 (1971).
10. A. V. Kiselev, *Quart. Rev. Chem. Soc.* XV, 116 (1961).
11. R. B. Gammage and S. J. Gregg, *J. Colloid Interface Sci.* **38**, 118 (1972); R. B. Gammage, Ph.D. Thesis, Exeter University (1964).
12. C. L. Cutting and D. C. Jones, *J. Chem. Soc.* 4067 (1955).
13. R. Stock, Ph.D. Thesis, London University (1955); S. J. Gregg and R. Stock, *in* "Gas Chromatography" (ed. D. H. Desty), p. 90, Butterworths, London (1958).
14. R. K. Packer, Ph.D. Thesis, London University (1952).
15. P. A. Cutting, Ph.D. Thesis, Brunel University (1970); "Vacuum Microbalance Techniques", Vol. 7, p. 71, Plenum Press, New York (1970).
16. W. F. Diano, Ph.D. Thesis, Exeter University (1969); W. F. Diano and S. J. Gregg, Colloques Int. C.N.R.S., No. 201 (1971).
17. P. A. Cutting and K. S. W. Sing, *Chem. and Ind.* 268 (1969).
18. K. S. W. Sing, *in* "Surface Area Determination" (eds. D. H. Everett and R. H. Ottewill), p. 25, Butterworths, London (1970).
19. A. V. Kiselev, *in* "The Structure and Properties of Porous Materials" (eds. D. H. Everett and F. S. Stone), p. 51, Butterworths, London (1958).
20. A. V. Kiselev, *in* "Proceedings of the Second International Congress on Surface Activity", II, p. 219, Butterworths, London (1957).
21. A. V. Kiselev and N. V. Kovaleva, *Izvest. Akad. Nauk S.S.S.R., Otd. Khim. Nauk* 955 (transl.) (1959).
22. P. L. Walker and J. Janov, *J. Colloid Interface Sci.* **28**, 499 (1968).
23. J. C. Arnell and H. L. McDermott, *Canad. J. Chem.* **30**, 177 (1952).
24. M. M. Dubinin, *in* "Chemistry and Physics of Carbon" (ed. P. L. Walker), Vol. 2, p. 51, Marcel Dekker, New York (1966).
25. F. M. W. Olds, Ph.D. Thesis, Exeter University (1959).

26. C. Pierce, R. N. Smith, J. W. Wiley and H. Cordes, *J. Amer. Chem. Soc.* **73**, 4551 (1951).
27. E. Cremer, T. Kraus and P. Stoever, *Chem.-Ing.-Tech.* **43**, 614 (1971); M. Voll and H. P. Boehm, *Carbon* **9**, 473 (1971); D. Rivin, *Rubber Chem. Technol.* **44**, 307 (1971).
28. R. K. Iler, "The Chemistry of Silica", p. 650, Wiley-Interscience, New York (1979); K. K. Unger, "Porous Silica", p. 195, Elsevier, Amsterdam (1979); N. D. Parkyns and K. S. W. Sing, *in* "Colloid Science", Vol. 2, p. 37, Specialist Periodical Reports, Chemical Society, London (1975); R. M. Pashley and J. A. Kitchener, *J. Colloid Interface Sci.* **71**, 491 (1979).
29. H. Naono, R. Fujiwara and M. Yagi, *J. Colloid Interface Sci.* **76**, 74 (1980).
30. S. Kondo, F. Fujiwara and M. Muroya, *J. Colloid Interface Sci.* **55**, 421 (1976).
31. J. J. Fripiat and J. Uytterhoeven, *J. Phys. Chem.* **66**, 800 (1962).
32. A. V. Kiselev and L. T. Zhuralev, *Zhur. Fiz. Khim.* **39**, 236 (1965).
33. J. A. G. Taylor, Ph.D. Thesis, Manchester University (1966); J. A. G. Taylor and J. A. Hockey, *J. Phys. Chem.* **70**, 2169 (1966).
34. D. Barby, *in* "Characterization of Powder Surfaces" (eds. G. D. Parfitt and K. S. W. Sing), p. 407, Academic Press, London and New York (1976).
35. F. S. Baker and K. S. W. Sing, *J. Colloid Interface Sci.* **55**, 605 (1976).
36. J. F. Goodman, Ph.D. Thesis, London University (1955).
37. T. Morimoto, M. Nagao and F. Tokuda, *Bull. Chem. Soc. Japan*, **41**, 1533 (1968); *J. Phys. Chem.* **73**, 243 (1969); T. Morimoto, M. Nagao and J. Imai, *Bull. Chem. Soc. Japan* **44**, 1282 (1971).
38. C. M. Hollabaugh and J. J. Chessick, *J. Phys. Chem.* **65**, 109 (1961).
39. E. McCafferty and A. C. Zettlemoyer, *J. Colloid Interface Sci.* **34**, 452 (1970); *Disc. Faraday Soc.* No. 52, 239 (1971).
40. P. T. Dawson, *J. Phys. Chem.* **71**, 838 (1967).
41. R. E. Day and G. D. Parfitt, *Trans. Faraday Soc.* **63**, 708 (1967); R. E. Day, G. D. Parfitt and J. Peacock, *Disc. Faraday Soc.* **52**, 215 (1971); *J. Colloid Interface Sci.* **46**, 17 (1974).
42. D. N. Furlong, Ph.D. Thesis, Brunel University (1975).
43. G. Munuera and F. S. Stone, *Disc. Faraday Soc.* **52**, 205 (1971); P. Jackson and G. D. Parfitt, *Trans. Faraday Soc.* **67**, 2469 (1971); P. Jones and J. A. Hockey, *Trans. Faraday Soc.* **67**, 2669 (1971); C. H. Rochester, *Chem and Ind.* 175 (1981).
44. D. N. Furlong, F. Rouquerol, J. Rouquerol and K. S. W. Sing, *J. Chem. Soc. Faraday Trans.* I, **76**, 774 (1980).
45. G. Dalla Gatta, B. Fubini and G. Venturello, *J. Chim. Phys.* **70**, 60 (1973).
46. G. C. Bye and K. S. W. Sing, *in* "Particle Growth in Suspensions" (ed. A. L. Smith), p. 29, Academic Press, London and New York (1973); N. D. Parkyns and K. S. W. Sing, *in* "Colloid Science", Vol. 2, pp. 40, 51, Specialist Periodical Reports, Chemical Society, London (1975); H. F. Holmes, E. L. Fuller and R. A. Beb, *J. Colloid Interface Sci.* **47**, 365 (1974).
47. K. S. W. Sing, *in* "Thermochimie", Colloques Int. C.N.R.S. No. 201, Paris (1972); F. S. Baker, J. D. Carruthers, R. E. Day, K. S. W. Sing and L. J. Stryker, *Disc. Faraday Soc.* No. 52, 173 (1971); A. A. Rahman and K. S. W. Sing, *Thermochim. Acta* **29**, 277 (1979); R. B. Gammage, W. S. Brey and B. W. Davis, *J. Colloid Interface Sci.* **32**, 256 (1970).
48. L. D. Beljakova, A. V. Kiselev and N. V. Kovaleva, *Bull. Soc. Chim.-Mém.* 285 (1967).
49. A. Nonaka and E. Ishizaki, *J. Colloid Interface Sci.* **62**, 381 (1977); P. G. Hall, A. Pidduck and C. J. Wright, *J. Colloid Interface Sci.* **79**, 339 (1981).

6

The Use of Gas Adsorption for the Determination of Surface Area and Pore Size Distribution

GENERAL RECOMMENDATIONS

The following recommendations are based on the material in Chapters 2 to 5. For the reasoning behind the individual recommendations, the appropriate sections should be consulted.

6.1 Choice of adsorptive

For evaluation of both the surface area and the pore size distribution of a solid from a single isotherm, nitrogen is the most suitable adsorptive. For determination of surface area alone, argon provides an alternative to nitrogen, but argon cannot be used at temperatures around 77 K for the assessment of pore size distribution. If the specific surface is relatively low ($< 5\,m^2\,g^{-1}$, say) krypton, also at ~ 77 K, offers the possibility of higher precision in the actual measurement of the adsorption, but not necessarily higher accuracy, than that obtained with nitrogen or argon in the resultant value of specific surface. The use of other adsorptives is not recommended except for the study of the structure of the surface (e.g. by water or alcohols), or as molecular probes for evaluation of micropore size (e.g. using molecules of different size and shape).

6.2 Choice of experimental method

A volumetric technique is generally to be preferred especially when reasonable accuracy is required in the region of high relative pressure, as in

the estimation of pore size distribution. A gravimetric technique (e.g. recording vacuum microbalance or silica spring), is useful however, if changes in the mass of the adsorbent itself (as a result, say, of oxidation, reduction or thermal decomposition) need to be measured at the same time as the isotherm. In the use of the sorption balance at low temperatures for the determination of pore size distribution it is essential to allow for the difference in temperature between the adsorbent sample and the refrigerant bath—preferably by means of a reference isotherm measured under identical conditions on a suitable nonporous sample. The reliability of data obtained with the automatic equipment now commercially available should be similarly checked.

6.3 Outgassing of the adsorbent

Prior to determination of an isotherm, all physisorbed material has to be removed from the surface of the adsorbent. This is best achieved by exposure of the surface to high vacuum, the exact conditions required (temperature and residual pressure) being dependent on the particular gas–solid system. In routine determinations of surface area it is generally advisable not to remove any chemisorbed species which may be present: thus, the hydroxylated oxides are usually outgassed at ~150°C. Microporous adsorbents such as zeolites or active carbons however require higher temperatures (350–400°C, say) for complete removal of physisorbed material from their narrowest pores. An outgassing period of 6–10 hours (e.g. overnight) is usually sufficient to reduce the residual pressure to $\sim 10^{-4}$ Torr.

6.4 Construction of the adsorption isotherm

A number of potential sources of error must be taken into account. In the volumetric method the following items need attention: (a) constancy of the level of liquid nitrogen; (b) depth of immersion of the sample bulb ($\geqslant 5$ cm); (c) temperature of sample (monitoring with vapour pressure thermometer close to sample bulb); (d) purity of adsorptive (preferably 99·9 per cent); (e) temperature of gas volumes (doser, dead space), controlled to ~0·1°C.

With gravimetric methods, the magnitude of the buoyancy correction should be assessed. Particular attention must be paid to the adsorbent temperature because of the unavoidable gap between the sample and the balance "case" (cf. Section 6.2).

6.5 Reproducibility and reversibility of the isotherm

For a given system at a given temperature, the adsorption isotherm should be reproducible, but the possibility of ageing of the adsorbent—e.g. through the addition or removal of water—must always be borne in mind. The reproducibility of the adsorption should be checked whenever possible by measurement of an isotherm on a second sample (of different mass) of the given adsorbent. Adsorption hysteresis is of two kinds: (a) the hysteresis loop, which is normally associated with capillary condensation; and (b) low-pressure hysteresis, which is due either to "activated entry" or to a change in the adsorbent, such as the swelling of a nonrigid structure.

6.6 Type of isotherm and type of hysteresis loop

The first stage in the interpretation of a physisorption isotherm is to identify the isotherm type and hence the nature of the adsorption process(es): monolayer–multilayer adsorption, capillary condensation or micropore filling. If the isotherm exhibits low-pressure hysteresis (i.e. at $p/p^\circ < 0{\cdot}4$, with nitrogen at 77 K) the technique should be checked to establish the degree of accuracy and reproducibility of the measurements. In certain cases it is possible to relate the hysteresis loop to the morphology of the adsorbent (e.g. a Type B loop can be associated with slit-shaped pores or platey particles).

6.7 BET analysis

The BET method is unlikely to yield a value of the true surface area if the isotherm is of either Type I or Type III; on the other hand, both Type II and Type IV isotherms are, in general, amenable to the BET analysis, provided that the value of c is not too high and that the BET plot is linear for the region of the isotherm containing Point B. It is recommended that both the value of c and the range of linearity of the BET plot be recorded. If the value of c is found to be higher than normal for the particular gas–solid system, the presence of microporosity is to be suspected even if the isotherm is of Type II or Type IV; the validity of the BET area then needs checking e.g. by the α_s-method, in order to ascertain how closely the shape of the isotherm conforms to that of the standard isotherm in the monolayer range.

6.8 Assessment of mesopore size distribution

The computation of mesopore size distribution is valid only if the isotherm is of Type IV. In view of the uncertainties inherent in the application of the Kelvin equation and the complexity of most pore systems, little is to be gained by recourse to an elaborate method of computation, and for most practical purposes the Roberts method (or an analogous procedure) is adequate—particularly in comparative studies. The decision as to which branch of the hysteresis loop to use in the calculation remains largely arbitrary. If the desorption branch is adopted (as appears to be favoured by most workers), it needs to be recognized that neither a Type B nor a Type E hysteresis loop is likely to yield a reliable estimate of pore size distribution, even for comparative purposes.

6.9 Assessment of microporosity

If a Type I isotherm exhibits a nearly constant adsorption at high relative pressure, the micropore volume is given by the amount adsorbed (converted to a *liquid* volume) in the plateau region, since the mesopore volume and the external surface are both relatively small. In the more usual case where the Type I isotherm has a finite slope at high relative pressures, both the external area and the micropore volume can be evaluated by the α_s-method provided that a standard isotherm on a suitable non-porous reference solid is available. Alternatively, the nonane pre-adsorption method may be used in appropriate cases to separate the processes of micropore filling and surface coverage. At present, however, there is no reliable procedure for the computation of micropore size *distribution* from a single isotherm; but if the size extends down to micropores of molecular dimensions, adsorptive molecules of selected size can be employed as molecular probes.

Appendix

A manual entitled "Reporting Physisorption Data for Gas/Solid Systems with Special Reference to the Determination of Surface Area and Porosity" has been prepared as a "provisional" publication by Commission I.6 of the International Union of Pure and Applied Chemistry (IUPAC). The purpose of the manual is to draw attention to problems involved in reporting physisorption data and to provide guidance on the evaluation and interpretation of isotherm data. The general conclusions and recommendations are very similar to those contained in Chapter 6.

A new classification of hysteresis loops, as recommended in the IUPAC manual, consists of the four types shown in the Figure below. To avoid confusion with the original de Boer classification (p. 117), the characteristic types are now designated H1, H2, H3 and H4; but it is evident that the first three types correspond to types A, E and B, respectively, in the original classification. It will be noted that H1 and H4 represent extreme types: in the former the adsorption and desorption branches are almost vertical and nearly parallel over an appreciable range of gas uptake, whereas in the latter they are nearly horizontal and parallel over a wide range of relative pressure. Types H2 and H3 may be regarded as intermediate between the two extremes.

As pointed out earlier (Section 3.5), certain shapes of hysteresis loops are associated with specific pore structures. Thus, type H1 loops are often obtained with agglomerates or compacts of spheroidal particles of fairly uniform size and array. Some corpuscular systems (e.g. certain silica gels) tend to give H2 loops, but in these cases the distribution of pore size and shape is not well defined. Types H3 and H4 have been obtained with adsorbents having slit-shaped pores or plate-like particles (in the case of H3). The Type I isotherm character associated with H4 is, of course, indicative of microporosity.

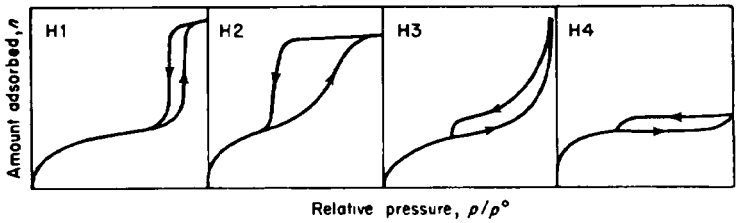

Author Index

(Numbers in parentheses indicate the citation, to be found at the end of the relevant chapter.)

Subject Index